Synthesis and Study of Peptidic Bacterial Siderophores

by

"Damon" Xin Wen

A thesis submitted in partial fulfilment of the requirements for the degree of

Doctor of Philosophy

March 2023

Acknowledgements

I would like to give my highest appreciation to my supervisor, Dr Michael Hall, for his unwavering guidance over the past four years. Thank you for meticulously supporting every part of my research and upholding my work to high standards. Dr Michael Hall has not only been an academic mentor but also a life mentor, and our supervisor meetings over pints have been very enjoyable.

Furthermore, I would like to extend my gratitude to all the past and present members of the MJH research group, with whom I have had the pleasure of working with. I must give a special mention to Dr Ronnie Ragbirsingh for his early guidance, advice during my rookie time, lots of jokes, delicious foods, and continued support as a big brother in my life. In addition, thanks to DJ Dr Kin Lok Ho for helping me improve as a chemist, rapping with me and ensuring that our voices are always heard throughout the building.

I would also like to thank Dr ZhengGuang Xiao, Dr Oliver Gray, Felicity Frank, Aminah Almarshad, and Jay Tromans for creating a wonderful working environment, caring about me, enjoying my witty jokes and engaging in insightful discussions with me.

I am grateful to my best 'Newcastle Soldier Team' members, Dr Omar Alatawi and Fehmi Benli, for the mutual support that we shared during our research journeys, since our master's studies, and continued strong friendship through all the stresses and joys.

Additionally, I extend my gratitude to Professor William McFarlane and Dr Corinne Wills for their invaluable support with NMR spectroscopy, and to Dr Paul Waddell for his assistance with X-ray crystallography.

Last but not least, I want to show my best appreciation to my grandparents; parents Ying Deng and GuiLing Wen; and girlfriend Esther May. Without your boundless support and encouragement, I could not have come this far. I love you all, and you are always in my deep heart.

Thank you all again, and please allow me to do one more time, "Allllllright mate?!" (with my loudest voice, special retroflex accent and heavy head nodding). I hope I have made you all proud and happy, AS ALWAYS AYE? PROPER!

Abstract

Siderophores are natural products found in many organisms, such as bacteria, which show high binding affinities for metals. Siderophores are an essential component of bacterial metabolism as they allow uptake of metal ions into the cells. The synthesis and study of siderophores are therefore useful in the understanding of bacterial metabolism and for the development of future antibiotics. This thesis will focus on the synthesis and investigation of two nonribosomal peptide bacterial siderophores.

Firstly, we will discuss our work on mirubactin C, an NRPs siderophore isolated from *Actinobacteria* sp. DEM60616 which was thought to inhibit bacterial lipoteichoic acid synthase (*ltaS*). Both the natural (*R*,*R*)- and unnatural (*S*,*S*)- enantiomers of mirubactin C were synthesised over 12 steps in 12% overall yield, with absolute stereochemistry confirmed by Marfey's analysis, and the biological activity of both synthetic enantiomers versus the isolated natural product was examined (Scheme 1).

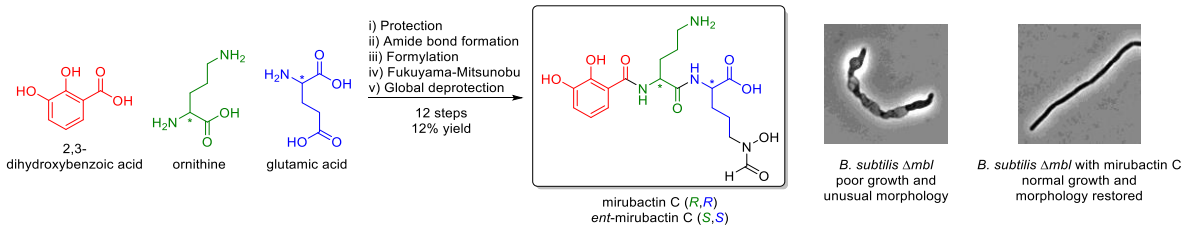

Scheme 1. Synthesis of mirubactin C, including biological activity testing.

Secondly, we have worked towards the synthesis of madurastatin C1, a siderophore isolated from *Actinomadura* sp. DEM31376. We present our construction of the complete backbone of madurastatin C1 over 14 steps with a 17% overall yield, and our exploration of the final steps involving oxazoline formation and global deprotection (Scheme 2).

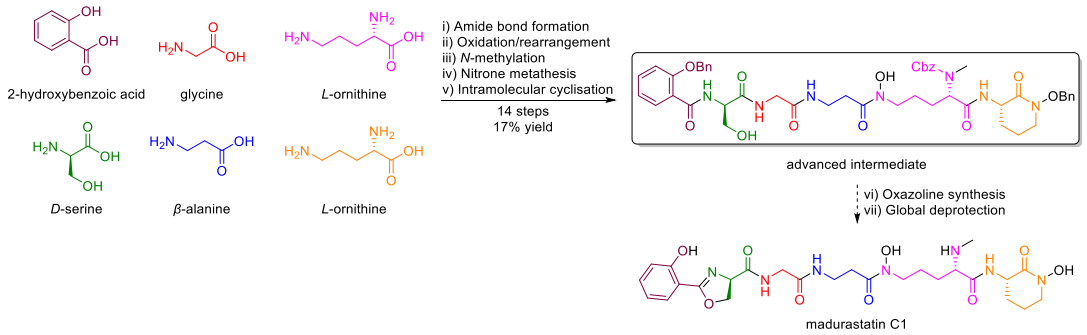

Scheme 2. Towards the synthesis of madurastatin C1.

Covid-19 Impact Statement

I am undertaking a laboratory-based PhD in organic chemistry, which is heavily reliant on access to the chemistry research laboratories and supporting analytical facilities (NMR, X-ray, Mass Spec).

From 17/3/20 all laboratory and analytical research work was stopped due to COVID-19, until 13/7/20, a period of 17 weeks. Despite reopening, the laboratories and analytical facilities are still subject to COVID restrictions and thus the rate of research work is still impaired.

I was unable to conduct practical research work over the closure period. Furthermore, a number of key intermediate compounds, prepared prior to the laboratory closures, decomposed during the closure period despite low temperature storage, requiring several months of additional work to re-prepare them.

Research delays and associated uncertainty around the situation have also caused me significant stress and anxiety. Despite the effects of COVID-19 on my research timeline and mental health, I worked to the best of my abilities to complete PhD projects.

Abbreviations

Ac	Acetyl
Ala	Alanine
aq.	Aqueous
Ar.	Aromatic
Bn	Benzyl
Boc	*tert*-Butyloxycarbonyl
calcd	Calculated
Cbz	Carbobenzyloxy
COSY	Correlation spectroscopy
d	Doublet
DAST	Diethylaminosulfur trifluoride
DCM	Dichloromethane
de	Diastereoisomeric excess
DEAD	Diethyl azodicarboxylate
DIPEA	N,N-Diisopropylethylamine
DMF	Dimethylformamide
DMSO	Dimethyl sulfoxide
ee	Enantiomeric excess
Eq.	Equivalents
Et	Ethyl
Et_2O	Diethyl ether
Et_3N	Triethylamine
EtOAc	Ethyl Acetate
g	Gram
Gly	Glycine
h	hours
HATU	1-[Bis(dimethylamino)methylene]-1H-1,2,3-triazolo[4,5-b]pyridinium 3-oxide hexafluorophosphate

HMBC	Heteronuclear multiple bond correlation spectroscopy
HRMS	High resolution mass spectrometry
HSQC	Heteronuclear single quantum correlation spectroscopy
IR	Infrared
J	Coupling constant
KOH	Potassium hydroxide
lit.	Literature
LTA	Lipoteichoic acid
LtaS	Lipoteichoic acid synthase
M	Molar
m	Multiplet
*m*CPBA	*meta*-Chloroperoxybenzoic acid
Me	Methyl
mg	milligram
min	minute
mL	millilitre
mol.	Molecular
Mp.	Melting point
mRNA	messenger ribonucleic acid
nm	nanometers
NMR	Nuclear magnetic resonance
NRP	Nonribosomal peptide
o	ortho
p	para
PBP	Penicillin-binding protein
PG	Peptidoglycan
Ph	Phenyl
ppm	parts per million
q	Quartet
R_f	Retention factor

r.t.	Room temperature
s	Singlet
t	Triplet
TFA	Trifluoroacetic acid
THF	Tetrahydrofuran
TLC	Thin layer chromatography
WTA	Wall teichoic acid

Contents

Chapter 1. Introduction

This PhD thesis focuses on the total synthesis and investigation of two nonribosomal peptides, mirubactin C and madurastatin C1. Both mirubactin C and madurastatin C1 are bioactive siderophores, isolated from Gram-positive bacteria. In this section we will therefore focus on an introduction to bioactive natural products, nonribosomal peptides and siderophores, as well discussing the biology of bacterial cell walls (e.g., LTA biosynthesis) as targets for the development of new antibiotics.

1.1 Natural Products

1.1.1 Natural Products - Applications in Drug Discovery

Natural products are small organic molecule secondary metabolites isolated from living organisms, such as bacteria, fungi, and plants. Primary metabolism occurs in all living organisms and is essential for function, including the synthesis of proteins, DNA and RNA. In contrast secondary metabolism involves the production of molecules that are not directly essential for survival, but that can provide an evolutionary advantage for the organism.

In 2016, research by Gloer *et al*. estimated that 500,000 natural products had been reported in the literature at that time, isolated from plants (~350,000), animals (~100,000), and microbes (~70,000).[1] Natural products are normally classified by their functional groups and biosynthetic pathways, with commonly occurring classes being terpenoids, phenolics, alkaloids, polyketides, and nonribosomal peptides. Phenolics, alkaloids and terpenoids are more commonly found in plants, polyketides and nonribosomal peptides are more commonly produced by bacteria, and fungi can produce terpenoids, polyketides and nonribosomal peptides.

Natural product research is important, as many natural products show biological activity and have been used in the development of medicines for the treatment of cancer, pain management, and infectious diseases.[2] Examples of natural products that have been used in medicine include the terpenoid artemisinin (first isolated from sweet wormwood, *Artemisia annua*)[3] used in the treatment of malaria, the phenolic aspirin

(first isolated from willow tree (genus *Salix*))[4] used as a painkiller, the alkaloid paclitaxel (first isolated from the pacific yew, *Taxus brevifolia*)[5] used as an anticancer drug, and rifampicin, a semi-synthetic antibiotic made from the polyketide rifamycin (first isolated from *Amycolatopsis rifamycinica*)[6] that is used to treat tuberculosis and leprosy (**Figure 1.1**).

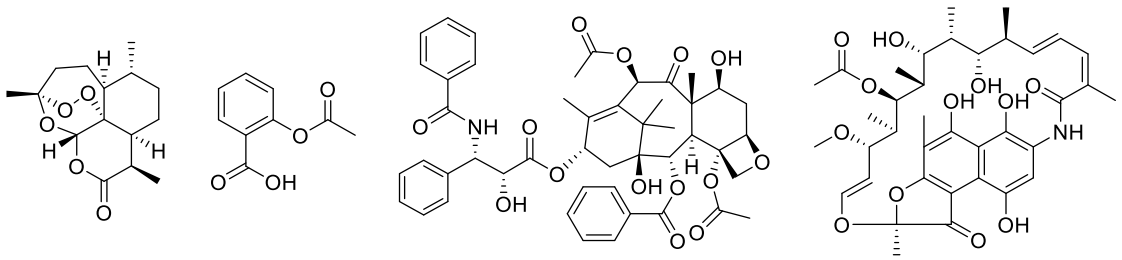

Figure 1.1. Natural products used in medicine.

1.1.2 Nonribosomal Peptide Natural Products - Applications in Drug Discovery

In living organisms peptides, such as proteins, are normally biosynthesised by the ribosome which translates mRNA into polypeptide sequences using natural amino acids. In contrast nonribosomal peptides are produced by nonribosomal peptide synthetases, which only make a specific polypeptide sequence but are capable of using non-natural amino acids (e.g., *D*-amino acids) and can include post-synthesis modification steps.

Nonribosomal peptide (NRP) natural products have a variety of important biological activities, and as such have been employed in the development of drug molecules, particularly antibiotics. For example, the antibiotic bacitracin A (first isolated from *Bacillus licheniformis* (ATCC 10716))[7] is used in the treatment of skin and eye infections (**Figure 1.2**).

1.2 Siderophore

1.2.1 Microbial Siderophores

Siderophores are a large group of natural products, many of which are nonribosomal

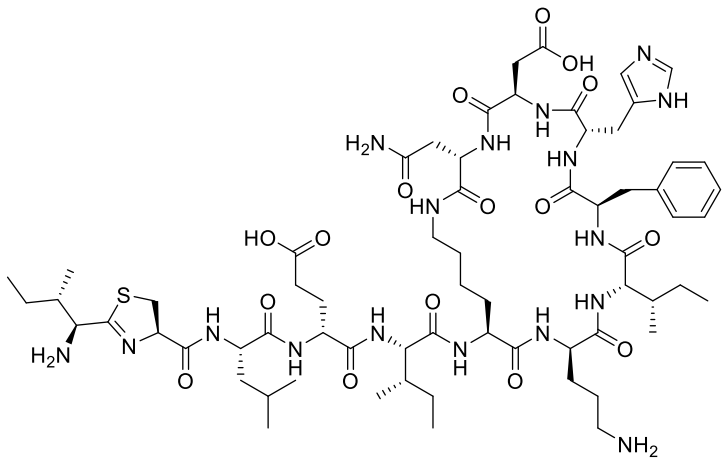

Figure 1.2. Nonribosomal peptide natural product used in medicine.

peptides. Siderophores are small molecules produced by microorganisms such as bacteria and fungi, which show high binding affinities for Fe^{3+} and other metal ions (e.g., Mg^{2+}, Zn^{2+}, Mn^{2+}). Iron is an essential element required for the growth and survival of most microorganisms. However, iron is often limited in the environment due to its tendency to form insoluble complexes, such as iron oxides and iron sulphides.

In order to take up Fe^{3+} from the environment, microorganisms can synthesise natural product siderophores, which are then exported through the cell wall. The siderophores then chelate Fe^{3+} from the environment to form stable complexes. Iron-complexed siderophores are then uptaken into the cell, by transport across the cell wall. Once inside the cell, the Fe^{3+} is released, making it available for use by the microorganism (**Figure 1.3**).[8-11]

1.2.2 Structure and Iron Binding in Natural Product Siderophores

In 2009, research by Hider *et al.* reported that there are more than 500 different siderophores, 270 of which have been structurally characterised.[8] Siderophores can be divided into three main types based on their functional groups: catecholates, hydroxamates, and carboxylates. These functional groups typically contain hard bidentate, singly charged, oxygen based ligands, which can interact with Fe^{3+} through a combination of ionic and dative bonding. Three of these bidentate chelating groups

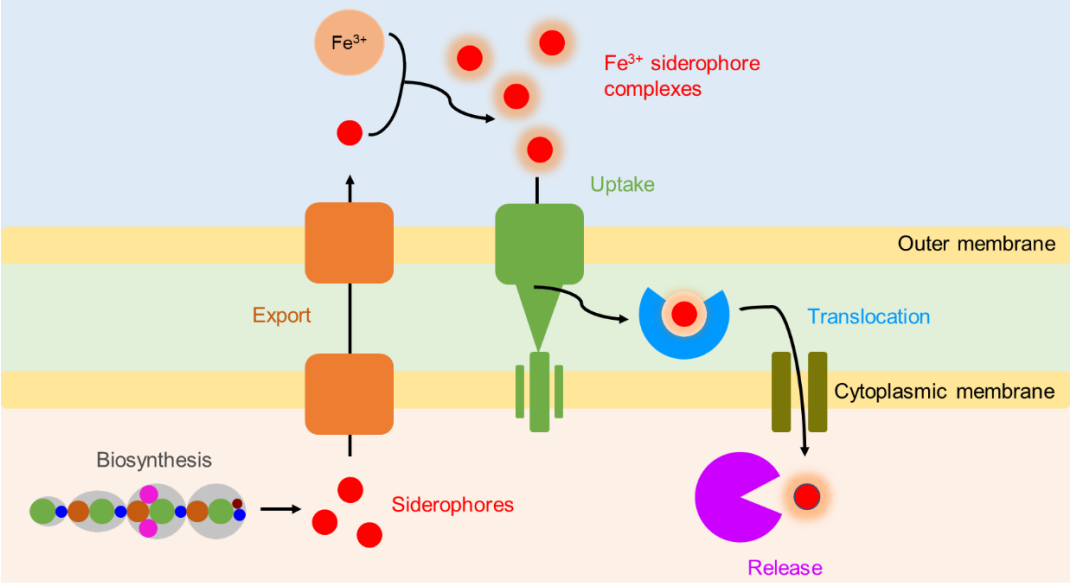

Figure 1.3. Siderophore mediated uptake of Fe^{3+} by microorganisms.[12]

can then bind one Fe^{3+} with an octahedral geometry (**Figure 1.4**).[13,14]

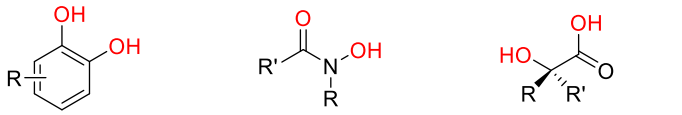

catechol hydroxamic acid α-hydroxycarboxylic acid

Figure 1.4. Typical chelating functional groups of siderophores.

Natural product siderophores can also be assessed for their binding affinities for Fe^{3+}, for comparison the commonly used multidentate ligand ethylenediaminetetraacetic acid (EDTA) is employed, which has a strong binding affinity for Fe^{3+} ($K_f = 10^{25}$).[15] Natural product siderophores have evolved to bind Fe^{3+} very strongly with the catecholate containing siderophore enterochelin (also known as enterobactin), produced by *Escherichia coli*, having the strongest known binding affinity for Fe^{3+} ($K_f = 10^{49}$).[16] Desferrioxamine B, produced by *Streptomyces* sp., is an example of a hydroxamate containing siderophore. The three hydroxamic acid groups form a strongly bound hexadentate complex with Fe^{3+}, resulting in a high binding affinity ($K_f = 10^{31}$).[17,18] Interestingly, desferrioxamine B is actually used as a drug for the treatment

of hemochromatosis and iron overdose (**Figure 1.5**).

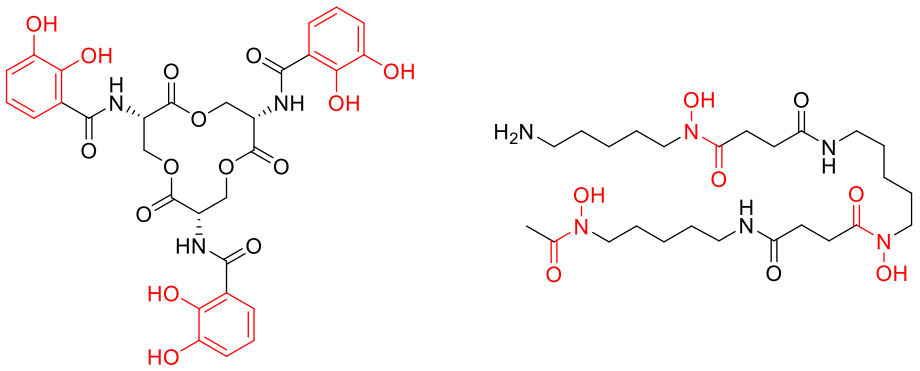

enterochelin (**6**)
(catecholate type)

desferrioxamine B (**7**)
(hydroxamate type)

Figure 1.5. Examples of natural product siderophores containing catecholate and hydroxamate groups.

1.2.3 Nonribosomal Peptide Siderophores

Brasilibactin A is a nonribosomal peptide siderophore, first isolated from *Nocardia brasiliensis* IFM 0995, which is classed as a mixed siderophore as it contains several different chelating functional groups.[19] Brasilibactin A can bind Fe^{3+} (K_f = 10^{27}) using one *ortho*-hydroxyphenyl substituted oxazoline group and two hydroxamic acid groups.[20] Brasilibactin A has shown promising bioactivity and has therefore been the target for total synthesis (**Figure 1.6**).[21]

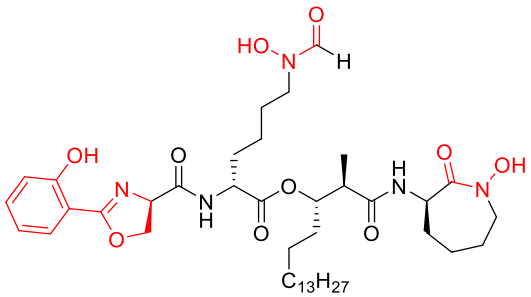

brasilibactin A (**8**)

Figure 1.6. Example of a nonribosomal peptide siderophore containing one *ortho*-hydroxyphenyl substituted oxazoline and two hydroxamic acid chelating groups.

1.3 Madurastatin C1 and Related Nonribosomal Peptide Siderophores

One of the target molecules of this project is the nonribosomal peptide siderophore madurastatin C1, a mixed siderophore containing one *ortho*-hydroxyphenyl substituted oxazoline and two hydroxamic acid chelating groups, first isolated from *Actinomadura* sp. in 2012.[22] Previous work in the group by Dr Andrew Tyler involved the reassignment of the structure of madurastatin C1, confirming the presence of an oxazoline ring instead of the originally proposed aziridine (**Figure 1.7**).[23]

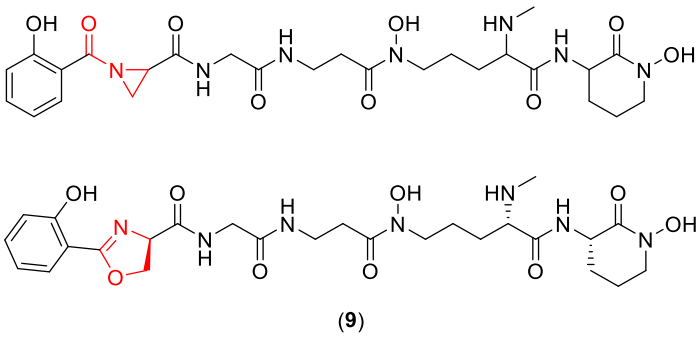

(**9**)

Figure 1.7. First proposed structure of madurastatin C1 (top) and revised structure of madurastatin C1 (**9**) (bottom).

Madurastatin C1 is related to a large number of known bacterial natural product siderophores which contain terminal *ortho*-hydroxyphenyl substituted oxazoline groups, which include madurastatins A-G. Madurastatin A1-3 and B1-2 were the first published examples of this family, isolated by Harada *et al*. in 2004 from pathogenic *Actinomadura madurae*.[24] It should be noted that for the ring closed molecules madurastatin A1 and B1, the structures were originally proposed to contain aziridine rings, now thought to be oxazoline rings. Structurally, A1 is the compound most closely related to madurastatin C1,[22] differing only in the second amino acid residue (Ala vs Gly). In 2017, Song *et al*. reported the isolation of madurastatin B3 from *Nocardiopsis* sp.,[25] and in 2019, Bugni *et al*. isolated madurastatins D1 and D2 along with *ent*-madurastatin C1 from a marine *Actinomadura* sp. WMMA-1423 (cultivated from the sponge *Tedania* sp.). Interestingly the madurastatin D series contain an imidazolidinone ring, formed by the cyclisation of one of the ornithine residues.[26] More

recently in 2022, Schuler *et al*. isolated a large number of additional madurastatins from *Actinomadura* sp. ST100801, including B4, C2, *ent*-D1, *ent*-D2, D3, D4, E1, E2, F1, G1 and G2 (**Figure 1.8**).[27]

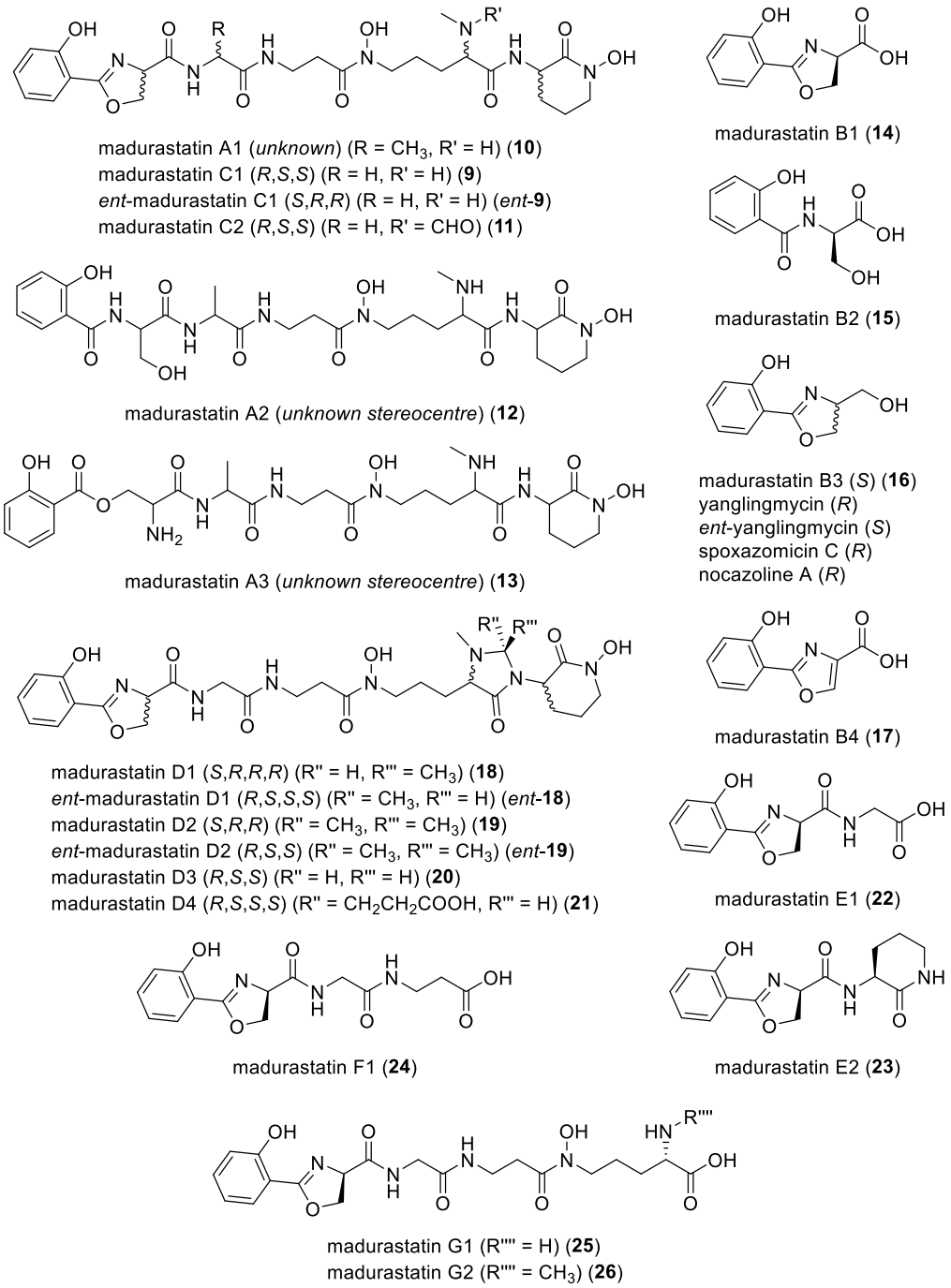

Figure 1.8. The madurastatin natural product siderophores family. For examples originally proposed to contain an aziridine ring, the revised oxazoline containing structures are shown.

In Chapter 3, we will present our work towards the total synthesis of madurastatin C1. In the next section of Chapter 1, we will discuss the biology of bacterial cell walls as targets for the development of new antibiotics, moving towards discussion of our second target molecule the NRP muribactin C.

1.4 The Bacterial Cell Wall as a Target for New Antibiotics

Due to the emergence of pathogenic bacteria which have high levels of resistance to existing antibiotics, there is a need for the development of new mode-of-action antibiotics.[28] Natural products have been widely used in the development of antibiotics and remain an important source for new drugs.[2, 29]

1.4.1 The Bacterial Cell Wall

The bacterial cell wall is an important target for the development of antibiotics. Since human cells lack a cell wall, drugs that target the bacterial cell wall can be very specific in their bioactivity. In addition, the bacteria cell wall is very important for bacterial growth and replication, thus inhibiting cell wall biosynthesis pathways can result in bacterial cell death.

For example, the well-known antibiotic penicillin interferes with bacterial cell wall biosynthesis by inhibiting the enzymes responsible for building the peptidoglycan layer, the penicillin-binding proteins (PBPs), inhibiting cell growth and division, and ultimately leading to rupture of the bacterial cell wall and cell death.[30,31]

The two main classes of bacteria, Gram-positive and Gram-negative bacteria, have different cell wall structures, consisting of layers of peptidoglycan and plasma membrane(s) (**Figure 1.9**).[32]

Peptidoglycan (PG) is an important element of the bacterial cell wall, consisting of a glycan backbone with side chain polypeptides, which are cross-linked to form a rigid polymer.[33] The peptidoglycan helps to maintain the shape of the bacterial cell and protects against changes in osmotic pressure. Therefore, peptidoglycan plays a crucial role in the growth and division of both Gram-positive and Gram-negative bacterial cells.

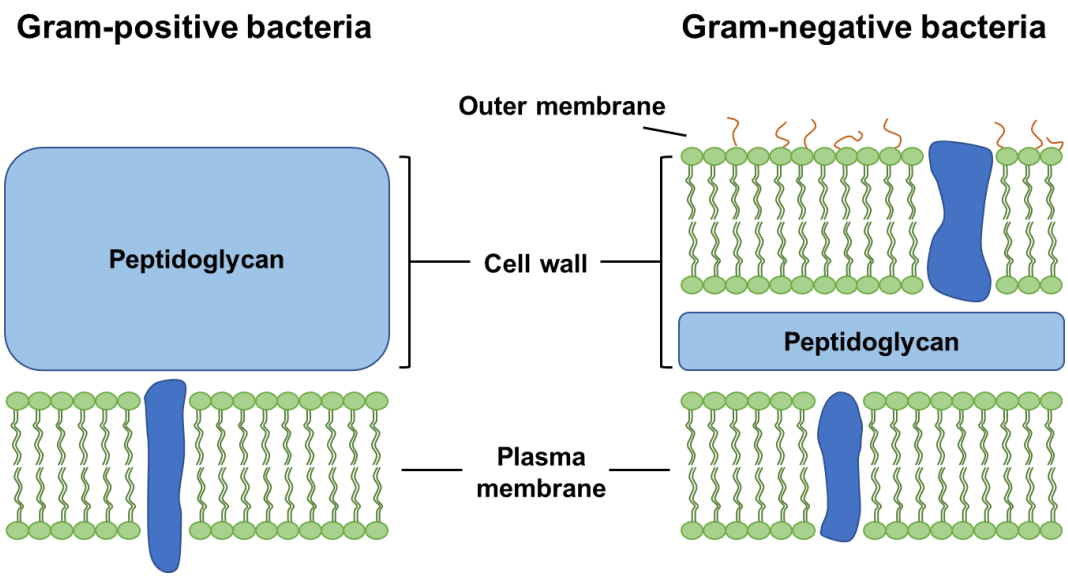

Figure 1.9. Bacterial cell envelopes of Gram-positive and-Gram negative bacteria.

Another critical component of the cell wall are the teichoic acids, which are a common feature of Gram-positive bacterial cell walls and can make up 50% of the cell wall weight, but are rarely found in Gram-negative bacteria. Teichoic acid helps to maintain the structural integrity of the Gram-positive bacterial cell wall by extending through the peptidoglycan and cross-linking the peptidoglycan layer with the plasma membrane.

1.4.2 Teichoic Acids - WTA and LTA

Teichoic acids are water-soluble, multiply negatively charged polymers of glycerol and ribitol phosphate linked to carbohydrates through phosphodiester bonds. Teichoic acids can be grouped into two classes, the wall teichoic acids (WTA) and the lipoteichoic acids (LTA),[34] with wall teichoic acids (WTA) being the most prevalent.[35] A major difference between WTA and LTA is the way in which they are attached within the cell envelope. WTA is covalently attached to the peptidoglycan layer, whilst LTA is anchored to the bacterial membrane via a glycolipid tail.[36] Since LTA is essential for the maintenance of the bacterial cell envelope, interfering with LTA biosynthesis can disrupt bacterial growth, making LTA a promising target for the development of new drugs (**Figure 1.10**).

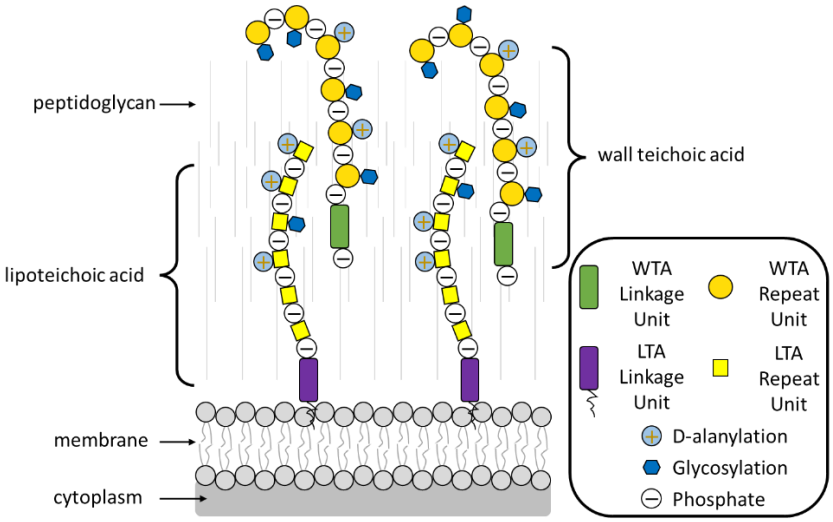

Figure 1.10. Gram-positive cell envelopes showing wall teichoic acids (WTA) covalently bound to peptidoglycan while lipoteichoic acids (LTA) are attached to the cell membrane.[34]

1.4.3 LTA Synthases

The enzyme, lipoteichoic acid (LTA) synthase (LtaS), was first identified in the Gram-positive bacteria *Staphylococcus aureus* in 2007 by Gründling and Schneewind.[37] LtaS is an Mg^{2+} dependent enzyme involved in the synthesis of lipoteichoic acid, an important component of the bacterial cell wall of Gram-positive bacteria. In particular, LtaS is responsible for the synthesis of the polyglycerol phosphate component of LTA (**Figure 1.11**).

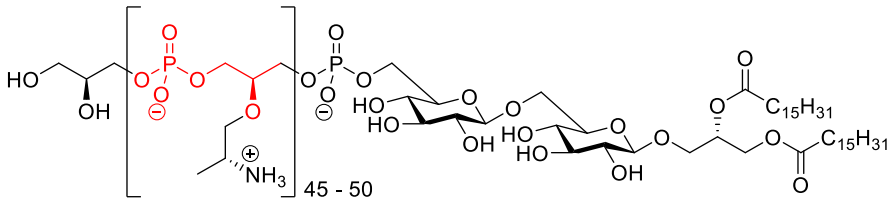

(**27**)

Figure 1.11. Lipoteichoic acid (LTA) (**27**), with polyglycerol phosphate component highlighted (red).

It has been shown that Gram-positive bacteria must produce LTA in order to maintain the cell wall structure, cell shape and in order to grow and divide.[38-40] This makes LtaS

an essential enzyme in *S. aureus* and similarly LtaS homologues are essential in other bacterial species. Essential enzymes in bacteria make good targets for the development of new antibiotics, as inhibition of an essential enzyme can result in bacterial cell death (bactericidal) or stop replication (bacteriostatic).

1.4.4 LtaS-like Enzymes in Gram-positive Bacteria

LtaS-like enzymes, or homologues, exist in many Gram-positive bacteria and play an important role in cell wall synthesis. There is interest in the development of LtaS inhibitors as potential antibiotics for the treatment of infections caused by Gram-positive bacteria such as *S. aureus* (wound infections), *Bacillus anthracis* (anthrax), *Bacillus cereus* (gastrointestinal infections) and *Listeria monocytogenes* (listeriosis).

For example, a search of the genome sequences of the commonly studied bacteria *Bacillus subtilis* shows the presence of four genes which encode for LtaS orthologues, enzymes with similar structure and function to LtaS. Gründling *et al.* have shown that the *B. subtilis* 168 contains the four LtaS orthologues, $LtaS_{BS}$ (YflE), YfnI, YqgS and YvgJ which are all involved in the synthesis of LTA.[41] . As part of their work exploring the structure and function of LtaS, the group of Lewis and Errington have also reported the crystal structure of $LtaS_{BS(215–649)}$, the extracellular functional domain of LtaS (eLtaS) (**Figure 1.12**).[39]

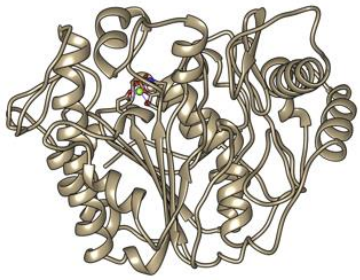

Figure 1.12. Crystal structure of the extracellular functional domain of lipoteichoic acid synthase interaction with Mg^{2+} (green), $LtaS_{BS(215–649)}$ (PDB code:2W8D).[39]

Of the four LtaS orthologues in *B. subtilis* only the crystal structure of $LtaS_{BS(215–649)}$

has been reported and even in this case only the crystal structure of the extracellular functional domain. Therefore, to better understand the protein structure of the other three LtaS orthologues, we undertook a search of the AlphaFold Protein Structure Database. AlphaFold has predicted the 3D structure of all four of the LtaS orthologues, $LtaS_{BS}$ (YflE), YfnI, YqgS and YvgJ, based on the full amino acid sequence including the non-functional domain. Through structural comparisons, we can see that the four orthologues have highly similar 3D structures, helping to explain their main function, i.e. the synthesis of the polyglycerol phosphate component of LTA (**Figure 1.13**).

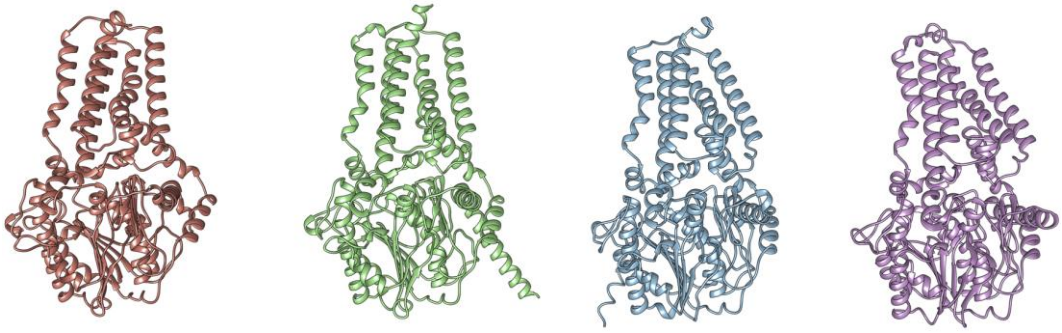

Figure 1.13. AlphaFold predicted 3D-structure of lipoteichoic acid synthase orthologues $LtaS_{BS}$ (YflE) (brown), YfnI (green), YqgS (blue) and YvgJ (purple) (https://alphafold.ebi.ac.uk).[42,43]

Gründling *et al*. have shown[41] that the *B. subtilis* LtaS orthologues, $LtaS_{BS}$ (YflE), YfnI, YqgS and YvgJ, have overlapping functions with *S. aureus* LtaS in the synthesis of LTA. The study started with mutant strain *S. aureus* ANG499, in which LtaS production is regulated by an inducible promoter, isopropyl β-D-1-thiogalactopyranoside (IPTG). *S. aureus* ANG499 grew normally and produced LTA in the presence of IPTG but grew poorly and did not produce LTA when IPTG was not added. A further mutant strain of *S. aureus* ANG499 was explored, in which native LtaS production was regulated by IPTG, but which also contained the *B. subtilis* gene *yflE* (which encodes for $LtaS_{BS}$) regulated by a tetracycline-inducible promoter. Now normal growth and LTA production of *S. aureus* ANG499 could be recovered through the addition of tetracycline to the growth media, showing that the *B. subtilis* enzyme $LtaS_{BS}$ could restore normal LTA

synthesis even in a different Gram-positive bacterium, *S. aureus*.[37]

In conclusion, this shows that LtaS-like enzymes are widely present in Gram-positive bacteria (e.g., *S aureus* or *B. subtilis*) and have the potential to be targeted in the development of new antibiotics for the treatment of Gram-positive bacterial infections.

1.4.5 Validation of LtaS as an Antibiotic Target

LtaS has been validated as an antibiotic target through the discovery and development of a small number of small molecule inhibitors. Walker *et al.* observed that the commonly used dye Congo red showed antibiotic activity against *S. aureus* mutant strains which lacked enzymes involved in the wall teichoic acid (WTA) synthesis pathway (e.g., Δ*tarO*). For *S. aureus* mutants lacking WTA, LtaS becomes an essential enzyme, thus Walker *et al.* suggested that Congo red could be acting as an LtaS inhibitor in their studies (**Figure 1.14**).

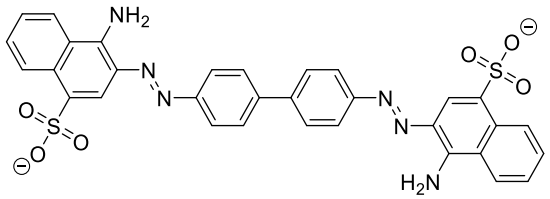

(**28**)

Figure 1.14. Congo red (**28**) an LtaS inhibitor.

In order to provide more evidence that Congo red may act as an LtaS inhibitor, Walker *et al.* undertook a whole cell assay in which they grew wild-type *S. aureus* RN4220 in the presence of different concentrations of Congo red. They then used western blotting, using an α-LTA antibody, to detect the concentration of LTA present versus the concentration of Congo red, showing a dose-dependent reduction in LTA production thus demonstrating that Congo red inhibits LTA biosynthesis (**Figure 1.15**).

To show that Congo red acts as a specific inhibitor of LtaS Walker *et al.* developed an assay for LtaS activity. First *C*-terminal His_6-tagged *S. aureus* LtaS was expressed

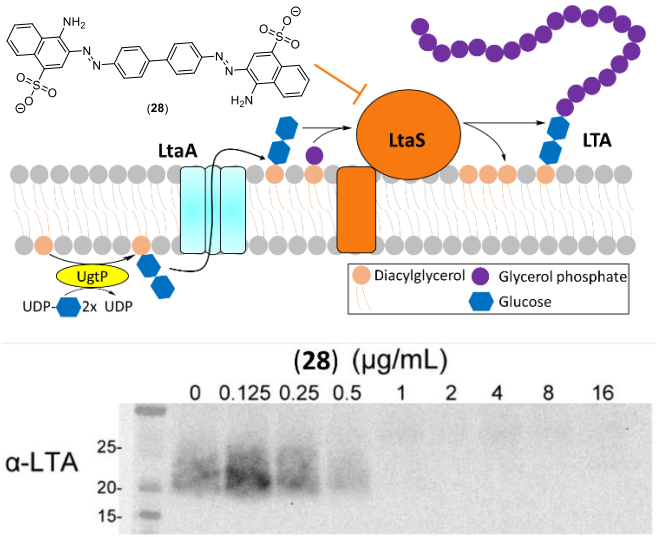

Figure 1.15. (Top) Proposed inhibition of LTA biosynthesis pathway by Congo red. (Bottom) Western blot showing dose response of LTA production by wild-type *S. aureus* in the presence of Congo red.[44]

and purified from *Escherichia coli*. Then they demonstrated that purified LtaS could be used to add units of glycerol phosphate onto phosphatidylglycerol, forming LTA polymer in a cell free system, which could be detected by western blot. On addition of Congo red the synthesis of LTA polymer was prevented, showing that Congo red is an inhibitor of LtaS (**Figure 1.16**).[44]

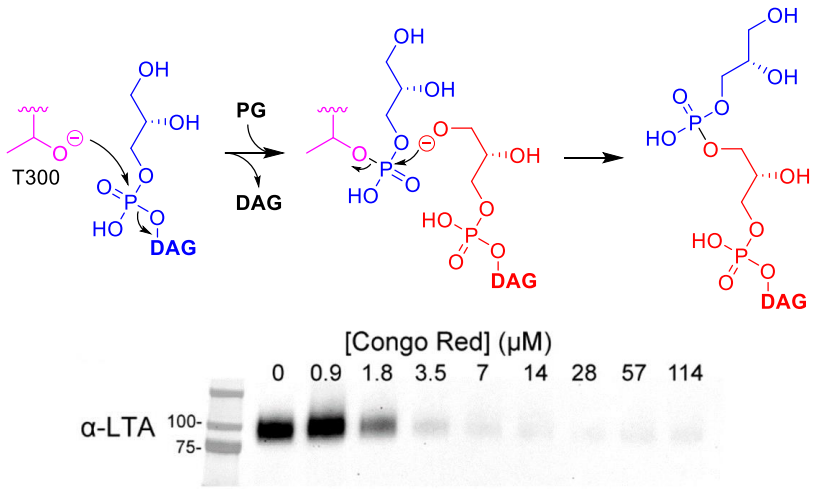

Figure 1.16. (Top) LTA polymer formation from the reaction of the amino acid T300 (purple) in the catalytic pocket with glycerol phosphate (blue) with another glycerol phosphate (red). (Bottom) Western blot showing dose-response inhibition of LTA polymerisation by Congo red in an isolated enzyme assay (IC_{50} of 2 μM).[44]

Missiakas *et al*. have also described a small molecule inhibitor of LtaS, “compound 1771”. Following a series of high-throughput whole cell screens, of more than 167,000 molecules from the compound libraries at the National Screening Laboratory for the Regional Centres of Excellence in Biodefense and Emerging Infectious Disease (NSRB), compound 1771 was identified as a potential inhibitor of LtaS (**Figure 1.17**).[45]

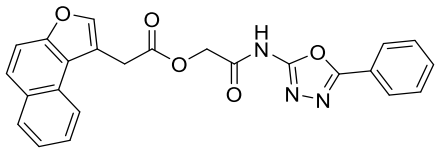

(**29**)

Figure 1.17. LtaS inhibitor “compound 1771” (LtaS-IN-1) (**29**).

Compound 1771 was shown to inhibit the LTA pathway, through the use of whole cell assays in *S. aureus* using western blotting to detect LTA production, which showed a dose-dependent decrease in LTA production in the presence of 1771. Further experiments used mutant *E. coli* to express two homologues of LtaS (*S. aureus* ($LtaS_{SA}$) and *B. anthracis* ($LtaS2_{BA}$)) capable of making LTA, which was abolished in the presence of 1771, confirming LtaS as the target for 1771. Competition experiments between 1771 and nitrobenzoxadiazole glycerol-phosphate (NBD-GP) and the extracellular functional domain of LtaS (eLtaS), provided evidence that 1771 binds in the glycerol-phosphate binding pocket. Compound 1771 was also shown to be effective in a mouse model of *S. aureus* infection, resulting in a significant increase in survival rate, suggesting that 1771 could be used as an antibiotic in the future (**Figure 1.18**).[45]

In recent work, Welch and Rahman *et al*. have used a combination of molecular docking and molecular dynamics (MD) simulations to design new LtaS inhibitors. Based on this computational evidence they then followed a lead optimisation approach to develop improved LtaS inhibitors based on compound 1771, resulting in the synthesis and biological evaluation of compound 4. Compound 4 was shown to be an

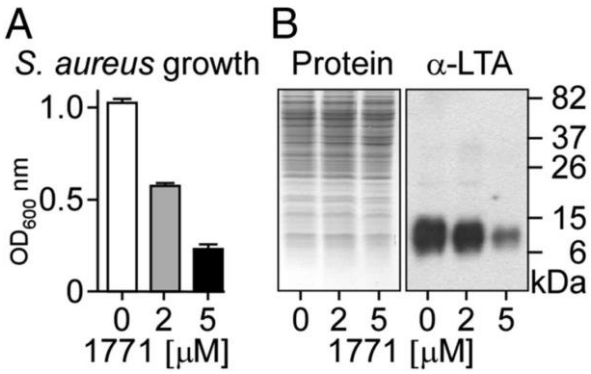

Figure 1.18. (A) Dose response of compound 1771 versus growth of *S. aureus*. (B) (left) Control experiment showing that compound 1771 does not affect bacterial protein production (SDS/PAGE with Coomassie staining), (right) Western blot showing dose response of LTA synthesis by *S. aureus* in the presence of compound 1771.[45]

improved inhibitor of eLtaS (IC_{50} = 4.06 μM (4) vs 14.90 μM (1771)) and showed promising results in a preliminary animal model of *S. aureus* infection in mice (**Figure 1.19**).[46]

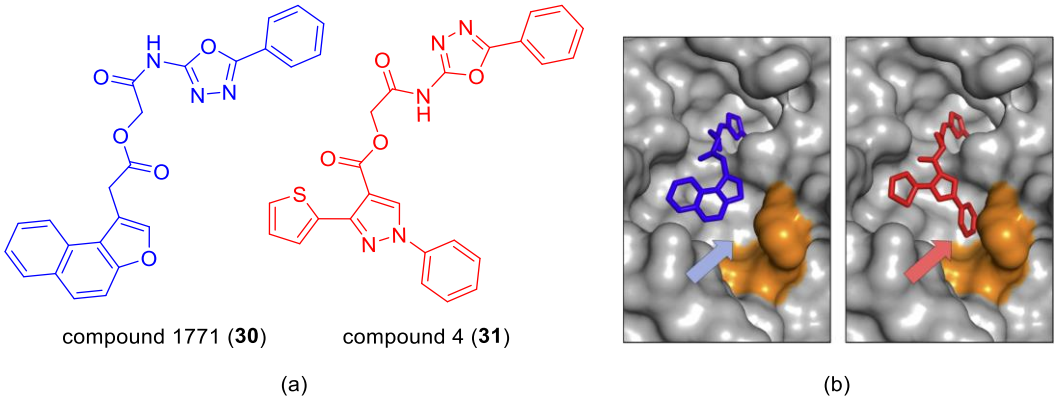

Figure 1.19. (a) Compound 1771 vs improved LtaS inhibitor "compound 4". (b) Predicted binding of compounds 1771 (blue) and 4 (red) against eLtaS, residues Lys299 and Tyr477 highlighted in orange showing increased binding to compound 4.[46]

1.5 Conclusions

Natural products, including non-ribosomal polypeptides, have been widely used in the development of new drugs, particularly in the area of antibiotics. In addition, we have

introduced lipoteichoic acid synthase (LtaS) as a validated target for the development of novel antibiotics.

We have also discussed bacterial siderophores, many of which are also based on NRPs structures, including madurastatin C1. Siderophore NRPs are also interesting molecules to study due to their role in bacterial metal transport, offering potential for the development of new antibiotic approaches.

The next chapters will focus on the synthesis and biological investigation of two bacterial NRPs. In Chapter 2, we will present our work on mirubactin C as a potential LtaS inhibitor, whilst in Chapter 3, we will discuss the synthesis towards the siderophore madurastatin C1.

Chapter 2. Total Synthesis of the Natural and Unnatural Enantiomers of Mirubactin C and Associated Biological Studies

2.1 Introduction

In this chapter, we will present our work on the polypeptide siderophore mirubactin C, including a discussion of the determination of the absolute stereochemistry and the synthesis of both the natural and unnatural enantiomers. Subsequent metal binding and biological studies will also be discussed in relation to the potential role of mirubactin C as a cell wall active antibiotic.

2.1.1 Δ*mbl Bacillus subtilis* for the Discovery of LtaS Inhibitors

Alongside enzymes which synthesise cell wall components, such as LtaS, Gram-positive bacteria also contain proteins with actin-like functions, which are responsible for the maintenance of cell shape and morphology. For example, *B. subtilis* contains three proteins with actin-like functions, MreB, Mbl (MreB-like) and MreBH (MreB homologue).[48] Lewis and Errington *et al.* have shown that *B. subtilis* Δ*mbl* mutants have the potential for use in the discovery of LtaS inhibitors.

During their investigation into the role of Mbl in *B. subtilis,* Errington *et al*. prepared Δ*mbl B. subtilis* mutants, which were shown to be non-viable due to the essential nature of Mbl. However, Δ*mbl B. subtilis* mutants were shown to grow normally in the presence of high concentrations of Mg^{2+} (20 mM).[49]

Following this work, Lewis and Errington *et al*. prepared a further Δ*mbl* Δ*ltaS B. subtilis* mutant and assessed its growth with and without the presence of Mg^{2+} (20 mM). Interestingly the Δ*mbl* Δ*ltaS B. subtilis* mutant grew normally, showing classical rod-like morphology, without the need for the addition of Mg^{2+}, suggesting that the suppression of LTA synthesis can rescue cell growth in a Δ*mbl B. subtilis* mutant (**Figure 2.1**).[39]

Based on these results it was suggested that Δ*mbl B. subtilis* mutants could be used

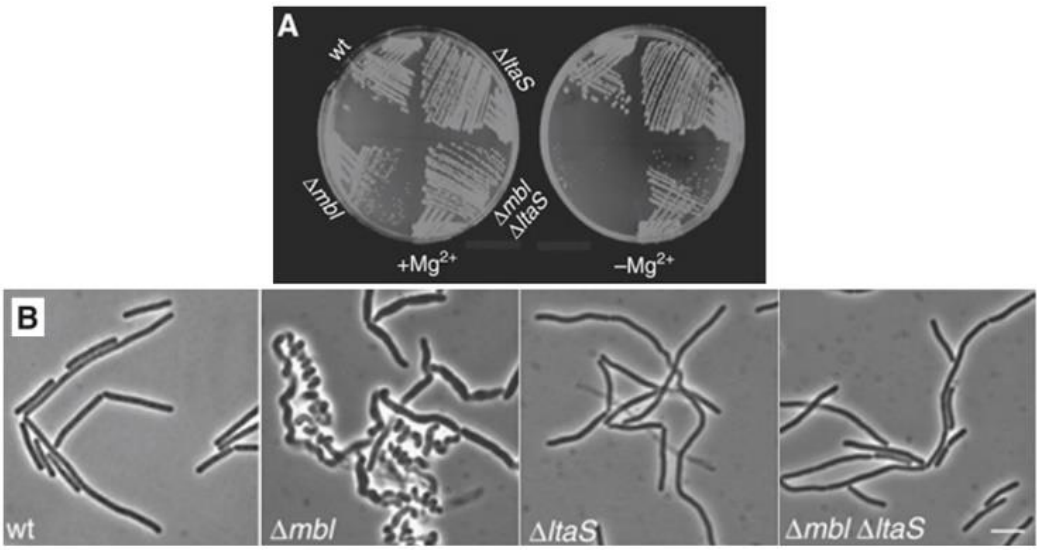

Figure 2.1. (A) Growth of wild-type *B. subtilis* and mutants, Δ*mbl*, Δ*ltaS* and Δ*mbl* Δ*ltaS* with (left) or without (right) the presence of Mg^{2+} (20 mM). (B) Bright-field microscopy showing cell morphology of wild-type *B. subtilis* and mutants under standard growth conditions.

for the detection of LtaS inhibitors. If a Δ*mbl B. subtilis* mutant was treated with an LtaS inhibitor, this should have a similar effect to the deletion of *ltaS* (Δ*ltaS)* and as such should rescue the growth of the Δ*mbl B. subtilis* mutant.

2.1.2 Discovery of LtaS Inhibitors using Δ*mbl Bacillus subtilis*

As part of a project to find small molecule natural products which can inhibit LtaS, our collaborators Kepplinger and Errington at the Centre for Bacterial Cell Biology screened more than 2,000 natural products containing extracts from actinobacteria. The extracts were tested for their capability to rescue normal growth of *B. subtilis Δmbl* in the absence of 20 mM Mg^{2+}, to screen for new natural products as potential LtaS inhibitors. Crude extracts from three different bacteria DEM30549, DEM30616 and DEM20435 showed activity, which were then purified by HPLC and size exclusion chromatography. A new molecule, initially named “DC616”, was identified from DEM30616 which showed the ability to rescue normal growth of *B. subtilis Δmbl* mutant and, as such, has the potential to be an LtaS inhibitor (**Figure 2.2**).

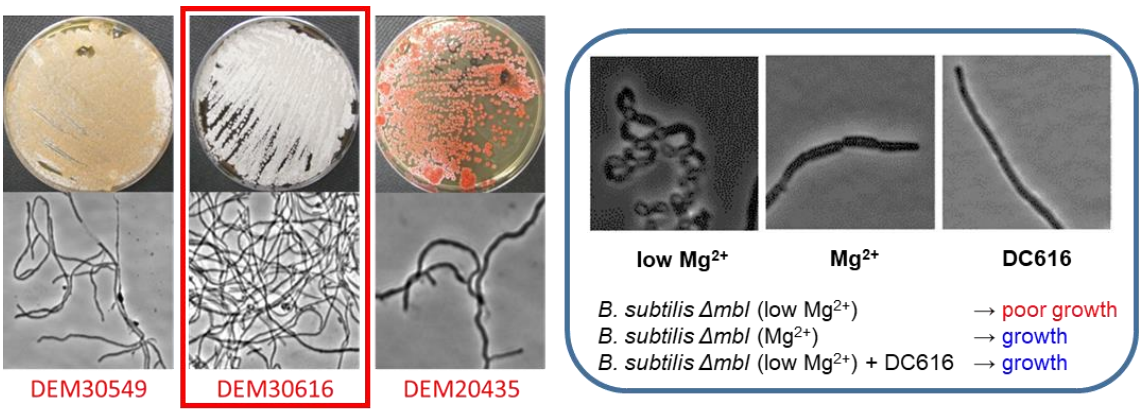

Figure 2.2. (a) Rescue of normal cell growth in Δ*mbl B. subtilis* by extracts from the bacteria DEM30549, DEM30616 (red) and DEM20435. (b) Bright-field microscopy showing growth and morphology in Δ*mbl B. subtilis* in the presence of low Mg^{2+} (3.8 μg/mL), high Mg^{2+} (20 mM) and low Mg^{2+} (3.8 μg/mL) plus "DC616".

Further work by the groups of Errington and Hall subsequently showed that "DC616" was a new dipeptide siderophore, named mirubactin C (**Figure 2.3**).

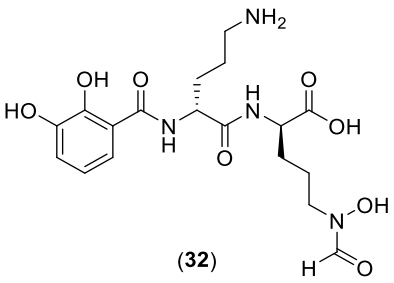

Figure 2.3. Mirubactin C (**32**).

It should be noted that during the preparation of this thesis, Huang *et al.* also published the structure of mirubactin C.[50]

2.1.3 Natural Product Siderophores Structurally Related to Mirubactin C

It should be noted that the natural product mirubactin C is related to a number of known natural product siderophores. Related siderophores include chlorocatechelin A, chlorocatechelin B,[51] mirubactin,[52,53] mirubactin B and mirubactin D.[50] Marahiel *et al*. first isolated mirubactin from *Actinosynnema mirum*, and attempted structure

elucidation,[52] however the original structure of mirubactin was misassigned. Following this work, as part of a synthetic project to synthesise de-chlorocatechelins, Kakeya *et al*. corrected the structure of mirubactin (**Figure 2.4**).[53]

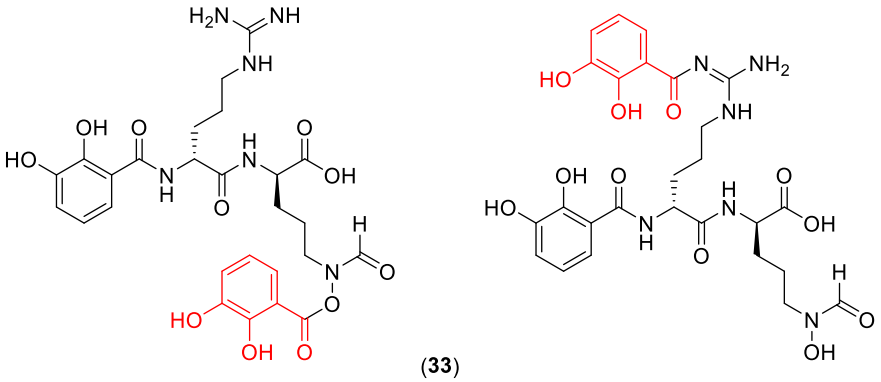

Figure 2.4. Originally proposed structure of mirubactin (left) and revised structure of mirubactin (**33**) (right).

The chlorocatechelins and the mirubactins are closely related, differing in the substituents of the 2,3-dihydroxybenzyl groups, the chlorocatechelins having a *para*-chloro substituent. They are also related to heterobactin, which also lacks the chloro substituent, but replaces the terminal hydroxamic acid with a cyclic hydroxamic acid formed from the *C*-terminal ornithine.[54] Chlorocatechelin A, mirubactin and heterobactin are all hexadentate siderophores, each containing three bidentate chelating groups. In each case, there are two 2,3-dihydroxybenzyl groups and one hydroxamic acid group, which can chelate trivalent metal ions preferentially, such as Fe^{3+} (**Figure 2.5**).

In recent work, Huang *et al*. have demonstrated that mirubactin B, mirubactin C and mirubactin D can all be obtained from mirubactin through degradation of the natural product during isolation during silica gel chromatography.[50] Mirubactin B, C, D and chlorocatechelin B are all tetradentate siderophores, each containing two bidentate chelating groups. In each case, there is one 2,3-dihydroxybenzyl group and one hydroxamic acid group which together can chelate divalent metal ions preferentially,

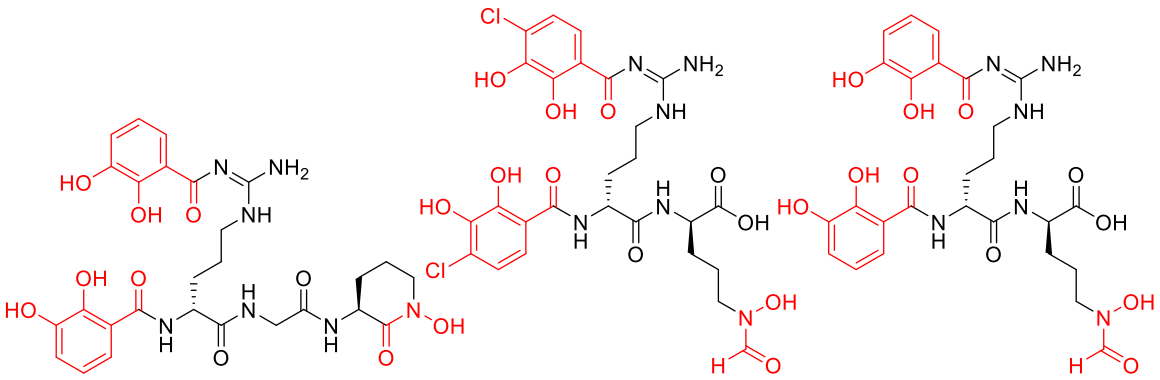

heterobactin (**34**) chlorocatechelin A (**35**) mirubactin (**33**)

Figure 2.5. Hexadentate siderophores heterobactin (**34**) chlorocatechelin A (**35**) and mirubactin (**33**), bidentate chelating groups (2,3-dihydroxybenzyl and hydroxamic acid) highlighted (red).

such as Mg^{2+} (**Figure 2.6**).

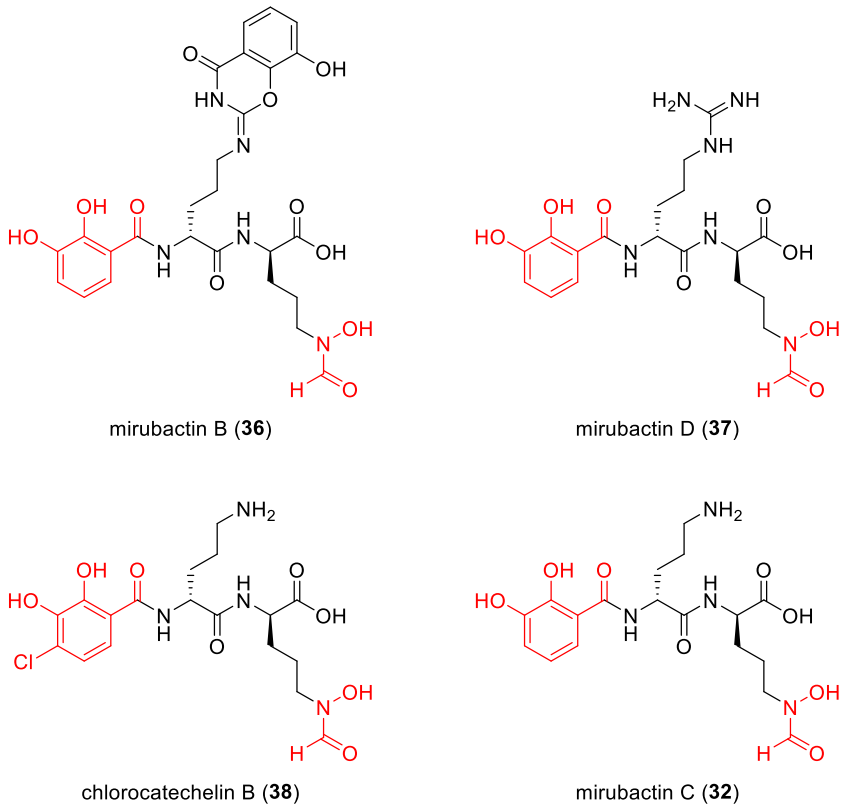

mirubactin B (**36**) mirubactin D (**37**)

chlorocatechelin B (**38**) mirubactin C (**32**)

Figure 2.6. Tetradentate siderophore mirubactin B (**36**) mirubactin D (**37**) chlorocatechelin B (**38**) and mirubactin C (**32**), bidentate chelating groups (2,3-dihydroxybenzyl and hydroxamic acid) highlighted (red).

2.2 Project Aim

In this chapter, our primary aim will be the enantioselective total synthesis of mirubactin C, followed by evaluation against *Δmbl B. subtilis* to validate mirubactin C as a potential LtaS inhibitor. This will involve analysis of the absolute stereochemistry of mirubactin C, prior to the commencement of synthetic work.

Our secondary aim is to use synthetic mirubactin C to probe the biological mechanism (mode-of-action) by which mirubactin C rescues growth in *Δmbl B. subtilis*, in a similar manner to the high concentration of Mg^{2+}.

We propose two possible modes-of-action of mirubactin C in *Δmbl B. subtilis*, which we will investigate. Firstly, that mirubactin C may act as a direct inhibitor of LtaS and secondly that mirubactin C be involved in metal transport in the bacteria, bringing higher than normal concentrations of Mg^{2+} into the bacterial cell.

Mirubactin C resembles a siderophore and contains two common siderophore chelating groups, a catecholate and a hydroxamate group. This means that mirubactin C may have the ability to coordinate and transport M^{2+} ions, such as Mg^{2+}. To better understand the potential binding of M^{2+} ions, we modelled mirubactin C with Mg^{2+} coordinated in a number of possible positions, thus suggesting that coordination is possible via the catecholate and a hydroxamate group (**Figure 2.7**).

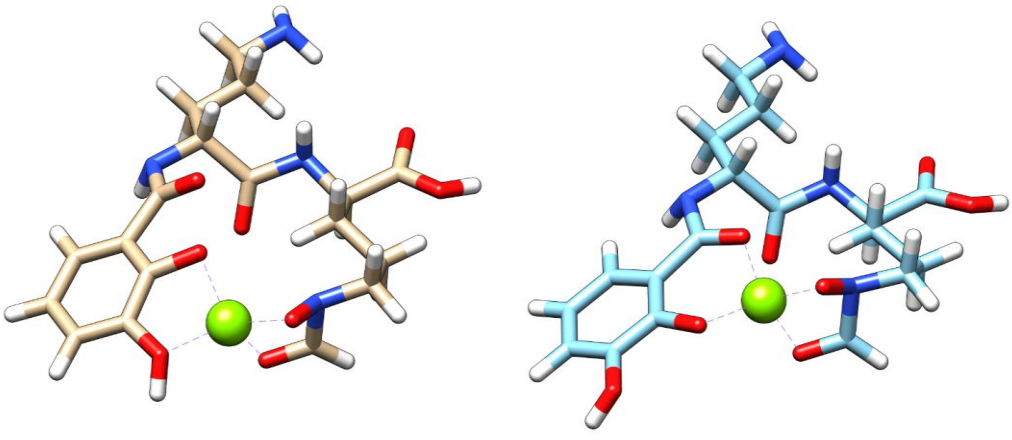

-1721.5704 a.u. -1721.5698 a.u.

Figure 2.7. Proposed binding of mirubactin C to Mg^{2+} predicted by Chimera, based on molecular mechanics method with steepest descent and conjugate gradient algorithm minimum energy.

To help to understand if the mode-of-action of mirubactin C involves acting as an inhibitor of LtaS or acting to transport metals, we decided to synthesise both possible enantiomers of mirubactin C (mirubactin C and *ent*-mirubactin C) and to evaluate their biological activity. If mirubactin C is an inhibitor of LtaS, then we would expect mirubactin C and *ent*-mirubactin C will give different biological activities, as mirubactin C and *ent*-mirubactin C would form diastereoisomeric complexes with LtaS with different binding energies and therefore different levels of inhibition.

However, mirubactin C and *ent*-mirubactin C should form complexes with metals with the same binding affinity. Thus, if the biological activities of mirubactin C and *ent*-mirubactin C are the same, it would suggest that the mode-of-action involves metal transport.

Therefore, the third aim of this chapter is to synthesise the enantiomer of mirubactin C (*ent*-mirubactin C) and to compare the biological activities of the two mirubactin C enantiomers.

2.3 Structure Determination and Absolute Stereochemistry of Mirubactin C

The elucidation of the molecular structure of naturally occurring mirubactin C was performed previously within the group by Dr Tyler[55] and later confirmed by the group of Huang.[50] Tyler completed the full structural assignment of mirubactin C, which is composed of a di-peptide formed from two ornithine amino acids, one of which is functionalised with a benzoic acid derivative and the other contains a hydroxamic acid group (**Figure 2.8**).

2.3.1 Introduction to Marfey's analysis

With the chemical structure of mirubactin C determined, the first task that we carried out was the determination of the absolute stereochemistry using Marfey's analysis.

The first example of "Marfey's analysis" was published in 1984 by Marfey, which is used to determine the absolute stereochemistry of amino acids and polypeptides.[56] Marfey's analysis involves the functionalisation of test enantiomeric amino acids with enantiopure Marfey's reagents, to form a diastereoisomer which can then be analysed

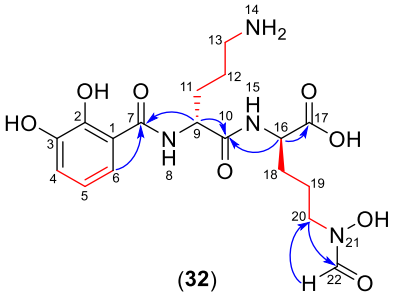

Figure 2.8. Elucidation of the structure of mirubactin C (**32**) by NMR, selected COSY (red) and HMBC (blue) correlations shown.

by HPLC or LCMS against prepared standards.

Commonly used Marfey's reagents consist of an electron-deficient aromatic ring containing a fluorine atom connected to an enantiopure amino acid, typically L-alanine (FDAA) or L-leucine (FDLA) (**Figure 2.9**).

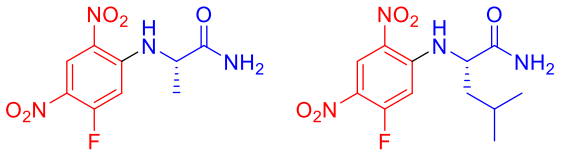

Figure 2.9. Commonly used Marfey's reagents FDAA and FDLA.

Marfey's analysis of a polypeptide starts with the hydrolysis of the amide bonds under strongly acidic conditions, typically using hydroiodic acid, to give the individual amino acids. The mixture of amino acids is then reacted with a suitable Marfey's reagent by nucleophilic aromatic substitution (S_NAr) of the fluorine atom, to give a series of diastereomeric products. This mixture is then analysed by HPLC, the aromatic ring of the Marfey's reagent fragment providing a UV chromophore (340 nm), or in more modern approaches by LCMS in comparison to previously prepared standards (**Figure 2.10**).

In an improvement to the original Marfey's procedures, Harada *et al.* demonstrated

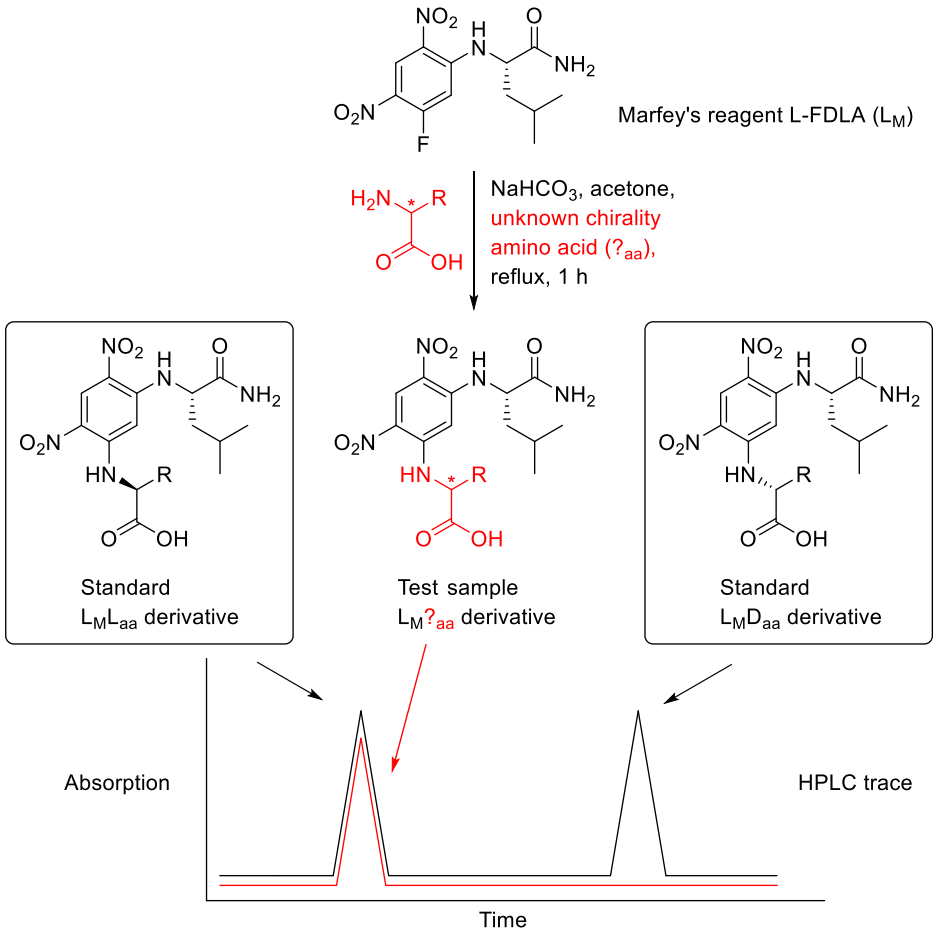

Figure 2.10. Determination of the absolute stereochemistry of an amino acid (red) by comparison of HPLC retention time against preprepared Marfey's standards.

the use of FDLA for improved detection by LCMS.[57] In addition, Harada *et al.* have also shown that in the case of difficult to access enantiopure amino acids, such as some D-amino acids or unnatural amino acids, the required Marfey's standards can be prepared by reacting a single enantiopure test amino acid with the two different enantiomeric Marfey's reagents, e.g., D-FDLA and L-FDLA, to generate the required pair of diastereoisomers.

2.3.2 Marfey's Analysis of Mirubactin C

To determine the absolute stereochemistry of mirubactin C, the first step is to prepare suitable standards for Marfey's analysis. As mirubactin C contains two ornithine fragments of unknown stereochemistry, we first needed to make Marfey's standards

for both L-ornithine and D-ornithine.

Therefore, we prepared an aqueous solution of L-ornithine hydrochloride and $NaHCO_3$, to form the corresponding free base, followed by the addition of a 1% L-FDLA in acetone. The reaction mixture was heated at 40 °C for 1 hour, after which samples containing L-FDLA/L-ornithine adducts were diluted with HPLC grade water and stored at -20 °C for later analysis by LCMS. The corresponding L-FDLA/D-ornithine adducts were also prepared following a similar procedure.

It should be noted that since ornithine contains two nucleophilic amine functional groups, three possible products can be formed, from both L- and D- ornithine, via S_NAr reactions with L-FDLA. The three possible products that can be formed include two mono-substituted ornithines (**42** and **43**) and one di-substituted ornithine (**44**) (**Figure 2.11**).[58]

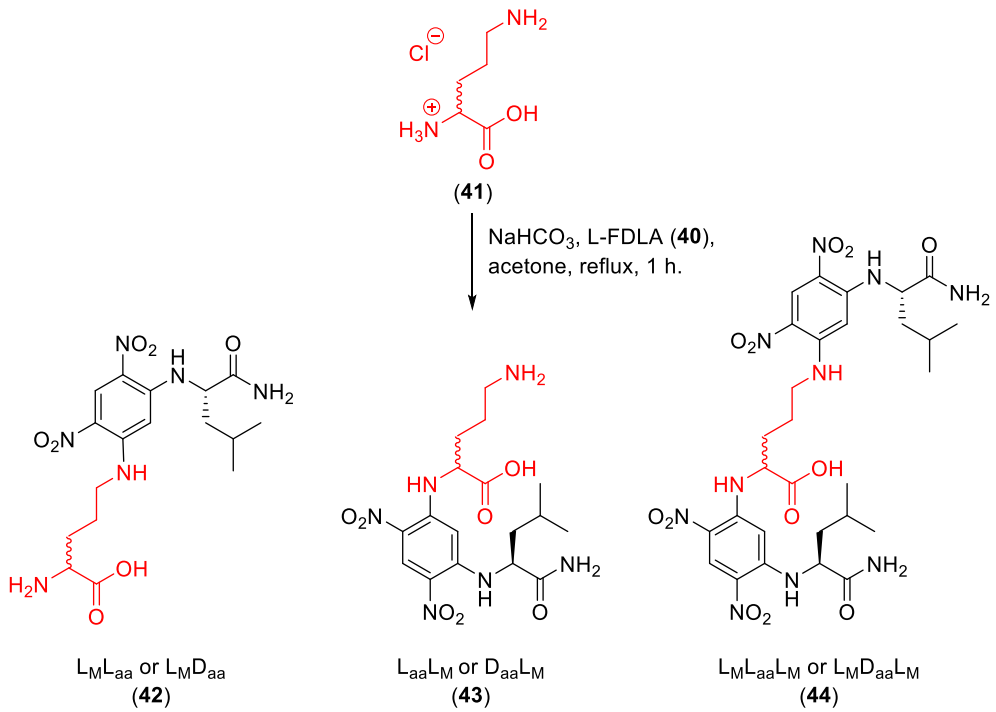

Figure 2.11. Marfey's derivatives formed through the reaction of ornithine with L-FDLA.

LCMS analysis of both the L-FDLA/L-ornithine and L-FDLA/D-ornithine Marfey's standards, as prepared previously, was performed. In the case of the L-FDLA/L-ornithine Marfey's standard, the total ion chromatogram (TIC) showed two major peaks

corresponding to the two mono-substituted ornithine derivatives with *m/z* = 427.20 at 8.17 min, and 427.20 at 8.69 min (L_ML_{aa} **42** and $L_{aa}L_M$ **43**; calc. 427.19 $[M+H]^+$). Note that using only MS data, it can not be determined which of the two observed peaks for the mono-substituted ornithine derivatives corresponds to which of the two isomers L_ML_{aa} **42** and $L_{aa}L_M$ **43**.

For the corresponding L-FDLA/D-ornithine Marfey's standard, a similar pattern was observed in the LCMS (TIC) with two peaks observed for the mono-substituted ornithine derivatives with *m/z* = 427.2 at 7.67 min, and 427.2 at 8.69 min (L_MD_{aa} **42** and $D_{aa}L_M$ **43**; calc. 427.19 $[M+H]^+$).

In both LCMS experiments, two additional peaks were observed. The peak at 11.12 min gave a major *m/z* signal of 274.32, which was also present in the total ion chromatogram (TIC) of the solvent blank, suggesting that this is an impurity present in the solvent or HPLC column. The second peak at ~12.28 min was also observed in both LCMS experiments, with a major *m/z* signal of ~270.03, which did not appear in the solvent blank but which we could not assign to any likely reaction by-products. The peaks at ~12.28 min do also not correspond to the expected di-substituted ornithine derivatives ($L_ML_{aa}L_M$ **44** and $L_MD_{aa}L_M$ **44**), although these may have been missed as the LCMS experiments were carried out with a mass range of 200-500 Da (**Figure 2.12**).

Examination of the LCMS for both the L-FDLA/L-ornithine and L-FDLA/D-ornithine Marfey's standards, shows that one set of mono-substituted ornithine derivatives has very similar retention times (~8.69 min). However, one set of mono-substituted ornithine derivatives have retention times of 7.67 min for L-FDLA/D-ornithine, or 8.17 min for L-FDLA/L-ornithine, which are well separated and this second set of signals can therefore be used for absolute stereochemistry determination.

To improve signal to noise in subsequent LCMS based Marfey's analysis of mirubactin C, where sample concentrations are low, we will use extracted ion chromatograms with an *m/z* range 427.2, +/- 0.25 Da to allow easy identification of mono-substituted ornithines L_ML_{aa} **42** / $L_{aa}L_M$ **43** and L_MD_{aa} **42** / $D_{aa}L_M$ **43**.

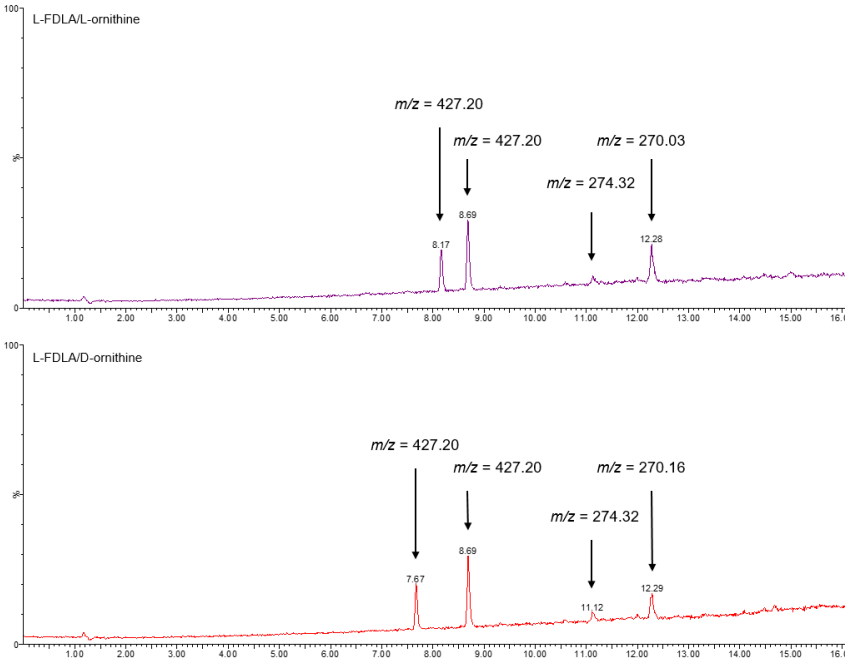

Figure 2.12. LCMS (TIC) analysis of L-FDLA/L-ornithine and L-FDLA/D-ornithine Marfey's standards.

With an LCMS method and suitable ornithine Marfey's standards available, we next carried out the determination of the absolute stereochemistry of the natural product, mirubactin C (provided by Dr B Kepplinger). We anticipated that the use of reductive hydrolysis conditions (hydroiodic acid) would result in the cleavage of all of the amide bonds as well as the conversion of the terminal hydroxamic acid into the corresponding amine.[59-63] Following reductive hydrolysis, the resulting free ornithines will be reacted with L-FDLA and the generated Marfey's derivatives will be compared with our standards by LCMS (**Figure 2.13**).

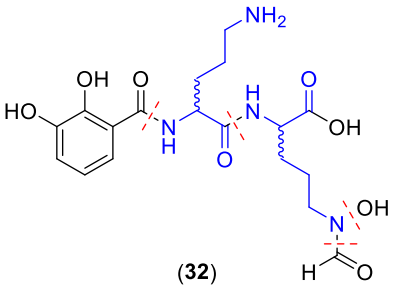

(**32**)

Figure 2.13. Reductive hydrolysis of mirubactin C with hydrogen iodide, for Marfey's analysis.

Therefore, 500 µg of mirubactin C (natural product) was reacted with 57% aqueous hydroiodic acid at 110 °C for 3 hours. Hydroiodic acid was removed under a gentle flow of nitrogen gas, and the reaction residue dissolved in aqueous $NaHCO_3$. A solution of L-FDLA in acetone was added, and the reaction mixture was heated to reflux for 1 hour, cooled to room temperature and acidified with aqueous HCl. The reaction mixture was then diluted with HPLC grade water prior to LCMS analysis (**Figure 2.14**).

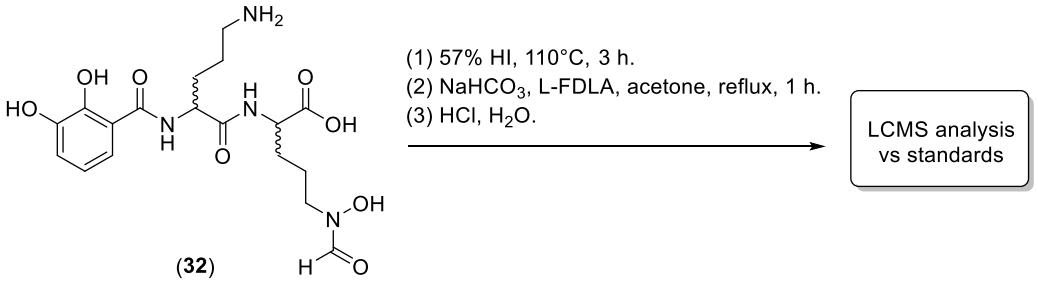

Figure 2.14. Preparation of mirubactin C for Marfey's analysis by LCMS.

Marfey's analysis of mirubactin C was performed against standards by LCMS with a UV/Vis detector (200-500 nm) and a mass detection range of 200-500 Da, with data shown as extracted ion chromatograms (*m/z* range 427.2, +/- 0.25 Da) (**Figure 2.15**).

LCMS analysis showed that L-FDLA derivatised mirubactin C gave the same retention times as the L-FDLA/D-ornithine Marfey's standard. Therefore we conclude that both of the ornithines in the natural product mirubactin C have a D-configuration. With the assignment of the absolute configuration of natural product mirubactin C, our next task was to examine the total synthesis of both the natural D,D-mirubactin C and unnatural L,L-mirubactin C.

2.4 Total Synthesis of Naturally Occurring (D,D)-Mirubactin C and its Enantiomer *ent*-(L,L)-Mirubactin C

2.4.1 Introduction

In this section, we will discuss the synthesis of mirubactin C and its enantiomer, which

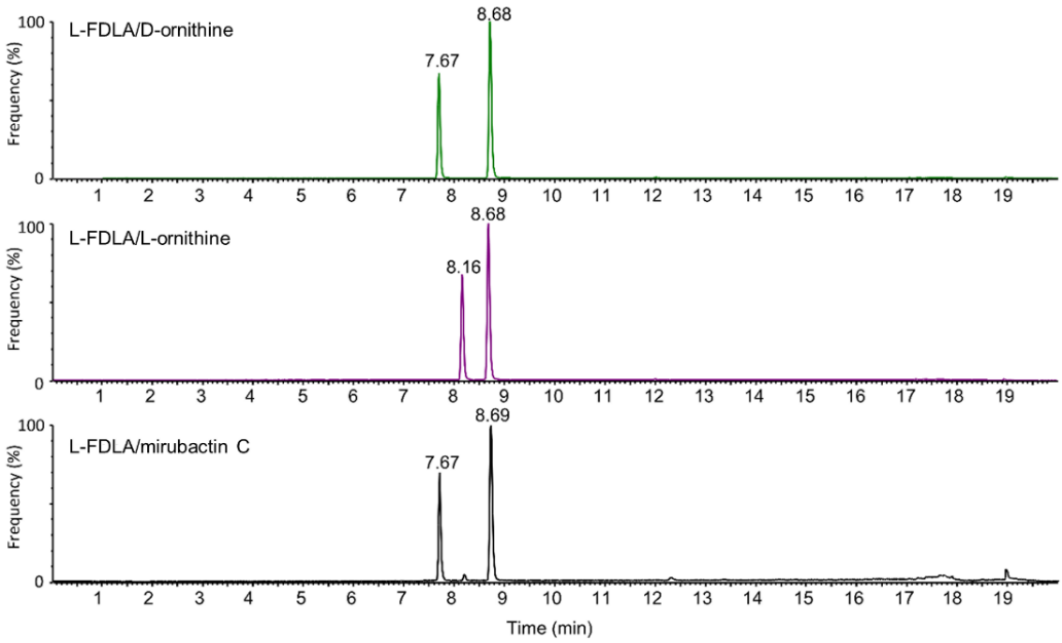

Figure 2.15. LCMS extracted ion chromatogram (EIC *m*/*z* = 427.2, +/- 0.25 Da) showing Marfey's standards L-FDLA/D-ornithine (top), L-FDLA/L-ornithine (middle) and L-FDLA derivatized mirubactin C (bottom).

we will call *ent*-mirubactin C. Following our previous Marfey's analysis mirubactin C is composed of two D-ornithine units, thus we will refer to this molecule as D,D-mirubactin C or (*R*,*R*)-mirubactin C. The ordering of the stereochemical centres will start from the *N*-terminus of mirubactin C (**Figure 2.16**).

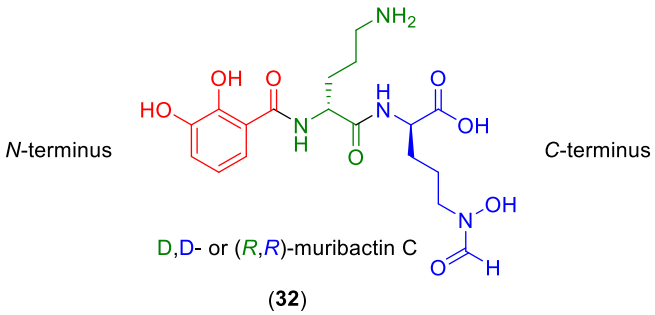

Figure 2.16. D,D-mirubactin C/(*R*,*R*)-mirubactin C showing *N*- and *C*-terminus.

Following the synthesis of both (*R*,*R*)-mirubactin C (**32**) and *ent*-(*S*,*S*)-mirubactin C (**32**) we will confirm the absolute stereochemistry of the synthetic material by Marfey's analysis and evaluate both enantiomers in our biological assays with *Δmbl B. subtilis*.

2.4.2 Retrosynthesis of Mirubactin C

Based on previous work by Kakeya *et al.* on the total synthesis of the related molecule, chlorocatechelin A,[64] we planned to synthesise mirubactin C from three fragments, the left-hand (red), middle (green) and right-hand (blue) fragments (**Scheme 2.1**).

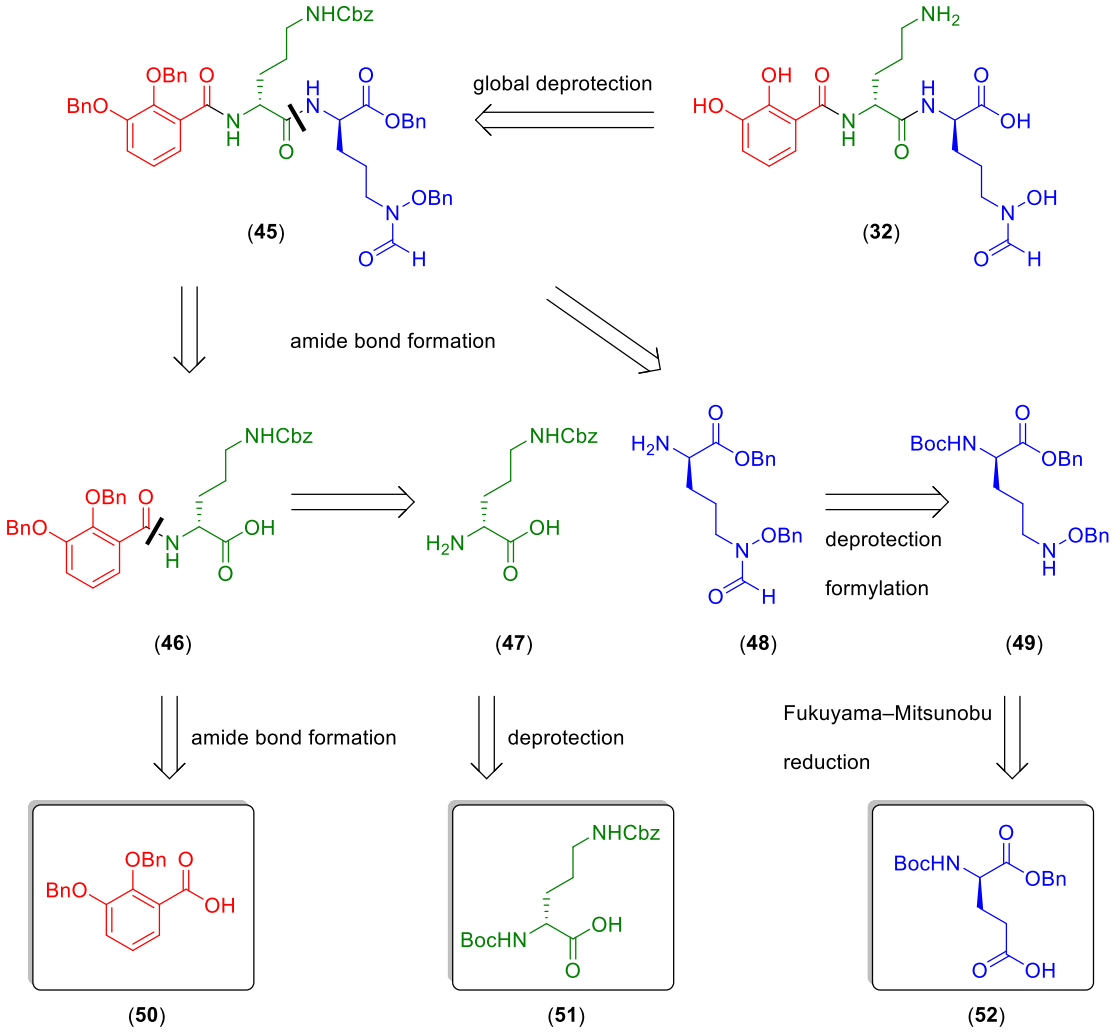

Scheme 2.1. Retrosynthetic analysis of mirubactin C showing the key left-hand (red), middle (green) and right-hand (blue) fragments.

For the left-hand fragment, we planned to start from benzyl protected 2,3-dihydroxybenzoic acid (**53**). The middle fragment will be based on ornithine, in which the amine groups are orthogonally protected. We planned to synthesise the right-hand fragment from protected glutamic acid, where the carboxylic acid side chain can be converted to the desired hydroxamic acid. Once we have completed the synthesis of

all three fragments, they will be joined together with amide bond coupling reactions followed by a global deprotection step.

2.4.3 Synthesis of the Left-hand Fragment of Mirubactin C

To begin our total synthesis of mirubactin C, we decided to start with the construction of the left-hand fragment, benzyl protected aryl carboxylic acid (**50**). Based on research by Kakeya *et al.*,[64] we planned to access benzyl protected aryl carboxylic acid (**50**) starting from 2,3-dihydroxybenzoic acid (**53**), via a global benzyl protection of both the phenolic and carboxylic acid groups to form benzyl 2,3-bis(benzyloxy)benzoate (**54**), followed by selective hydrolysis of the benzyl ester (**Scheme 2.2**).

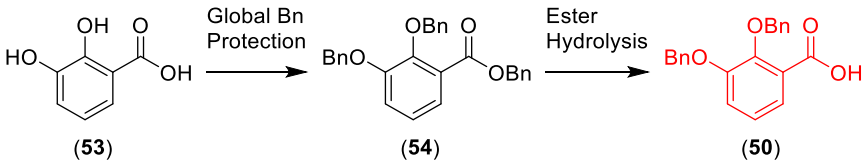

Scheme 2.2. Global benzyl protection/selective hydrolysis strategy for the synthesis of left-hand fragment benzyl protected aryl carboxylic acid (**50**).

Therefore, we started by reacting 2,3-dihydroxybenzoic acid (**53**) with 3.3 equivalents of benzyl bromide and 3.3 equivalents of potassium carbonate in DMF at room temperature on a 5 mmol scale. After 16 hours, TLC showed that the reaction had gone to completion. Subsequent purification of the crude reaction material by column chromatography on silica gel gave the corresponding benzyl 2,3-bis(benzyloxy)benzoate (**54**) in a 75% isolated yield (**Scheme 2.3**).

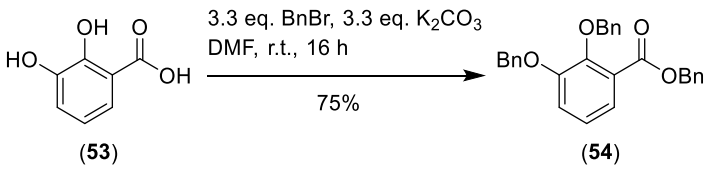

Scheme 2.3. Benzyl protection of 2,3-dihydroxybenzoic acid (**53**).

We confirmed the structure of benzyl 2,3-bis(benzyloxy)benzoate (**54**) by ^{1}H-NMR analysis, which showed the appearance of three new 2H singlets, at 5.32, 5.14 and 5.07 ppm, corresponding to three benzylic methylene groups.

To further confirm the structure, single crystals of benzyl 2,3-bis(benzyloxy)benzoate (**54**) were grown through slow evaporation of an ethyl acetate solution and examined by single crystal X-ray diffraction. Benzyl 2,3-bis(benzyloxy)benzoate (**54**) crystallised in the monoclinic space group $P2_1/c$, with 4 molecules in the unit cell (Z = 4) (**Figure 2.17**).

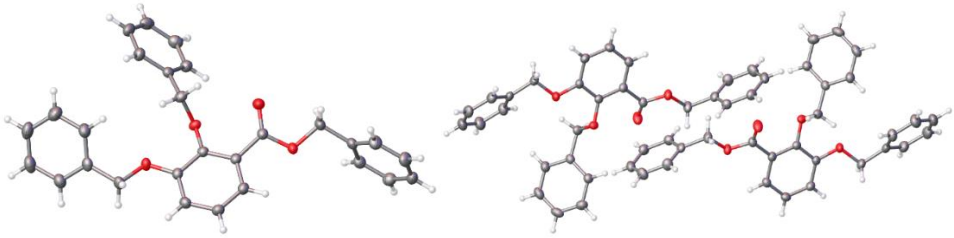

Figure 2.17. (left) ORTEP diagram showing single crystal X-ray structure of benzyl 2,3-bis(benzyloxy)benzoate (**54**). (right) crystal packing.

To provide more starting material for the next steps, the benzyl protection of 2,3-dihydroxybenzoic acid (**53**) was repeated twice on a 5 mmol scale, and a further two times on a 10 mmol scale giving high isolated yields in all cases following column chromatography, 78-89% (**Table 2.1**).

Entry	Reaction Scale/mmol	Isolated Yield
1[a]	5	75%
2	5	84%
3	5	86%
4	10	78%
5	10	89%

Table 2.1. Benzyl protection of 2,3-dihydroxybenzoic acid (**53**) on 5 and 10 mmol scales. [a] Entry repeated from **Scheme 2.3** for comparison.

The following step involved the selective hydrolysis of the benzyl ester of benzyl 2,3-bis(benzyloxy)benzoate (**54**) under basic conditions. Therefore, benzyl 2,3-bis(benzyloxy)benzoate (**54**) was refluxed in the presence of 2 M aqueous NaOH. After 16 hours the starting material could not be observed by TLC, so the reaction was cooled to room temperature and then acidified with a dropwise addition of 2 M aqueous HCl until a pH of 2 was obtained. On acidification, a white precipitate was formed, which was isolated by filtration, washed with water and dried to give the desired 2,3-bis(benzyloxy)benzoic acid (**50**) in a 71% yield without further purification required (**Scheme 2.4**; **Table 2.2**, Entry 1).

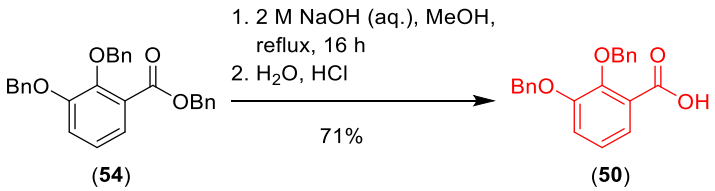

Scheme 2.4. Basic hydrolysis of benzyl 2,3-bis(benzyloxy)benzoate (**54**) to give 2,3-bis(benzyloxy)benzoic acid (**50**).

To check for hydrolysis of the benzyl ester we examined the ^{13}C NMR spectra focusing on the carbonyl carbon, however both benzyl 2,3-bis(benzyloxy)benzoate (**54**) and 2,3-bis(benzyloxy)benzoic acid (**50**) showed very similar shifts of 165.6 ppm. However, the infrared spectroscopy showed a new broad peak at 2935-2572 cm^{-1} which we assigned to the O-H stretch of the newly formed carboxylic acid and a shift of the C=O stretch from 1716 cm^{-1} (conjugated ester) to 1683 cm^{-1} (conjugated acid).

Upon acidification at the end of the reaction 2,3-bis(benzyloxy)benzoic acid (**50**) tended to form a fine powder which was difficult to recover by filtration. Therefore, we worked to improve the reaction work-up to produce more material for the next steps. Following a repeat hydrolysis of benzyl 2,3-bis(benzyloxy)benzoate (**54**) on a slightly increased scale of 4 mmol, upon completion, the reaction was acidified as previously described to precipitate the product. EtOAc was added to the crude reaction mixture to dissolve the solid 2,3-bis(benzyloxy)benzoic acid (**50**) present and the biphasic

mixture was transferred to a separating funnel. Separation of the layers, followed by two further extractions with EtOAc and solvent removal under reduced pressure gave a slightly improved yield of 76% (**Table 2.2**, Entry 2). Repeating this reaction on a 4 mmol scale gave very similar yields (**Table 2.2**, Entry 3), with further slight improvements of the yield on a larger 8 mmol scale with no further purification required in all cases (**Table 2.2**, Entry 4-5).

Entry	Reaction Scale/mmol	Isolation Method	Isolated Yield
1[a]	3	Filtration	71%
2	4	Extraction	75%
3	4	Extraction	76%
4	8	Extraction	78%
5	8	Extraction	79%

Table 2.2. Basic hydrolysis of benzyl 2,3-bis(benzyloxy)benzoate (**54**) on 3, 4 and 8 mmol scale with different collecting methods (filtration and extraction). [a] Entry repeated from **Scheme 2.4** for comparison.

We have successfully completed our target left-hand fragment of mirubactin C, which will be used in the future synthesis of both (*R*,*R*)-mirubactin C (**32**) and *ent*-(*S*,*S*)-mirubactin C (**32**).

2.4.4 Synthesis of the Middle Fragments of Mirubactin C and *ent*-Mirubactin C and Coupling with Left-Hand Fragment

To make the middle fragment of both enantiomers of mirubactin C, (*R*,*R*)-mirubactin C (**32**) and *ent*-(*S*,*S*)-mirubactin C (**32**), we planned to start from commercial orthogonally *N*-protected (*R*)- and (*S*)-ornithines followed by deprotection of the *N*-terminal amine. These middle fragments will then be coupled with the previously prepared left-hand fragment, 2,3-bis(benzyloxy)benzoic acid (**50**) (**Scheme 2.5**).

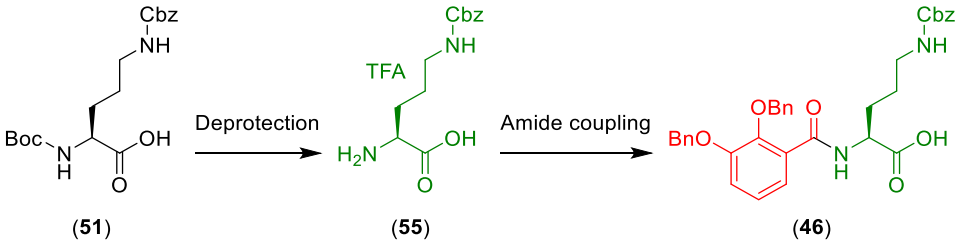

(**51**) (**55**) (**46**)

Scheme 2.5. Planned synthesis of the middle fragment of *ent*-(*S*,*S*)-mirubactin C (**46**) starting from (*S*)-5-(((benzyloxy)carbonyl)amino)-2-((*tert*-butoxycarbonyl)amino)pentanoic acid (**51**), and subsequent coupling with the left-hand fragment (**50**). Note for (*R*,*R*)-mirubactin C (**32**), (*R*)-5-(((benzyloxy)carbonyl)amino)-2-((*tert*-butoxycarbonyl)amino)pentanoic acid will be used.

In this section we decided to optimise our reaction chemistry with the natural L-amino acids to make *ent*-(*S*,*S*)-mirubactin C (**32**) due to their lower commercial costs, we then planned to replicate successful reaction conditions with the more expensive D-amino acids to make (*R*,*R*)-mirubactin C (**32**).

Therefore starting with commercial (*S*)-5-(((benzyloxy)carbonyl)amino)-2-((*tert*-butoxycarbonyl)amino)pentanoic acid (**51**) we planned to carry out a selective Boc deprotection under acidic conditions.[65] (*S*)-5-(((benzyloxy)carbonyl)amino)-2-((*tert*-butoxycarbonyl)amino)pentanoic acid (**51**) was treated with trifluoroacetic acid in dichloromethane at room temperature on a 4 mmol scale. After 1 hour TLC showed the reaction was complete, after which the solvent was removed and the solid crude product was triturated with diethyl ether to remove residual trifluoroacetic acid and unreacted starting material. This gave the desired Boc deprotected (*S*)-ornithine (**55**) in a quantitative yield as the trifluoroacetate salt without further purification, as assessed by ^{1}H NMR (**Scheme 2.6**; **Table 2.3**, Entry 1).

The structure of TFA•Boc deprotected (*S*)-ornithine (**55**) was confirmed by ^{1}H NMR analysis which showed the loss of the signal corresponding to the Boc *tert*-butyl group. Following the success of this initial experiment, the deprotection of (*S*)-5-

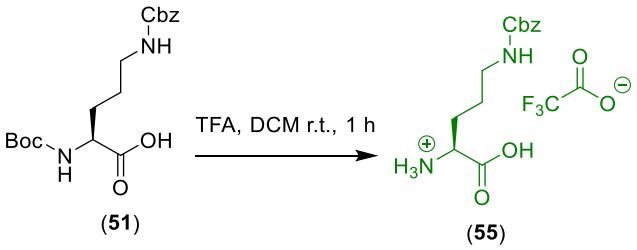

(**51**) (**55**)

Scheme 2.6. Selective Boc deprotection of (*S*)-5-(((benzyloxy)carbonyl)amino)-2-((*tert*-butoxycarbonyl)amino)pentanoic acid (**51**) to give TFA•Boc deprotected (*S*)-ornithine (**55**)

(((benzyloxy)carbonyl)amino)-2-((*tert*-butoxycarbonyl)amino)pentanoic acid (**51**) was repeated four more times, on a 3 to 4 mmol scale, to prepare enough material for the next steps. In all cases high yields were observed (**Table 2.3**).

Entry	Reaction Scale/mmol	Isolated Yield
1	4	95%
2	3	71%
3	4	93%
4	4	92%
5	4	90%

Table 2.3. Boc deprotection of (*S*)-5-(((benzyloxy)carbonyl)amino)-2-((*tert*-butoxycarbonyl)amino)pentanoic acid (**51**) with TFA in DCM.

It should be noted that for the preparation of the middle fragment of (*R*,*R*)-mirubactin C (**46**), the required (*R*)-2-amino-5-(((benzyloxy)carbonyl)amino)pentanoic acid was purchased directly and no Boc deprotection step was needed.

In the next step, we planned to form an amide bond between the left-hand fragment, 2,3-bis(benzyloxy)benzoic acid (**50**), and the Cbz protected ornithines ((*R*)-**55** and (*S*)-**55**) to provide the left-middle fragment of both enantiomers of mirubactin C. In this project, we chose to focus on the use of HATU as our preferred amide bond forming

reagent, due to its reliability, low racemisation potential and ease of work-up. Because of the presence of free carboxylic acid groups on both the 2,3-bis(benzyloxy)benzoic acid (**50**) and the Cbz protected ornithines ((*R*)-**55** and (*S*)-**55**), to make the coupling reactions selective we planned to first activate the 2,3-bis(benzyloxy)benzoic acid (**50**) with HATU before the addition of the nucleophilic amines.

Starting with synthesis towards the middle fragment of *ent*-(*S*,*S*)-mirubactin C (**46**), we reacted 2,3-bis(benzyloxy)benzoic acid (**50**) on a 2 mmol scale with 1.1 equivalents of HATU in DMF at 0 °C for 20 min, to form the OAt-activated ester intermediate. Then, 1.05 equivalents of Cbz protected ornithine (*S*)-**55** were added to the reaction, followed by 5 equivalents of DIPEA. After being stirred for 30 min at 0 °C, the reaction mixture was allowed to warm slowly to room temperature and stirred for an additional 15 hours and quenched with saturated aqueous NH_4Cl. The reaction mixture in DMF/water was then extracted with EtOAc, washed with aqueous 2M HCl, brine, dried over Na_2SO_4 and the solvent removed. The crude product was then purified by column chromatography, with the use of 0.5% acetic acid in the eluent to prevent streaking (**Scheme 2.7**).

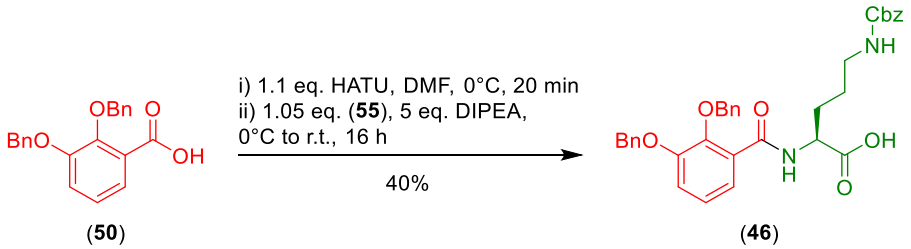

(**50**) (**46**)

Scheme 2.7. HATU coupling of 2,3-bis(benzyloxy)benzoic acid (**50**) with Cbz protected ornithine (*S*)-**55** to give (*S*)-5-(((benzyloxy)carbonyl)amino)-2-(2,3-bis(benzyloxy)benzamido)pentanoic acid (*S*)-**46**.

^{1}H NMR analysis of the column fractions showed that our desired benzoyl substituted ornithine (*S*)-**46** had co-eluted with an unknown by-product. The by-product showed a single peak at 2.81 ppm in ^{1}H NMR, which correlated with a peak at 38.5 ppm in the ^{13}C NMR by HSQC, indicating a methyl group on a nitrogen atom. This methyl group also showed a correlation to a ^{13}C NMR signal at 165.9 ppm by HMBC, suggesting a

carbonyl carbon. This allowed us to assign the by-product as tetramethylurea (**56**), produced during the formation of the HOAt-activated ester (**Scheme 2.8**).

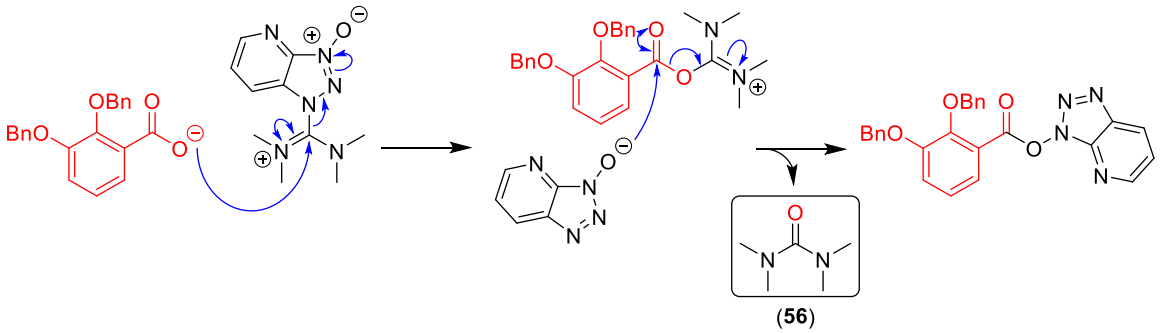

Scheme 2.8. Formation of tetramethylurea (**56**) during HOAt-activation of 2,3-bis(benzyloxy)benzoic acid (**50**).

Since tetramethylurea is highly soluble in water (116.2 g/L),[66] while we anticipated that benzoyl substituted ornithine (*S*)-**46** would be much less soluble in water, we dissolved the column fractions containing both molecules in EtOAc and washed three times with water. Following separation, drying over Na_2SO_4 and evaporation of the organic solvent, benzoyl substituted ornithine (*S*)-**46** was obtained in a 40% yield with no tetramethylurea present.

The structure of benzoyl substituted ornithine (*S*)-**46** was confirmed by NMR analysis, through the observation of a new amide proton at 8.59 ppm (broad d, J = 7.1 Hz) which was shown by COSY to couple to the ornithine α-proton at 4.70-4.58 ppm (m). This was also supported by high-resolution mass spectrometry which showed a molecular ion $[M+Na]^+$ with m/z = 605.2274, which is consistent with a molecular formula of $C_{34}H_{34}N_2O_7Na$ (calc. m/z = 605.2264).

Following further analysis of the ^{13}C NMR, we observed that several of the ^{13}C signals showed associated small signals, which were close in shift. We proposed that this was due to the presence of rotamers. The new signals in the ^{13}C NMR correspond to the carbon atoms at positions C-31 and C-37, adjacent to the carbamate group, therefore the rotamers observed at likely due to restricted rotation around the carbamate (**Figure 2.18**).[67,68]

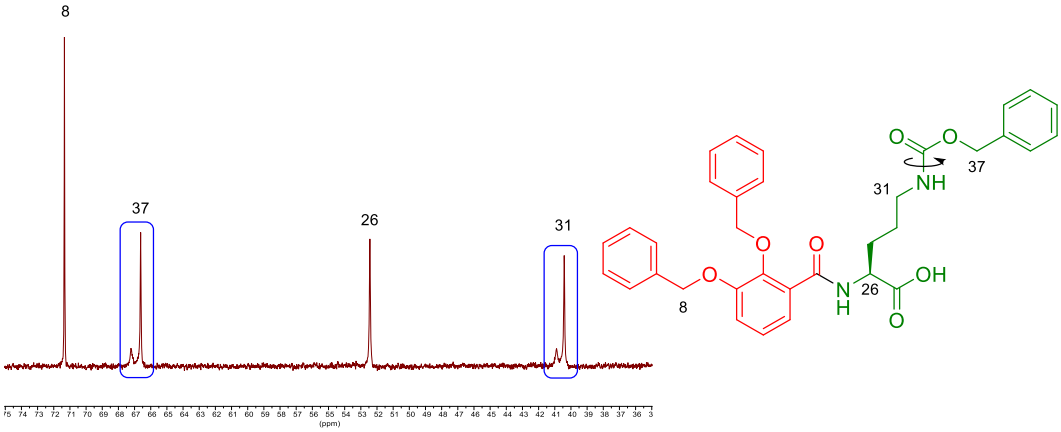

Figure 2.18. Rotamers (*S*)-5-(((benzyloxy)carbonyl)amino)-2-(2,3-bis(benzyloxy)benzamido)pentanoic acid (**46**) observed in ^{13}C NMR.

Next we repeated the HATU coupling of 2,3-bis(benzyloxy)benzoic acid (**50**) with Cbz protected ornithine (*S*)-**55**, again on a 2 mmol scale to generate more of the desired left-middle fragment, benzoyl substituted ornithine (*S*)-**46**, and to optimise the purification steps. Following the work-up, the crude reaction mixture was washed an additional three times with water to remove the tetramethylurea (**56**) and then purified by column chromatography giving an isolated yield of 41% (**Table 2.4**, Entry 2). A further reaction following this improved procedure, with slight optimisation of the column chromatography step, gave a similar isolated yield of 49% (**Table 2.4**, Entry 3).

Following this optimised procedure, we then used 2,3-bis(benzyloxy)benzoic acid (**50**) and Cbz protected ornithine (*R*)-**55** to generate the left-middle fragment, benzoyl substituted ornithine (*R*)-**46** on a 1.0 and 3.9 mmol scale, giving benzoyl substituted ornithine (*R*)-**46** in a 33% and 45% isolated yield (**Table 2.4**, Entry 4-5).

The chemical structure of benzoyl substituted ornithine (*R*)-**46** was confirmed by comparison with the ^{1}H-NMR and ^{13}C-NMR spectra of benzoyl substituted ornithine (*S*)-**46**, showing identical spectra.

Specific rotation was also measured for both benzoyl substituted ornithine (*S*)-**46** (**Table 2.4**, Entry 3) and (*R*)-**46** (**Table 2.4**, Entry 5) giving values of -14.0° and +2.0°

(*c* = 1, MeOH). The opposite sign helps to confirm the majority absolute stereochemistry of each sample, however the difference in value may indicate some racemisation of the samples, which will be addressed later through chiral HPLC analysis.

Entry	Stereochemistry (*R*/*S*)	Reaction Scale/mmol	Isolated Yield
1	*S*	2.0	40%
2	*S*	2.0	41%
3	*S*	2.0	49%[a]
4	*R*	3.9	33%
5	*R*	1.0	45%[a]

Table 2.4. HATU amide coupling of 2,3-bis(benzyloxy)benzoic acid (**50**) with Cbz protected ornithine (S)-**55** and (*R*)-**55**, on 1.0 to 3.9 mmol scales. [a] Specific rotation measured for these samples.

2.4.5 Synthesis of the Right-hand Fragments of Mirubactin C and *ent*-Mirubactin C

To make the right-hand fragment of both enantiomers of mirubactin C, (*R*,*R*)-mirubactin C (**32**) and *ent*-(*S*,*S*)-mirubactin C (**32**), we planned to start from commercial protected (*R*)- and (*S*)-glutamic acid (**52**) followed by reduction to obtain the corresponding alcohol (**57**). Then we planned to substitute the terminal hydroxy group for protected hydroxylamine, using a Fukuyama-Mitsunobu reaction, followed by formylation to give the corresponding protected hydroxamic acid group. Finally, Boc deprotection of the *N*-terminal amine will give our desired right-hand fragments (*R*)-**58** and (*S*)-**58** (**Scheme 2.9**).

2.4.5.1. Reduction of Protected (*R*)- and (*S*)-Glutamic acid (52) to Give Protected (*R*)- and (*S*)-2-Amino-5-hydroxypentanoic Acid (57)

Inspired by the total synthesis of the chlorocatechelin A,[64] we decided to begin the

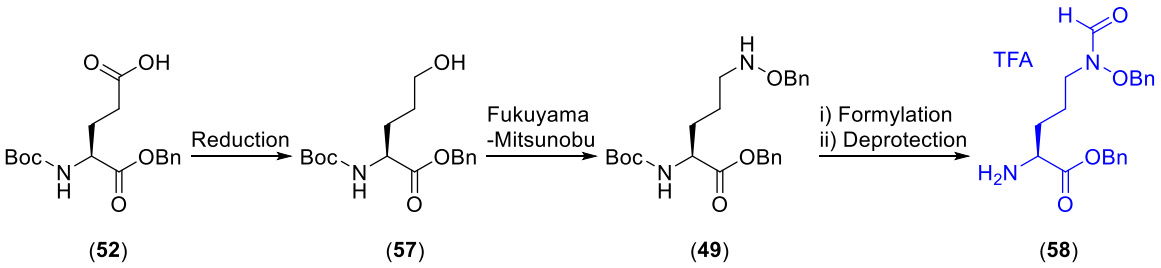

Scheme 2.9. Planned synthesis of the right-hand fragment of *ent*-(*S*,*S*)-mirubactin C (**58**) starting from (*S*)-5-(benzyloxy)-4-((*tert*-butoxycarbonyl)amino)-5-oxopentanoic acid (**52**) via reduction, Fukuyama-Mitsunobu reaction, formylation and Boc deprotection. Note for (*R*,*R*)-mirubactin C (**32**), (*R*)-5-(benzyloxy)-4-((*tert*-butoxycarbonyl)amino)-5-oxopentanoic acid will be used as the starting material.

synthesis of the right-hand fragment from a protected glutamic acid derivative, which would be reduced to the corresponding alcohol. This selective reduction could be achieved by activation of the terminal carboxylic acid, to form an acid anhydride, followed by hydride reduction. We chose to use a Boc protecting group on the *N*-terminus and a benzyl protecting group on the *C*-terminus of glutamic acid (**Scheme 2.10**).

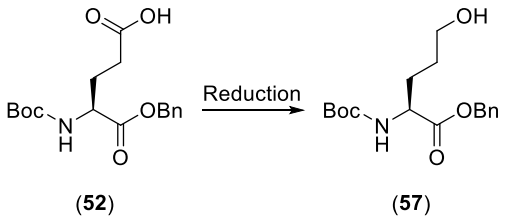

Scheme 2.10. Planned reduction of protected glutamic acid (*S*)-**52**.

We therefore started with the reaction of protected glutamic acid (*S*)-**52** with 1.14 equivalents of ethyl chloroformate and 1.04 equivalents of DIPEA on a 2 mmol scale to generate the corresponding anhydride over 45 minutes at -10 °C. Following this 3 equivalents of solid sodium borohydride were added in one portion to the reaction mixture, the cooling bath was removed and 6 mL of water was added via syringe. Upon the addition of water, considerable gas evolved (H_2) from the reaction, causing

significant bubbling. The reaction was then stirred at room temperature and after 20 mins a faint new spot could be observed on TLC when illuminated with UV light (254 nm). Following the aqueous work-up, the crude product was purified by column chromatography to give the desired protected (*S*)-2-amino-5-hydroxypentanoic acid (*S*)-**57** in a 38% yield (**Scheme 2.11**).

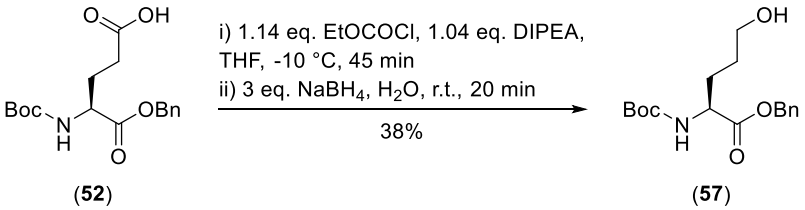

Scheme 2.11. Reduction of protected glutamic acid (*S*)-**52** to give protected (*S*)-2-amino-5-hydroxypentanoic acid (*S*)-**57**.

The structure of protected (*S*)-2-amino-5-hydroxypentanoic acid (**57**) was confirmed by both ^{1}H NMR, which showed the appearance of a new triplet (t, *J* = 6.1 Hz, 2H, H-17) at 3.53 ppm corresponding to the two protons adjacent to the OH and ^{13}C NMR which showed a loss of the carbonyl carbon (177.9 ppm) of the starting material and the appearance of a new signal at 61.6 ppm for the carbon adjacent to the newly formed alcohol group. Successful reduction was also confirmed via high resolution mass spectrometry which showed the correct molecular ion ([M+Na]$^{+}$) with *m/z* = 346.1631.

Analysis of the ^{1}H NMR spectra showed two signals at 4.37 – 4.18 ppm (m) and 4.18 – 3.97 ppm (m), corresponding to the α-proton (C-11) appearing in a 3 : 1 ratio, indicating the presence of two rotamers. To confirm the presence of rotamers we reexamined the sample with ^{1}H NMR in acetone-d_6. Interestingly, in this new solvent we also observed a pair of rotamer signals at 4.21 ppm (td, *J* = 8.6, 5.1 Hz) and 4.14 – 4.02 ppm (m) corresponding to the α-proton (C-11). In this case, the two rotamers were present in a ratio of approximately 9 : 1 by integration (**Figure 2.19**).

In order to confirm the presence of rotamers in the ^{1}H NMR of (*S*)-2-amino-5-

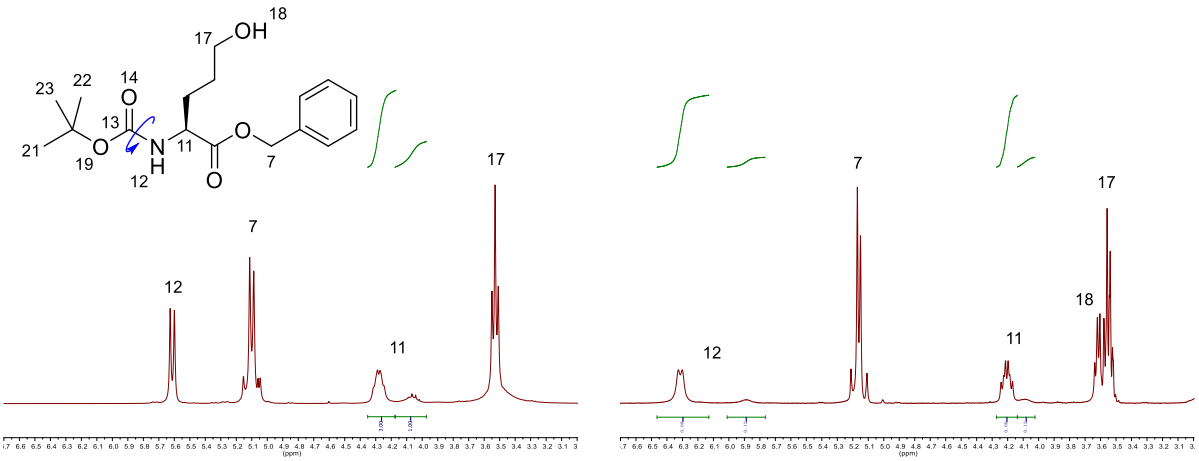

Figure 2.19. Rotamers of benzyl (*S*)-2-((*tert*-butoxycarbonyl)amino)-5-hydroxypentanoate as observed by ^{1}H NMR in $CDCl_3$ (left) and acetone d_6 (right).

hydroxypentanoic acid (**57**) we next carried out a variable temperature NMR experiment. Since we will need to access higher temperatures we decided to use dimethyl sulfoxide-d_6 as our NMR solvent, due to its high boiling point. ^{1}H NMR spectra were run at a range of temperatures from 298 to 378 K.

At 298 K, the two rotamer peaks of the α-proton (C-11) were observed at 3.98 ppm (ddd, J = 9.4, 7.8, 5.1 Hz) and 3.88 – 3.83 ppm (m). On heating of the sample, the two signals merged to form a single peak at 4.06 – 3.95 ppm (m) at around 338 K. A similar effect was seen for the two rotamer peaks corresponding to *t*-butyl group of the Boc (C-21, 22, 23), with the peaks at 1.37 and 1.27 ppm observed at 298 K merging to form a single peak at 1.37 ppm at around 338 K. These experiments confirm that (*S*)-2-amino-5-hydroxypentanoic acid (**57**) has two carbamate rotamers.

It should also be noted that several of the signals in the NMR show significant changes in their chemical shifts and show increased broadening on the heating of the sample. For example, the signal associated with the proton of the terminal hydroxyl group (O-18) appears at 4.42 ppm (t, J = 5.1 Hz) at 298 K. Upon heating, broadening of the peak is observed likely due to an increase in the rate of proton exchange with the solvent, whilst shift changes are likely due to changes in the H-bonding with the DMSO (**Figure 2.20**).

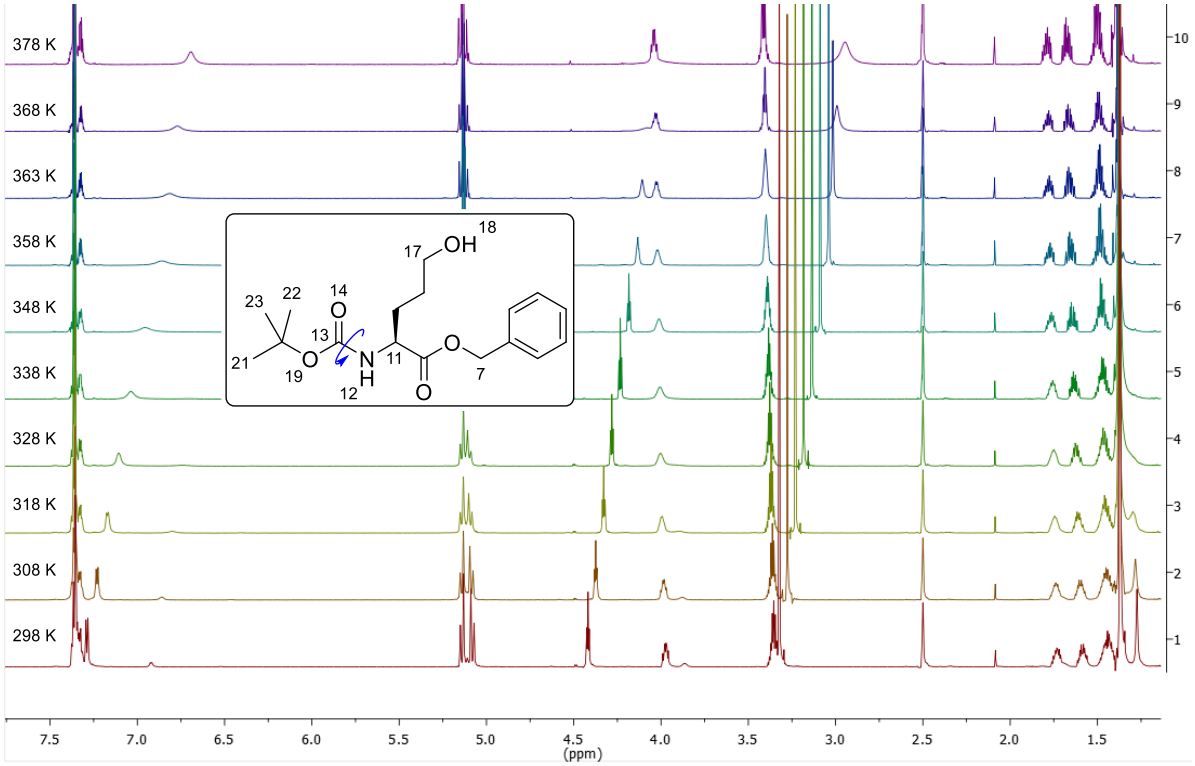

Figure 2.20. ^{1}H NMR (DMSO-d$_6$, 700 MHz) of protected (*S*)-2-amino-5-hydroxypentanoic acid (**57**) from 298 K (bottom) to 378 K (top), showing the presence of rotamers.

Following confirmation of rotamers by ^{1}H NMR, we continued with the synthesis of protected (*S*)-2-amino-5-hydroxypentanoic acid (**57**) to make more material for later steps. Even after purification from previous experiments, protected (*S*)-2-amino-5-hydroxypentanoic acid (**57**) showed only faint spots on TLC under UV light, likely due to a lack of conjugation in the molecule. This made detection and purification using TLC difficult. Therefore we decided to use potassium permanganate solution to stain TLC plates to improve the detection of the product. We therefore repeated the reduction of protected glutamic acid (*S*)-**52** on a 4 mmol scale. Using our new TLC conditions yields following chromatography were improved, giving a 72% isolated yield (**Table 2.5**, Entry 2). Two further 4 mmol scale reactions gave similar isolated yields of 69% and 76%, with a similar isolated yield of 64% obtained at an 8 mmol scale (**Table 2.5**, Entry 3-5).

To make the corresponding protected (*R*)-2-amino-5-hydroxypentanoic acid (**57**), we

started with protected glutamic acid (*R*)-**52**. Two reactions on a 7 mmol scale using similar reaction conditions, gave the desired protected (*R*)-2-amino-5-hydroxypentanoic acid (*R*)-**57** in excellent 89 and 90% isolated yields (**Table 2.5**, Entry 6-7).

Entry	Stereochemistry (*S*/*R*)	Reaction Scale/ mmol	Isolated Yield
1[a]	*S*	2	38%
2	*S*	4	72%
3	*S*	4	69%
4	*S*	4	76%
5	*S*	8	64%
6	*R*	7	90%
7	*R*	7	89%

Table 2.5. Reduction of protected glutamic acid (*S*)-**52** and (*R*)-**52** to the corresponding protected 2-amino-5-hydroxypentanoic acid (*S*)-**57** and (*R*)-**57**. [a] Entry repeated from **Scheme 2.11** for comparison.

The chemical structure of protected (*R*)-2-amino-5-hydroxypentanoic acid was confirmed by comparison with the spectral data for protected (*S*)-2-amino-5-hydroxypentanoic acid.

To assess the absolute stereochemistry of both protected 2-amino-5-hydroxypentanoic acid (*S*)-**57** and (*R*)-**57**, we examined the specific rotation of each compound. The specific rotation ($[\alpha]_D$) of protected (*S*)-2-amino-5-hydroxypentanoic acid (**Table 2.5**, Entry 2) was -23.6° (*c* = 1, MeOH), whilst the specific rotation ($[\alpha]_D$) of protected (*R*)-2-amino-5-hydroxypentanoic acid (**Table 2.5**, Entry 7) was +21.2° (*c* = 1, MeOH). The measured specific rotation for both enantiomers was of approximately the same value but opposite in sign, suggesting that both enantiomers were present with similar %*ee*.

It should also be noted that the specific rotation of protected (*R*)-2-amino-5-hydroxypentanoic acid has been previously reported in the literature, giving a similar value to what we have observed ($[\alpha]_D$ = +28.5°, *c* = 2.8, MeOH).[64]

In conclusion, the reduction of protected glutamic acid (*S*)-**52** and (*R*)-**52** to the corresponding protected 2-amino-5-hydroxypentanoic acid (*S*)-**57** and (*R*)-**57** was successfully achieved providing enough material for the next steps.

2.4.5.2 Synthesis of Nosyl Protected (*R*)- and (*S*)-2-amino-5-(hydroxyamino)pentanoic acid (62) via a Fukuyama-Mitsunobu *N*-alkylation

In the next synthetic step, we planned to substitute the terminal hydroxy group with a hydroxylamine group, using a Fukuyama-Mitsunobu *N*-alkylation. The Fukuyama-Mitsunobu *N*-alkylation is used in the synthesis of amines from the corresponding alcohols, including the synthesis of *N*-substituted hydroxylamines, through the use of nitrobenzenesulfonamides (Ns-amides) as an acidic nucleophile (pKa value 8~10) in a Mitsunobu reaction.[69] In amine synthesis, the nosyl group is then removed with aromatic thiolate nucleophiles, such as thiophenol (**Scheme 2.12**).[70]

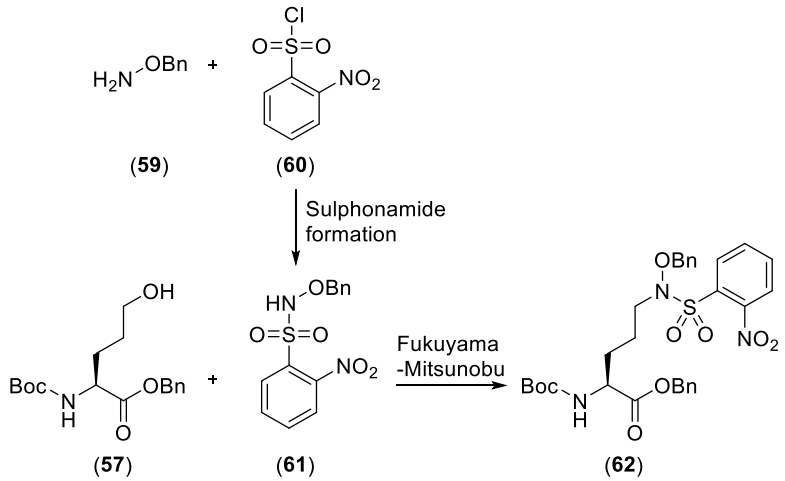

Scheme 2.12. Synthetic route to nosyl protected (*S*)-2-amino-5-(hydroxyamino)pentanoic acid (**62**) via a Mitsunobu type reaction.

In order to carry out the planned Fukuyama-Mitsunobu *N*-alkylation, to synthesise (*R*)- and (*S*)-2-amino-5-(hydroxyamino)pentanoic acid (**62**), first we have to prepare the

starting material *N*-(benzyloxy)-2-nitrobenzenesulfonamide (**61**). This can be prepared from commercial 2-nitrobenzenesulfonyl chloride and *O*-benzylhydroxylamine hydrochloride.[71,72]

We therefore dissolved 2-nitrobenzenesulfonyl chloride (**60**) and the HCl salt of *O*-benzylhydrolamine in pyridine at 0 °C, on a 4 mmol scale. The pyridine is used as the solvent in excess in order to provide the free base of *O*-benzylhydrolamine (**59**), to act as a nucleophilic catalyst and to deprotonate the product. The reaction mixture was stirred and allowed to warm slowly to room temperature over 5 hours. DCM and water were added to the reaction mixture, followed by two further extractions with DCM, washing with saturated NH_4Cl and brine, drying over Na_2SO_4 and solvent removal under reduced pressure to give a pale yellow powder, which was then purified by recrystallisation. Our recrystallisation protocol involved dissolving 763 mg of crude *N*-(benzyloxy)-2-nitrobenzenesulfonamide (**61**) in 8 mL of warm chloroform, followed by the addition of 16 mL of methanol, cooling to 0° C and allowing to stand overnight to warm to room temperature. Precipitation was observed and the solids were collected by filtration, washed with 10 mL methanol and dried under air to give colourless crystals of *N*-(benzyloxy)-2-nitrobenzenesulfonamide (**61**) in a 32% yield (**Scheme 2.13**; **Table 2.6**, Entry 1).

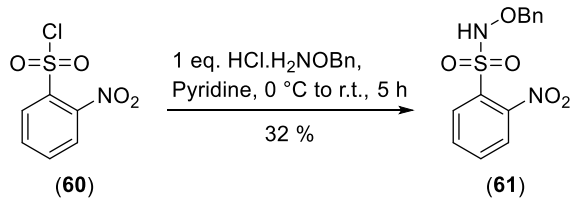

(**60**) (**61**)

Scheme 2.13. Nucleophilic substitution of 2-nitrobenzenesulfonyl chloride (**60**) to give *N*-(benzyloxy)-2-nitrobenzenesulfonamide (**61**)

The structure of *N*-(benzyloxy)-2-nitrobenzenesulfonamide (**61**) was confirmed by comparison of the NMR spectrum with that previously reported.[64] In addition, infrared spectroscopy showed a new peak at 3253 cm^{-1} (N-H stretch), corresponding to the newly formed sulphonamide group. High quality single crystals were grown via liquid-

liquid diffusion from a 1 : 1 solution of chloroform/methanol and water, which were submitted for single crystal X-ray diffraction analysis. The X-ray crystal structure showed that *N*-(benzyloxy)-2-nitrobenzenesulfonamide (**61**) had crystallised in the monoclinic space group $P2_1/_n$, in which the molecules are connected via a chain of intermolecular H-bonds (**Figure 2.21**).

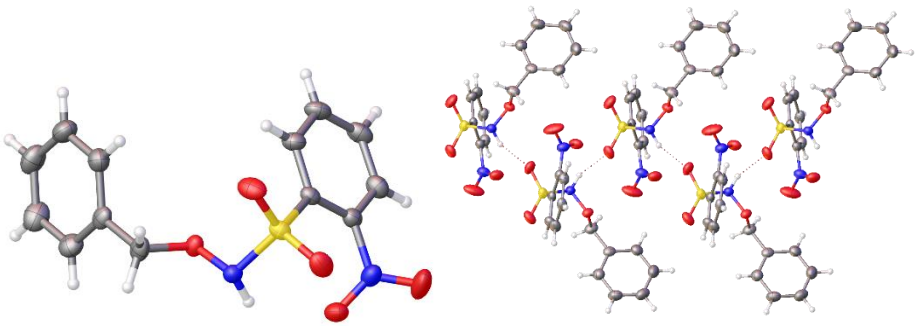

Figure 2.21. (left) ORTEP diagram showing single crystal X-ray structure of *N*-(benzyloxy)-2-nitrobenzenesulfonamide (**61**) (right) intermolecular H-bonding network.

To provide more starting material for the next steps, the nucleophilic substitution of 2-nitrobenzenesulfonyl chloride (**60**) was repeated on a 15 mmol scale, following the same purification protocol, giving a very similar 38% yield (**Table 2.6**, Entry 2).

To improve the isolated yield, we decided to examine the optimisation of the recrystallisation conditions. Following a repeat reaction on the 15 mmol scale and after aqueous work-up, the crude *N*-(benzyloxy)-2-nitrobenzenesulfonamide (**61**) (3 g) was dissolved in 20 mL of refluxing chloroform. Afterwards, the solution was allowed to cool slightly and 40 mL of methanol was added. The solution was then cooled to 0 °C and allowed to stand overnight to warm to room temperature, which upon isolation by filtration gave a slightly improved yield of 49% (**Table 2.6**, Entry 3).

To further improve the crystallisation conditions, following a 15 mmol scale reaction, the crude material was again dissolved in 20 mL of refluxing chloroform with the addition of 40 mL of methanol as before. The solution was then cooled to 0 °C for 5 hours and the solid was isolated directly from the cold solution by filtration, to give a slightly improved yield of 52% (**Table 2.6**, Entry 4). Finally, following another 15 mmol

reaction, the recrystallisation was repeated as previously from 20 mL of refluxing but now with the addition of only 30 mL of methanol. After 5 hours at 0 °C, the solution was filtered to give an improved isolated yield of 63% (**Table 2.6**, Entry 5).

Entry	Reaction Scale/ mmol	Recrystallisation Solvents $CHCl_3$: MeOH	Recrystallisation Conditions: Temperatures (Time)	Isolated Yield
1	4	1:2	warm → 0 °C → r.t. (16 h)	32%
2	15	1:2	warm → 0 °C → r.t. (16 h)	38%
3	15	1:2	refluxing → 0 °C → r.t. (16 h)	49%
4	15	1:2	refluxing → 0 °C (5 h)	52%
5	15	1:1.5	refluxing → 0 °C (5 h)	63%

Table 2.6. Optimisation of recrystallisation procedures for isolation of *N*-(benzyloxy)-2-nitrobenzenesulfonamide. [a] Entry repeated from **Scheme 2.13** for comparison.

Following optimisation of the recrystallisation conditions, sufficient *N*-(benzyloxy)-2-nitrobenzenesulfonamide (**61**) was prepared to supply the following synthetic step, the synthesis of nosyl protected (*R*)- and (*S*)-2-amino-5-(hydroxyamino)pentanoic acid (**62**).

To achieve access to nosyl protected (*R*)- and (*S*)-2-amino-5-(hydroxyamino)pentanoic acid (**62**), we decided to use a Fukuyama-Mitsunobu *N*-alkylation[69,73,74] to substitute the terminal hydroxy group of protected (*R*)- and (*S*)-2-amino-5-hydroxypentanoic acid (**57**) with *N*-(benzyloxy)-2-nitrobenzenesulfonamide (**61**) following the work done by Yokoshima *et al*. on related procedures.[75]

We therefore started by dissolving 2.9 mmol of protected (*S*)-2-amino-5-hydroxypentanoic acid (**57**), 1.1 equivalents of nitrobenzenesulfonamide (**61**) and 1.1 equivalents of triphenylphosphine in tetrahydrofuran and then the reaction mixture was cooled to 0 °C. Then 1.1 equivalents of diethyl azodicarboxylate (DEAD) were added dropwise over 30 minutes and the reaction mixture was allowed to warm slowly to room temperature for over 1 hour. Following the aqueous work-up, the crude product

was purified by column chromatography to give the desired nosyl protected (*S*)-2-amino-5-(hydroxyamino)pentanoic acid (**62**) in a 59% isolated yield as a colourless oil (**Scheme 2.14**; **Table 2.7**, Entry 1).

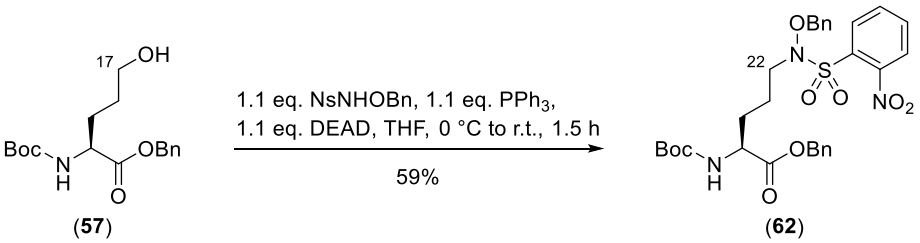

Scheme 2.14. Substitution of protected (*S*)-2-amino-5-hydroxypentanoic acid (**57**) to give nosyl protected (*S*)-2-amino-5-(hydroxyamino)pentanoic acid (**62**) via a Fukuyama-Mitsunobu *N*-alkylation.

The structure of protected nosyl protected (*S*)-2-amino-5-(hydroxyamino)pentanoic acid (**62**) was confirmed by ^{1}H NMR, which showed the appearance of several new signals in the aromatic region at 7.99 (d, *J* = 8.0 Hz, 1H), 7.74 (t, *J* = 7.8 Hz, 1H), 7.64 (t, *J* = 7.8 Hz, 1H) and 7.53 ppm (d, *J* = 8.0 Hz, 1H) which correspond to the four aromatic protons of the nosyl group. Also we compared the ^{13}C NMR shift of C-17 of protected (*S*)-2-amino-5-hydroxypentanoic acid (**57**), which is substituted with an OH group, with C-22 of nosyl protected (*S*)-2-amino-5-(hydroxyamino)pentanoic acid (**62**), which is substituted with the *N*-atom of the nosyl protected hydroxyamino group, and observed the expected change in the shift from 61.6 ppm to 52.9 ppm.

In the Mitsonubu reaction, the DEAD and triphenylphosphine react first to form an activated intermediate, in several papers these two reagents are reacted together first prior to the addition of the alcohol and nucleophile.[76] Therefore in an attempt to improve the isolated yield we tested an alternative addition order for the reaction.
Therefore we attempted a test reaction on a 1.8 mmol scale, in which we started with dropwise addition of 1.1 eq. of DEAD to 1.1 eq. of triphenylphosphine in tetrahydrofuran at 0 °C, the mixture was stirred for a further 30 minutes. Afterwards, protected (*S*)-2-amino-5-hydroxypentanoic acid (**57**) was added as a solution in THF,

followed by 1.1 equivalents of solid *N*-(benzyloxy)-2-nitrobenzenesulfonamide (**61**). After 1.5 hours at room temperature, the reaction was worked-up as previously described and the crude product was purified by column chromatography to give an improved isolated yield of 71% (**Table 2.7**, Entry 2). Following this improved procedure, we repeated the reaction on a 2.8 mmol scale giving an isolated yield of 88% (**Table 2.7**, Entry 3).

We applied this improved procedure to the synthesis of nosyl protected (*R*)-2-amino-5-(hydroxyamino)pentanoic acid (**62**), giving consistently high yields (> 80%) on scales from 2 to 6.1 mmol (**Table 2.7**, Entry 4-6).

Entry	Stereochemistry (*R*/*S*)	Reaction Scale/ mmol	Isolated Yield
1	*S*	2.9	59%[a]
2	*S*	1.8	71%
3	*S*	2.8	88%
4	*R*	2.0	85%
5	*R*	3.3	87%
6	*R*	6.1	82%

Table 2.7. Substitution of protected (*R*)- and (*S*)-2-amino-5-hydroxypentanoic acid (**57**) to the corresponding nosyl protected (*R*)- and (*S*)-2-amino-5-(hydroxyamino)pentanoic acid (**62**) via a Fukuyama-Mitsunobu *N*-alkylation. [a] Entry repeated from **Scheme 2.14** for comparison.

The structure of nosyl protected (*R*)-2-amino-5-(hydroxyamino)pentanoic acid (**62**) was confirmed by comparison with the spectral data for the corresponding (*S*)-(**62**). Specific rotation was measured for both nosyl protected (*S*)- and (*R*)-2-amino-5-(hydroxyamino)pentanoic acid (**62**) giving -0.8° (**Table 2.7**, Entry 3) and +3.8° (**Table 2.7**, Entry 6) (*c* =1, MeOH) respectively, suggesting a similar %*ee* for each enantiomer at this stage of the reaction sequence.

In conclusion, we successfully completed the synthesis of nitrobenzenesulfonamide (**61**), confirmed by single crystal X-ray diffraction. We have then completed the synthesis of both nosyl protected (*R*)- and (*S*)-2-amino-5-(hydroxyamino)pentanoic acid (**62**) via an optimised Fukuyama-Mitsunobu *N*-alkylation reaction.

2.4.5.3. Synthesis of the TFA Salt of (*R*)- and (*S*)-Benzyl 2-amino-5-(*N*-(benzyloxy)formamido)pentanoate (58) via De-nosylation, Formylation and Deprotection

To complete the synthesis of the right-hand fragment of both enantiomers of mirubactin C, the TFA salts of (*R*)- and (*S*)-benzyl 2-amino-5-(*N*-(benzyloxy)formamido)pentanoate (**58**), we planned to first deprotect nosyl protected (*R*)- and (*S*)-2-amino-5-(hydroxyamino)pentanoic acid (**62**) to remove the nosyl group, then formylate the secondary hydroxyamino group to form the desired benzyl protected hydroxamate group, followed by a Boc deprotection prior to the planned amide coupling steps with the left-middle fragment (**Scheme 2.15**).

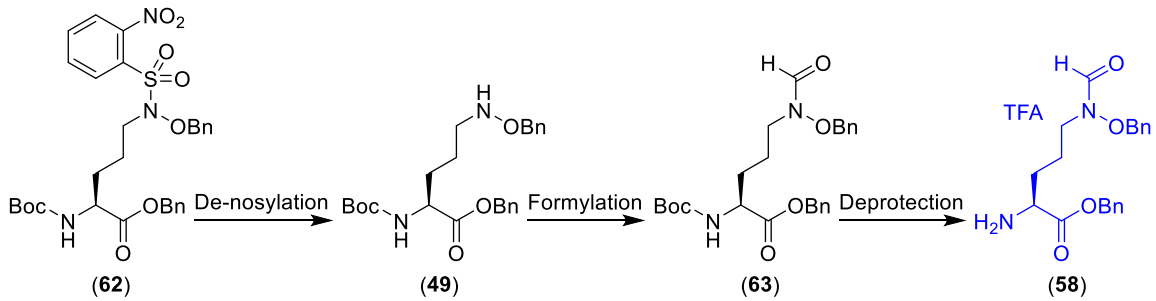

Scheme 2.15. Synthetic route to TFA salt of (*R*)- and (*S*)-benzyl 2-amino-5-(*N*-(benzyloxy)formamido)pentanoate (**58**).

The nosyl group is stable to strong acids and hydroxides but can be removed by thiolate nucleophiles in the presence of a base.[69,70] Therefore, we attempted the de-nosylation of nosyl protected (*S*)-2-amino-5-(hydroxyamino)pentanoic acid (**62**) with thiophenol.

On a 0.88 mmol scale, nosyl protected (*S*)-2-amino-5-(hydroxyamino)pentanoic acid

(**62**) and 1.1 equivalents of potassium carbonate were dissolved in DMF, followed by addition of 1.2 equivalents of thiophenol at room temperature. The colour of the reaction mixture slowly changed from light green to orange and after 1 h TLC indicated that the reaction was complete. Following the work-up, purification of the crude reaction material by column chromatography gave the corresponding benzyl (*S*)-5-((benzyloxy)amino)-2-((*tert*-butoxycarbonyl)amino)pentanoate (**49**) in a 63% isolated yield (**Scheme 2.16**; **Table 2.8**, Entry 1).

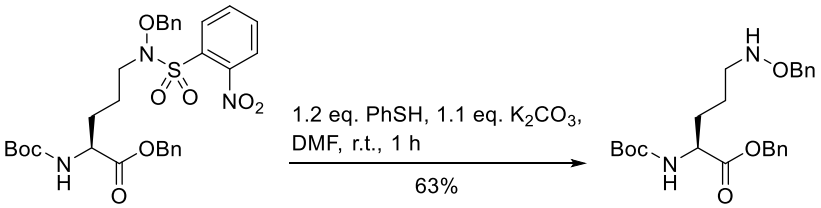

(**62**) (**49**)

Scheme 2.16. Deprotection of nosyl protected (*S*)-2-amino-5-(hydroxyamino)pentanoic acid (**62**) to give benzyl (*S*)-5-((benzyloxy)amino)-2-((*tert*-butoxycarbonyl)amino)pentanoate (**49**).

The structure of benzyl (*S*)-5-((benzyloxy)amino)-2-((*tert*-butoxycarbonyl)amino)pentanoate (**49**) was confirmed by ^{1}H NMR analysis, which showed the loss of the signals corresponding to the four aromatic protons of the nosyl group, and high-resolution mass spectrometry which showed a molecular ion $[M+H]^{+}$ (*m/z* = 429.2394) which matched the expected molecular formula ($C_{24}H_{32}N_2O_5H$).

In an attempt to improve the isolated yield and to prepare more material for the next synthetic step, we repeated the de-nosylation reaction on a 1.16 mmol scale. Increasing the reaction time to 1.5 hours gave a slightly improved isolated yield of 70% (**Table 2.8**, Entry 2), with further scale-up to 1.32 mmol giving further improvements to an isolated yield of 82% (**Table 2.8**, Entry 3).

Following our previous procedure, we carried out several de-nosylation reactions, preparing benzyl (*R*)-5-((benzyloxy)amino)-2-((*tert*-butoxycarbonyl)amino)pentanoate (**49**) giving consistently high yields of over 81% (**Table 2.8**, Entry 4-6).

Entry	Stereochemistry (*R*/*S*)	Reaction Scale/ mmol	Time/ h	Isolated Yield
1[a]	*S*	0.88	1.0	63%
2	*S*	1.16	1.5	70%
3	*S*	1.32	1.5	82%
4	*R*	1.51	1.5	96%
5	*R*	2.42	1.5	90%
6	*R*	5.06	1.5	81%

Table 2.8. Deprotection of nosyl protected (*R*)- and (*S*)-2-amino-5-(hydroxyamino)pentanoic acid (**62**) to give (*R*)- and (*S*)-benzyl 5-((benzyloxy)amino)-2-((*tert*-butoxycarbonyl)amino)pentanoate (**49**). [a] Entry repeated from **Scheme 2.16** for comparison.

The structure of (*R*)-benzyl 5-((benzyloxy)amino)-2-((*tert*-butoxycarbonyl)amino)pentanoate (**49**) was confirmed by comparison with the spectral data for the corresponding enantiomer. Specific rotation was measured for both protected (*S*)- and (*R*)-benzyl 5-((benzyloxy)amino)-2-((*tert*-butoxycarbonyl)amino)pentanoate (**49**) giving -13.4° (**Table 2.8**, Entry 3) and +10.4° (**Table 2.8**, Entry 6) (*c* = 1, MeOH) respectively, suggesting a similar %*ee* for each enantiomer.

Following successful removal of the nosyl group, next we focussed on formylation of the secondary hydroxyamino group. Based on research by Huffman,[77] we planned to formylate the secondary hydroxyamino group with acetic anhydride and formic acid.
The formylation of (*S*)-benzyl 5-((benzyloxy)amino)-2-((*tert*-butoxycarbonyl)amino)pentanoate (**49**) was carried out on a 0.47 mmol scale. First we reacted 2.1 equivalents of acetic anhydride with 4.2 equivalents of formic acid in dichloromethane for 30 min at room temperature, after which (*S*)-benzyl 5-((benzyloxy)amino)-2-((*tert*-butoxycarbonyl)amino)pentanoate (**49**) was added to the

reaction mixture. After an additional 1 hour, following an aqueous workup the desired benzyl (*S*)-5-(*N*-(benzyloxy)formamido)-2-((*tert*-butoxycarbonyl)amino)pentanoate (**63**) was obtained with an 80% yield without further purification (**Scheme 2.17**; **Table 2.9**, entry 1).

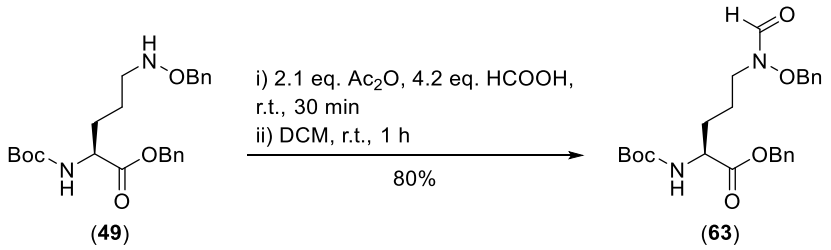

Scheme 2.17. *N*-Formylation of (*S*)-benzyl 5-((benzyloxy)amino)-2-((*tert*-butoxycarbonyl)amino)pentanoate (**49**).

The introduction of a formyl group was confirmed by ^{1}H NMR analysis, which showed the appearance of two broad singlets at 8.20 and 8.02 ppm which integrate for one proton, and ^{13}C NMR which showed a new peak at 163.3 ppm. To further understand the observation of two ^{1}H NMR signals corresponding to the aldehyde-like proton of the new formyl group, we carried out a variable temperature NMR experiment in $CDCl_3$. At a high temperature (328 K) the two peaks of the formyl group appeared as a single broad peak. As the sample was cooled two sharp peaks appeared, around 273 K corresponding to the presence of a major and minor rotamer present in the sample (**Figure 2.22**).

In an attempt to optimise the reaction conditions, we repeated the formylation reaction on a similar scale but with an increase in the time allowed for the acetic anhydride and formic acid to react from 0.5 h to 1 h, resulting in an increased yield of 99%. (**Table 2.9**, Entry 2). In a third attempt, we repeated the reaction on a reduced 0.14 mmol scale with a shorter reaction time for the last step, but in this case the product was isolated in 92% yield following column chromatography (**Table 2.9**, Entry 3).
Finally, we applied our optimised formylation conditions to the synthesis of the (*R*)-

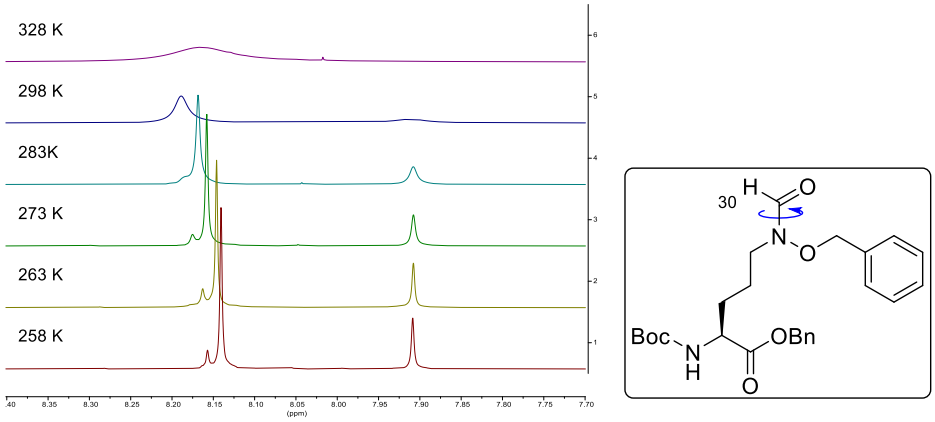

Figure 2.22. ^{1}H NMR ($CDCl_3$, 700 MHz) of benzyl (*S*)-5-(*N*-(benzyloxy)formamido)-2-((*tert*-butoxycarbonyl)amino)pentanoate (**63**) from 258 K (bottom) to 328 K (top), showing the prescence of rotamers.

benzyl 5-(*N*-(benzyloxy)formamido)-2-((*tert*-butoxycarbonyl)amino)pentanoate (**63**) on a 5.16 mmol scale, but extending the time of both the first and second steps of the reaction to 2 hours. Following aqueous work-up and column chromatography, the desired product was isolated in a 98% yield (**Table 2.9**, Entry 4).

Entry	Stereochemistry (*R*/*S*)	Reaction Scale/mmol	Time Step 1/h	Time Step 2/h	Isolated Yield
1	*S*	0.47	0.5	1.0	80%[a]
2	*S*	0.42	1.0	1.0	99%
3	*S*	0.14	1.0	0.5	92%[b]
4	*R*	5.16	2.0	2.0	98%[b]

Table 2.9. *N*-Formylation of (*R*)- and (*S*)-benzyl 5-((benzyloxy)amino)-2-((*tert*-butoxycarbonyl)amino)pentanoate (**49**) to give (*R*)- and (*S*)-benzyl 5-(*N*-(benzyloxy)formamido)-2-((*tert*-butoxycarbonyl)amino)pentanoate (**63**). [a] Entry repeated from **Scheme 2.17** for comparison. [b] Purification by column chromatography.

We confirmed the structure of (*R*)-benzyl 5-(*N*-(benzyloxy)formamido)-2-((*tert*-

butoxycarbonyl)amino)pentanoate (**63**) by comparison with the spectral data for the corresponding enantiomer. The specific rotation ($[\alpha]_D$) was measured for both enantiomers giving -8.3° of the (*S*)- (**Table 2.9**, Entry 2) and +17.6° for the (*R*)-enantiomer (**Table 2.9**, Entry 4) (*c* = 1, MeOH). The opposite signs of the specific rotations show the presence of an excess of each enantiomer, however the different values suggest that some racemisation may have occurred particularly with the (*S*)-sample. It should also be noted that the specific rotation of (*R*)-benzyl 5-(*N*-(benzyloxy)formamido)-2-((*tert*-butoxycarbonyl)amino)pentanoate (**63**) has been previously reported in the literature ($[\alpha]_D$ = +14.9°, *c* = 1.2, MeOH).[64] However no additional supporting data was given in the literature to examine %*ee*, therefore it is difficult at this stage to easily assess the %*ee* of our samples.

In the next step we wished to carry out the Boc deprotection of the *N*-terminal amine of (*R*)- and (*S*)-benzyl 5-(*N*-(benzyloxy)formamido)-2-((*tert*-butoxycarbonyl)amino)pentanoate (**63**), following the report of Haufe *et al*., using acidic conditions.[65]

Therefore, we started with the deprotection of (*S*)-benzyl 5-(*N*-(benzyloxy)formamido)-2-((*tert*-butoxycarbonyl)amino)pentanoate (**63**) on a 0.38 mmol scale by reaction, by reaction with excess trifluoroacetic acid in dichloromethane at room temperature. After 2 hours, the starting material could not be observed by TLC after staining with ninhydrin solution, and a new spot appeared on the baseline. The solvent was then removed under reduced pressure to give the desired right-hand fragment of *ent*-mirubactin C as the corresponding TFA salt, TFA•(*S*)-benzyl 2-amino-5-(*N*-(benzyloxy)formamido)pentanoate (**58**), in a 92% yield without further purification (**Scheme 2.18**; **Table 2.10**, Entry 1).

^{1}H NMR analysis confirmed the loss of the Boc group, with the loss of the *tert*-butyl signal. Following the success of this initial experiment, the Boc deprotection was repeated on the same scale to prepare more material to use in subsequent steps, resulting in a similarly high yield of 96% (**Table 2.10**, Entry 2).

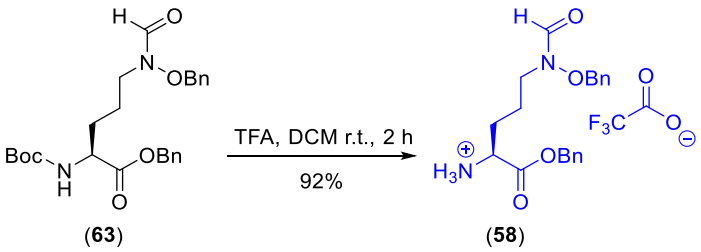

Scheme 2.18. Boc deprotection of (*S*)-benzyl 5-(*N*-(benzyloxy)formamido)-2-((*tert*-butoxycarbonyl)amino)pentanoate (**63**) to give TFA•(*S*)-benzyl 2-amino-5-(*N*-(benzyloxy)formamido)pentanoate (**58**)

To make the corresponding TFA•(*R*)-benzyl 2-amino-5-(*N*-(benzyloxy)formamido)pentanoate (**58**), we carried out the deprotection of (*R*)-benzyl 5-(*N*-(benzyloxy)formamido)-2-((*tert*-butoxycarbonyl)amino)pentanoate (**63**) on a 3.36 mmol scale under similar reaction conditions giving a satisfactory yield of 84% yield (**Table 2.10**, Entry 3).

Entry	Stereochemistry (*R*/*S*)	Reaction Scale/mmol	Yield
1[a]	*S*	0.38	92%
2	*S*	0.38	96%
3	*R*	3.36	84%

Table 2.10. Boc deprotection of (*R*)- and (*S*)-benzyl 5-(*N*-(benzyloxy)formamido)-2-((*tert*-butoxycarbonyl)amino)pentanoate (**63**) with TFA in DCM.

It should be noted that we decided to take use the TFA salts of (*R*)- and (*S*)-benzyl 2-amino-5-(*N*-(benzyloxy)formamido)pentanoate (**58**) directly in the next coupling step, without further purification, due to the difficulties in purification of amine salts.

2.4.6 Final Steps in the Synthesis of Protected Mirubactin C and *ent*-Mirubactin C and Absolute Stereochemistry Analysis

To complete our synthesis of both enantiomers of mirubactin C, we planned to

assemble the previously prepared left-middle fragments (**46**) with the corresponding right-hand fragments (**58**), via a HATU amide coupling.

To make protected *ent*-(*S*,*S*)-mirubactin C (*S*,*S*-**45**), we therefore reacted benzoyl substituted ornithine (*S*)-**46** (left-middle fragment) on a 0.25 mmol scale with 1.1 equivalents HATU in DMF at 0 °C for 25 min. Then 1.05 equivalent of TFA•(*S*)-benzyl 2-amino-5-(*N*-(benzyloxy)formamido)pentanoate (**58**) (right-hand fragment) was added to the reaction as a DMF solution, followed by dropwise addition of 4 equivalents of DIPEA over 5 minutes. The reaction mixture was allowed to warm slowly to room temperature, stirred for an additional 2.5 hours and quenched with saturated aqueous NH_4Cl. Following aqueous work-up and column chromatography, the desired protected *ent*-(*S*,*S*)-mirubactin C (*S*,*S*-**45**) was isolated in 55% yield (**Scheme 2.19**).

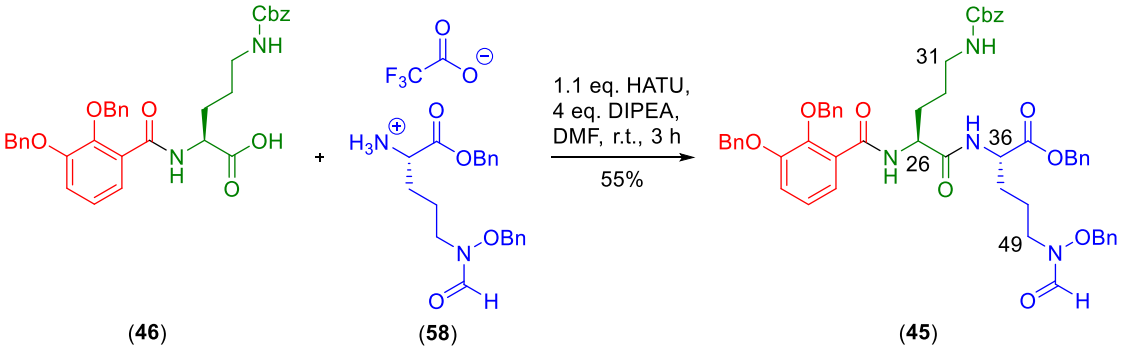

Scheme 2.19. Amide coupling of benzoyl substituted ornithine (*S*)-**46** (left-middle fragment) and TFA•(*S*)-benzyl 2-amino-5-(*N*-(benzyloxy)formamido)pentanoate (**58**) (right-hand fragment) to give protected *ent*-(*S*,*S*)-mirubactin C (*S*,*S*-**45**).

It was challenging to confirm the final structure of protected *ent*-(*S*,*S*)-mirubactin C (*S*,*S*-**45**) by simple ^{1}H NMR analysis, due to the presence of a large number of overlapping broad signals, which may be due to rotamers or diastereoisomers. However, ^{1}H and ^{13}C assignments could be carried out through the use of 2D-NMR experiments, HSQC and HMBC. Moreover, the formation of protected *ent*-(*S*,*S*)-mirubactin C (*S*,*S*-**45**) could be confirmed by high resolution mass spectrometry, which showed the expected molecular ion (experimental $[M+Na]^+$ = 943.3925; calculated for $C_{54}H_{56}N_4O_{10}Na$ $[M+Na]^+$ 943.3894).

We next repeated the reaction to form protected *ent*-(*S*,*S*)-mirubactin C (*S*,*S*-**45**) on a very similar scale (0.32 mmol), but with an increase in the reaction time to 16 h. After purification by column chromatography, we still observed the presence of a small tetramethylurea peak. At this point, we had to suspend our research due to the spread of COVID-19 and the samples were stored in the freezer under an N_2 atmosphere at -20 °C for future analysis. After approximately six months we reaccessed the same sample with additional 3 times water wash and removed the tetramethylurea, which resulted in an improved isolated yield of 75% (**Table 2.11**, Entry 2).

It should be noted that after six months the sample had undergone some minor degradation, with additional peaks present in the ^{1}H NMR. To look for potential rotamers of protected *ent*-(*S*,*S*)-mirubactin C (*S*,*S*-**45**), we carried out further analysis using high-field NMR (700 MHz) to obtain improved spectral dispersion and to undertake variable temperature experiments (**Figure 2.23**).

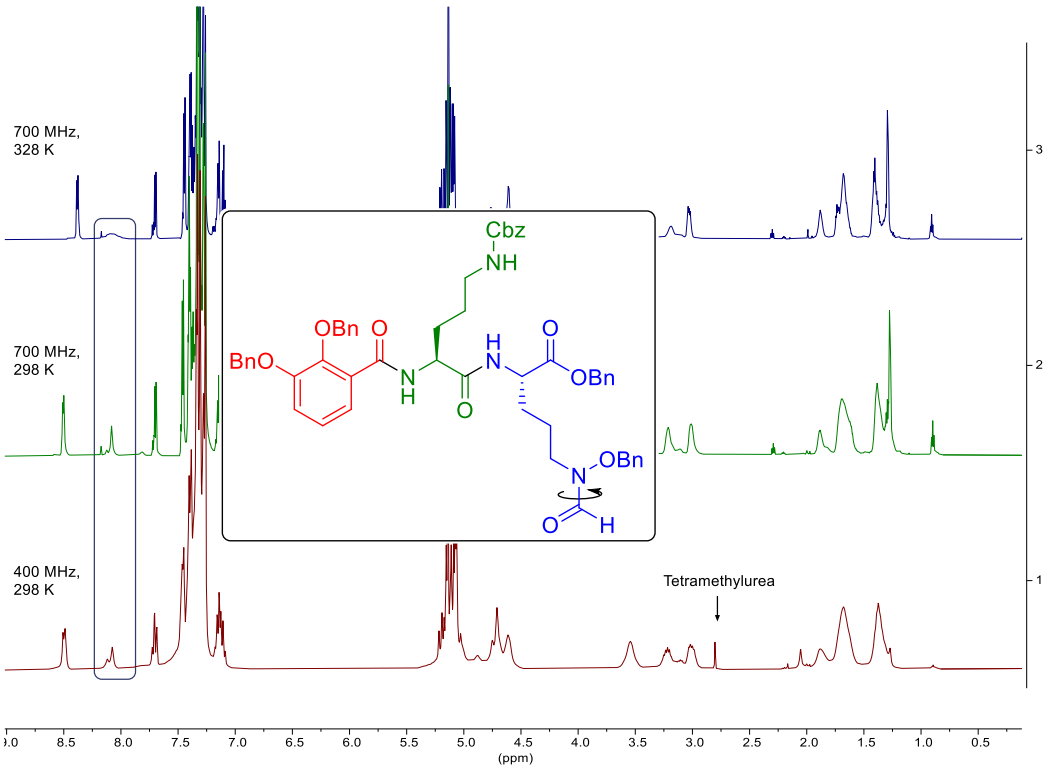

Figure 2.23. ^{1}H NMR ($CDCl_3$) of protected *ent*-(*S*,*S*)-mirubactin C (*S*,*S*-**45**) with rotamer peaks highlighted: (bottom) showing contaminating tetramethylurea; (middle) spectra at 298 K; (top), spectra at 328 K.

^{1}H NMR spectral analysis showed two signals at 8.12 ppm (m) and 8.08 ppm (m), corresponding to the aldehyde-like protons merging into a broad peak at 8.08 ppm (m), indicating that two rotamers were present in a ratio of approximately 1:7 by integration due to restricted rotation of the formyl group as before.

Next we applied the same amide coupling conditions to the synthesis of protected (*R*,*R*)-mirubactin C (*R*,*R*-**45**) on a 1.25 mmol scale, achieving a satisfactory isolated yield of 65% (**Table 2.11**, Entry 3).

Entry	Stereochemistry (*R*/*S*)	Reaction Scale /mmol	Time /h	Isolated Yield
1[a]	*S,S*	0.25	3	55%
2	*S,S*	0.32	16	75%
3	*R,R*	1.25	16	65%

Table 2.11. Amide couplings to give protected (*R*,*R*)-mirubactin C (*R*,*R*-**45**) and protected *ent*-(*S*,*S*)-mirubactin C (*S*,*S*-**45**).

The structure of the protected (*R*,*R*)-mirubactin C (*R*,*R*-**45**) was confirmed by comparison with the 700 MHz ^{1}H NMR spectrum of protected *ent*-(*S*,*S*)-mirubactin C (*S*,*S*-**45**), supported by 2D NMR studies. The aromatic region showed good agreement between the two enantiomers, but a number of differences are observable in the region containing the benzylic methylenes and α-protons, indicating the potential for diastereoisomers (**Figure 2.24**).

In addition, we also examined the 700 MHz ^{1}H NMR spectrum of protected (*R*,*R*)-mirubactin C (*R*,*R*-**45**) in DMSO-d_6 in an attempt to improve spectral dispersion (e.g., benzylic methylenes) and to better understand the presence of any rotamers. In DMSO-d_6 several peaks corresponding to potential rotamers (or diastereoisomers) were observed, including the two signals corresponding to the amide proton N-35 (major peak, 8.51 ppm, d, J = 7.5 Hz; minor peak, 8.57 ppm, d, J = 7.6 Hz) appearing in a 3 : 1 ratio. The same splitting with 3 : 1 ratio situation was also present with amide

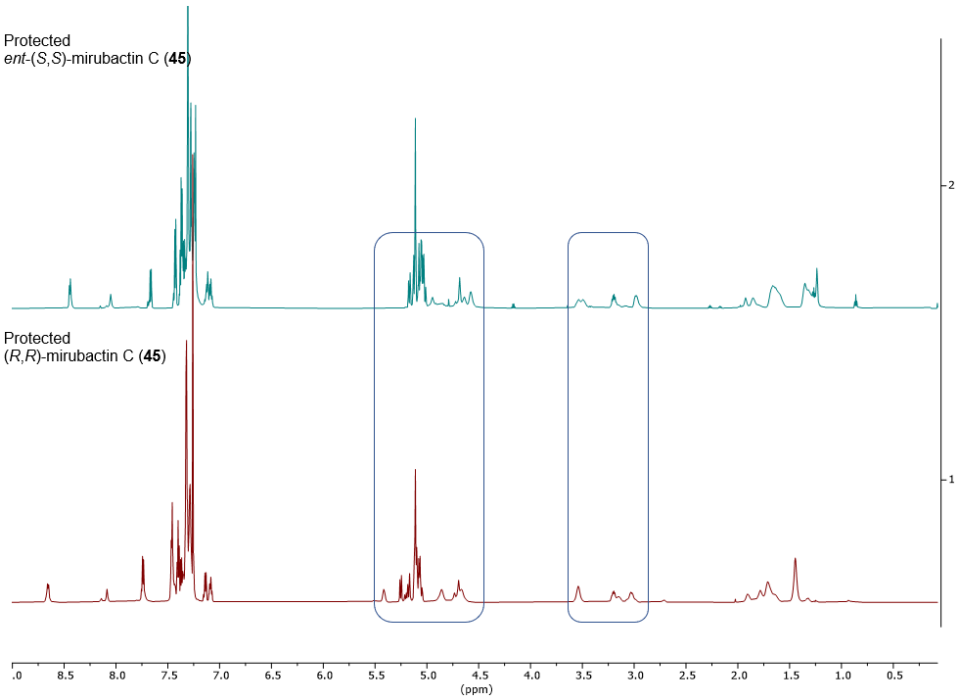

Figure 2.24. ^{1}H NMR ($CDCl_3$, 700 MHz) comparison of (top) protected *ent*-(*S*,*S*)-mirubactin C (*S*,*S*-**45**) and (bottom) protected (*R*,*R*)-mirubactin C (*R*,*R*-**45**) at 298 K. Highlighted box showing potential diastereoisomers.

proton N-25 (major peak, 8.46 ppm, d, *J* = 7.9 Hz; minor peak, 8.49 ppm, d, *J* = 8.3 Hz) and with α-proton C-26 (major peak, 4.56 – 4.49 ppm, m; minor peak, 4.62 – 4.57 ppm, m). The data suggests that one set of rotamers (or diastereoisomers) are present in a 3 : 1 ratio, potentially due to restricted rotation around the C-23 to N-25 and/or C-27 to N-35 amide bonds. In addition, the peak corresponding to the formyl group aldehyde-like proton C-67 is also split into two peaks (major peak, 8.18 ppm, br s; minor peak, 7.96 ppm, br s) giving an approximate ratio of 5 : 3, which indicates that a second set of rotamers are present, as discussed previously for compound (*S*)-benzyl 5-((benzyloxy)amino)-2-((*tert*-butoxycarbonyl)amino)pentanoate (**49**) (**Figure 2.25**).

With the synthesis of protected *ent*-(*S*,*S*)-mirubactin C (*S*,*S*-**45**) and protected (*R*,*R*)-mirubactin C (*R*,*R*-**45**) completed, we next worked on confirming the absolute chemistry via the previously used Marfey's method (**Figure 2.26**).

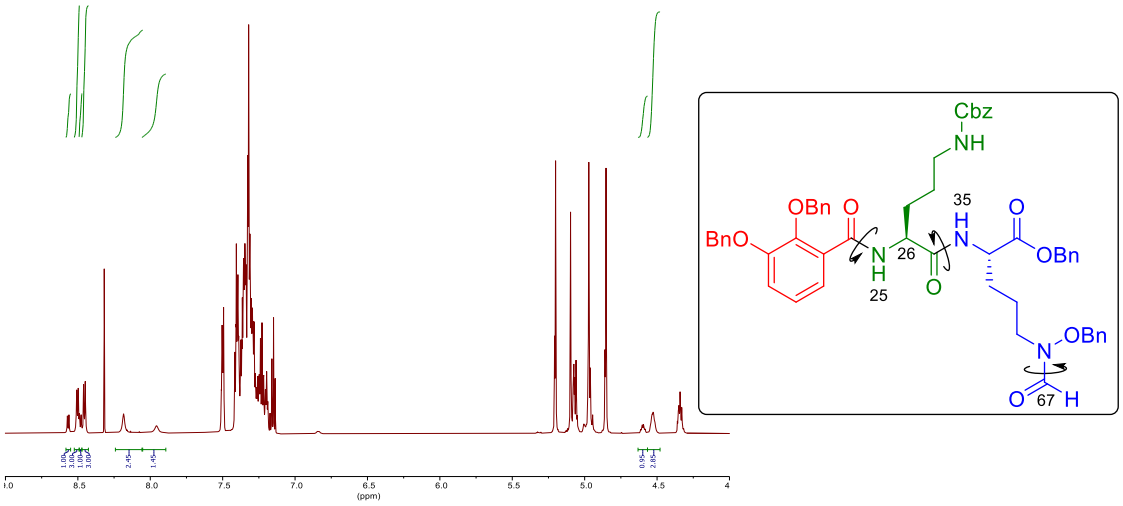

Figure 2.25. ^{1}H NMR (DMSO-d$_6$, 700 MHz) of protected (*R*,*R*)-mirubactin C (*R*,*R*-**45**) showing the presence of rotamers (or diastereoisomers).

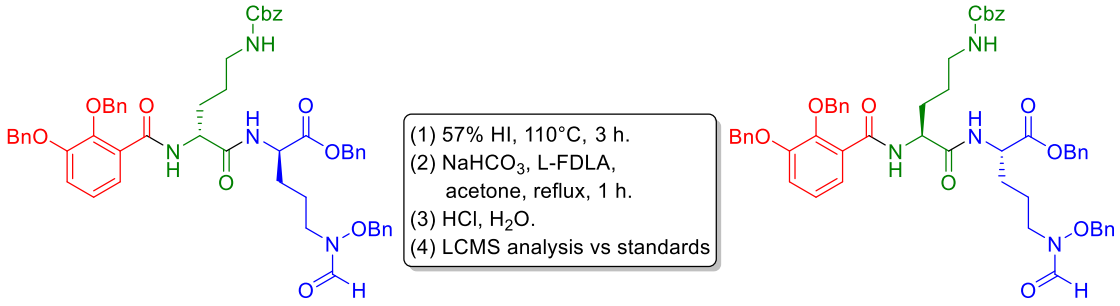

Figure 2.26. Marfey's analysis of protected (*R*,*R*)-mirubactin C (*R*,*R*-**45**) and protected *ent*-(*S*,*S*)-mirubactin C (*S*,*S*-**45**) by LCMS.

Therefore, 500 µg of protected (*R*,*R*)-mirubactin C (*R*,*R*-**45**) or protected *ent*-(*S*,*S*)-mirubactin C (*S*,*S*-**45**) were analysed by Marfey's method. Following degradation with hydriodic acid and reaction with L-FDLA, both samples were analysed by LCMS against the natural product mirubactin C (**32**) and the previously prepared Marfey's standards (L$_M$L$_{aa}$ **42** and L$_M$D$_{aa}$ **42**) (**Figure 2.27**).

For comparison we examined the natural product mirubactin C (**32**) by Marfey's analysis. L-FDLA derivatized natural product mirubactin C showed two major peaks, at 7.77 and 8.68 min, and a minor peak at 8.26 min. The two major peaks correspond

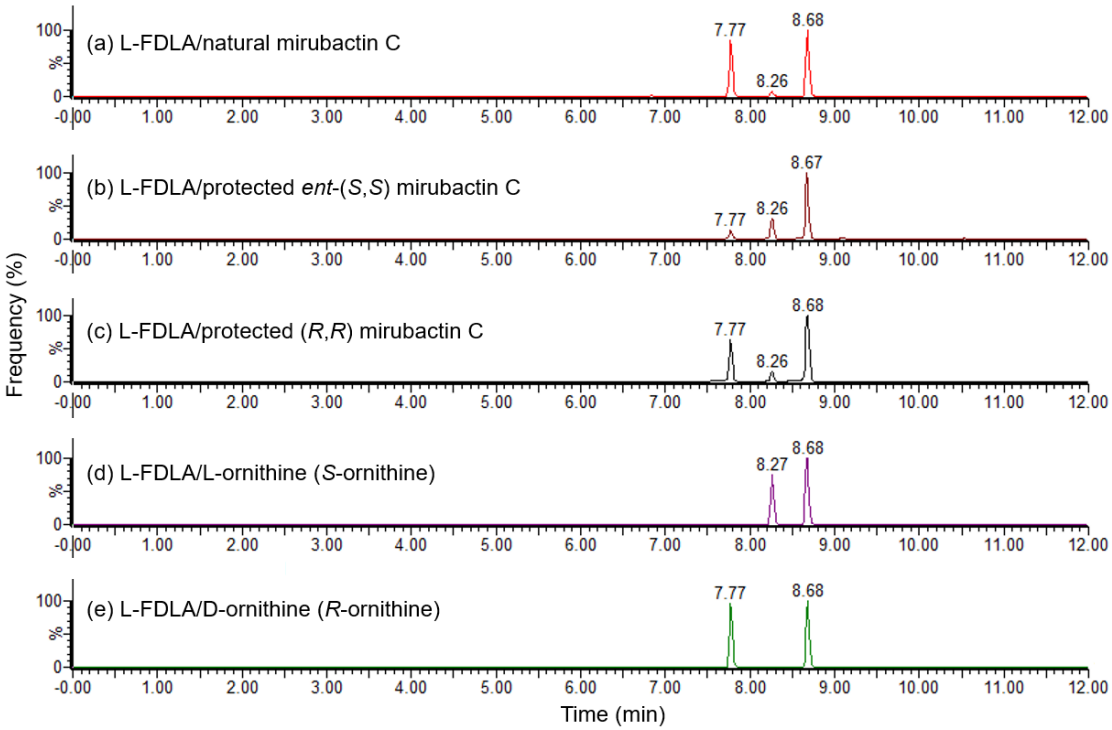

Figure 2.27. LCMS extracted ion chromatogram (EIC *m*/*z* = 427.2, +/- 0.25 Da) showing (a) L-FDLA derivatised natural product mirubactin C; (b) L-FDLA derivatised protected *ent*-(*S*,*S*)-mirubactin C; (c) L-FDLA derivatised protected (*R*,*R*)-mirubactin C; Marfey's standards (d) L-FDLA/L-ornithine and (e) L-FDLA/D-ornithine.

to those observed for the L-FDLA/D-ornithine (*R*-ornithine) standard, confirming the (*R*,*R*)-stereochemistry for natural product mirubactin C (**32**) as observed previously.

However, the minor peak at 8.26 min corresponds to the presence of a small amount of *S*-ornithine (*cf*. peak at 8.27 min for L-FDLA/L-ornithine (*S*-ornithine) standard), corresponding to an approximate ratio of 10 : 1 of (*R*) to (*S*) in the overall sample. Assuming that the natural product mirubactin C (**32**) consists of a mixture of only (*R*,*R*) and (*R*,*S*)/(*S*,*R*), and does not have significant quantities of (*S*,*S*), this would equate to a diastereomeric ratio (*dr*) of 4.5 : 1 (*R*,*R*) to (*R*,*S*)/(*S*,*R*) for the sample examined. The presence of *S*-ornithine in the sample suggests that racemisation has occurred in natural mirubactin C, either during isolation/storage or during the degradation by hydriodic acid during sample preparation. It should also be noted that the two Marfey's standards, L-FDLA/D-ornithine (*R*-ornithine) and L-FDLA/L-ornithine (*S*-ornithine)

show peaks with similar retention times at 8.68 min and cannot be used for comparison. Marfey's analysis of protected (*R*,*R*)-mirubactin C (*R*,*R*-**45**) showed a similar result with natural product mirubactin C (**32**), and also closely matched the L-FDLA/D-ornithine (*R*-ornithine) standard, confirming (*R*,*R*)-stereochemistry for protected (*R*,*R*)-mirubactin C (*R*,*R*-**45**). However, again a minor peak at 8.26 min was observed corresponding to the presence of (*S*)-ornithine, giving an overall 4 : 1 (*R*) to (*S*) ratio and a predicated 1.5 : 1 *dr* for the synthetic material.

Finally, Marfey's analysis of protected *ent*-(*S*,*S*)-mirubactin C (*S*,*S*-**45**) gave the major peaks at 8.26 and 8.67 min, matching the L-FDLA/L-ornithine (*S*-ornithine) standard, showing (*S*,*S*)-stereochemistry for synthetic protected (*S*,*S*)-mirubactin C (*S*,*S*-**45**). Again the peak at 7.77 min corresponding to (*R*)-ornithine was also present, showing an overall ratio of 1 : 3 (*R*) to (*S*), and a predicated 1 : 1 *dr*.

Therefore, based on these experiments we can conclude that both protected (*R*,*R*)-mirubactin C (*R*,*R*-**45**) and protected *ent*-(*S*,*S*)-mirubactin C (*S*,*S*-**45**) have the expected (*R*,*R*)- and (*S*,*S*)-stereochemistry as the predominant component, but in both cases significant quantities of the (*R*,*S*)/(*S*,*R*) diastereoisomer can be observed arising from racemisation during the synthesis.

To further understand to the stereochemistry of our protected *ent*-(*S*,*S*)-mirubactin C (*S*,*S*-**45**) and protected (*R*,*R*)-mirubactin C (*R*,*R*-**45**) samples, we examined both by chiral HPLC. Three samples were prepared in HPLC grade water: protected *ent*-(*S*,*S*)-mirubactin C (*S*,*S*-**45**), protected (*R*,*R*)-mirubactin C (*R*,*R*-**45**), and a racemic sample prepared by mixing protected *ent*-(*S*,*S*)-mirubactin C (*S*,*S*-**45**) and protected (*R*,*R*)-mirubactin C (*R*,*R*-**45**) in a 1 : 1 ratio. Following chiral HPLC method development (see appendix 1), all three samples were analysed on a CHIRALPAK® IC chiral column using a gradient iPrOH/MeOH system (**Figure 2.28**).

Chiral HPLC of the 1:1 mixture of both protected *ent*-(*S*,*S*)-mirubactin C (*S*,*S*-**45**) and protected (*R*,*R*)-mirubactin C (*R*,*R*-**45**) enantiomers analysis showed two major and one minor peak at 38.0, 50.9 and 45.3 min respectively. This demonstrated sufficient

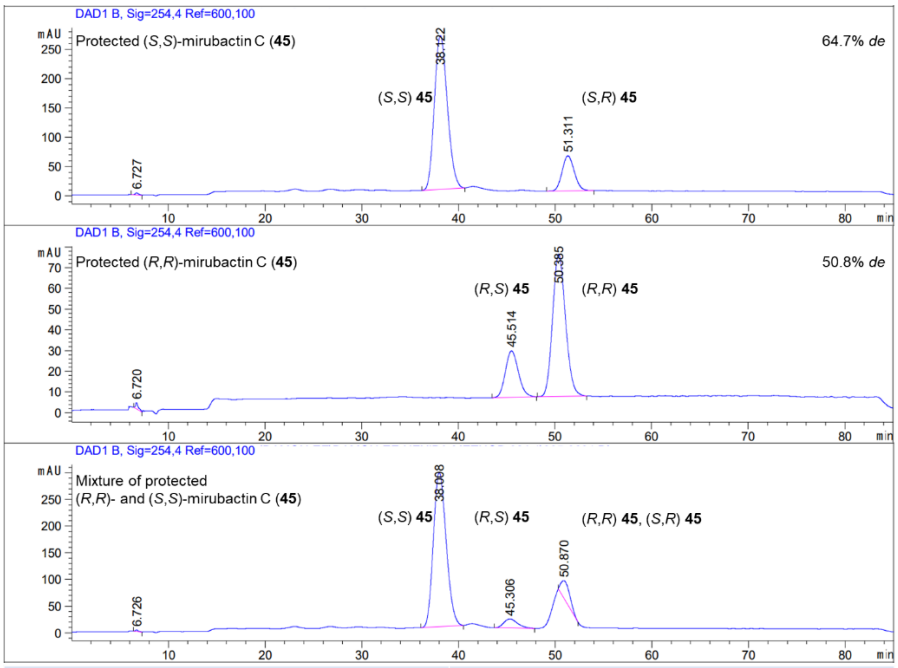

Synthetic Sample	Diastereomeric Ratio
Protected (*S*,*S*)-mirubactin C (*S*,*S*-**45**)	4.7 : 1 (*S*,*S* : *S*,*R*)
Protected (*R*,*R*)-mirubactin C (*R*,*R*-**45**)	1 : 3.1 (*R*,*S* : *R*,*R*)

Figure 2.28. Chiral HPLC (CHIRALPAK® IC, iPrOH/MeOH) analysis of: (top) protected *ent*-(*S*,*S*)-mirubactin C (*S*,*S*-**45**); (middle) protected (*R*,*R*)-mirubactin C (*R*,*R*-**45**); and (bottom) a 1:1 mixture of protected *ent*-(*S*,*S*)-mirubactin C (*S*,*S*-**45**) and protected (*R*,*R*)-mirubactin C (*R*,*R*-**45**).

separation of the stereoisomers present, suitable for further analysis.

Analysis of protected *ent*-(*S*,*S*)-mirubactin C (*S*,*S*-**45**) showed a major peak at 38.1 min and a minor peak at 51.3 min. By comparison to the other samples, we can assign the peak at 38.1 min as protected *ent*-(*S*,*S*)-mirubactin C (*S*,*S*-**45**), whilst the minor peak at 51.3 min is likely to be the corresponding (*R*,*S*)/(*S*,*R*)-diastereoisomer as observed by the supporting Marfey's analysis. Similarly, protected (*R*,*R*)-mirubactin C (*R*,*R*-**45**) showed a major peak at 50.4 min and a minor peak at 45.5 min, which we also assigned as protected (*R*,*R*)-mirubactin C (*R*,*R*-**45**) and the corresponding (*R*,*S*)/(*S*,*R*)-diastereoisomer respectively.

To determine which (*R*,*S*)- or (*S*,*R*)-diastereoisomer might be present in each sample we re-examined of the specific rotations ($[\alpha]_D$) of the synthetic intermediates leading to protected *ent*-(*S*,*S*)-mirubactin C (*S*,*S*-**45**) and protected (*R*,*R*)-mirubactin C (*R*,*R*-

45). The two enantiomeric left-middle fragments, benzoyl substituted ornithine (*S*)-**46** (-14.0°) and (*R*)-**46** (+2.0°), give opposite specific rotations, suggesting that in the final products the first stereocentre remained intact particularly in the case of benzoyl substituted ornithine (*S*)-**46**. However the specific rotations of the enantiomeric right-hand fragments prior to coupling, (*S*)-benzyl 5-(*N*-(benzyloxy)formamido)-2-((*tert*-butoxycarbonyl)amino)pentanoate (**63**) (-8.3°) and (*R*)- (**63**) (+17.6°), showed significant differences suggesting more racemisation in this fragment, particular in the synthesis of protected *ent*-(*S*,*S*)-mirubactin C (*S*,*S*-**45**). Therefore, we propose that the observed diastereoisomers had epimerised at the second stereocentre, near to the *N*-terminus, the protected *ent*-(*S*,*S*)-mirubactin C (*S*,*S*-**45**) sample containing a (*S*,*R*)-diastereoisomer and the protected (*R*,*R*)-mirubactin C (*R*,*R*-**45**) sample containing a (*R*,*S*)-diastereoisomer.

Integration of the major and minor peaks gave an approximate 5 : 1 *dr* for protected *ent*-(*S*,*S*)-mirubactin C (*S*,*S*-**45**) and a 3 : 1 *dr* for protected (*R*,*R*)-mirubactin C (*R*,*R*-**45**). It should be noted that the *dr*'s calculated from chiral HPLC do not match those seen with previous Marfey's analysis, thus further investigation of this will be required in the future.

Since we planned to use semi-preparative HPLC for final purification, after global deprotection, we decided at this stage to continue with a mixture of diastereoisomers.

2.4.7 Synthesis of (*R*,*R*)-Mirubactin C (*R*,*R*-32) and *ent*-(*S*,*S*)-Mirubactin C (*S*,*S*-32) via Global Deprotection

After confirming that our samples of protected (*R*,*R*)-mirubactin C (*R*,*R*-**45**) and protected *ent*-(*S*,*S*)-mirubactin C (*S*,*S*-**45**) contained the desired enantiomer as the major component, we proceeded to examine the final synthetic step, in which we will plan to remove four benzyl and one Cbz protecting groups at the same time. Based on research by Kakeya *et al.* in which hydrogenolysis was used to fully deprotect chlorocatechelin A,[64] we planned to use excess hydrogen as a reducing agent with catalytic Pd/C to perform a global deprotection of both protected (*R*,*R*)-mirubactin C (*R*,*R*-**45**) and *ent*-(*S*,*S*)-mirubactin C (*S*,*S*-**45**).

We therefore started by reacting 0.087 mmol of protected *ent*-(*S*,*S*)-mirubactin C (*S*,*S*-**45**) with excess hydrogen, at atmospheric pressure, in the presence of 10% Pd/C at room temperature for 2 hours. Afterwards, the Pd/C was removed using a C8 SPE cartridge, which was then eluted with MeOH and the filtrate was concentrated under reduced pressure to give 35 mg of crude material (**Scheme 2.20**).

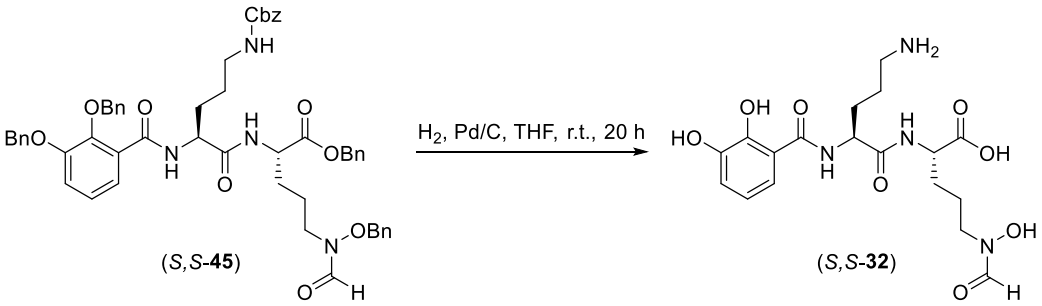

Scheme 2.20. Global deprotection of protected *ent*-(*S*,*S*)-mirubactin C (*S*,*S*-**45**) to give *ent*-(*S*,*S*)-mirubactin C (*S*,*S*-**32**)

Analysis of the crude sample by ^{1}H NMR spectra showed a number of signals corresponding to benzyl methylenes, suggesting that the reaction had not gone to completion. Therefore the crude material was resubmitted to the reaction conditions for an additional 18 h. Following work up as previously described, approximately 8 mg of crude material was recovered. ^{1}H NMR spectrum showed no signals in the benzylic region, suggesting that all protecting groups had been successfully removed (**Figure 2.29**).

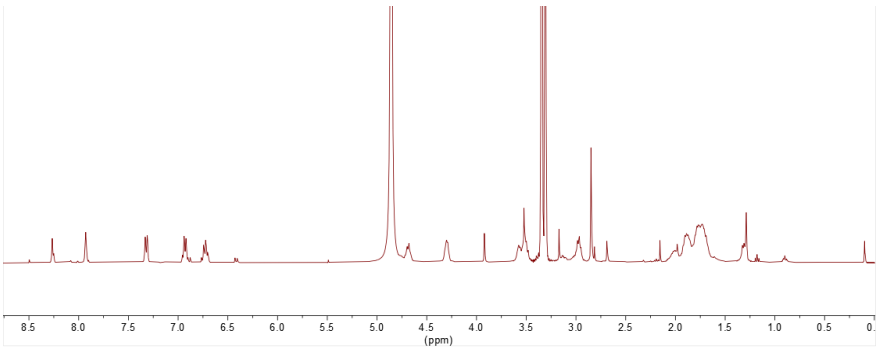

Figure 2.29. ^{1}H NMR (CD_3OD) of crude deprotected *ent*-(*S*,*S*)-mirubactin C (*S*,*S*-**32**).

^{1}H NMR of the crude *ent*-(*S*,*S*)-mirubactin C (*S*,*S*-**32**) showed the presence of diastereoisomers, thus the sample was separated by semi-preparative HPLC (C18, gradient 5%-15% ACN) and the individual peaks were analysed by LCMS, in comparison to a sample of the natural product. Semi-preparative HPLC and LCMS analysis were carried out by Dr Bernhard Kepplinger.

Semi-preparative HPLC of crude *ent*-(*S*,*S*)-mirubactin C (*S*,*S*-**32**) gave four main peaks at 31.7, 39.1, 42.0 and 43.1 min. In addition, natural product mirubactin C (**32**) was also purified by semi-preparative HPLC, and gave a single peak at 39.2 min, suggesting that peak 2 of crude *ent*-(*S*,*S*)-mirubactin C (*S*,*S*-**32**) corresponds to the correct relative stereochemistry. Each of the peaks from *ent*-(*S*,*S*)-mirubactin C (*S*,*S*-**32**) was collected and analysed by HR-LCMS (**Figure 2.30**).

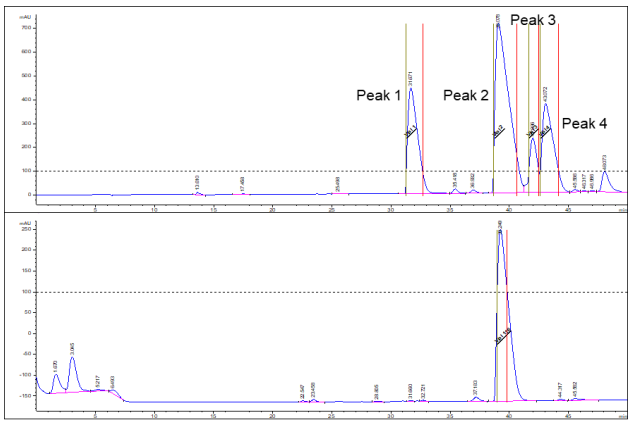

Figure 2.30. HPLC of crude *ent*-(*S*,*S*)-mirubactin C (top) and natural product (bottom)

HR-LCMS of peaks 1 and 2 showed the presence of ions with *m/z* = 427.1833 and 427.1785 respectively, which matched those observed for the natural product mirubactin C, *m/z* = 427.1783 $[M+H]^+$. The natural product has a molecular formula of $C_{18}H_{26}N_4O_8H$ which gives a calculated *m/z* = 427.1829 $[M+H]^+$, suggesting that both peaks 1 and 2 from *ent*-(*S*,*S*)-mirubactin C (*S*,*S*-**32**) have the same molecular formula as the natural product. In addition, peak 2 (39.1 min) also has similar retention to the natural product (39.2 min), therefore peak 2 can be assigned as the (*S*,*S*)-enantiomer of the natural product. Whilst peak 1 (31.7 min) is likely the (*S*,*R*)-(**32**) diastereoisomer (**Figure 2.31**).

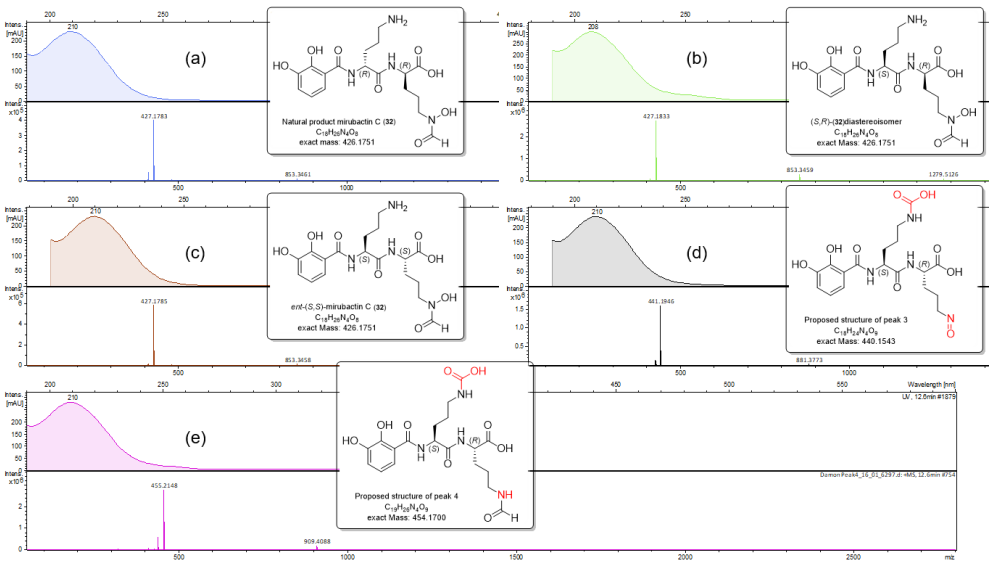

Figure 2.31. HR-LCMS analysis showing UV/Vis and mass spectra of (a) natural product mirubactin C (**32**); (b) peak 1 (31.7 min), (*S*,*R*)-(**32**) diastereoisomer; (c) peak 2 (39.1 min), *ent*-(*S*,*S*)-mirubactin C (*S*,*S*-**32**); (d) peak 3 (42.0 min), with proposed structure; (e) peak 4 (43.1 min), with proposed structure.

The remaining two peaks, 3 and 4, were also analysed by HR-LCMS giving major ions with *m/z* = 441.1946 and 455.2148. These were both assigned as $[M+H]^+$ by observation of the associated $[2M+H]^+$ ions in the spectra. We propose that peaks 3 and 4 correspond to by-products from the hydrogenation step. Peak 3 (**Figure 2.31**; (d)) potentially shows a by-product arising from the incomplete removal of the Cbz group along with an unexpected formation of a nitroso group. Whilst peak 4 (**Figure 2.31**; (e)) may arise from incomplete removal of the Cbz group, and reduction of the hydroxamic acid.[78] The purified samples of peaks 1 to 4 were subsequently used by Dr Bernhard Kepplinger in biological studies.

Following these promising results, next we decided to continue to examine the global deprotection of our synthetic (*R*,*R*)-mirubactin C (**45**) and *ent*-(*S*,*S*)-mirubactin C (**45**), to provide sufficient material for characterisation and additional biological evaluation. Since at this stage, the amount of protected (*S*,*S*)-mirubactin C (*S*,*S*-**45**) was limited, we focussed on the global deprotection of protected (*R*,*R*)-mirubactin C (*R*,*R*-**45**).

Therefore, 0.11 mmol of protected (*R*,*R*)-mirubactin C (*R*,*R*-**45**) was hydrogenated at atmospheric pressure, with 10% Pd/C at room temperature. After 3 hours the Pd/C was removed using a C8 SPE cartridge, which was then eluted with MeOH and the filtrate concentrated under reduced pressure, as previously. However, ^{1}H NMR showed that the reaction was incomplete and the crude material was resubmitted to the reaction conditions for a further 16 hours. Following work-up as before, 24 mg of crude material was obtained and ^{1}H NMR showed the presence of one major diastereoisomer (**Figure 2.32**).

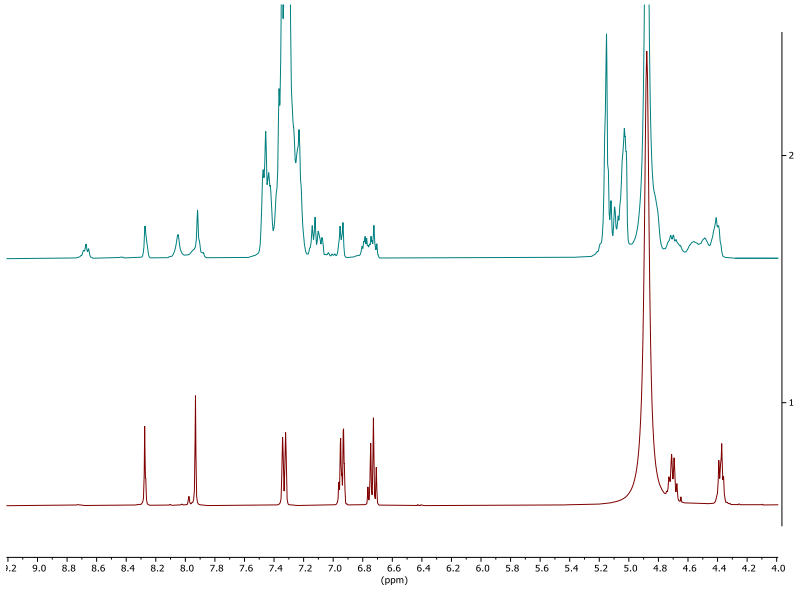

Figure 2.32. Comparison of ^{1}H NMR of crude protected (*R*,*R*)-mirubactin C (*R*,*R*-**45**) following global deprotection for 3 hours (top) and following global deprotection for a total of 19 hours (bottom).

Then the crude (*R*,*R*)-mirubactin C (*R*,*R*-**32**) was purified by a C18 reversed phase semi-preparative HPLC column using a similar method as previously (a gradient MeCN/H_2O system with 0.1% formic acid), using the natural product mirubactin C (**32**) as a standard. It should be noted that synthetic (*R*,*R*)-mirubactin C (*R*,*R*-**32**) shows slightly different retention times (24.8 vs 27.0 min) and peak shapes to natural product mirubactin C (**32**), due to differences in the injection volume (**Figure 2.33**).

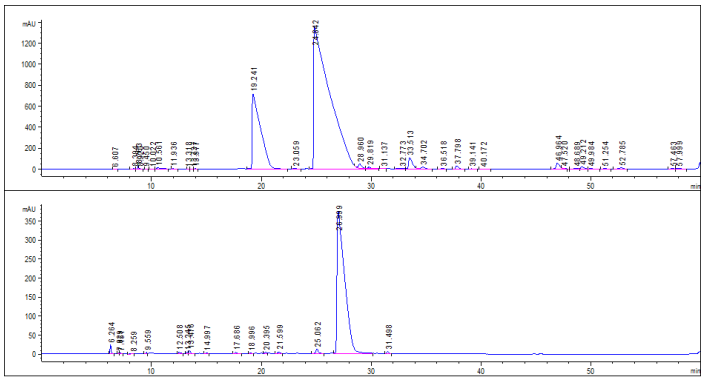

Figure 2.33. Semi-preparative HPLC purification of (*R*,*R*)-mirubactin C (*R*,*R*-**32**) (top), compared to the natural product mirubactin C (**32**) (bottom).

The semi-preparative HPLC of crude (*R*,*R*)-mirubactin C (*R*,*R*-**32**) gave our two main peaks at 19.2 and 24.8 min. Based on previous experience and in comparison to the natural product (27.0 min), we suggest that peak 1 is the diastereomeric (*R*,*S*)-mirubactin C (*R*,*S*-**32**) and peak 2 is our desired (*R*,*R*)-mirubactin C (*R*,*R*-**32**).

Therefore, peak 2 was collected and the formic acid (from the HPLC eluent) was neutralised by dropwise addition of 2 M aqueous NaOH until a pH of 7 was obtained, then the solvent was removed under reduced pressure. To aid in removal of water, multiple portions of MeCN were added periodically and solvent removal continued over the course of a day. Finally, the sample was dried under a flow of nitrogen gas.

The residue was then dissolved in 5 mL HPLC grade water and injected to the LH-20 size exclusion chromatography (eluent, HPLC grade water), to allow for desalting and final purification. A fraction containing (*R*,*R*)-mirubactin C (*R*,*R*-**32**) was obtained, the solvent was removed under reduced pressure, with the periodic addition of portions of MeCN to aid in removal of the water, and the sample was finally dried under a flow of nitrogen gas over 24 hours to give a white solid.

Unfortunately, ^{1}H NMR showed that sodium formate (8.49 ppm) was still present in the sample. Therefore we resubmitted the sample to LH-20 size exclusion chromatography for further purification, following which solvent removal as before afforded a light brown solid.

^{1}H NMR showed that we had successfully removed sodium formate, but unfortunately (*R*,*R*)-mirubactin C (*R*,*R*-**32**) had been contaminated by an unknown impurity, with

peaks at 3.77 – 3.67 ppm (m), 3.21 ppm (q, J = 7.3 Hz), 1.38 – 1.31 ppm (m) and 1.29 ppm (t, J = 7.2 Hz). Further NMR studies, including 2D NMR, failed to identify the impurity.

In order to clean up our (*R*,*R*)-mirubactin C (*R*,*R*-**32**) sample, it was dissolved in water and washed with EtOAc, subjected to high vacuum overnight, and twice resubmitted to size exclusion chromatography. Size exclusion chromatography led to a substantial decrease in impurity levels, but with decreasing sample recovery and the appearance of some degradation products (**Figure 2.34**).

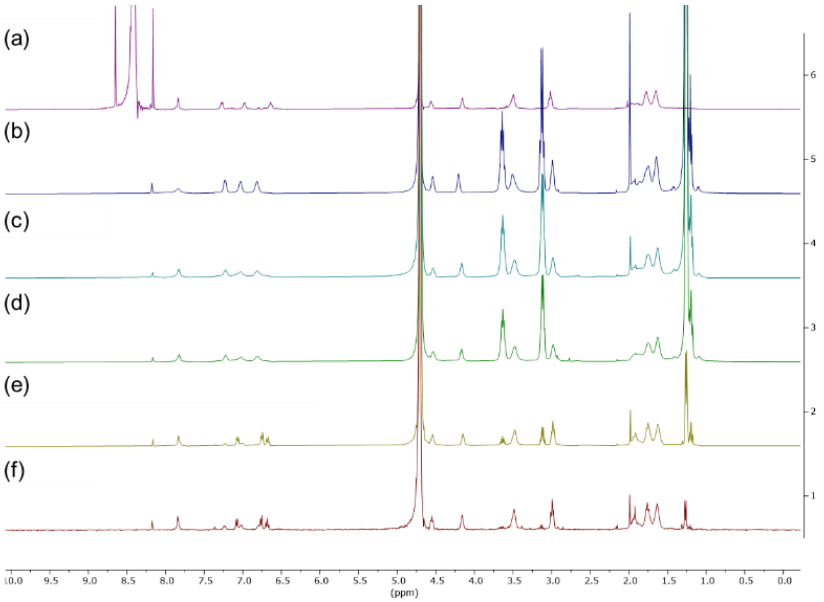

Figure 2.34. ^{1}H NMR (D_2O) comparison of (*R*,*R*)-mirubactin C (*R*,*R*-**32**) (a) After first attempt size exclusion chromatography; (b) After second attempt size exclusion chromatography; (c) After washed with EtOAc; (d) After high vacuum overnight; (e) After third attempt size exclusion chromatography; (f) After fourth attempt size exclusion chromatography.

Therefore, to obtain new material for purification, we then repeated the global deprotection of protected (*R*,*R*)-mirubactin C (*R*,*R*-**45**) on a 0.228 mmol scale, with an increased reaction time of 24 hours. After removing the Pd/C by filtration through a C8 SPE cartridge, the crude product was analysed by Marfey's analysis to check absolute stereochemistry (**Figure 2.35**).

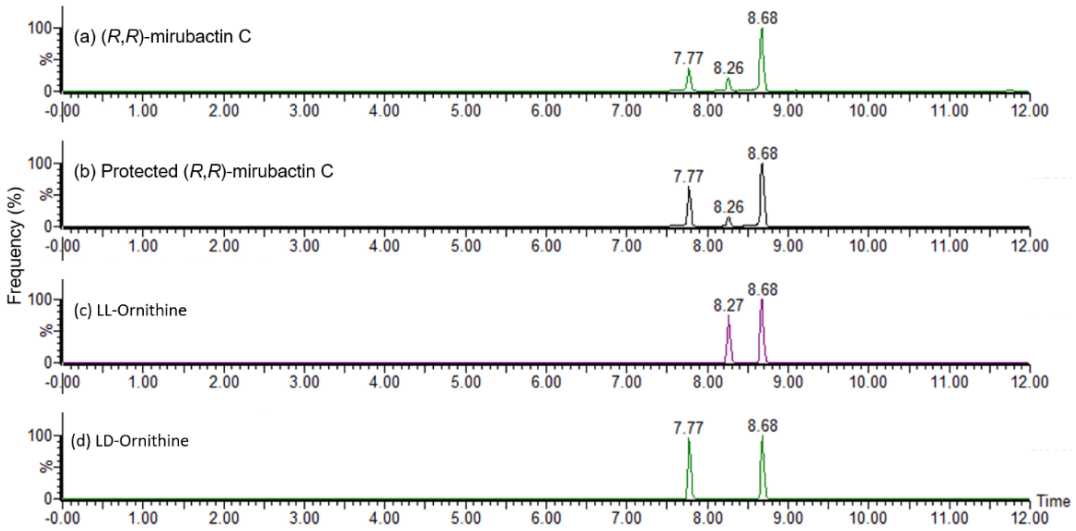

Figure 2.35. LCMS extracted ion chromatogram (EIC *m*/*z* = 427.2, +/- 0.25 Da) showing: (a) L-FDLA derivatised deprotected (*R*,*R*)-mirubactin C (*R*,*R*-**32**); (b) L-FDLA derivatised protected (*R*,*R*)-mirubactin C (*R*,*R*-**45**) and Marfey's standards (c) L-FDLA/L-ornithine and (d) L-FDLA/D-ornithine.

Previous analysis of protected (*R*,*R*)-mirubactin C (*R*,*R*-**45**) (shown again in **Figure 2.35**) showed that the presence of both (*R*)-ornithine and (*S*)-ornithine derivatives in a ~ 4.2 : 1 (*R*) to (*S*) ratio, allowing an estimation of the diastereomeric ratio (*dr*) for the molecule of 1.6 (*R*,*R*) : 1 (*R*,*S*)/(*S*,*R*). Following global deprotection, Marfey's analysis of the resulting synthetic (*R*,*R*)-mirubactin C (*R*,*R*-**32**) showed a ratio of 1.8 : 1 (*R*) to (*S*) ratio of ornithine derivatives, resulting in an estimated *dr* for the molecule of approximately 0.4 (*R*,*R*) : 1 (*R*,*S*)/(*S*,*R*).

Since our (*R*,*R*)-mirubactin C (*R*,*R*-**32**) sample still likely contained the desired enantiomer as the major component, we continued the purification by semi-preparative HPLC. However, comparison against the natural product mirubactin C (**32**) (23.6 min) showed the presence of (*R*,*R*)-mirubactin C (*R*,*R*-**32**) (24.3 min) and the diastereomeric (*R*,*S*)-mirubactin C (*R*,*S*-**32**) (17.5 min), showing a *dr* of approximately 3.4 (*R*,*R*) : 1 (*R*,*S*). The HPLC result of the synthetic (*R*,*R*)-mirubactin C (*R*,*R*-**32**) sample indicated that the desired (*R*,*R*)-mirubactin C (*R*,*R*-**32**) was still the dominant component. In order to isolate (*R*,*R*)-mirubactin C (*R*,*R*-**32**), peak 2 was collected, neutralised and the solvent removed as before (**Figure 2.36**).

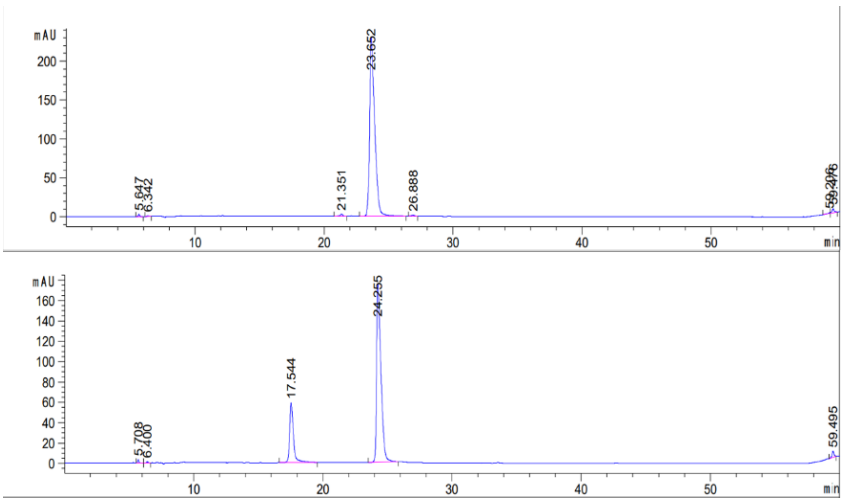

Figure 2.36. Semi-preparative HPLC purification of (*R*,*R*)-mirubactin C (*R*,*R*-**32**) (bottom), compared to the natural product mirubactin C (**32**) (top)

Next we carried out further purification by size exclusion chromatography. Following collection of the peak containing (*R*,*R*)-mirubactin C (**32**), ^{1}H NMR showed that sodium formate was still present, some remaining even after two additional attempts at purification by size exclusion chromatography. However, due to prolonged purification efforts, some degradation was observed (**Figure 2.37**).

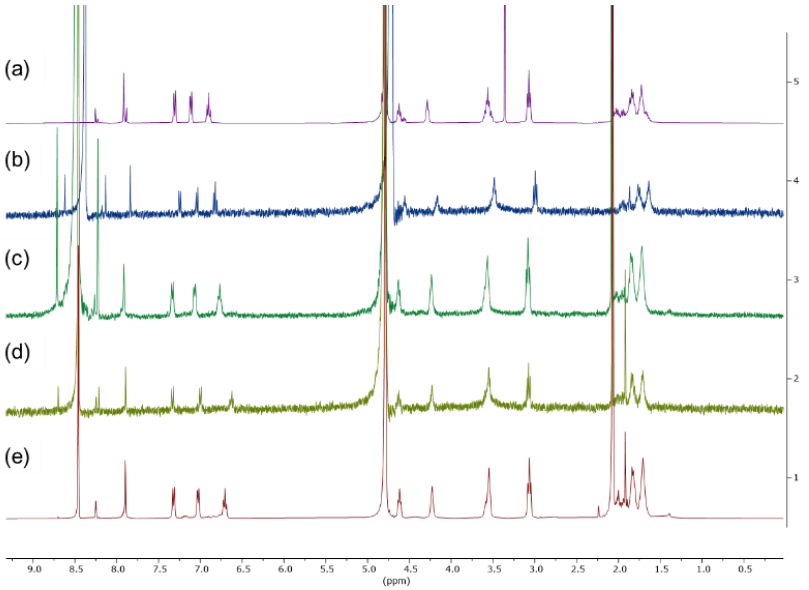

Figure 2.37. ^{1}H NMR (D_2O) comparison of (a) After hydrogenation; (b) After purification from HPLC and neutralisation; (c) After first attempt size exclusion chromatography; (d) After second attempt size exclusion chromatography; (e) After third attempt size exclusion chromatography.

Due to the continued difficulties in removing sodium formate, we decided not to use formic acid during any new purifications by semi-preparative HPLC. Also we decided to investigate the use of freeze-drying to reduce decomposition during the solvent removal stage.

Therefore we prepared a new sample of deprotected (*R*,*R*)-mirubactin C (*R*,*R*-**32**), by reacting 0.27 mmol of protected (*R*,*R*)-mirubactin C (*R*,*R*-**45**) in THF at room temperature, with 110 mg of 10% Pd/C, under a flow of hydrogen gas over 2 hours, followed by an additional 16 hours under a static atmosphere of hydrogen. After the removal of Pd/C by filtration through a C8 SPE cartridge, the crude reaction mixture was purified using semi-preparative HPLC using a gradient MeCN/H_2O eluent system without any formic acid. By comparison with the retention time of natural product mirubactin C (**32**) (23.3 min), a fraction (peak 2) was identified which contained the desired (*R*,*R*)-mirubactin C (*R*,*R*-**32**) (22.4 min), whilst peak 1 contained the diastereomeric (*R*,*S*)-mirubactin C (*R*,*S*-**32**) (17.7 min). Peaks 1 and 2 were collected and the solvent was removed over 16 hours using a freeze-drier to give us a colourless crystalline solid (**Figure 2.38**).

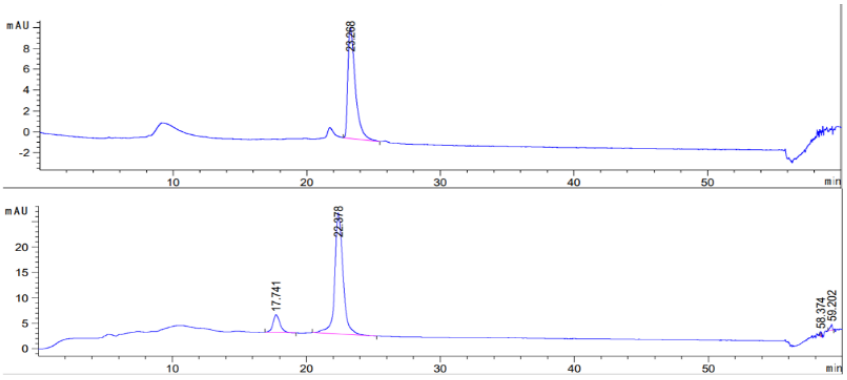

Figure 2.38. Semi-preparative HPLC (without formic acid) purification of (*R*,*R*)-mirubactin C (*R*,*R*-**32**) (bottom), compared to the natural product mirubactin C (**32**) (top).

^{1}H NMR comparison against natural product mirubactin C (**32**), showed that we had successfully made the (*R*,*R*)-mirubactin C (*R*,*R*-**32**) as well as the diastereomeric (*R*,*S*)-mirubactin C (*R*,*S*-**32**). However (*R*,*R*)-mirubactin C (*R*,*R*-**32**) appeared to

decompose on storage, even at -20 °C in D_2O, as further analysis using high-field NMR (700 MHz) showed an increasing quantity of a new unidentified molecule appearing in the spectra over time. (**Figure 2.39**).

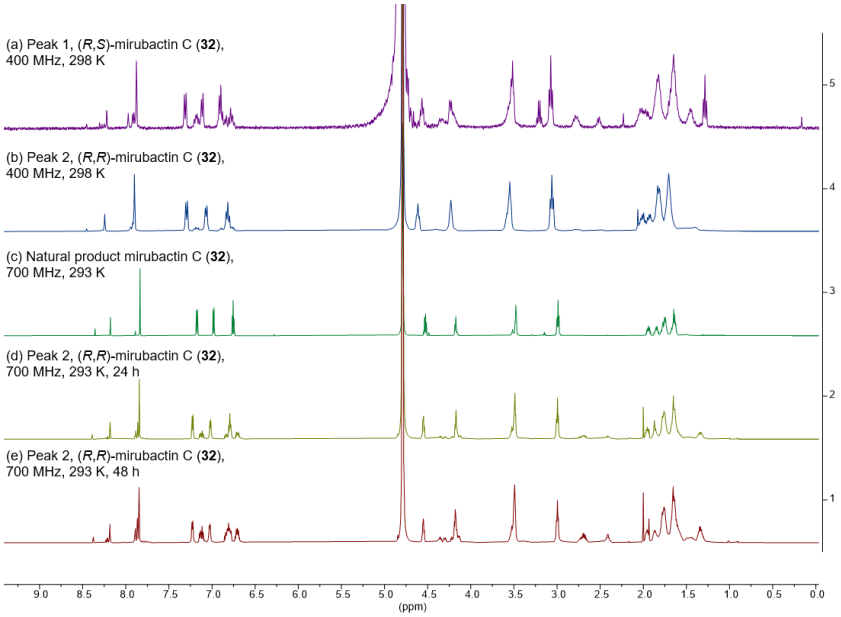

Figure 2.39. ^1H NMR (D_2O) comparison of (a) Distereomeric (*R*,*S*)-mirubactin C (*R*,*S*-**32**); (b) (*R*,*R*)-mirubactin C (*R*,*R*-**32**); (c) Natural product mirubactin C (**32**); (d) (*R*,*R*)-mirubactin C (*R*,*R*-**32**) over 24 hours; (e) (*R*,*R*)-mirubactin C (*R*,*R*-**32**) over 48 hours.

In conclusion, global deprotection of both protected (*R*,*R*)-mirubactin C (*R*,*R*-**45**) and *ent*-(*S*,*S*)-mirubactin C (*R*,*R*-**45**) was successful, but we encountered multiple purification issues. Our optimised purification involves semi-preparative HPLC (without formic acid) followed by solvent removal by freeze drying. However the samples obtained appear to suffer from a degradation problem over time.

2.5 Metal Binding Affinity Investigation of Mirubactin C

For a better understanding of the mode-of-action of mirubactin C, we planned to measure the metal binding affinity of natural product mirubactin C (**32**) with different metals. Isothermal titration calorimetry (ITC) is a technique for determining the thermodynamic parameters (affinity, enthalpy, and stoichiometry) of a binding interaction through an experiment in which one reactant is titrated to a second reactant

under isothermal conditions.[79] Binding affinity (K_D) and stoichiometry (N) can be determined from the fitted curve (**Figure 2.40**).[80,81]

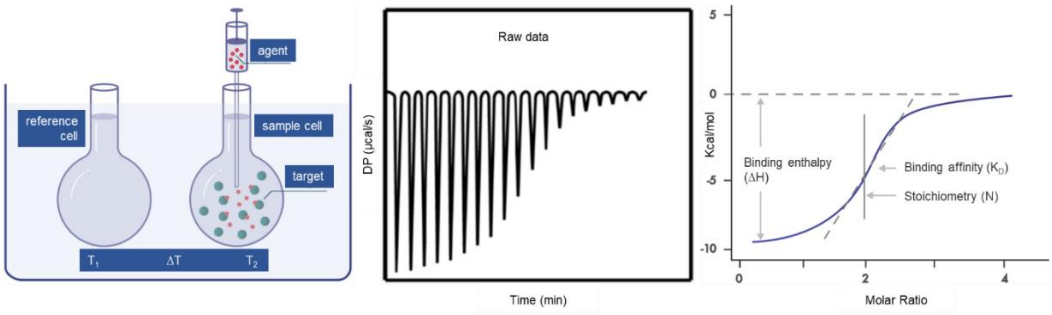

Figure 2.40. An ITC experiment (left) experimental setup module, the heat absorbed or generated during the binding reaction is measured and allows the calculation of various interaction parameters; (middle) raw data output, each titrant and integrated area of each peak corresponding to enthalpy is measured. (right) Sigmoidal curve of the released or consumed enthalpy per mol against the molar ratio in order to derive binding affinity (K_D) and reaction stoichiometry (N).[82,83]

Before we measured the metal binding affinity of natural product mirubactin C, we planned to validate the method by running test experiments using a well-known metal-chelating agent, Ethylenediaminetetraacetic acid (EDTA) and a series of M^{2+} ions, such as Ca^{2+}, Mn^{2+} and Mg^{2+}.

Therefore we first examined the binding of $CaCl_2$ with EDTA. Using a MicroCal PEAQ-ITC, a 1mM $CaCl_2$ solution in 10 mM MES buffer (pH = 6.0), in a syringe, was titrated into a 0.1 mM EDTA solution in 10 mM MES buffer (pH = 6.0), in the sample cell. Starting from the first injection of 0.4 µL, an additional 19 injections of 2 µL each, every 150 sec, occurred over 50 min at 25 °C. The binding affinity of EDTA-$CaCl_2$ was analysed using the MicroCal PEAQ-ITC Analysis Software, giving a binding curve which was a similar shape to that reported, with a stoichiometry (N = 0.89) and dissociation constant (K_D = 5.69E-07 M) also similar to that reported (N = 0.97 +/- 5% sites and K_D = 534E-9 +/- 20% M, PEAQ-ITC manual). This demonstrated that 1 equivalent of EDTA was binding approximately 1 equivalent of Ca^{2+} (**Figure 2.41**).

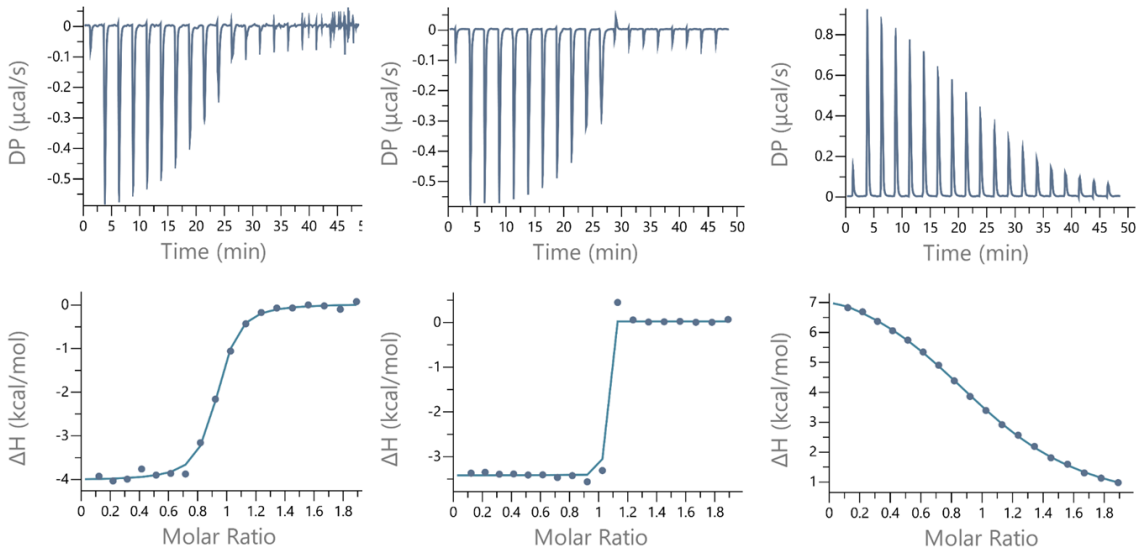

Figure 2.41. ITC analysis of Ca^{2+} (left), Mn^{2+} (middle) and Mg^{2+} (right) binding to EDTA. Baseline corrected raw ITC titrations (top) and the derived binding isotherm (bottom) in the presence of 10 mM $CaCl_2$, $MnSO_4$ and $MgSO_4$.

Then we undertook the same procedure to measure the metal binding affinity of Mn^{2+} and Mg^{2+} with EDTA respectively. ITC analysis for both metals showed the expected 1 : 1 binding stoichiometry (N = 1.01 [Mn^{2+} + EDTA], N = 1.03 [Mg^{2+} + EDTA]). Furthermore, the Mn^{2+} binds to EDTA more strongly than Ca^{2+} as can be seen by the sharp response in the binding curve. Interestingly the binding of Mg^{2+} with EDTA shows an endothermic process, as seen by the decreasing binding curve, which has been previously reported (**Table 2.12**).[84]

Entry	1	2	3
Sample	$CaCl_2$ + EDTA	$MnSO_4$ + EDTA	$MgSO_4$ + EDTA
N (sites)	0.89	1.01	1.03
K_D (M)	5.69E-07	1.00E-12	1.69E-05
ΔH (kcal/mol)	-4.04	-3.44	8.1
ΔG (kcal/mol)	-8.52	-16.4	-6.52
-TΔS (kcal/mol)	-4.48	-12.9	-14.6

Table 2.12. Thermodynamic properties of [Ca^{2+}/ Mn^{2+}/ Mg^{2+} +EDTA] binding obtained.

Following these test experiments, we used a similar procedure to examine the metal binding affinity of Mg^{2+} with the natural product mirubactin C (**32**). A freshly prepared 10 mM solution of $MgSO_4$ in 10 mM CHES buffer (pH = 10.2), in a syringe, was titrated into a 1 mM natural product solution in 10 mM CHES buffer (pH = 10.2), in the sample cell. Starting from the first injection of 0.4 µL, an additional 19 injections of 2 µL each, every 150 sec, occurred over 50 min at 25 °C. Analysis of the binding affinity of Mg^{2+} and natural product mirubactin C (**32**), gave a binding curve with a stoichiometry (N = 1.1) and dissociation constant (K_D = 1.21E-06 M), which demonstrated that 1 equivalent of natural product mirubactin C (**32**) was binding approximately 1 equivalent of Mg^{2+}. The first 10 injections gave the expected response, however after this the baseline showed significant noise, which may be due to issues with sample solubility. (**Figure 2.42**, (left); **Table 2.13**, Entry 1).

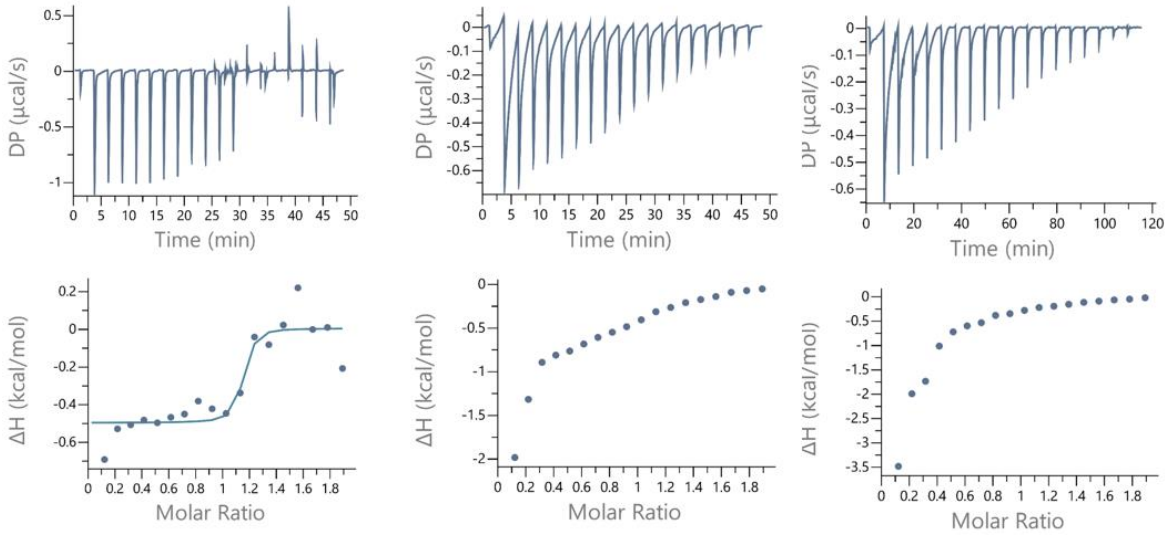

Figure 2.42. ITC analysis of Mg^{2+} interacting with mirubactin C (**32**).

We postulated that the problems observed in our first binding titration, may have been due to changes in pH during the experiment, or interactions with the buffer. Thus we repeated the metal binding affinity study between Mg^{2+} and the natural product mirubactin C (**32**) with an increased CHES buffer concentration (50 mM). However no binding was observed (**Figure 2.42**, (middle); **Table 2.13**, Entry 2). We next examined

increasing the time between each injection, to allow for the baseline to stabilise. Repeating the experiment with an increased “space time” of 360 s, gave better baseline recovery, but did not allow us to observe any binding effect (**Figure 2.42**, (right); **Table 2.13**, Entry 3).

Entry	1	2	3	4	5	6
Sample	$MgSO_4$ + mirubactin C (**32**)					
N (sites)	1.10	NA	NA	0.97	1.01	NA
K_D (M)	1.21E-06	NA	NA	1.02E-06	5.31E-06	NA
Concentration buffer (mM)	10	50	50	10	10	10
Space time (S)	150	150	360	150	150	150

Table 2.13. ITC analysis of Mg^{2+} interacting to mirubactin C (**32**) with optimise conditions.

We were concerned that both $MgSO_4$ and natural product mirubactin C may be unstable in the high pH conditions of the CHES buffer solution (pH = 10.2), or that the buffer itself may be interfering with the observation of binding. Therefore we then repeated the binding experiment at a lower concentration of CHES buffer (10 mM) with 150 s “space time” with freshly prepared samples. Similar “binding” results were observed, with similar issues with the baseline following stoichiometric addition of $MgSO_4$ (**Figure 2.43**, (left); **Table 2.13**, Entry 4). One hour later, the experiment was repeated again with the sample samples, giving very similar experimental outcomes. (**Figure 2.43**, (middle); **Table 2.13**, Entry 5). However, after the samples were stored overnight at stored at -20 °C, poor binding data was obtained (**Figure 2.43**, (right); **Table 2.13**, Entry 6). This strongly suggests sample degradation has occurred in the CHES buffer.

In conclusion, our preliminary data suggest that the natural product mirubactin C (**32**) binds 1 equivalent of Mg^{2+}. However difficulties in the experimental set-up have

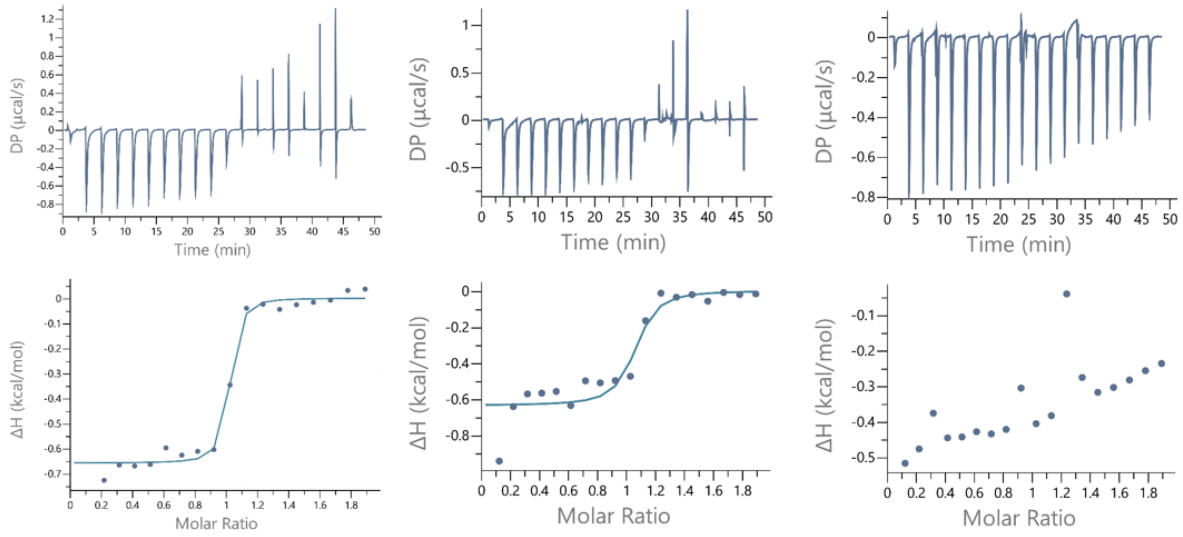

Figure 2.43. ITC analysis of Mg^{2+} interacting with mirubactin C (**32**).

prevented us from obtaining definitive binding data. In the future we would want to explore an alternative method to measure metal binding affinity, such as titration measured by UV absorption spectra.

2.6 Biological Evaluation of Synthetic Enantiomers of Mirubactin C

Now that we had access to synthetic *ent*-(*S*,*S*)-mirubactin C (*S*,*S*-**32**), we wished to measure the biological activity of the natural product against its enantiomer. We had previously postulated that if the observed biological activity arises from the molecule's ability to bind and transport metals than we would expect that synthetic *ent*-(*S*,*S*)-mirubactin C (*S*,*S*-**32**) and natural product mirubactin C to show the same biological activity. If differences are observed, then the mode-of-action may involve interaction with an enzyme target (such as LtaS).

Therefore, our synthetic *ent*-(*S*,*S*)-mirubactin C (*S*,*S*-**32**) (**Figure 2.30**, Peak 2) was used for biological studies in comparison to natural product mirubactin C (**32**) and synthetic (*R*,*R*)-mirubactin C (*R*,*R*-**32**) (provided by Dr Andrew Tyler). The biological evaluation was carried out by Dr Bernhard Kepplinger.

First the impact of natural and synthetic (*R*,*R*)-mirubactin C (*R*,*R*-**32**) on bacterial cell morphology was examined. Mutant *B. subtilis* (Δ*mbl B. subtilis*) was grown in low Mg^{2+}

growth media along with either natural or synthetic (*R*,*R*)-mirubactin C (*R*,*R*-**32**), alongside a high Mg^{2+} concentration experiment. In low Mg^{2+} growth media the expected unusual cell morphology was observed, whilst in the other three conditions the cell morphology is rescued and the normal rod-shape is seen, showing that synthetic (*R*,*R*)-mirubactin C (*R*,*R*-**32**) gives the same effect as the natural product (**Figure 2.44**).

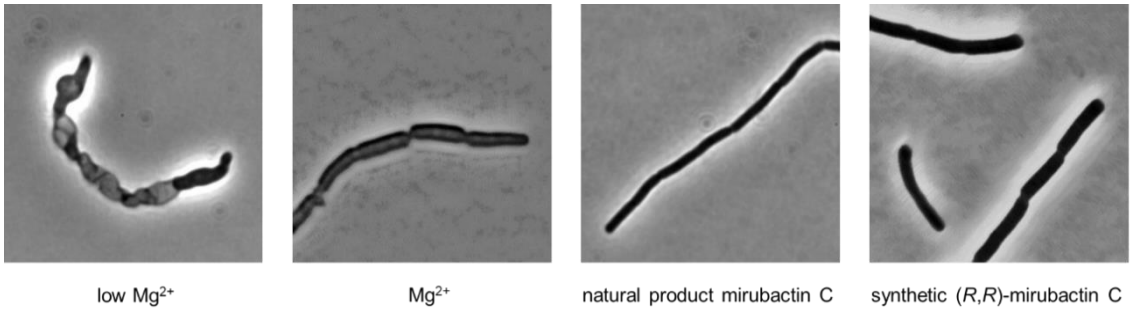

Figure 2.44. Bright-field microscopy showing growth and morphology in Δ*mbl B. subtilis* in the presence of low Mg^{2+} (3.8 μg/mL), high Mg^{2+} (20 mM), low Mg^{2+} (3.8 μg/mL) plus natural product mirubactin C and low Mg^{2+} (3.8 μg/mL) plus synthetic (*R*,*R*)-mirubactin C (*R*,*R*-**32**).

Next an *mbl*-recovery assay was undertaken in the presence of synthetic (*R*,*R*)-, (*S*,*S*)-, and natural mirubactin C (**32**). The *mbl*-recovery assay monitors the rate of cell growth of the Δ*mbl B. subtilis* mutant. Typically added Mg^{2+} is required to see normal cell growth, whilst low Mg^{2+} growth media results in very slow growth. This therefore allows us to quantify the impact of synthetic (*R*,*R*)-, (*S*,*S*)-, and natural mirubactin C (**32**) on the growth of Δ*mbl B. subtilis.*

In an early set of experiments, synthetic (*R*,*R*)-mirubactin C (*R*,*R*-**32**) and natural product mirubactin C (**32**) were compared. Both showed similar activity, with growth rescue occurring at a concentration of 32 μg/mL. This helps to confirm that the natural product mirubactin C (**32**) was the responsible factor for rescuing cell growth in a Δ*mbl B. subtilis* mutant (**Figure 2.45**).

Subsequently the rescue effects of synthetic of *ent*-(*S*,*S*)-mirubactin C (*S*,*S*-**32**) were

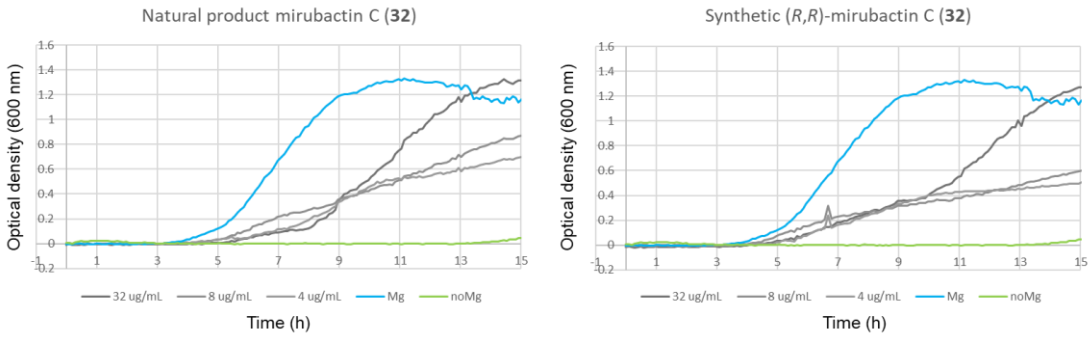

Figure 2.45. Δ*mbl B. subtilis* mutant recovery assay of natural product mirubactin C (**32**) and synthetic (*R*,*R*)-mirubactin C (*R*,*R*-**32**).

compared to natural product mirubactin C (**32**). The natural product mirubactin C (**32**) showed the optimal growth rescue at 6.25 µg/mL. Interestingly, dose-response growth rescue was observed up to 6.25 µg/mL, above which growth of the Δ*mbl* mutant was suppressed at higher concentrations.

In our synthetic *ent*-(*S*,*S*)-mirubactin C (*S*,*S*-**32**) sample, a positive dose-response for growth rescue was also observed up to 25 µg/mL, beyond which growth was suppressed. (**Figure 2.46**).

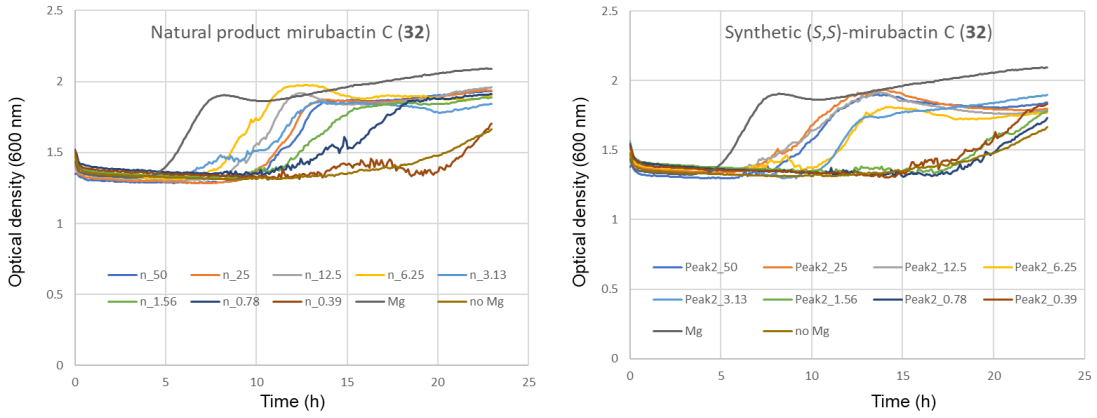

Figure 2.46. Δ*mbl B. subtilis* mutant recovery assay of natural product mirubactin C (**32**) and synthetic *ent*-(*S*,*S*)-mirubactin C (*S*,*S*-**32**).

From these results, it can be seen that both synthetic *ent*-(*S*,*S*)-mirubactin C (*S*,*S*-**32**) and natural product/(*R*,*R*)-mirubactin C (**32**) show similar growth rescue, although at

slightly different concentrations. Furthermore high concentrations of these molecules show suppression of growth. This suggests that the observed biological activity arises from a mode-of-action involving metal binding. The growth rescue of the Δ*mbl* mutant may therefore be occurring as the mirubactins tested help the bacteria to uptake Mg^{2+} even at lower overall concentrations, thus a metal transport mode-of-action.

In addition, the *mbl*-recovery assay was also performed with the diastereoisomeric (*S*,*R*)-mirubactin C (*S*,*R*-**32**), isolated by HPLC. This also showed growth rescue up to 50 μg/mL, a higher concentration than the previous samples. We would expect diastereoisomeric (*S*,*R*)-mirubactin C (*S*,*R*-**32**) to be a weaker binder of Mg^{2+}, thus needing a high concentration to observe similar growth rescue (**Figure 2.47**).

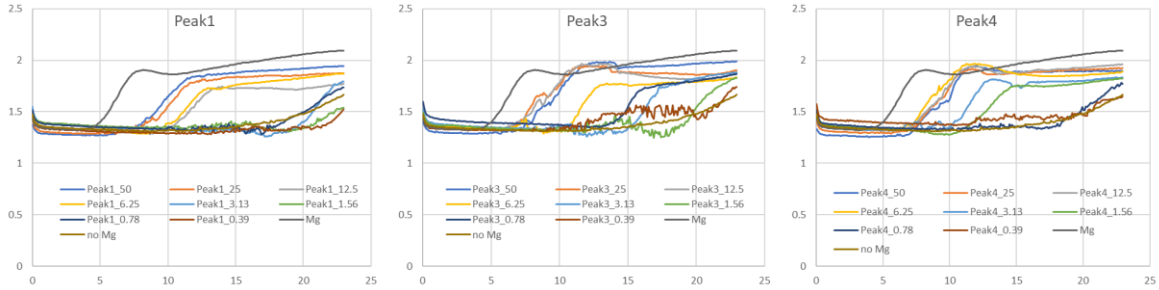

Figure 2.47. Δ*mbl B. subtilis* mutant recovery assay of synthetic (*S*,*R*)-mirubactin C (**32**) (**Figure 2.30**, Peak 1), Peak 3 (from **Figure 2.30**) and Peak 4 (from **Figure 2.30**).

2.7 Conclusions

In this chapter, we have confirmed the absolute stereochemistry of mirubactin C (**32**) by Marfey's analysis. Following which we have successfully developed a total synthesis of both enantiomers of mirubactin C (**32**) over 12 synthetic steps, although the final global deprotection and isolation still require optimisation.

We have also attempted to measure the metal binding affinity of the natural product mirubactin C (**32**) by ITC. Although binding stoichiometry was obtained, solubility and stability issues have prevented further binding data to be obtained.

Associated biological studies have shown that both mirubactin C and *ent*-mirubactin C show similar rescue activity, which leads us to believe that they are involved in metal

transport in the bacteria, aiding the bacteria in uptaking Mg^{2+} into the bacterial cell from their environment, and that these compounds are unlikely to be direct inhibitors of LtaS.

It also should be noted that during the preparation of this thesis, we have published a manuscript covering the structure determination of mirubactin C and its biological studies.[85]

Chapter 3. Total Synthesis of the Natural Product Siderophore Madurastatin C1

3.1 Introduction

In this chapter, we will present our work on the total synthesis of the polypeptide siderophore natural product madurastatin C1.

3.2 Madurastatin C1

Madurastatin C1 was isolated from a bacteria *Actinomadura* sp. DEM31376, by our collaborator Dr Hamed Mosaei Sejzi. *Actinomadura* sp. DEM31376 was isolated from a deep sea marine sediment from the Canary Basin in the Atlantic Ocean.[86] Madurastatin C1 showed potential antibiotic bioactivity and therefore was investigated further, of particular interest was the role of madurastatin C1 (**9**) as a bacterial siderophore in the *Actinomadura*, a known pathogenic species of bacteria.

3.3 Structure Determination and Relative Absolute Stereochemistry Assignment of Madurastatin C1

Madurastatin C1 was first isolated by Sosio *et al.* from *Actinomadura* sp.,[22] however the structure of madurastatin C1 was initially misassigned. Previous work in the group, by Dr Andrew Tyler, corrected the structure of madurastatin C1 (**9**) and solved the absolute stereochemistry (**Figure 3.1**).[23]

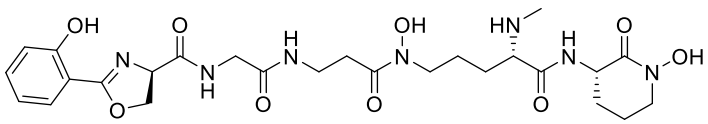

(**9**)

Figure 3.1. Structure of madurastatin C1 (**9**).

3.4 Retrosynthesis of Madurastatin C1

It should be noted that a number of the simpler madurastatins have been the targets

of total synthesis (rac)-madurastatin B1,[87] (rac)-madurastatin B3 etc.,[88] and considerable efforts have been made to synthesise related oxazoline containing NRP siderophores.[89] However a total synthesis of madurastatin C1 (**9**) has yet to be completed.

Based on previous work by Miller *et al*. on the total synthesis of related NRP siderophores,[90] we planned to synthesise madurastatin C1 (**9**) from three main fragments: the left-hand, middle and right-hand fragment (**Scheme 3.1**).

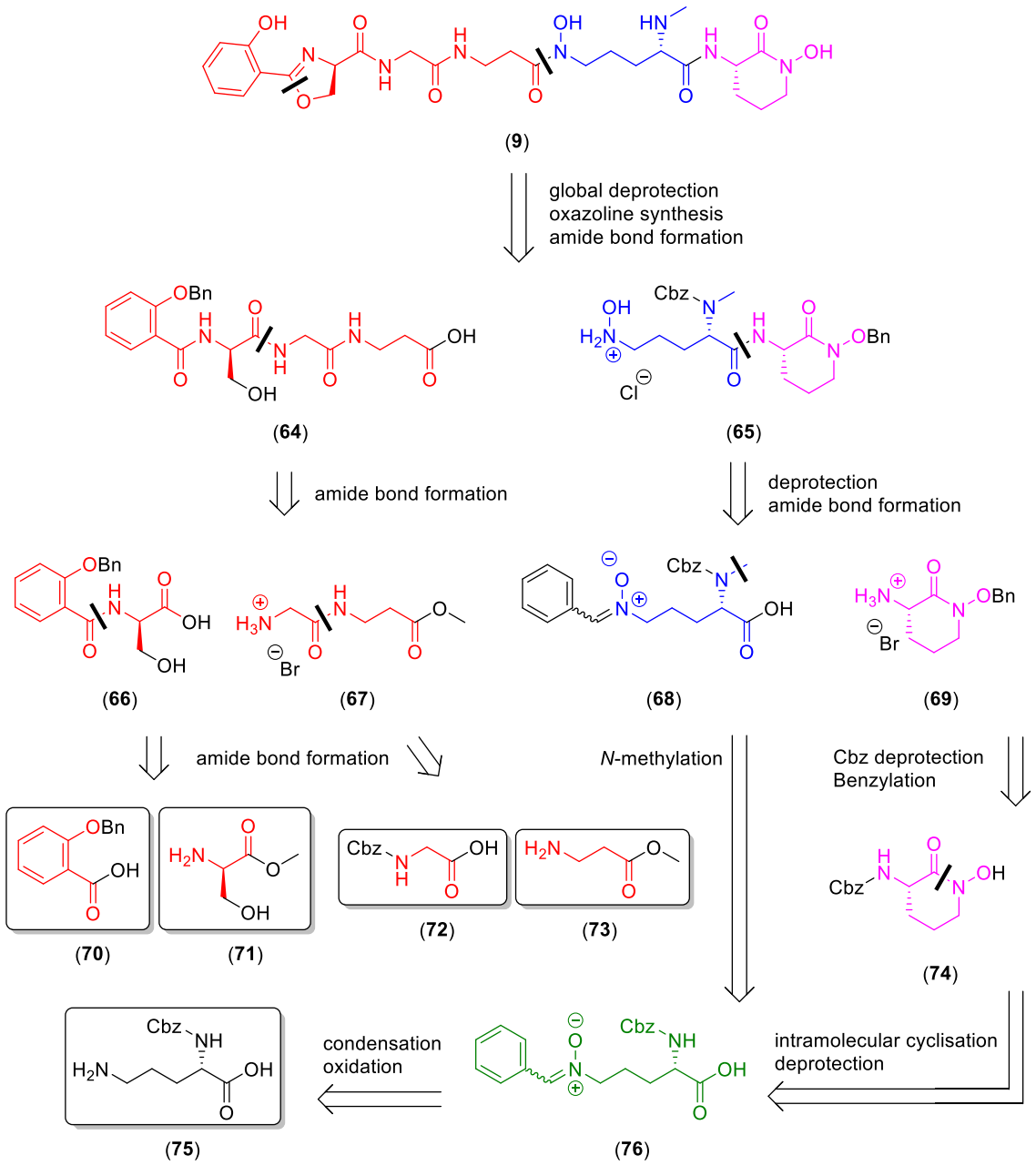

Scheme 3.1. Retrosynthetic analysis of madurastatin C1

The left-hand fragment would be made from four molecules, protected 2-hydroxybenzoic acid, D-serine hydrochloride, Cbz protected glycine and *β*-alanine methyl ester coupled together through amide bond formation. The middle and right-hand fragments will be based on a common intermediate, *N*-terminal Cbz protected L-ornithine. The three completed fragments will then be joined together with amide bond coupling reactions followed by a final oxazoline synthesis and a global deprotection step.

3.5 Synthesis of the Left-hand Fragment of Madurastatin C1

To begin our total synthesis of madurastatin C1, we decided to start with the synthesis of the left-hand fragment, from two key intermediates (2-(benzyloxy)benzoyl)-*D*-serine (**66**) and methyl 3-(2-aminoacetamido)propanoate (**79**) (**Scheme 3.2**).

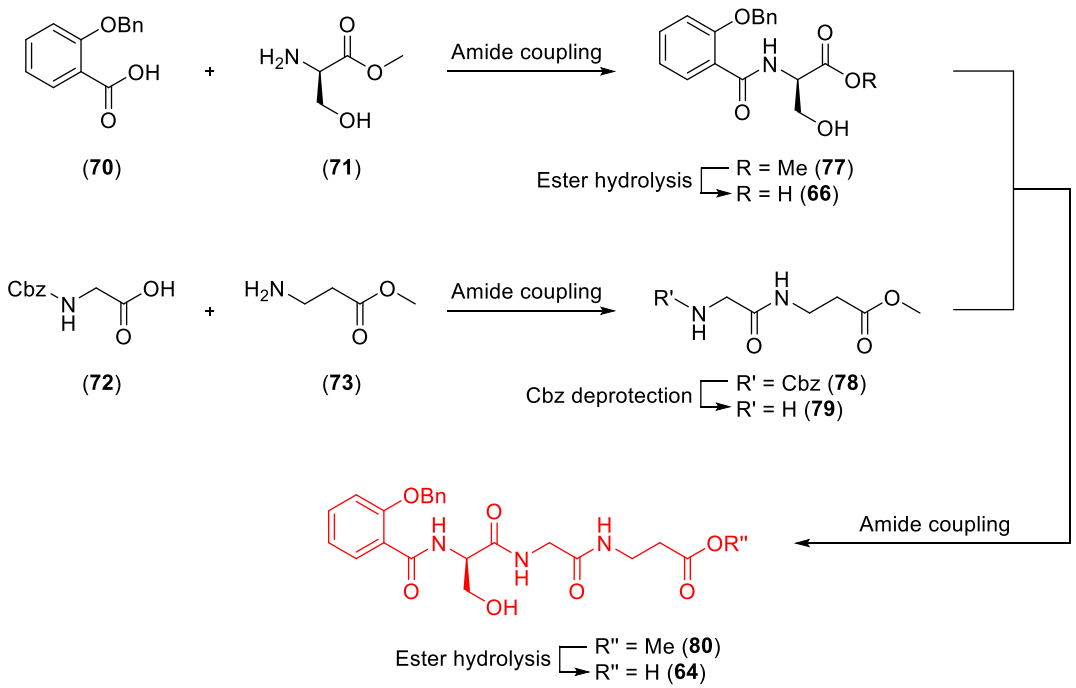

Scheme 3.2. Synthetic strategy for the left-hand fragment of madurastatin C1 (**64**).

Based on previous experience as described in chapter 2, we planned to couple 2-(benzyloxy)benzoic acid (**70**) and methyl *D*-serinate (**71**) using HATU, followed by hydrolysis of the methyl ester to give our first key intermediate (2-(benzyloxy)benzoyl)-

D-serine (**66**). In parallel, we planned to construct our second key intermediate methyl 3-(2-aminoacetamido)propanoate (**79**), through the HATU coupling of ((benzyloxy)carbonyl)glycine (**72**) and methyl 3-aminopropanoate (**73**), followed by a Cbz deprotection. Afterwards, the two intermediates will be joined together via an additional amide bond coupling reaction and finally hydrolysis to give our desired left-hand fragment (**64**).

3.5.1 Synthesis of (2-(Benzyloxy)benzoyl)-*D*-serine (66)

In order to synthesise (2-(benzyloxy)benzoyl)-*D*-serine (**66**), we first had to prepare the corresponding methyl ester, methyl (2-(benzyloxy)benzoyl)-*D*-serinate (**77**), via an amide coupling of two commercially available components.

Therefore, on a 0.2 mmol scale 2-(benzyloxy)benzoic acid (**70**) was first activated with HATU in DMF at 0 °C for 15 min. Then methyl *D*-serinate hydrochloride (**81**) was added to the reaction in DMF, followed by dropwise addition of 3.9 equivalents of DIPEA over 5 minutes. The reaction mixture was allowed to warm slowly to room temperature, stirred for an additional 15 hours and quenched with saturated aqueous NH_4Cl. Following aqueous work-up and column chromatography, the desired benzyl methyl (2-(benzyloxy)benzoyl)-*D*-serinate (**77**) was isolated in a 95% yield as a colourless crystalline solid (**Scheme 3.3**).

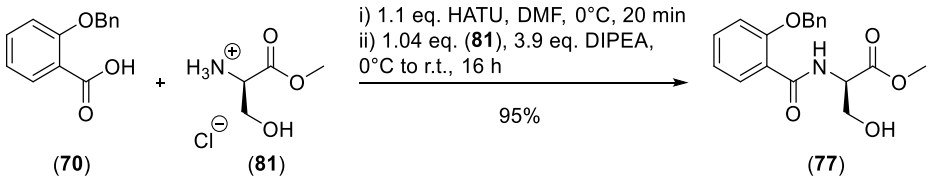

Scheme 3.3. Amide coupling of 2-(benzyloxy)benzoic acid (**70**) and methyl *D*-serinate hydrochloride (**81**) to give methyl (2-(benzyloxy)benzoyl)-*D*-serinate (**77**).

The structure of methyl (2-(benzyloxy)benzoyl)-*D*-serinate (**77**) was confirmed by NMR analysis, through the observation of a new amide proton at 8.78 ppm (d, J = 7.0 Hz) which was also shown by COSY to couple to the serine α-proton at 3.81 ppm (dt,

J = 7.5, 3.9 Hz). The specific rotation ($[\alpha]_D$) of methyl (2-(benzyloxy)benzoyl)-*D*-serinate (**77**) was -16.2 ° (*c* = 1, MeOH), demonstrating a %*ee* of 64% in comparison to the $[\alpha]_D$ of the known enantiomer (+25.3 ° (*c* = 1.4, MeOH)).[91] High quality single crystals were also grown via slow evaporation of a methanol solution, which were submitted for single crystal X-ray diffraction analysis.

Methyl (2-(benzyloxy)benzoyl)-*D*-serinate (**77**) crystallised in the orthorhombic space group $P2_12_12_1$, with 4 molecules in the unit cell (Z = 4), and the absolute stereochemistry was confirmed to be *R* (*D*) (Flack parameter = -0.07(13)) (**Figure 3.2**).

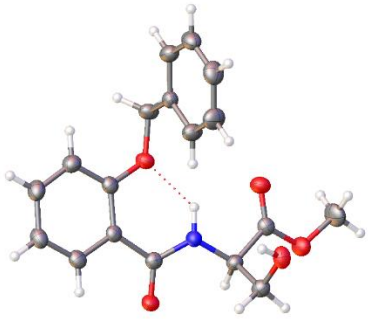

Figure 3.2. ORTEP diagram showing one molecule in the single crystal X-ray structure of methyl (2-(benzyloxy)benzoyl)-*D*-serinate (**77**).

To provide more starting material for the next steps, the amide coupling of 2-(benzyloxy)benzoic acid (**70**) and methyl *D*-serinate hydrochloride (**81**) was repeated several times (≥ 5 mmol) giving high isolated yields of 79-93% in all cases following column chromatography (**Table 3.1**).

The next synthetic step involved the hydrolysis of methyl (2-(benzyloxy)benzoyl)-*D*-serinate (**77**) under basic conditions, to give the corresponding carboxylic acid ready for a second HATU coupling.

Therefore, methyl (2-(benzyloxy)benzoyl)-*D*-serinate (**77**) was hydroysed in 2M aqueous NaOH on a 4.2 mmol scale, with THF as the cosolvent. After 1 hour at room temperature the reaction was completed by TLC. Following aqueous work-up and acid-base extraction, the solvent was removed to give the desired (2-(benzyloxy)benzoyl)-*D*-serine (**66**) in an 84% yield (**Scheme 3.4**; **Table 3.2**, Entry 1).

Entry	Reaction Scale/mmol	Isolated Yield
1[a]	0.2	85%
2	5.2	93%
3	5.2	81%
4	5.0	89%
5	5.0	79%

Table 3.1. HATU coupling of 2-(benzyloxy)benzoic acid (**70**) with methyl *D*-serinate hydrochloride (**81**) to give methyl (2-(benzyloxy)benzoyl)-*D*-serinate (**77**). [a] Entry repeated from **Scheme 3.3** for comparison.

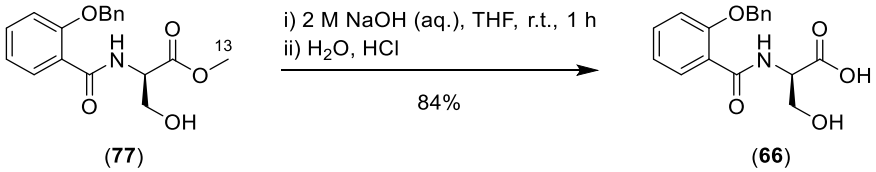

(**77**) (**66**)

Scheme 3.4. Basic hydrolysis of methyl (2-(benzyloxy)benzoyl)-*D*-serinate (**77**) to give (2-(benzyloxy)benzoyl)-*D*-serine (**66**).

Successful hydrolysis of methyl (2-(benzyloxy)benzoyl)-*D*-serinate (**77**) was confirmed by NMR which showed the loss of the methyl group (C-13). NMR analysis also showed that (2-(benzyloxy)benzoyl)-*D*-serine (**66**) was present in the sample with no significant impurities following the work-up, thus no further purification was required for further reactions. However, to obtain an analytically pure sample for further analysis, a portion of (2-(benzyloxy)benzoyl)-*D*-serine (**66**) was purified by column chromatography. Measurement of specific rotation gave α_D = -24.8 ° (*c* = 1, MeOH), suggesting that the sample was enantioenriched and that the *R* (*D*) configuration is still the main component.

To produce more material for the next steps, hydrolysis of methyl (2-(benzyloxy)benzoyl)-*D*-serinate (**77**) was repeated on a range of scales from 1.7 to 4.2 mmol, giving excellent yields from 91-95% of our first key intermediate, (2-(benzyloxy)benzoyl)-*D*-serine (**66**), ready for future coupling reactions (**Table 3.2**,

Entry 2-4).

Entry	Reaction Scale/mmol	Isolation Method	Isolated Yield
1[a]	4.2	acid-base extraction	84%
2	2.4	acid-base extraction	91%
3	1.7	acid-base extraction	95%
4	4.2	acid-base extraction and chromatography	93%

Table 3.2. Basic hydrolysis of methyl (2-(benzyloxy)benzoyl)-*D*-serinate (**77**). [a] Entry repeated from **Scheme 3.4** for comparison.

3.5.2 Synthesis of Methyl 3-(2-Aminoacetamido)propanoate Hydrobromide

In the next step, we focussed on the second key intermediate for the preparation of the left-hand fragment, methyl 3-(2-aminoacetamido)propanoate hydrobromide (**67**). We planned to synthesise this by an amide coupling of ((benzyloxy)carbonyl)glycine(**72**) with methyl 3-aminopropanoate hydrochloride (**82**) to give *N*-Cbz-gly-β-ala-OMe (**78**) followed by a Cbz deprotection step (**Scheme 3.5**).

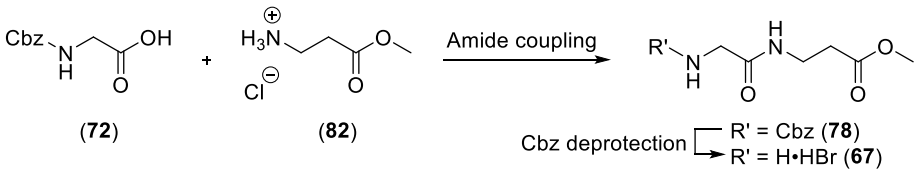

Scheme 3.5. Synthetic strategy for the second key intermediate (**67**) of the left-hand fragment of madurastatin C1.

N-Cbz-gly-β-ala-OMe (**78**) has been previously synthesised by Zeldes *et al.*, using TEA and DCC in chloroform.[92] Due to our previous success with HATU, we decided to continue to use HATU coupling conditions but used DCM as our reaction solvent to simplify the workup.

Therefore 4.8 mmol of ((benzyloxy)carbonyl)glycine (**72**), 1.1 equivalents of both methyl 3-aminopropanoate hydrochloride (**82**) and HATU were dissolved in DCM, cooled to 0 °C and 4.0 equivalents of DIPEA was added. After 1 hour, the reaction mixture was allowed to warm slowly to room temperature over 15 hours, and was quenched with saturated aqueous NH_4Cl. Following aqueous work-up and column chromatography, the desired *N*-Cbz-gly-β-ala-OMe (**78**) was isolated in a 85% yield (**Scheme 3.6**; **Table 3.3**, Entry 1).

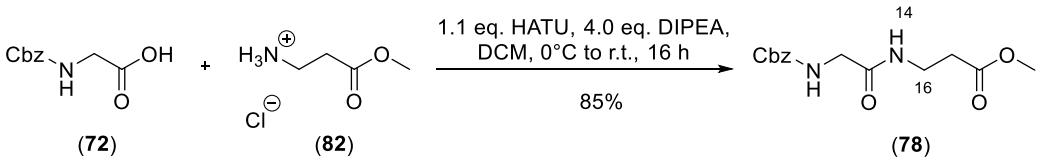

Scheme 3.6. Amide coupling of ((benzyloxy)carbonyl)glycine (**72**) and methyl 3-aminopropanoate hydrochloride (**82**) to give *N*-Cbz-gly-β-ala-OMe (**78**).

The structure of *N*-Cbz-gly-β-ala-OMe (**78**) was confirmed by NMR analysis, through the observation of a new amide proton (H-14) at 7.11 ppm (t, J = 6.0 Hz) which was also shown by COSY to couple to the β-alanine methylene protons (H-16) at 3.51 ppm (q, J = 6.2 Hz, 2H). In addition, the melting point of *N*-Cbz-gly-β-ala-OMe (**78**) was measured as 94-95 °C, which closely matched that previously reported in the literature (93-94 °C).[92]

To provide more material for later steps, the amide coupling of ((benzyloxy)carbonyl)glycine (**72**) and methyl 3-aminopropanoate hydrochloride (**82**) was repeated three times more on the same scale with the same procedure giving yields of 83% or more in all cases (**Table 3.3**).

Next we wished to carry out the Cbz deprotection of *N*-Cbz-gly-β-ala-OMe (**78**), which typically is carried out using hydrogenation or strongly acidic conditions.[93,94]

Therefore *N*-Cbz-gly-β-ala-OMe (**78**) was reacted on a 3.64 mmol, with excess hydrobromic acid in acetic acid and dichloromethane at room temperature. After 1 h, the reaction was complete by TLC with staining with potassium permanganate solution

Entry	Reaction Scale/mmol	Isolated Yield
1[a]	4.8	85%
2	4.8	88%
3	4.8	83%
4	4.8	89%

Table 3.3. HATU amide coupling of ((benzyloxy)carbonyl)glycine (**72**) and methyl 3-aminopropanoate hydrochloride (**82**) to give *N*-Cbz-gly-β-ala-OMe (**78**). [a] Entry repeated from **Scheme 3.6** for comparison.

showing the loss of starting material. The reaction was concentrated under a flow of nitrogen gas in the fume cupboard to remove excess HBr and any Br_2 present. The resulting residue was dissolved in chloroform, and the remaining solvent was removed under reduced pressure. The crude reaction material was then dissolved in the minimum amount of methanol, and twice the volume of hexane was added and the mixture was stirred overnight. The resulting solid was then collected via filtration to give our desired second key intermediate of the left-hand fragment, methyl 3-(2-aminoacetamido)propanoate hydrobromide (**67**) in an 84% yield (**Scheme 3.7**; **Table 3.4**, Entry 1).

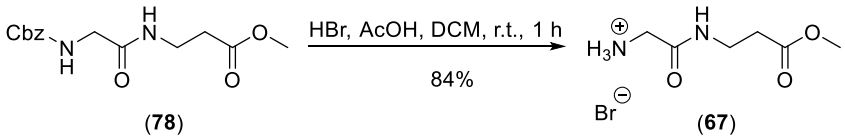

(**78**) (**67**)

Scheme 3.7. Cbz deprotection of *N*-Cbz-gly-β-ala-OMe (**78**) to give methyl 3-(2-aminoacetamido)propanoate hydrobromide (**67**).

Successful Cbz deprotection of *N*-Cbz-gly-β-ala-OMe (**78**) was confirmed by ^{13}C NMR analysis, which showed the loss of the six ^{13}C signals corresponding to the Cbz group, and ^{1}H NMR which showed a new broad peak at 7.95 ppm (br-s, 3H) corresponding to *N*-terminal ammonium.

Following the success of the initial experiment, the deprotection of *N*-Cbz-gly-β-ala-OMe (**78**) was repeated twice more on a 3.40 and 4.80 mmol scale, to prepare enough material for the further steps. In all cases high yields were observed (**Table 3.4**).

Entry	Reaction Scale/mmol	Isolated Yield
1[a]	3.64	84%
2	3.40	90%
3	4.80	89%

Table 3.4. Cbz deprotection of *N*-Cbz-gly-β-ala-OMe (**78**) with HBr.

3.5.3 Synthesis of the Left-hand Fragment of Madurastatin C1 via Coupling of the First and Second Intermediates and Methyl Ester Hydrolysis

To make the left-hand fragment (**64**) of madurastatin C1, we planned to assemble the first, (2-(benzyloxy)benzoyl)-*D*-serine (**66**), and second intermediate, methyl 3-(2-aminoacetamido)propanoate hydrobromide (**67**), via an amide bond formation, followed by hydrolysis of the methyl ester (**Scheme 3.8**).

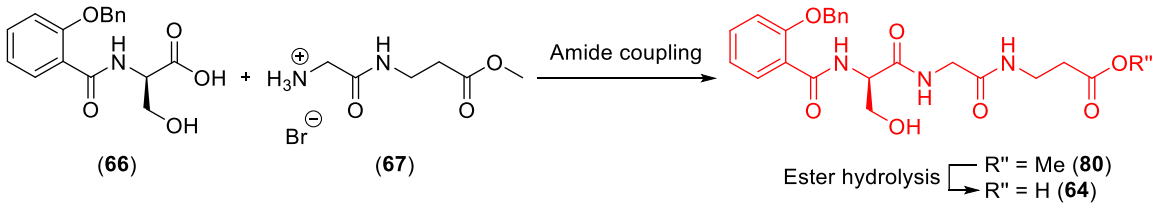

(**66**) (**67**)

Scheme 3.8. Planned synthesis left-hand fragment (**64**) of madurastatin C1.

First we made the corresponding *N*-functionalised (*R*)-ser-gly-β-ala-OMe (**80**) following our previously described HATU coupling conditions in DMF. Thus (2-(benzyloxy)benzoyl)-*D*-serine (**80**) on a 3.33 mmol scale was activated with HATU, and then reacted with 1.2 equivalents of methyl 3-(2-aminoacetamido)propanoate hydrobromide (**67**) in the presence of DIPEA. After aqueous work-up and column

chromatography, *N*-functionalised (*R*)-ser-gly-β-ala-OMe (**80**) was isolated in a 49% yield as a colourless solid (**Scheme 3.9**).

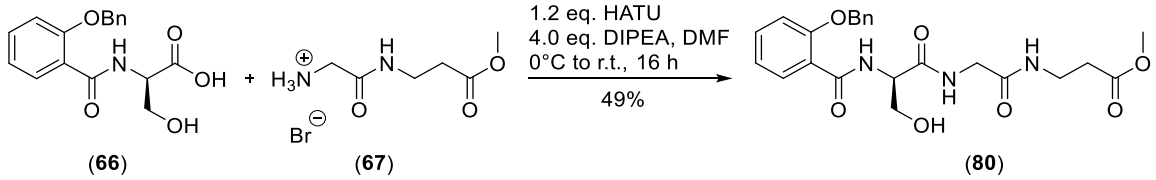

(**66**) (**67**) (**80**)

Scheme 3.9. Amide coupling of (2-(benzyloxy)benzoyl)-*D*-serine (**66**) and methyl 3-(2-aminoacetamido)propanoate hydrobromide (**67**) to give *N*-functionalised (*R*)-ser-gly-β-ala-OMe (**80**).

The structure of *N*-functionalised (*R*)-ser-gly-β-ala-OMe (**80**) was confirmed by ^{1}H NMR analysis which showed a total of three amide protons, including a new peak at 7.49 ppm (t, *J* = 6.1 Hz) as confirmed by COSY which showed coupling of the new amide proton to the glycine methylene protons (3.88 ppm, dd, *J* = 16.0, 6.1 Hz; 3.77 ppm, dd, *J* = 16.9, 5.8 Hz). Success of the amide coupling reaction was also supported by high-resolution mass spectrometry which showed a molecular ion $[M+Na]^{+}$ with m/z = 480.1740, giving a molecular formula of $C_{23}H_{27}N_3O_7Na$ (calc. m/z = 480.1747).
To make more material for later steps, we repeated the HATU coupling of (2-(benzyloxy)benzoyl)-*D*-serine (**66**) and methyl 3-(2-aminoacetamido)propanoate hydrobromide (**67**) twice on similar scales, resulting in slightly improved isolated yields (**Table 3.5**).

The final step for synthesising the left-hand fragment (**64**) of madurastatin C1 involved the methyl hydrolysis of *N*-functionalised (*R*)-ser-gly-β-ala-OMe (**80**) under basic conditions as previously described.
Therefore, 1.55 mmol of *N*-functionalised (*R*)-ser-gly-β-ala-OMe (**80**) was dissolved in a mixture of THF and 2M aqueous NaOH at room temperature. After 1 hour starting material could not be observed by TLC, following staining with potassium permanganate. Aqueous work-up, including acid-base extraction as before, followed

Entry	Reaction Scale/mmol	Isolated Yield
1[a]	3.3	49%
2	3.5	45%
3	4.0	58%

Table 3.5. HATU-mediated amide coupling of (2-(benzyloxy)benzoyl)-*D*-serine (**66**) and methyl 3-(2-aminoacetamido)propanoate hydrobromide (**67**) to give *N*-functionalised (*R*)-ser-gly-β-ala-OMe (**80**). [a] Entry repeated from **Scheme 3.9** for comparison.

by solvent removal gave the desired left-hand fragment (**64**) of madurastatin C1 as a colourless solid in a 90% yield (**Scheme 3.10**; **Table 3.6**, Entry 1).

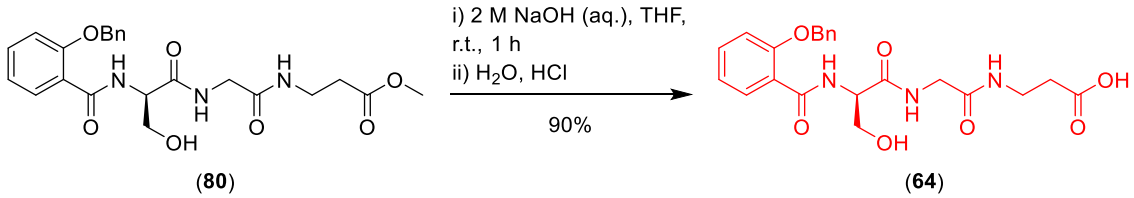

Scheme 3.10. Basic hydrolysis of *N*-functionalised (*R*)-ser-gly-β-ala-OMe (**80**) to give the left-hand fragment (**64**) of madurastatin C1.

^{1}H NMR analysis confirmed the loss of the methyl group, and the molecular formula ($C_{22}H_{25}N_3O_7Na$) was confirmed via high resolution mass spectrometry ($[M+Na]^+$, *m*/*z* = 466.1590).

Next we repeated the same methyl ester hydrolysis of *N*-functionalised (*R*)-ser-gly-β-ala-OMe (**80**) on a 1.14 mmol scale, achieving a satisfactory yield of 93% (**Table 3.6**).

Entry	Reaction Scale/mmol	Isolated Yield
1[a]	1.55	90%
2	1.14	93%

Table 3.6. Basic hydrolysis of *N*-functionalised (*R*)-ser-gly-β-ala-OMe (**80**). [a] Entry repeated from **Scheme 3.10** for comparison.

The specific rotation of the left-hand fragment (**64**) of madurastatin C1 (**Table 3.6**, Entry 1) was observed as α_D = -20.6°, showing that the sample remained enantioenriched with the *R* (*D*) configuration as the dominant component. However with no literature data available for comparison to determine %*ee*, future work will require both chiral HPLC and the growth of single crystals for X-ray analysis.

3.6 Synthesis of the Key "nitrone" Intermediate for Middle and Right-hand Fragment of Madurastatin C1

In order to synthesise the middle and right-hand fragments, we first need to prepare a key nitrone containing intermediate (**76**).

In the synthesis of our target nitrone intermediate (**76**), we planned to start from commercial protected *N*-α-Cbz-L-ornithine (**75**) which will undergo a condensation reaction with benzaldehyde to give the corresponding imine (**83**). Then we planned to oxidise the imine group to the corresponding oxaziridine (**84**) using *m*CPBA, followed by an acid catalysed rearrangement to give our target nitrone (**76**) (**Scheme 3.11**).

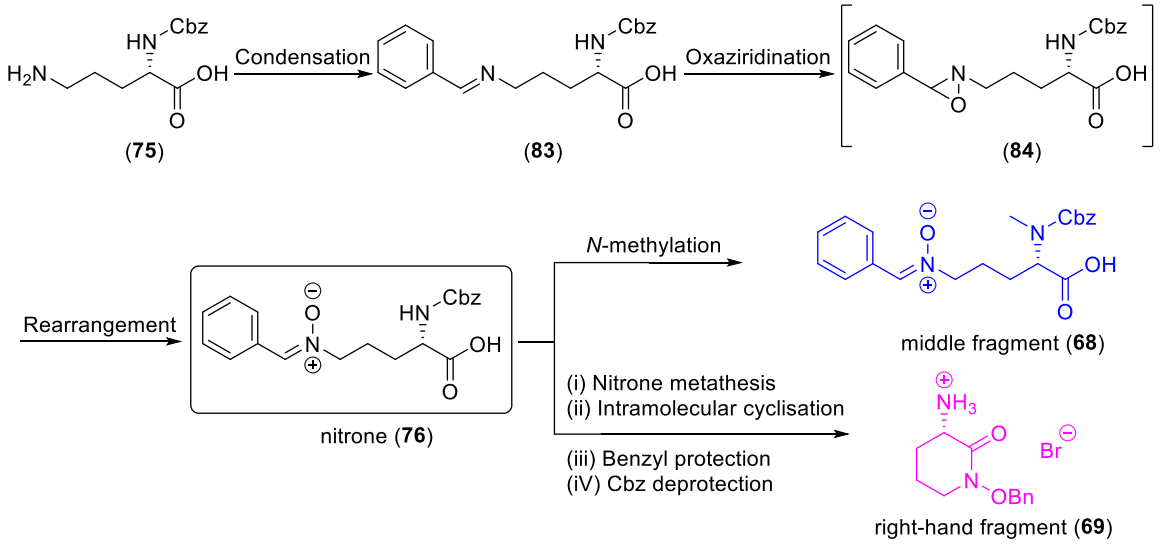

Scheme 3.11. Planned synthesis of the key nitrone intermediate (**76**) starting from *N*-α-Cbz-L-ornithine via a condensation, oxaziridination, rearrangement reaction sequence. Nitrone intermediate (**76**) will then be used in the synthesis of both the middle (blue) (**68**) and right-hand (purple) (**69**) fragments of madurastatin C1.

In order to synthesise benzaldehyde-derived imine (**83**), we adapted a procedure from the group of Miller.[95] Therefore, we dissolved 18.8 mmol of *N*-α-Cbz-L-ornithine (**75**) in MeOH, along with 1.1 equivalents of KOH. Afterwards, 1.1 equivalents of benzaldehyde and pre-dried 3 Å molecular sieves (beads) were added. After stirring at room temperature for 16 hours, the molecular sieves were removed by filtration and the filtrate was concentrated under reduced pressure to give benzaldehyde-derived imine (**83**) in a quantitative yield as assessed by ^{1}H NMR (**Scheme 3.12**; **Table 3.7**, Entry 1).

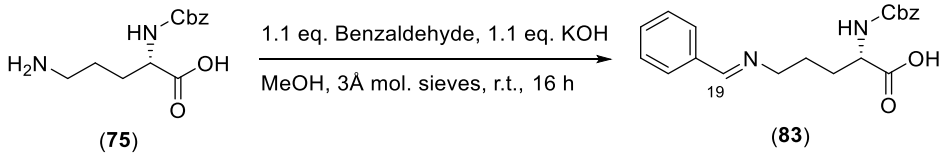

Scheme 3.12. Condensation reaction of *N*-α-Cbz-L-ornithine (**75**) to give benzaldehyde-derived imine (**83**).

The structure of benzaldehyde-derived imine (**83**) was confirmed by ^{1}H and ^{13}C NMR, which showed a 1H singlet (8.27 ppm) for the newly formed imine, correlated by HSQC to a carbon peak at 160.3 ppm. Furthermore, infrared spectroscopy showed a new peak at 1688.2 cm^{-1} which we assigned to the C=N stretch of the newly formed imine. Following the success of this initial reaction, we repeated the reaction six more times with the 3 Å molecular sieves (beads) replaced with the corresponding powder for easier purification. In all cases quantitative yields were obtained for the crude product (**Table 3.7**).

Following successful imine formation, next we focussed on oxidation/rearrangement of benzaldehyde-derived imine (**83**) to give our target nitrone (**76**), via an intermediate oxaziridine (**84**).

Since the oxidation reaction required the use of *m*CPBA, we first purified commercially available ≥77% *m*CPBA by washing an Et_2O solution with an aqueous solution of NaOH and NaH_2PO_4, to remove the 3-chlorobenzoic acid present.[96] The Et_2O was

Entry	Reaction Scale/mmol	3 Å Molecular Sieves	Yield
1[a]	18.8	beads	quantitative
2	15.0	powder	quantitative
3	15.0	powder	quantitative
4	18.8	powder	quantitative
5	18.8	powder	quantitative
6	3.7	powder	quantitative
7	18.8	powder	quantitative

Table 3.7. Condensation reaction of protected *N*-α-Cbz-L-ornithine (**75**) with benzaldehyde in MeOH.

then removed under a flow of nitrogen gas to give high purity *m*CPBA.

Following this, we dissolved 0.6 mmol of benzaldehyde-derived imine (**83**) in methanol at 0 °C, and added 1.15 equivalents of freshly purified *m*CPBA in methanol solution dropwise over 20 mins. After 1.5 hours at 0 °C the reaction mixture was concentrated under a flow of nitrogen gas and the resulting residue was dissolved in water and washed with EtOAc. The aqueous layer was acidified with 2 M aqueous HCl to pH 2, then extracted into EtOAc. The organic extracts were washed with saturated aqueous $Na_2S_2O_3$ to reduce any *m*CPBA remaining. After washing with brine and drying with Na_2SO_4, the solvent was removed to give the crude oxaziridine intermediate (**84**) as a pale yellow solid, which was used directly in the next step (**Scheme 3.13**).

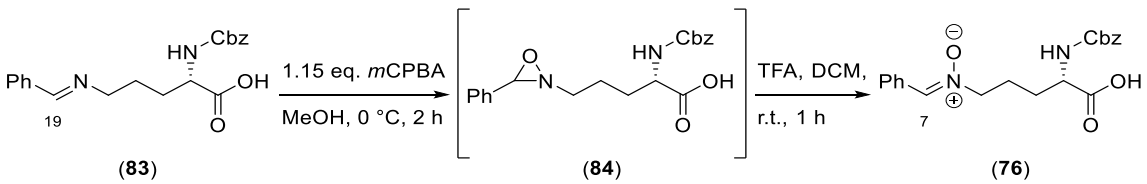

(**83**) (**84**) (**76**)

Scheme 3.13. Two step *m*CPBA oxidation and acid catalysed rearrangement of benzaldehyde-derived imine (**83**) to give nitrone (**76**).

The crude oxaziridine intermediate (**84**) was then reacted with excess trifluoroacetic

acid in dichloromethane at room temperature for 1 hour. Following solvent removal under reduced pressure, the crude product was slurried into stirred EtOAc : hexane (1 : 2), in the presence of 0.7 equivalents of benzaldehyde. After 16 hours the slurry was cooled to 0 °C, and the solids were collected via filtration, washed with cold EtOAc and dried to give the desired crude nitrone (**76**) as a pale pink sold in a 66% yield (**Scheme 3.13**; **Table 3.8**, Entry 1).

The structure of nitrone (**76**) was confirmed by ^{13}C NMR analysis with showed the nitrone carbon (C-7) at 133.4 ppm, which matched the literature.[95] To further confirm the structure, single crystals of nitrone (**76**) were grown through solvent diffusion from methanol/toluene (MJH-DW-20-0061) and slow evaporation from DMSO (MJH-DW-20-0065) and examined by single crystal X-ray diffraction. Two crystal structures were collected and analysed at the Diamond light source. Both samples gave the same crystal structure, showing that the nitrone (**76**) had crystallised in the monoclinic space group $P2_1$, with two molecules in the unit cell (Z = 2). Both structures contained continuous solvent-accessible channels along the crystallographic [010] direction, containing disordered MeOH or DMSO. The single crystal structure showed that the nitrone had adopted a (*Z*)-configuration in the solid state. Unfortunately, the Flack parameters obtained were -0.4(10) (MeOH/Toluene) and -0.2(5) (DMSO), thus the absolute stereochemistry could not be determined (**Figure 3.3**)

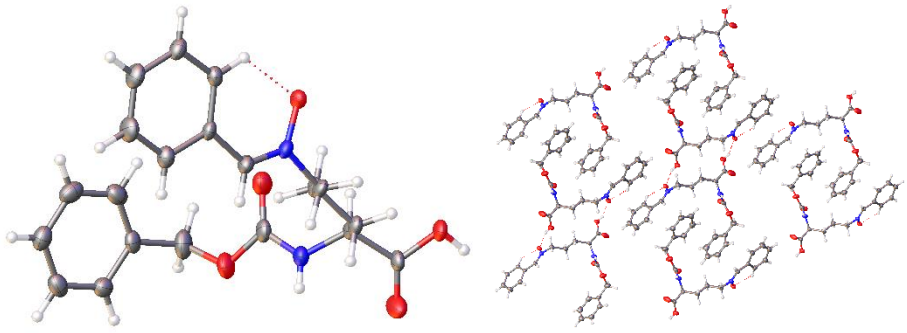

Figure 3.3. (left) ORTEP diagram showing one molecule in the crystal structure of nitrone (**76**), (right) intermolecular H-bonding network, showing solvent-accessible channels.

The oxidation/rearrangement reaction of imine (**83**) was then repeated four more times, on a large scale to provide sufficient material for further steps. In all cases moderate to good yields were obtained of the crude nitrone (**76**) (**Table 3.8**).

Entry	Reaction Scale/mmol	Crude Yield
1[a]	0.6	66%
2	19.5	74%
3	19.5	67%
4	19.5	58%
5	21.2	73%

Table 3.8. *m*CPBA oxidation and acid catalysed rearrangement of benzaldehyde-derived imine (**83**) to give nitrone (**76**). [a] Entry repeated from **Scheme 3.13** for comparison.

The observed melting points of prepared nitrone (**76**) (e.g. 148.4-149.7 °C, **Table 3.8**, Entry 2) showed slight decreases in comparison to the literature (150.5 – 151 °C),[95] suggesting the presence of small amounts of impurities in the sample. This was confirmed by careful examination of the ^{1}H NMR with showed small quantities of 3-chlorobenzoic acid and benzaldehyde present. However, attempts to purify nitrone (**76**) via silica gel chromatography were unsuccessful due to the decomposition on silica. Therefore crude nitrone (**76**) was carried on to next step.

Next we focused on the synthesis of middle fragment (**68**) and right-hand fragment (**69**), using nitrone (**76**) as a common starting material.

3.7 Synthesis of Middle Fragment of Madurastatin C1 via *N*-methylation

To complete our synthesis of the middle fragment of madurastatin C1, we planned to selectively *N*-methylate nitrone intermediate (**76**). Therefore, in our first attempt at this reaction we deprotonated nitrone (**76**) on a 2.7 mmol scale with 3 equivalents of NaH in THF at 0 °C for 30 min. 8 Equivalents of MeI were then added at 0 °C, the reaction

mixture was allowed to warm slowly to room temperature over 24 hours and then quenched with MeOH. The reaction mixture was concentrated overnight under a flow of nitrogen gas in the fume cupboard to remove excess MeI present. Following acid-base extraction and drying over Na_2SO_4, the solvent was removed and the resulting residue was triturated from hexane/Et_2O to give the crude *N*-methyl nitrone (**68**) in a 67% yield (**Scheme 3.14**; **Table 3.9**, Entry 1).

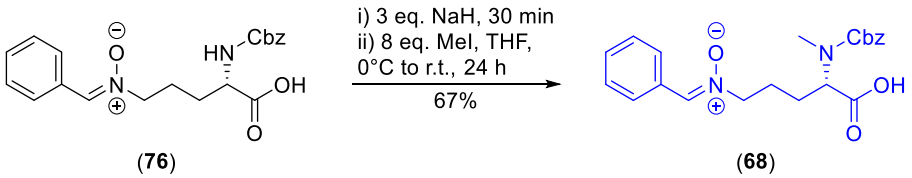

(**76**) (**68**)

Scheme 3.14. *N*-methylation of key intermediate nitrone (**76**) to give *N*-methyl nitrone (**68**).

Successful *N*-methylation of nitrone (**68**) was confirmed by ^{1}H NMR (DMSO-d_6), which showed the appearance of two new singlets at 2.81 and 2.79 ppm in a 1.4 : 1 ratio, corresponding to a total of three protons. This suggested the presence of restricted rotation around the carbamate group, confirmed by the observation of a broad peak at 30.4 ppm in the ^{13}C NMR corresponding to the methyl group.[90] The presence of rotamers was confirmed by variable temperature NMR experiments, which showed that the peaks corresponding to the *N*-methyl group coalesced in the ^{1}H NMR at higher temperatures (343 K). It should however also be noted that in the ^{1}H NMR of *N*-methyl nitrone (**68**) peaks corresponding to the starting material nitrone (**76**) were observed, suggesting that the reaction had not gone to completion and that the reaction conditions and purification method required optimisation (**Figure 3.4**).

In an attempt to improve the *N*-methylation reaction, we carried out the reaction again. Following deprotonation as before, the reaction time was increased from 24 to 41 hours, prior to quenching with MeOH and excess MeI removal as previously. Following aqueous work-up and trituration, *N*-methyl nitrone (**68**) was recovered in a 68% yield

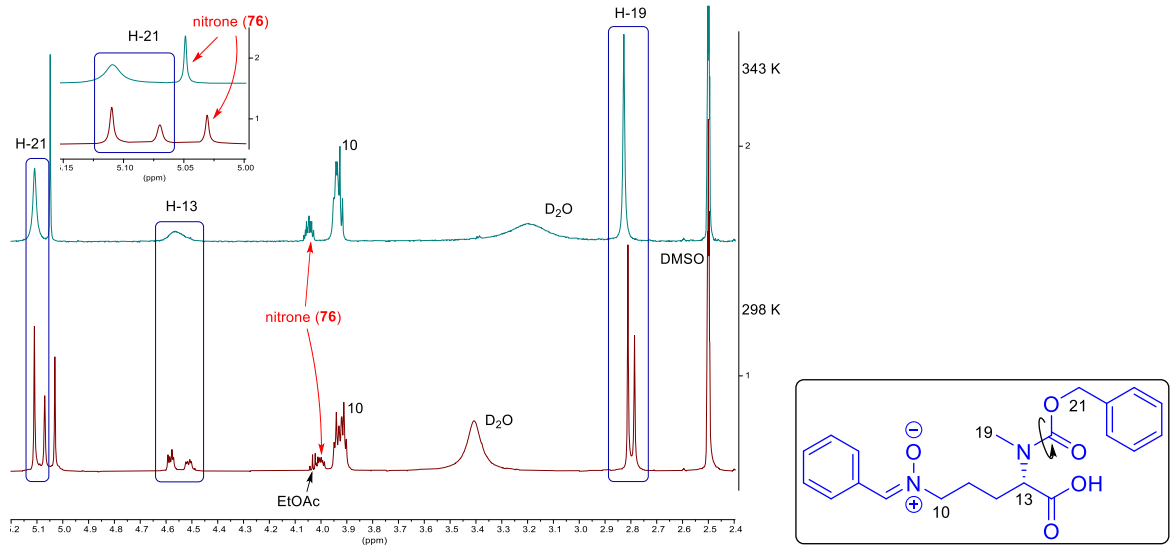

Figure 3.4. ^{1}H NMR (DMSO-d_6, 700 MHz) of *N*-methyl nitrone (**68**) recorded at 298 K (bottom) and at 343 K (top), showing the presence of rotamers and starting material.

with an improved ratio of 4 : 1 of *N*-methyl nitrone (**68**) to unreacted nitrone (**76**) (**Figure 3.5**; **Table 3.9**, Entry 2). To further improve the *N*-methylation, the reaction was repeated using 4 equivalents of NaH and further increasing the reaction time after deprotonation to 47 h, followed by quenching and aqueous work-up as before. ^{1}H NMR analysis of the crude showed that all of the starting material nitrone (**76**) had been consumed. The crude product was then purified by column chromatography to give the desired *N*-methyl nitrone (**68**) in a 25% isolated yield (**Figure 3.5**; **Table 3.9**, Entry 3).

Entry	Scale /mmol	Equivalents of NaH	Time /hour	Purification method	Ratio product : start material	Yield
1[a]	2.7	3	24	trituration	2 : 1	43%[b]
2	2.9	3	41	trituration	4 : 1	68%[b]
3	2.9	4	47	column chromatography	-	25%[c]

Table 3.9. *N*-methylation of key nitrone intermediate (**76**) to give *N*-methyl nitrone (**68**). [a] Entry repeated from **Scheme 3.14** for comparison. [b] Estimated yield by ^{1}H NMR. [c] Isolated yield.

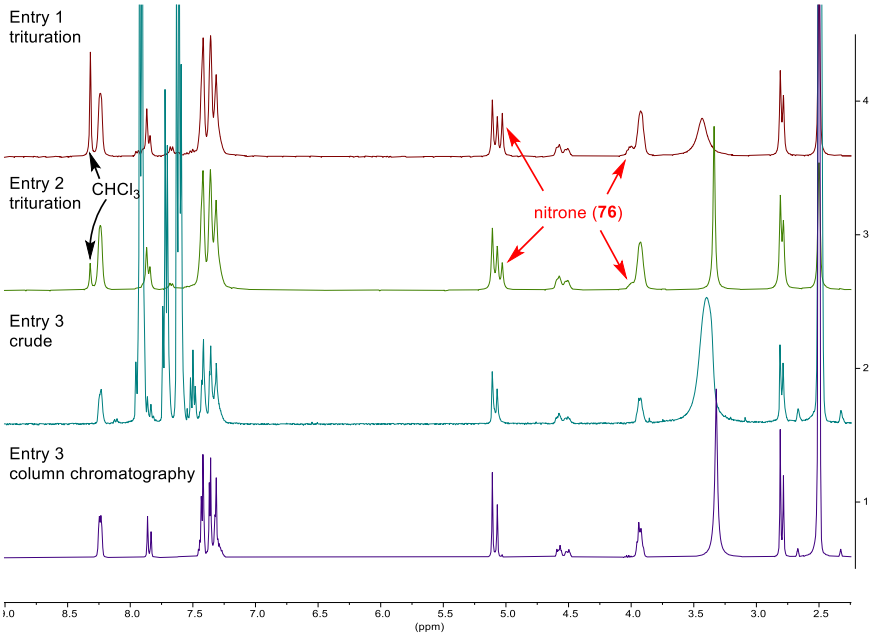

Figure 3.5. Comparison of the reaction outcomes of the formation of *N*-methyl nitrone (**68**) by ^{1}H NMR (DMSO-d$_6$, 400 MHz, 298 K).

3.8 Synthesis of Right-hand Fragment of Madurastatin C1 via Nitrone Metathesis/Cyclisation, Benzylation and Cbz Deprotection

Following a report from Miller *et al*.[90] we planned to synthesise the right-hand fragment of madurastatin C1, cyclised ornithine hydrobromide (**69**), from our previously prepared nitrone (**76**). This will involve forming the free hydroxylamine, through a nitrone metathesis reaction, which will undergo a spontaneous intramolecular cyclisation, and the cyclised product will be trapped as the benzylated species. Finally to access the right-hand fragment of madurastatin C1 to be used for future coupling reactions, we will deprotect the Cbz group and isolate the product as the cyclised ornithine hydrobromide (**69**) (**Scheme 3.15**).

We first attempted the one-pot nitrone metathesis/cyclisation and benzylation reaction sequence. Therefore, on an 8.1 mmol scale, nitrone (**76**) was reacted with 1.2 equivalents of hydroxylamine hydrochloride in MeOH at reflux for 1 hour. At this point the starting material nitrone (**76**) could not be observed by TLC, so 3 Å molecular sieves and 2.0 equivalents of Et$_3$N were added in order to promote the cyclisation.

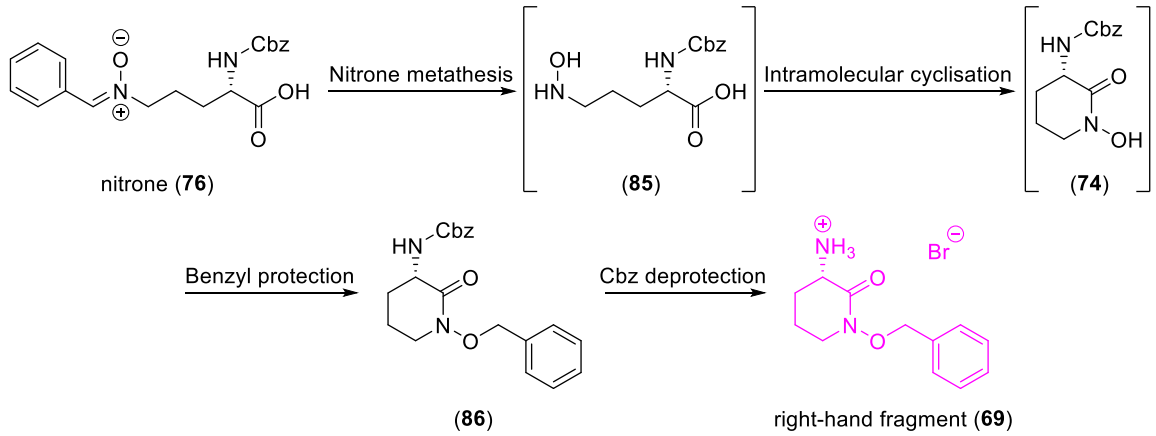

Scheme 3.15. Synthetic route to right-hand fragment of madurastatin C1, cyclised ornithine hydrobromide (**69**)

After an additional 2 hours at reflux, the reaction was cooled and filtered through a pad of celite to remove the molecular sieves. Following aqueous work-up, the crude cyclised hydroxamic acid (**74**) was obtained and directly reacted with 5 equivalents of benzyl bromide and 10 equivalents of potassium carbonate in DMF at room temperature for 16 hours. Following the aqueous work-up, purification of the crude reaction material by column chromatography gave the corresponding benzyl protected cyclised ornithine (**86**) as a colourless solid in a 71% isolated yield (**Scheme 3.16**).

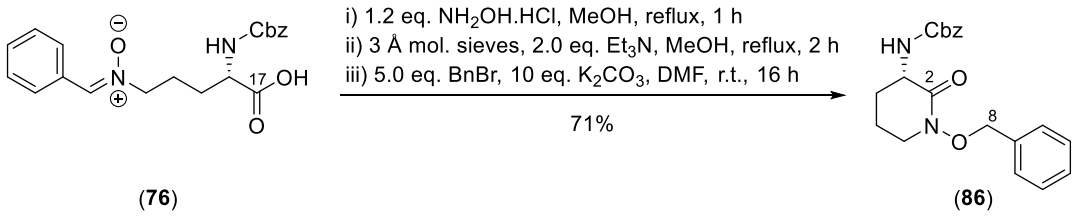

Scheme 3.16. One-pot nitrone metathesis/cyclisation and benzyl protection of nitrone (**76**) to give benzyl protected cyclised ornithine (**86**).

The structure of benzyl protected cyclised ornithine (**86**) was confirmed by ^{1}H-NMR analysis, which showed the appearance of new 2H singlets at 4.95 ppm (d, *J* = 10.5 Hz, 1H, H-8^{a}) and 4.87 (d, *J* = 10.4 Hz, 1H, H-8^{b}), corresponding to the newly formed diastereotopic *O*-benzyl methylene group. Moreover, the ^{13}C-NMR showed the loss of

the carbon peak (173.6 ppm) corresponding to carbonyl carbon (C-17) from nitrone (**76**), and the appearance of a new carbon peak (167.7 ppm) corresponding to the carbonyl carbon (C-2) of the hydroxamic acid. In addition the melting point of benzyl protected cyclised ornithine (**86**) was consistent with the literature 86-87 °C (lit = 86-88 °C),[90] and high resolution mass spectrometry showed the expected molecular ion (experimental $[M+Na]^+$ = 377.1477; calculated for $C_{20}H_{22}N_2O_4Na$ $[M+Na]^+$ = 377.1477). To prepare more starting material for following steps, the one-pot reaction was repeated as before on the same scale, giving a similar isolated yield of 77% (**Table 3.10**, Entry 2).

Entry	Reaction Scale/mmol	Isolated Yield
1[a]	8.1	71%
2	8.1	77%

Table 3.10. One-pot nitrone metathesis/cyclisation and benzyl protection of nitrone (**76**) to give benzyl protected cyclised ornithine (*S*-**86**). [a] Entry repeated from **Scheme 3.16** for comparison.

In order to examine the absolute stereochemistry of our synthesised benzyl protected cyclised ornithine (*S*-**86**) we measured the specific rotation ($[\alpha]_D$) giving a positive value of +22.0 ° (*c* = 1, MeOH) (**Table 3.10**, Entry 1). Benzyl protected cyclised ornithine (**86**) has been synthesised previously by Miller and Sridhar *et al*., utilising a number of different routes to make both of the enantiomers.[97,90,98] Examination of the literature gave seven reported specific rotations for this molecule, four for the (*S*)-enantiomer with an average value of +53.0 ° (over three reported numbers) and three for the (*R*)-enantiomer with an average value of -50.4 °, suggesting that we had obtained the correct enantiomer (**Table 3.11**).

Interestingly in our survey of specific rotation data for benzyl protected cyclised ornithine (**86**), we observed an unusual literature report in which the (*S*)-enantiomer had been previous prepared by the same method that we had followed, but the $[\alpha]_D$ is

Source	Stereochemistry (*R*/*S*)	Specific rotation ($[\alpha]_D$)	Concentration, Solvent
This work	*S*	+22.0 °	(*c* = 1, MeOH)
J. Org. Chem., 2002[90]	*S*	-45.0 °	(*c* = 1, DCM)
Org. Biomol. Chem., 2018[98]	*S*	+55.3 °	(*c* = 1, DCM)
J. Org. Chem., 1990[97]	*S*	+52.0 °	(*c* = 1.45, DCM)
J. Org. Chem., 1990[97]	*S*	+51.6 °	(*c* = 1.8, DCM)
J. Org. Chem., 1990[97]	*R*	-51.0 °	(*c* = 1.4, DCM)
J. Org. Chem., 1990[97]	*R*	-51.7 °	(*c* = 1.8, DCM)
J. Org. Chem., 1990[97]	*R*	-48.5 °	(*c* = 1, DCM)

Table 3.11. Specific rotation ($[\alpha]_D$) of benzyl protected cyclised ornithine (**86**) comparison with literature.[97,90,98]

reported to be -45.0 ° rather than the expected +53.0 ° suggesting an error in this report.[90]

Finally, variable temperature ^{1}H NMR experiments were undertaken for benzyl protected cyclised ornithine (*S*-**86**) (**Table 3.10**, Entry 1), showing the presence of rotamers due to the restricted rotation around the carbamate group (Appendix 2) (**Figure 3.6**).

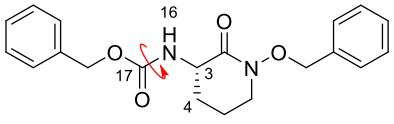

(**86**)

Figure 3.6. Rotamers present due to the hindered rotation of the nitrogen-carbon bond (N-16 to C-3) around the carbamate group (Appendix 2)

In the next step, we wished to carry out the Cbz deprotection of the *N*-terminal amine of benzyl protected cyclised ornithine (**86**), under acidic conditions as previously described in this chapter.

Therefore, we reacted benzyl protected cyclised ornithine (**86**) on a 4.23 mmol in dichloromethane with excess 33% hydrobromic acid in acetic acid at room temperature. After 1 hour, the starting material could not be observed by TLC (potassium permanganate) and the reaction was concentrated under a flow of nitrogen gas, in the fume cupboard, to remove excess HBr and any Br_2 present. The resulting residue was then dissolved in the minimum amount of chloroform, twice the volume of hexane was added, and the mixture was stirred overnight to precipitate the product. The resulting solid was then collected via filtration to give our desired right-hand fragment, cyclised ornithine hydrobromide (**69**) as a red powder in a 95% yield (**Scheme 3.17**; **Table 3.12**, Entry 1).

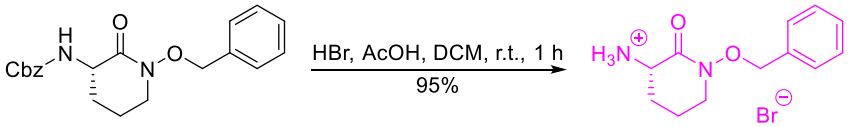

(**86**) (**69**)

Scheme 3.17. Cbz deprotection of benzyl protected cyclised ornithine (**86**) to give cyclised ornithine hydrobromide (**69**)

The structure of cyclised ornithine hydrobromide (**69**) was confirmed by ^{13}C NMR analysis which showed the loss of the signals corresponding to the Cbz protecting group, whilst the melting point (191 - 192 °C) closely matched that previously reported in the literature (194 - 195 °C).[97]

Following our successful initial experiment, the Cbz deprotection of benzyl protected cyclised ornithine (**86**) was repeated on a 5.54 mmol scale as previously to give similarly high yields (**Table 3.12**).

Entry	Reaction Scale/mmol	Isolated Yield
1[a]	4.23	95%
2	5.54	95%

Table 3.12. Cbz deprotection of benzyl protected cyclised ornithine (**86**) with HBr

At this stage we had successfully prepared sufficient right-hand fragment to provide material for the next steps. We then focussed on peptide coupling of cyclised ornithine hydrobromide (**69**) with the middle fragment of madurastatin C1.

3.9 Synthesis of Middle-Right Fragment of Madurastatin C1 via Amide Coupling and Nitrone Metathesis

To complete our synthesis of the middle-right fragment of madurastatin C1, we planned to assemble the previously prepared middle fragment, *N*-methyl nitrone (**68**) with the corresponding right-hand fragment, cyclised ornithine hydrobromide (**69**), via a HATU amide coupling. This will then be followed by nitrone metathesis to generate the desired middle-right fragment (**Scheme 3.18**).

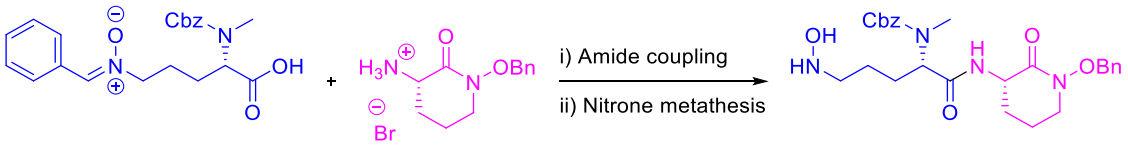

(**68**) (**69**) (**87**)

Scheme 3.18. Planned synthesis middle-right fragment (**87**) of madurastatin C1 starting from amide coupling of *N*-methyl nitrone (**68**) (middle fragment) and cyclised ornithine hydrobromide (**69**) (right-hand fragment), followed by nitrone metathesis.

Therefore, we first started with the synthesis of nitrone dipeptide (**88**) using our previously described HATU coupling conditions in DMF. Thus on a 3.83 mmol scale, 1.1 equivalents of *N*-methyl nitrone (**68**) were first activated with HATU in DMF and the reacted with cyclised ornithine hydrobromide (**69**) in the presence of DIPEA. After aqueous work-up and column chromatography, the desired nitrone dipeptide (**88**) was isolated in a 61% yield (**Scheme 3.19**).

The success of the amide coupling was confirmed by 2D-NMR analysis by the appearance of a new amide peak (8.26 ppm, N-16) in the ^{1}H NMR which were correlated by HMBC with corresponding to the ^{13}C NMR signals at 169.9 ppm (C-17),

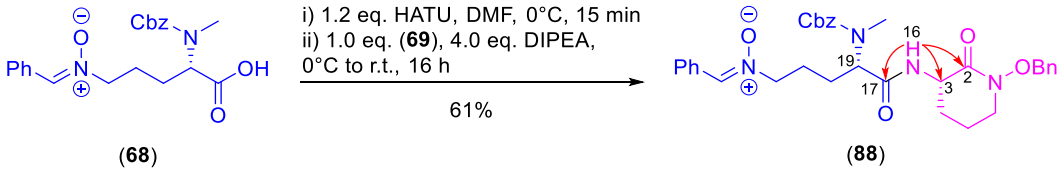

Scheme 3.19. Amide coupling of *N*-methyl nitrone (**68**) (middle fragment) and cyclised ornithine hydrobromide (**69**) (right-hand fragment) to give nitrone dipeptide (**88**). Selected HMBC (red) correlations shown.

50.1 ppm (C-3) and 165.2 ppm (C-2), corresponding to the neighbouring amide, carbamate and α-carbons respectively.

Again, rotamers were observed in both the ^{1}H and ^{13}C NMR spectra of nitrone dipeptide (**88**). Variable temperature ^{1}H NMR experiments showed that the signals for the nitrone proton (C-37), diastereotopic benzylic methylene protons (C-30) and α-proton (C-19) were all split at room temperature, but all coalesced by once the sample was warmed to 388 K. Likewise, the ^{13}C NMR of nitrone dipeptide (**88**), showed splitting of several carbon signals (C-21, C-19, C-28, and C-23), which also coalesced above 368 K (**Figure 3.7**).

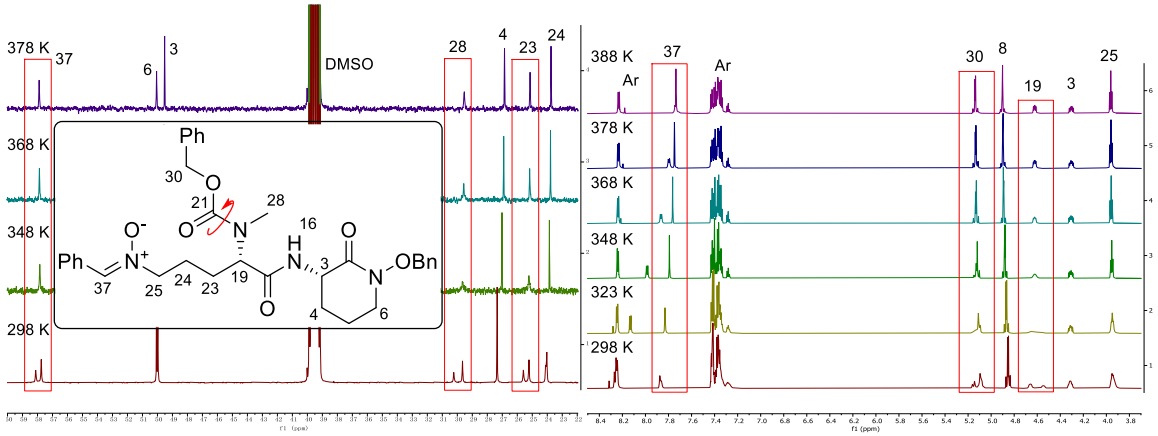

Figure 3.7. Rotamers of nitro dipeptide (**88**) as observed by ^{13}C NMR (left) from 298 K (bottom) to 378 K (top) and ^{1}H NMR (right) from 298 K (bottom) to 388 K (top) in DMSO-d_6 (700MHz).

It should be noted that following column chromatography we also isolated a by-product

from the HATU coupling reaction in 61% yield, which was confirmed as the corresponding unmethylated nitrone dipeptide (**89**) by NMR and HRMS. We believe that this molecule was produced by the HATU coupling of nitrone (**76**) with cyclised ornithine hydrobromide (**69**). The nitrone (**76**) likely being present as a minor impurity in the *N*-methyl nitrone (**68**) starting material prepared previously (**Figure 3.8**).

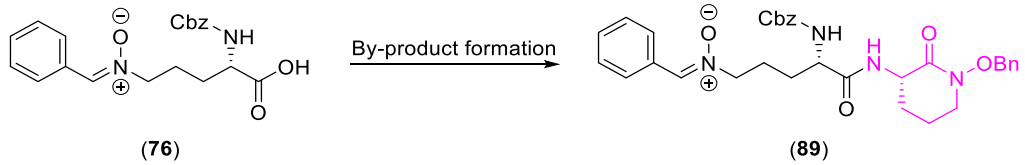

(**76**) (**89**)

Figure 3.8. Expected by product unmethylated nitrone dipeptide (**89**) formed by amide coupling from nitrone (**76**).

In the next step we planned to carry out a nitrone metathesis reaction on nitrone dipeptide (**88**) to give the free hydroxylamine.

Therefore following a similar procedure as before, 0.6 mmol of nitrone dipeptide (**88**) was reacted with 1.2 equivalents of hydroxylamine hydrochloride in MeOH at reflux for 40 minutes. After this, the solvent was removed under reduced pressure and the resulting residue was triturated with MeOH/Et_2O (1:3) to give the desired hydroxylamine functionalised dipeptide (**65**) (middle-right fragment) in a quantitative yield (**Scheme 3.20**; **Table 3.13**, Entry 1).

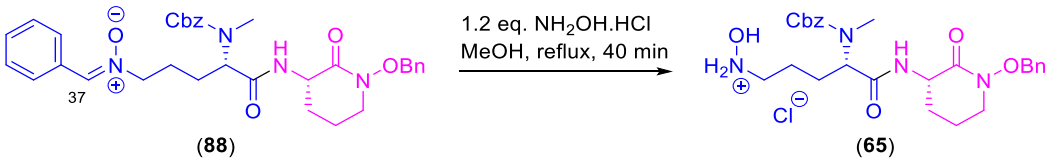

(**88**) (**65**)

Scheme 3.20. Nitrone metathesis of nitrone dipeptide (**88**) to give hydroxylamine functionalised dipeptide (**65**) (middle-right fragment).

^{1}H NMR analysis confirmed the presence of hydroxylamine functionalised dipeptide (**65**) through the loss of the nitrone signal (C-37), in combination with high resolution mass spectrometry which showed the expected molecular ion (experimental $[M+Na]^+$

= 521.2355; calculated for $C_{26}H_{34}N_4O_6Na$ $[M+Na]^+$ 521.2376). However, ^1H NMR also showed trace impurities within the sample, therefore a portion of triturated hydroxylamine functionalised dipeptide (**65**) was subjected to column chromatography in DCM:MeOH (24:1). Following solvent removal, ^1H NMR showed an increase in impurity levels in the sample, suggesting that hydroxylamine functionalised dipeptide (**65**) may be unstable on silica. We therefore decided to take hydroxylamine functionalised dipeptide (**65**) directly into the next coupling step without further purification. The nitrone metathesis reaction was then repeated on a similar scale to prepare more material to use in subsequent steps (**Table 3.13**).

Entry	Reaction Scale/mmol	Yield
1[a]	0.6	quantitative
2	0.9	quantitative

Table 3.13. Nitrone metathesis of nitrone dipeptide (**88**) to give hydroxylamine functionalised dipeptide (**64**). [a] Entry repeated from **Scheme 3.20** for comparison.

3.10 Synthesis of Madurastatin C1 via Final Amide Coupling, Oxazoline Synthesis and Global Deprotection

To complete our synthesis of madurastatin C1 (**9**), we planned to first assemble the previously prepared left-hand fragment (**64**) with the corresponding middle-right fragment (**65**), via a HATU amide coupling, followed by cyclisation to give our desired protected oxazoline pentapeptide (**91**), and finally a global deprotection (**Scheme 3.21**).

We first attempted the amide coupling between the two main fragments. Therefore, 1.2 mmol of *N*-functionalised (*R*)-ser-gly-β-ala-OH (**64**) was reacted with HATU, hydroxylamine functionalised dipeptide (**65**) and DIPEA in DMF at 0 °C for around 15 minutes. After this, the reaction mixture was allowed to warm slowly to room temperature over 22 hours. Following aqueous work-up, protected pentapeptide (**90**)

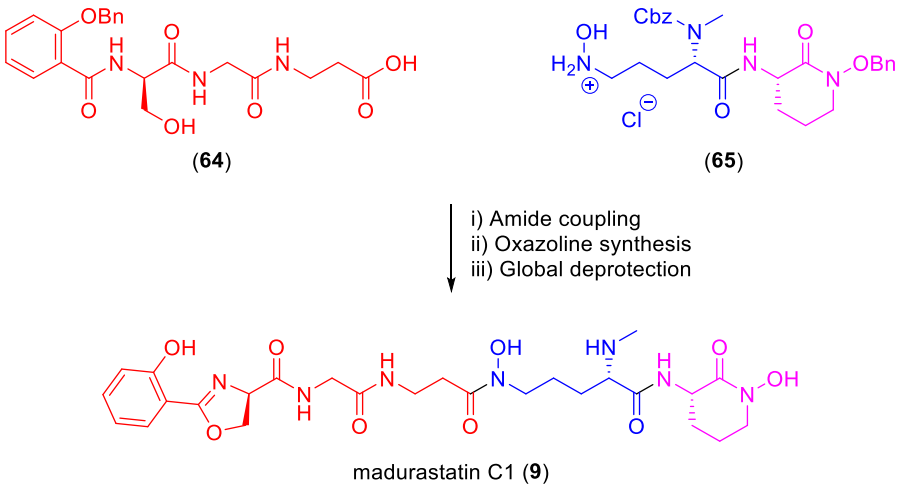

Scheme 3.21. Planned final steps in the synthesis of madurastatin C1 (**9**).

was purified by column chromatography (DCM:MeOH = 9:1). ^{1}H NMR analysis showed the presence of a number of impurities, thus the sample was purified by column chromatography a second time (DCM:MeOH = 19:1, R_f = 0.18). The desired protected pentapeptide (**90**) was isolated in a 53% yield as a colourless oil (**Scheme 3.22**).

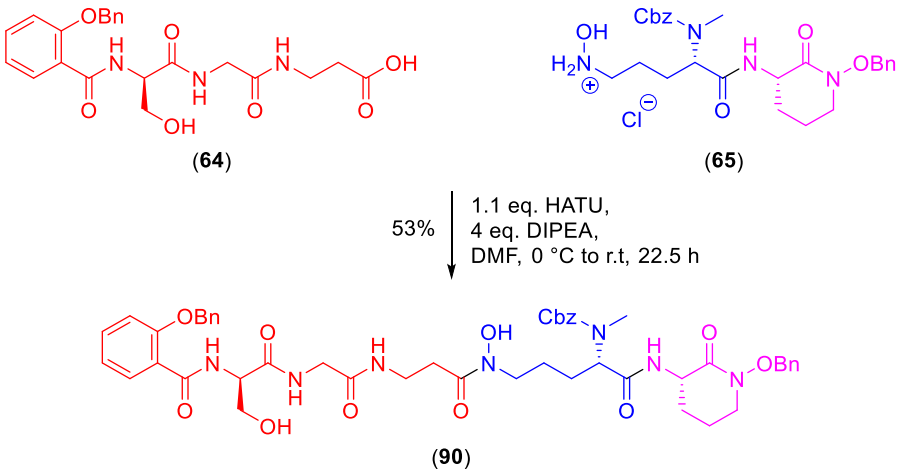

Scheme 3.22. Amide coupling of *N*-functionalised (*R*)-ser-gly-β-ala-OH (**64**) (left fragment) and hydroxylamine functionalised dipeptide (**65**) (middle-right fragment) to give protected pentapeptide (**90**).

The protected pentapeptide (**90**) was first analysed by LCMS. The base peak chromatogram showed one major peak at 14.7 min with *m/z* = 924.4 ([M+H$^+$]),

corresponding to the desired product. A minor peak was also observed at 10.6 min with *m/z* = 499.2 ([M+H]$^+$), corresponding to trace unreacted starting material hydroxylamine functionalised dipeptide (**65**). The extracted ion chromatogram (*m/z* range 924.4, +/- 0.5 Da) was also examined to check for the presence of other diastereoisomers, however only a single major peak was seen, suggesting a single diastereoisomer following purification. It should be noted that the two small peaks observed at 16.1 min and 16.6 min in the EIC, did not contain a major *m/z* = 924.4 signal in the mass spectra and as such are not diastereoisomers (**Figure 3.9**).

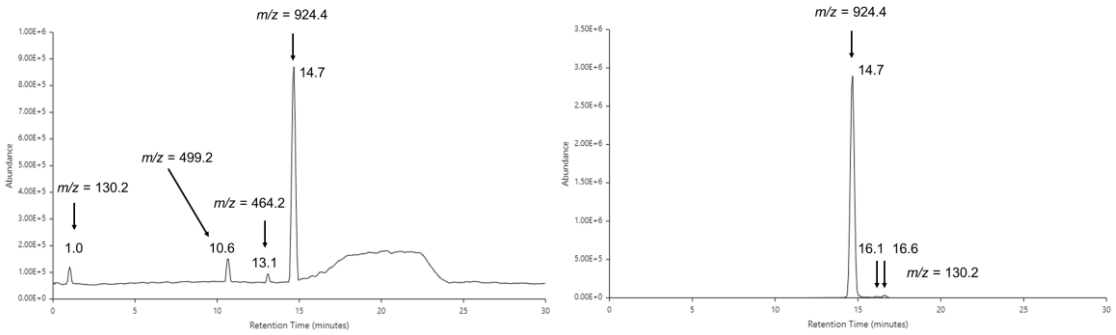

Figure 3.9. LCMS of protected pentapeptide (**90**): (A) base peak chromatogram (B) extracted ion chromatogram (EIC *m*/*z* = 924.4, +/- 0.5 Da).

Isolated protected pentapeptide (**90**) was also analysed by HRMS which gave *m/z* = 924.4192 (calculated for $C_{48}H_{57}N_7O_{12}H$ [M+H]$^+$ 924.4144) matching the expected formula.

^{1}H NMR analysis of protected pentapeptide (**90**) was complex due to the presence of a large number of overlapping broad signals even at high field (700 MHz). Therefore we used a number of 2D-NMR experiments (COSY, HSQC and HMBC) in order to assign the ^{1}H and ^{13}C signals, supported with ^{1}H-^{15}N HMBC experiments (for full assignment table see Appendix 3, **Figure 3.10**).

In addition, we also examined protected pentapeptide (**90**) by variable temperature NMR to examine the presence of rotamers. Due to the large number of overlapping signals in the ^{1}H NMR, we focused our attention on variable temperature ^{13}C NMR.

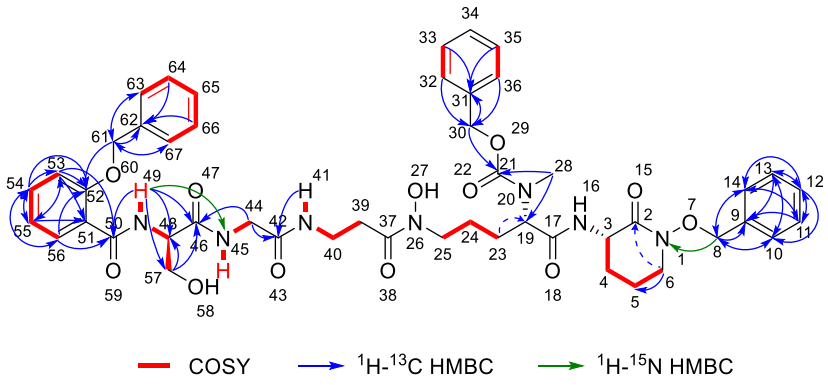

Figure 3.10. Selected 2D-NMR correlations for protected pentapeptide (**90**)

Several peaks corresponding to rotamers were observed, including those corresponding to C-25 (46.9 and 46.8 ppm at 298 K, coalescing to 47.0 ppm at 328 K) and C-39 (32.0 and 31.9 ppm at 298 K, shifting to 32.2 and 32.1 ppm at 328 K). These experiments confirm that protected pentapeptide (**90**) has two rotamers due to the restricted rotation of the central hydroxamic acid group (**Figure 3.11**).

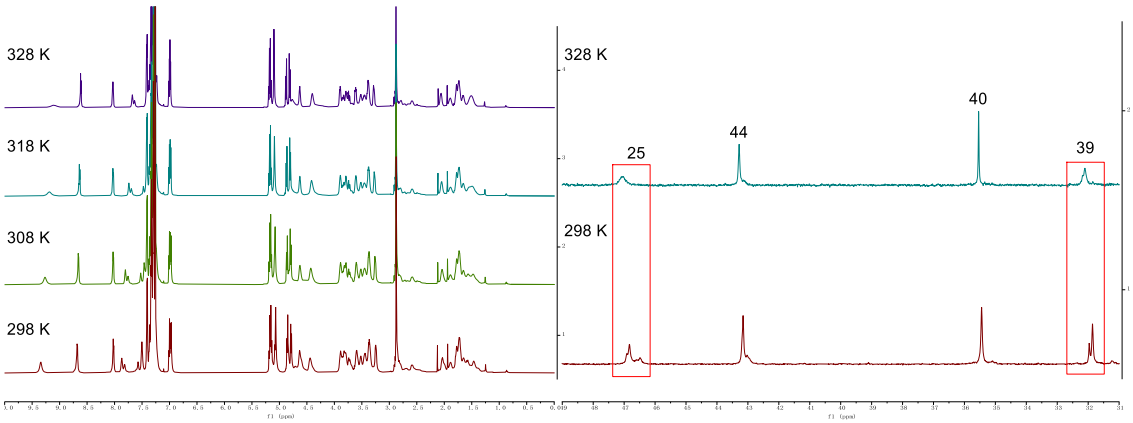

Figure 3.11. ^{1}H NMR ($CDCl_3$, 700 MHz) (left) and ^{13}C NMR ($CDCl_3$, 176 MHz) (right) of protected pentapeptide (**90**) from 298 K (bottom) to 328 K (top), showing the presence of rotamers.

In our variable temperature ^{13}C NMR experiments, a number of other rotamers were also observed involving the C-42, C-24, C-19, C-28 and C-21 positions, which suggests additional rotamers are present due to restricted rotation around one of the amide bonds and the CBz carbamate group (**Figure 3.12**).

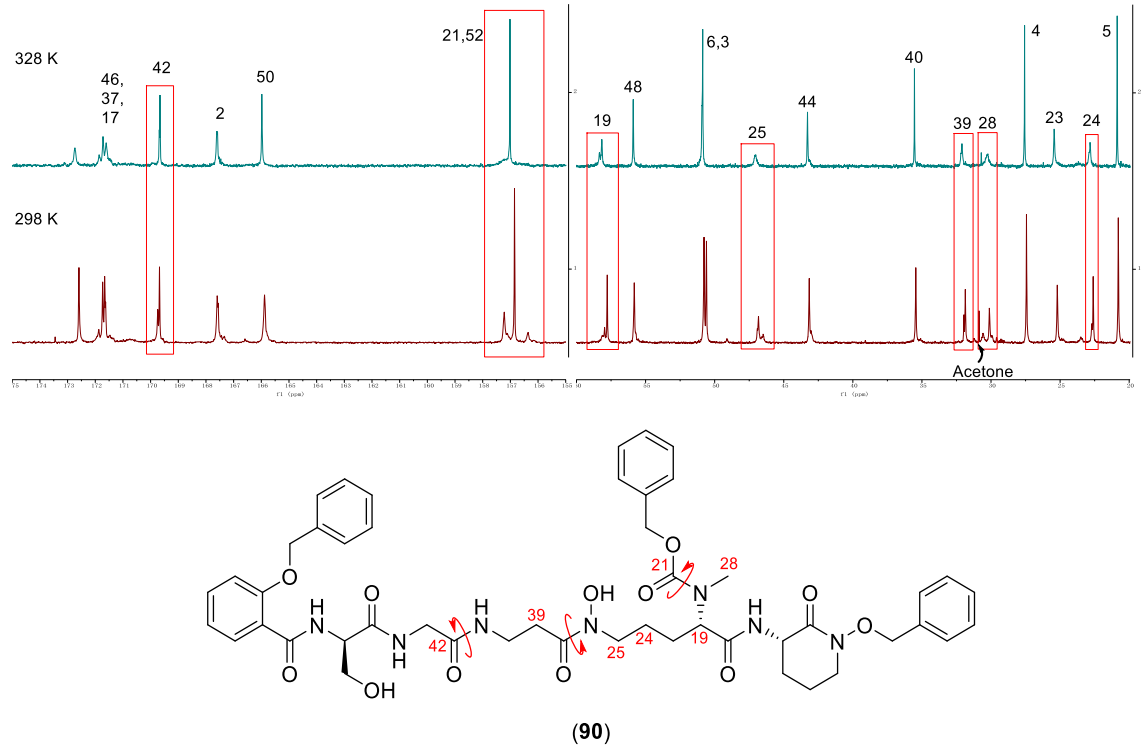

(**90**)

Figure 3.12. ^{13}C NMR ($CDCl_3$, 176 MHz) of protected pentapeptide (**90**) from 298 K (bottom) to 328 K (top), showing the presence of rotamers.

In the next step, we focused on the cyclisation reaction to form the desired oxazoline (**91**). We decided to use diethylamino-sulfur trifluoride (DAST) for the cyclisation reaction following a procedure by Wipf *et al*. in which they prepared oxazolines from serine-containing polypeptides.[99]

In our first test reaction, we reacted protected pentapeptide (**90**) on a 0.08 mmol scale, with 2 equivalents of DAST in dichloromethane at -78 °C. After 1 hour at -78 °C, the reaction mixture was allowed to warm to room temperature, and 4 equivalents of solid K_2CO_3 were added in one portion. After 30 minutes the reaction was quenched with saturated aqueous $NaHCO_3$. Following aqueous work-up and column chromatography (DCM:MeOH = 19:1), the major product (R_f = 0.31) from TLC was isolated (**Scheme 3.23**).

Unfortunately the ^1H NMR spectrum of the major fraction from the oxazoline forming reaction, only showed the presence of a complex mixture of compounds in which it

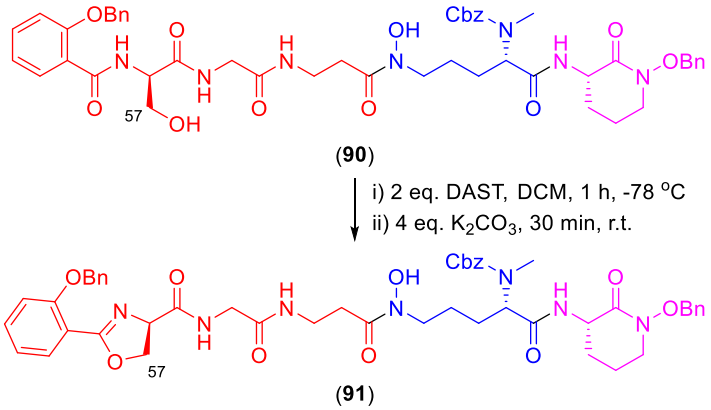

Scheme 3.23. Ring closing reaction with DAST in an attempt to form protected oxazoline pentapeptide (**91**).

was hard to identify the desired protected oxazoline pentapeptide (**91**).

Therefore, we attempted the ring closing reaction of protected pentapeptide (**90**) again on a similar scale, increasing the amount of DAST to 3 equivalents, K_2CO_3 to 5 equivalents, and the overall reaction time to 2.5 hours. Following aqueous work-up and column chromatography, a major fraction was obtained (**Table 3.14**).

Entry	Reaction Scale /mmol	Reaction Time/hour		Equivalents		Reaction Outcome
		Step 1	Step 2	DAST	K_2CO_3	
1[a]	0.08	1 h	0.5 h	2	4	Complex mixture
2	0.10	2 h	0.5 h	3	5	Trace by HRMS

Table 3.14. Attempted ring closing reaction of protected pentapeptide (**90**) with DAST to give protected oxazoline pentapeptide (**91**) [a] Entry repeated from **Scheme 3.23** for comparison.

Again ^{1}H NMR analysis proved inconclusive, so the major fraction from the column was analysed by HRMS. The mass spectra showed a small signal with *m/z* = 928.3868 (7%) which matched the calculated formula ($C_{48}H_{55}N_7O_{11}Na$ $[M+Na]^+$ 928.3857) of the protected oxazoline pentapeptide (**91**) suggesting that some of the desired molecules had been formed in the reaction (**Figure 3.13**).

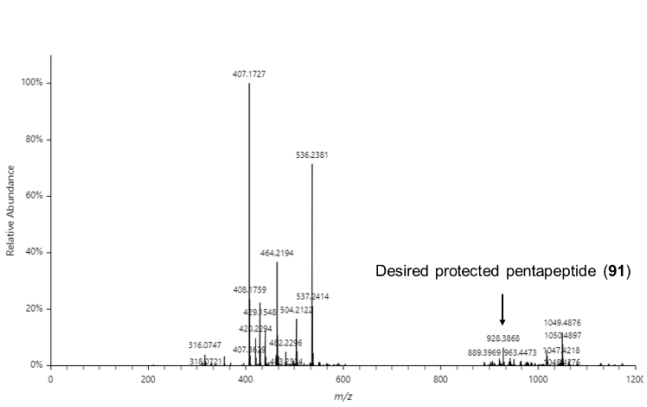

Figure 3.13. HRMS of isolated major fraction showing the expected molecular ion of protected oxazoline pentapeptide (**91**).

Unfortunately, due to time constraints we were unable to continue work on this molecule, including further purification and final global deprotection.

3.11 Conclusions and Future Work

In this chapter, we have successfully achieved 14 synthetic steps en route to the polypeptide siderophore natural product madurastatin C1, in a 17% overall yield to the backbone protected pentapeptide (**90**) based on the longest linear pathway. During the course of the synthesis, we have attempted to monitor the absolute stereochemistry by specific rotation ($[\alpha]_D$), which has given reasonable %*ee* for several key compounds (e.g., (2-(benzyloxy)benzoyl)-*D*-serine (**66**), left-hand fragment (**64**) of madurastatin C1, benzyl protected cyclised ornithine (*S*-**86**) and middle-right fragment component (**88**)) including the final product protected pentapeptide (**90**). However in the future this should be confirmed by chiral HPLC analysis following the synthesis of the enantiomers for comparison. Assignment of the absolute stereochemistry has also been supported through the use of single crystal X-ray diffraction for methyl (2-(benzyloxy)benzoyl)-*D*-serinate (**77**), which gave Flack parameters of -0.07(13), confirming that the major enantiomer was *R*. In addition, we have shown that the final product protected pentapeptide (**90**) was formed as a single diastereomer by LCMS analysis. Throughout this synthesis the ^{1}H NMR analysis was complicated by the presence of a number of rotamers. However we have shown that this can be

understood through the use of variable temperature NMR experiments.

Unfortunately, the second to last planned step in our synthetic sequence, the DAST mediated oxazoline synthesis was so far unsuccessful. In part due to the formation of multiple by-products and difficulties in purification.

In the future, in order to complete the synthesis of madurastatin C1 we would consider two alternative routes, assuming that the previously attempted late stage oxazoline synthesis could not be improved.

Firstly, we would examine the introduction of the oxazoline ring much earlier in the synthetic plan. In particular, we would test the introduction of the oxazoline ring directly from several early left-hand fragment precursors (**92**, **93**, **94**) which would be later coupled with the middle-right hand fragments, followed by global deprotection. However, this approach may be difficult as the oxazoline may ring open during the subsequent reaction chemistry (**Scheme 3.24**).

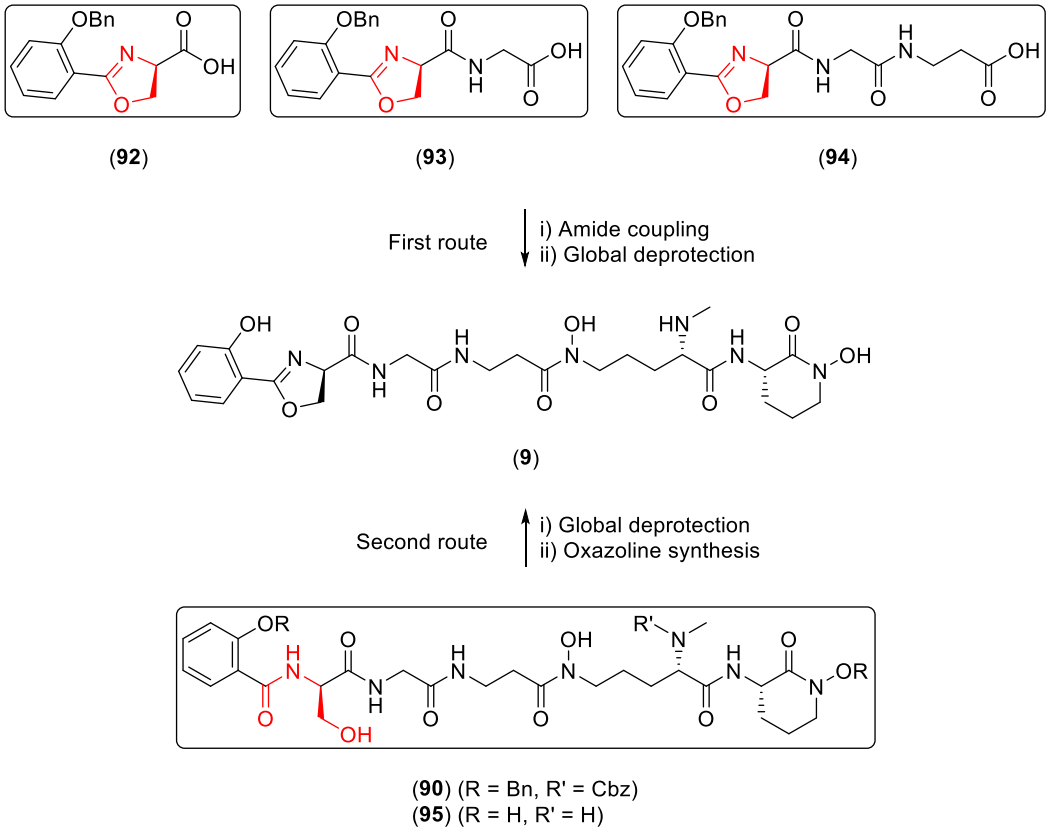

Scheme 3.24. Alternative routes to approach madurastatin C1 (**9**)

Secondly, we will attempt the global deprotection of protected pentapeptide (**90**) to give deprotected pentapeptide (**95**), followed by a final step of oxazoline synthesis. However, this also may be difficult as the deprotected pentapeptide (**95**) has the potential to undergo other reactions with DAST or similar reagents.

An advantage of our first route is that the planned oxazoline containing left-hand fragments would correspond to the benzyl protected versions of other natural products, namely madurastatin B1 (**14**), madurastatin E1 (**22**) and madurastatin F1 (**24**),[27] allowing us to access these other natural products as part of the same synthesis (**Figure 3.14**).

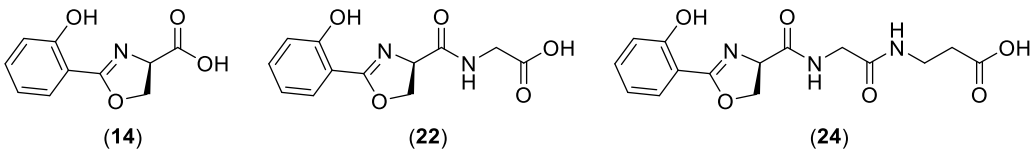

Figure 3.14. Natural products madurastatin B1 (**14**), madurastatin E1 (**22**) and madurastatin F1 (**24**).

Chapter 4. Experimental

4.1 General Experimental Information

Analysis

The melting points (MP) were determined using the Stuart SMP3 melting point apparatus. For thin layer chromatography (TLC), silica gel 60 F_{254} plates were used and visualization was done under ultraviolet light, unless a staining technique was specified. The ^{1}H NMR and $^{13}C\{1H\}$ NMR spectra were acquired using spectrometers such as Bruker Advance III 300 MHz, Jeol ECS-400 MHz, or Bruker Advance III HD 700 MHz. The Varian 800 FT-IR Scimitar Series spectrometer was used to obtain infrared (IR) spectra. The high resolution mass (HRMS) spectra were provided by SAgE Mass Spectrometry Facility (Newcastle University), performed by Dr Rachael Dack and Dr Alex Charlton.

Chemical Procedures

All chemical reactions involving air-sensitive reagents were conducted using the Schlenk technique under a nitrogen atmosphere. Anhydrous solvents were distilled under nitrogen and used without delay. THF and ether were distilled from sodium/benzophenone, while DCM was distilled from calcium hydride. Manual flash column chromatography was performed using Geduran silica gel 60 (40-63 μm).

4.2 Advanced Marfey's Analysis Experimental Section

All reagents were purchased from TCI UK Ltd (N^{α}-(5-fluoro-2,4-dinitrophenyl)-L-leucinamide, N^{α}-(5-fluoro-2,4-dinitrophenyl)-D-leucinamide), Alfa Aesar Ltd (L-ornithine hydrochloride, 57 % hydriodic acid) and Fluorochem Ltd (D-ornithine hydrochloride). LCMS was performed on a Waters LCMS system, ACQUITY Ultra Performance LC™ (UPLC™) coupled to ACQUITY Photodiode Array (PDA) UV detector and a Xevo TQ-S mass detector.

LCMS Method for Marfey's Analysis

HPLC separation was carried out using a linear gradient of 5 - 70 % MeCN:H_2O (0.1 % formic acid) over 15 minutes and a hold time at 100 % of MeCN (0.1 % formic acid) for 1 minute, with an injection volume of 1 µL, and a volume flow rate of 0.25 mL/min. Detection was carried out by UV (200-500 nm) and ESI-MS. Column (temp): ACQUITY UPLC® BEH C_{18} 1.7 µm, 2.1 x 150 mm Column (40 °C)

Marfey's Analysis of DC616 A (32)

To determine the absolute stereochemistry of DC616 A (**32**) by Marfey's analysis, 500 µg of (**32**) was dissolved in 400 µL of 57% HI and the reaction mixture was heated to 110 °C in an oil bath for 3 hours. After this time the reaction mixture was evaporated to dryness under a gentle stream of nitrogen gas overnight.

The residue material was dissolved in 240 µL of 1 M aq. $NaHCO_3$, to which was added 170 µL 1 % N^{α}-(5-fluoro-2,4-dinitrophenyl)-L-leucinamide in acetone and the reaction mixture was stirred for 1 hour at 40 °C. After this, the reaction was quenched with 60 µL of 2 M aq. HCl.

20 µL of this sample was diluted with 980 µL of HPLC grade water and analysed following the above LCMS method, versus standards.

Preparation of Standards for Marfey's Analysis

Marfey's standards for D-ornithine and L-ornithine were prepared by mixing 50 µL of a 50 mM aq. solution of either D-ornithine or L-ornithine hydrochloride with 20 µL of a 1 M aq. solution of $NaHCO_3$ and 100 µL of 1 % L-FDLA in acetone. The reaction mixtures were heated to 40 °C in a water bath for 1 hour to form the corresponding L-FDLA/D-ornithine and L-FDLA/L-ornithine adducts. 17 µL of each

of these sample was diluted with 983 µL of HPLC grade water and analysed following the above LCMS method.

Marfey's Analysis of DC616 A (32) vs Standards by LCMS

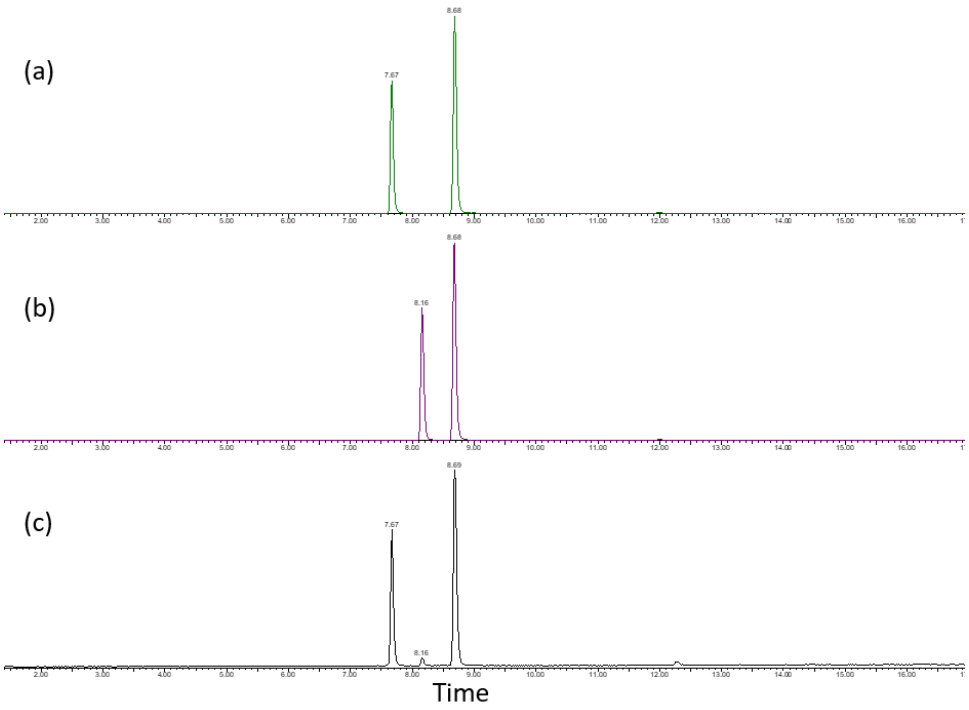

Figure. LCMS Extracted ion chromatograms (EIC *m/z* = 427.2, +/- 0.25 Da):

(a) L-FDLA + D-Ornithine (LD standard)

(b) L-FDLA + L-Ornithine (LL standard)

(c) L-FDLA + DC616 A

4.3 Experimental Procedures and Structural Characterisation

4.3.1 Benzyl 2,3-bis(benzyloxy)benzoate (54)

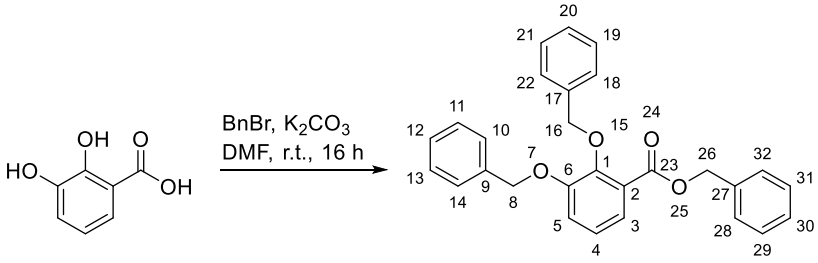

To a stirred solution of 2,3-dihydoxybenzoic acid (1.54 g, 10.00 mmol) in dry DMF (16 mL) at room temperature under nitrogen atmosphere was added K_2CO_3 (4.53 g, 32.78 mmol).

To the reaction mixture, BnBr (4.0 mL, 33.63 mmol) was added dropwise.

The reaction mixture was stirred for 38 h at room temperature.

After which the reaction mixture was diluted with H_2O (60 mL) and the aqueous extracted with EtOAc (3 X 50 mL) to obtain the benzyl ester. The combined organic layers were washed with sat. aq. $NaHCO_3$ (30 mL), sat. aq. NH_4Cl (30 mL), brine (60 mL), dried over anhydrous sodium sulphate and the solvent was removed under reduced pressure.

The crude product was purified via silica gel column chromatography (40-60 petrol/EtOAc = 15:1, column diameter = 5 cm, silica = 25 cm) to give the product as a colourless crystalline (needle) solid (3.95 g, 9.30 mmol) in a 93% yield.

Colourless solid (3.95 g, 93%).

Mp: 41 °C [lit. 40 °C].

R_f = 0.30 (40-60 petrol : EtOAc, 15:1; UV light 254nm).

^{1}H NMR (400 MHz, Chloroform-*d*) δ 7.45 - 7.08 (m, 16H, H-3, Ar), 7.15 (dd, *J* = 8.2, 1.8 Hz, 1H, H-5), 7.08 (t, *J* = 7.9 Hz, 1H, H-4), 5.32 (s, 2H, H-26), 5.14 (s, 2H, H-16), 5.07 (s, 2H, H-8).

^{13}C NMR (101 MHz, Chloroform-*d*) δ 165.6 (C-23), 152.4 (C-6), 147.8 (C-1), 137.2, 136.1, 135.6, 128.1, 128.1, 127.9, 127.8, 127.7, 127.6, 127.4, 127.1 (C-14 and C-10), 126.4 (C-4), 123.7 (C-3), 122.3 (C-2), 117.3 (C-5), 75.1 (C-16), 70.5 (C-8), 66.4 (C-26).

IR (neat) ν_{max}/cm^{-1}: 3029 (C-H, Ar, w), 1716 (C=O, s).

MS (ES+): 871.3 $[2M+Na]^+$ (20%), 447.1 $[M+Na]^+$ (100%).

HRMS (TOF ES+): calcd for $C_{28}H_{24}O_4Na$ $[M+Na]^+$ 447.1572, found 447.1577.

[lit.]: J. Deng, Y. Hamada and T. Shioiri, An efficient synthesis of alterobactin A
A super siderophore of marine origin. *Synthesis-Stuttgart*, 1998, 627-638.

4.3.2 2,3-Dibenzyloxybenzoic acid (50)

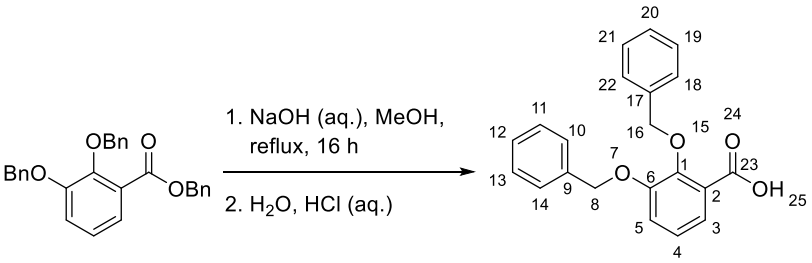

Benzyl 2,3-bis(benzyloxy) benzoate (1.79 g, 4.20 mmol) was dissolved in MeOH (15 mL), after which an aqueous solution of NaOH (10 mL, 2M) was added. The reaction mixture was heated to reflux and stirred for 16 h. After which the reaction mixture was cooled to room temperature, and the MeOH was removed under reduced pressure.

The resulting mixture was diluted with H_2O (40 mL) and washed with EtOAc (2 x 40 mL). The aqueous layer was acidified with a dropwise addition of 10% aq. HCl until pH 2 was reached (pH paper).

The acidified aqueous layer was then extracted with EtOAc (3 x 40 mL). The combined organic layers were then washed with brine (50 mL), dried over anhydrous sodium sulphate and the solvent was removed under reduced pressure to give 2,3-dibenzyloxybenzoic acid as a colourless powder (1.11 g, 3.32 mmol) in a 79% yield.

X-Ray grade crystals were grown from slow evaporation in methanol.

Colourless powder (1.11 g, 79%).

Mp: 124 – 125 °C [lit. 124.1 - 125.9 °C].

R_f = 0.35 (40-60 petrol : EtOAc, 2:1; UV light 254nm).

^{1}H NMR (400 MHz, Chloroform-*d*) δ 11.26 (br s, 1H, H-25), 7.67 (dd, *J* = 7.8, 1.7 Hz, 1H, H-3), 7.42 – 7.39 (m, 2H, H-14, H-10), 7.39 – 7.32 (m, 3H, H-13, H-12, H-11), 7.31 – 7.24 (m, 5H, Ar), 7.19 (dd, *J* = 8.2, 1.7 Hz, 1H, H-5), 7.12 (t, *J* = 8.0 Hz, 1H, H-4), 5.19 (s, 2H, H-16), 5.12 (s, 2H, H-8).

^{13}C NMR (101 MHz, Chloroform-*d*) δ 165.6 (C-23), 151.5 (C-6), 147.3 (C-1), 136.0 (C-9), 134.9 (C-17), 129.4 (C-22, C-18), 129.3 (20), 128.9 (Ar), 128.9 (Ar), 128.6 (C-12), 127.9 (C-14, C-10), 125.1 (C-4), 124.5 (C-3), 123.3 (C-2), 119.1 (C-5), 77.2 (C-16), 71.7 (C-8).

IR (neat) ν_{max}/cm^{-1}: 3032 (C-H, w), 2935-2572 (O-H, b, w), 1683 (C=O, s).

MS (ES+): 691.2 $[2M+Na]^+$ (64%), 357.1 $[M+Na]^+$ (100%).

HRMS (TOF ES+): calcd for $C_{21}H_{18}O_4Na$ $[M+Na]^+$: 357.1103, found 357.1122.

X-Ray code: MJH-DW-20-0065

[lit.]: D. J. Raines, O. V. Moroz, K. S. Wilson and A.-K. Duhme-Klair, Interactions of a Periplasmic Binding Protein with a Tetradentate Siderophore Mimic. *Angew. Chem. Int. Ed.*, 2013, **52**, 4595-4598.

4.3.3 (*S*)-4-(((benzyloxy)carbonyl)amino)-1-carboxybutan-1-aminium 2,2,2-trifluoroacetate (55)

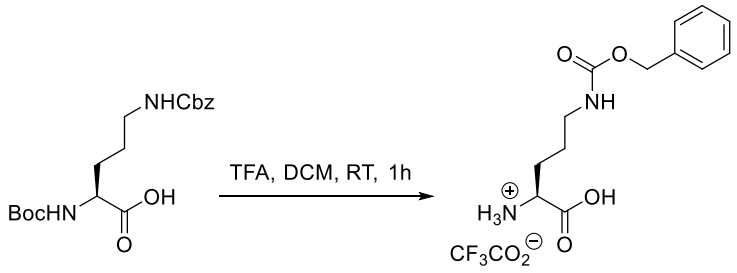

In a 150 mL round bottom flask, under an atmosphere of nitrogen, was added (*S*)-5-(((benzyloxy)carbonyl)amino)-2-((*tert*-butoxycarbonyl)amino)pentanoic acid (1.465 g, 4 mmol), anhydrous DCM (23 mL) and followed by TFA (23 mL). After which the reaction mixture was stirred for 1 hour at room temperature. The solvent was then removed under reduced pressure and the residue with precipitated with diethyl ether and filtered to give (*S*)-4-(((benzyloxy)carbonyl)amino)-1-carboxybutan-1-aminium 2,2,2-trifluoroacetate (1.4452 g, 3.8 mmol) as a pale pink solid in 95% yield without further purification.

Note: The ^{1}H NMR shows significant the broadening across all peaks, however signals corresponding the Boc group are no longer observed.

4.3.4 (*S*)-5-(((Benzyloxy)carbonyl)amino)-2-(2,3-bis(benzyloxy)benzamido)pentanoic acid (46)

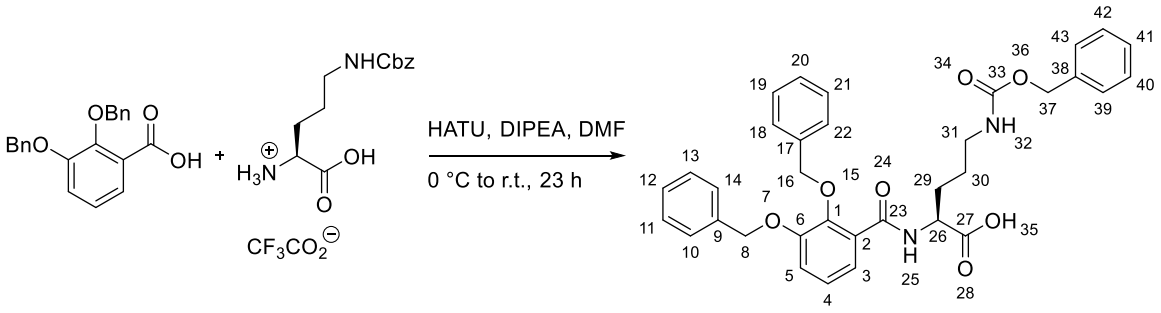

To a stirred solution of 2,3-bis(benzylox)benzoic acid (0.67 g, 2.00 mmol, 1.00 eq) in dry DMF (20 mL) at 0 °C under nitrogen atmosphere was added HATU (0.76 g, 2.00 mmol, 1.00 eq). The reaction mixture stirred for 15 min.

To a separate 25 mL round bottom flask, (*S*)-2-amino-5-(((benzyloxy)carbonyl)amino)pentanoic acid compound with 2,2,2-trifluoroacetaldehyde (1:1) (0.73 g 2.00 mmol) was dissolved in dry DMF (5 mL) at 0 °C under nitrogen atmosphere.

After which the second mixture was transferred into the first-round bottom flask by syringe.

To the reaction mixture, DIPEA (1.75 mL, 10.00mmol, 5.00 eq) was added dropwise over 5 min.

After being stirred for 30 min at the same temperature, the reaction mixture was allowed to warm slowly to room temperature stirred for 23 h.

After which the reaction mixture was quenched with sat. aq. NH_4Cl (10 mL), the resulting slurry was extracted with EtOAc (3 x 40 mL). The combined organic layers were washed with 0.2 M NaOH (2 x 30 mL), 0.4 M HCl (2 x 30 mL) and then brine (60 mL), dried over anhydrous sodium sulphate and the solvent was removed under reduced pressure.

The crude product was purified via silica gel column chromatography (MeOH/DCM/Acetic acid = 0.5:9.5:0.05, column diameter = 5 cm, silica = 25 cm) to give (*S*)-5-(((benzyloxy)carbonyl)amino)-2-(2,3-bis(benzyloxy)benzamido)pentanoic acid as a yellow foam, (0.57 g 0.98 mmol) in a 49% yield.

Yellow foam (0.57 g, 49%).

[α]$_D$ = -14° (*c* =1, MeOH).

R_f = 0.30 (MeOH : DCM : AcOH, 1:19:0.1; UV light 254nm).

^{1}H NMR (400 MHz, Chloroform-*d*) δ 10.49 (br s, 1H, H-35), 8.59 (d, *J* = 7.1 Hz, 1H, H-25), 7.69 (dd, *J* = 7.0, 2.5 Hz, 1H, H-3), 7.42 – 7.38 (m, 2H, Ar), 7.37 – 7.14 (m, 13H, Ar) 7.12 – 7.06 (m, 2H, H-5, H-4), 5.15 – 5.02 (m, 7H, H-8, H-16, H-37, H-32), 4.70 – 4.58 (m, H-26), 3.07 – 2.90 (m, 2H, H-31), 1.79 – 1.67 (m, 1H, H-29^a), 1.52 – 1.25 (m, 3H, H-29^b, H-30).

^{13}C NMR (101 MHz, Chloroform-*d*) δ 174.8 (C-27), 165.7 (C-23), 156.6 (C-33), 151.7 (C-6), 147.1 (C-1), 136.6 (C-38), 136.3, 136.3, 129.0, 128.9, 128.7, 128.6, 128.5, 128.5, 128.3, 128.2, 128.0, 127.8, 126.3 (C-2), 125.3, 124.4 (C-4), 123.3 (C-3), 117.6 (C-5), 76.2 (C-16), 71.3 (C-8), 66.6 (C-37), 52.4 (C-26), 40.4 (C-31), 29.0 (C-29), 25.8 (C-30).

IR (neat) ν_{max}/cm^{-1}: 3347 (O-H, b, w), 3033 (N-H, w), 2940 (C-H, w), 1713 (C=O, m).

MS: (ES+): 1187.5 $[2M+Na]^+$ (20%), 605.2 $[M+Na]^+$ (100%), 583.2 $[M+H]^+$ (61%).

HRMS (TOF ES+): calcd for $C_{68}H_{68}N_4O_{14}Na$ $[2M+Na]^+$: 1187.4630, found 1187.4634.

HRMS (TOF ES+): calcd for $C_{34}H_{34}N_2O_7Na$ $[M+Na]^+$: 605.2264, found 605.2274.

HRMS (TOF ES+): calcd for $C_{34}H_{34}N_2O_7H$ $[M+H]^+$: 583.2444, found 583.2444.

4.3.5 *N*-(Benzyloxy)-2-nitrobenzenesulfonamide (61)

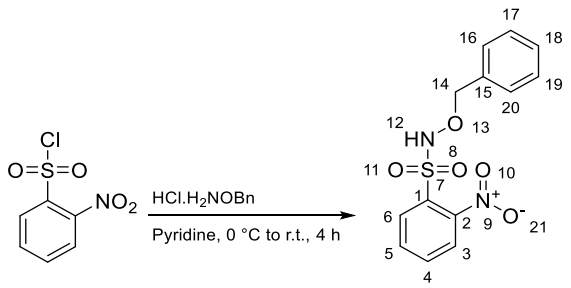

A stirred solution of *O*-benzylhydroxylamine hydrochloride (2.40 g, 15.00 mmol, 1.00 eq) in dry pyridine (20 mL) was cooled to 0 °C in an ice bath under a nitrogen atmosphere.

To this solution, a solution of 2-nitrobenzenesulfonyl chloride (3.37 g, 15.20 mmol, 1.01 eq) in dry pyridine (15 mL) was added dropwise over 30 min.

After being stirred for 1 h at the same temperature, the reaction mixture was allowed to warm slowly to room temperature stirred for an additional 4 h.

After which the reaction mixture was diluted with H_2O (35 mL), the resulting slurry extracted with DCM (2 x 20 mL). The combined organic layers were washed with 0.2 M HCl (3 x 10 mL), dried over anhydrous sodium sulphate and the solvent was removed under reduced pressure to give the crude nitrobenzenesulfonamide as a light-yellow powder.

The resulting solids were then dissolved in the minimum amount of $CHCl_3$ and cold MeOH was added to promote crystallisation overnight.

The crystals were collected via filtration and wash with cold MeOH (30 mL) to give *N*-(benzyloxy)-2-nitrobenzenesulfonamid as colourless crystals (2.45 g, 7.95 mmol) in a 53% yield.

X-Ray grade crystals were generated at the interface of a mixture of 1:1:1 $CHCl_3$, MeOH and H_2O.

Colourless crystal (2.45 g, 53%).

Mp: 153 °C [lit. 154 °C][64].

^{1}H NMR (400 MHz, Chloroform-*d*) δ 8.28 – 8.23 (m, 1H, H-3), 8.12 (s, 1H, H-12), 7.90 – 7.85 (m, 1H, H-6), 7.82 – 7.75 (m, 2H, H-5, H-4), 7.41 – 7.35 (m, 5H, Ar), 5.08 (s, 2H, H-14).

^{13}C NMR (101 MHz, Chloroform-*d*) δ 148.6, 134.9, 134.9, 133.8, 133.0, 130.6, 129.6 (2C), 129.0, 128.7 (2C), 125.7 (C-3), 80.0 (C-14).

IR (neat) ν_{max}/cm^{-1}: 3253 (N-H, m), 3063 (C-H, w).

HRMS (TOF ES+): calcd for $C_{13}H_{12}N_2O_5SNa$ $[M+Na]^+$: 331.0365, found 331.0372.

X-Ray code: MJH-DW-20-0049

4.3.6 Benzyl (*S*)-2-((*tert*-butoxycarbonyl)amino)-5-hydroxypentanoate (57)

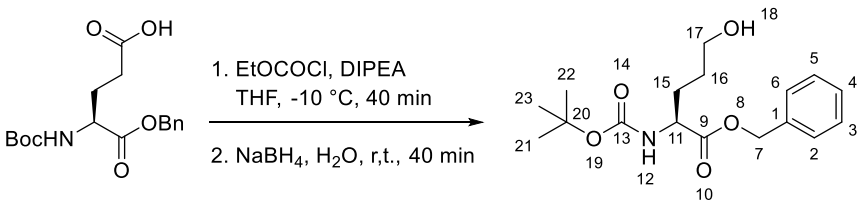

A stirred solution of (*S*)-5-(benzyloxy)-4-((*tert*-butoxycarbonyl)amino)-5-oxopentanoic acid (1.348 g, 4 mmol, 1 eq) in dry THF (22 mL) was cooled to -10 °C under nitrogen atmosphere.

DIPEA (0.73 mL, 4.16 mmol, 1.04 eq) and ethyl chlorocarbonate (0.44 mL, 4.56 mmol, 1.14 eq) were added dropwise from two separate syringes at the same time to the reaction mixture over 15 minutes.

Upon complete addition the reaction mixture was stirred for a further 30 minutes at the same temperature.

After which time sodium borohydride (0.454 g, 12 mmol, 3 eq) was added in one portion.

The reaction mixture then removed from the cold bath and allowed to warm slowly to room temperature and H_2O (11 mL) was added dropwise over 10 minutes.

Upon complete addition the mixture was left to stir for 30 minutes before 10 mL of brine was added to it.

After which the reaction mixture was extracted with EtOAc (3 x 30 mL). The combined organic layers were washed with sat. aq. $NaHCO_3$ (30 mL), sat. aq. NH_4Cl (30 mL) and then brine (40 mL), dried over anhydrous sodium sulphate and the solvent was removed under reduced pressure to give a clear colourless oil.

The crude product was purified via silica gel column chromatography (40-60 petrol/ethyl acetate = 2:1, column diameter = 5 cm, silica = 20 cm) to give benzyl (*S*)-2-((*tert*-butoxycarbonyl)amino)-5-hydroxypentanoate as clear colourless oil (0.95 g, 2.94 mmol) in a 73% yield

Colourless oil (0.95 g, 73%).

[α]$_D$ = -23.6° (*c* = 1, MeOH).

R_f = 0.14 (40-60 petrol : EtOAc, 2:1, UV light 254nm, $KMnO_4$);

^{1}H NMR (300 MHz, Acetone-d_6) δ 7.42 – 7.26 (m, 5H, Ar), 6.32 (d, *J* = 8.3 Hz, 1H, H-12) (minor rotamer 10% at 5.89), 5.19 (d, *J* = 12.4 Hz, 1H, H-7^a), 5.13 (d, *J* = 12.6 Hz, 1H, H-7^b), 4.21 (td, *J* = 8.6, 5.1 Hz, 1H, H-11), (minor rotamer 10% at 4.09), 3.62 (t, *J* = 5.1 Hz, 1H, H-18), 3.58 – 3.52 (m, 2H, H-17), 1.98 – 1.87 (m, 1H, H-15^a), 1.82 – 1.67 (m, 1H, H-15^b), 1.65 – 1.55 (m, 2H, H-16),1.39 (s, 9H, H-23, H-22, H-21).

^{1}H NMR (300 MHz, DMSO-d_6) δ 7.38 – 7.27 (m, 5H, Ar), 5.15 (d, *J* = 12.5 Hz, 1H, H-7^a), 5.08 (d, *J* = 12.7 Hz, 1H, H-7^b), 4.41 (t, *J* = 5.1 Hz, 1H, H-18), 3.97 (td, *J* = 8.5, 5.1 Hz, 1H, H-11), 3.39 – 3.33 (m, 2H. H-17, overlaps with residual water peak), 1.80 – 1.68 (m, 1H, H-15^a), 1.65 – 1.52 (m, 1H, H-15^b), 1.50 – 1.41 (m, 2H, H-16), 1.37 and 1.27 (s and s, 9H, H-23, H-22, H-21, major rotamer at 1.37, minor rotamer at 1.27).

^{13}C NMR (75 MHz, Acetone-d_6) δ 172.9 (C-9), 156.1 (C-13), 136.6 (C-1), 128.7 (C-5 and C-3), 128.3 (C-4), 128.2 (C-6 and C-2), 78.8 (C-20), 66.4 (C-7), 61.3 (C-17), 54.1 (C-11), 29.2 (C-16), 28.6 (C-15), 28.1 (C-23, C-22 and C-21).

IR (neat) ν_{max}/cm^{-1}: 3363 (O-H, b, w), 3976 (N-H, w).

MS (ES+): 346.2 $[M+Na]^+$ (100%).

HRMS (TOF ES+): calcd for $C_{17}H_{25}NO_5Na$ $[M+Na]^+$: 346.1630, found 346.1631.

4.3.7 Benzyl (*S*)-5-((*N*-(benzyloxy)-2-nitrophenyl)sulfonamido)-2-((*tert*-butoxycarbonyl)amino)pentanoate (62)

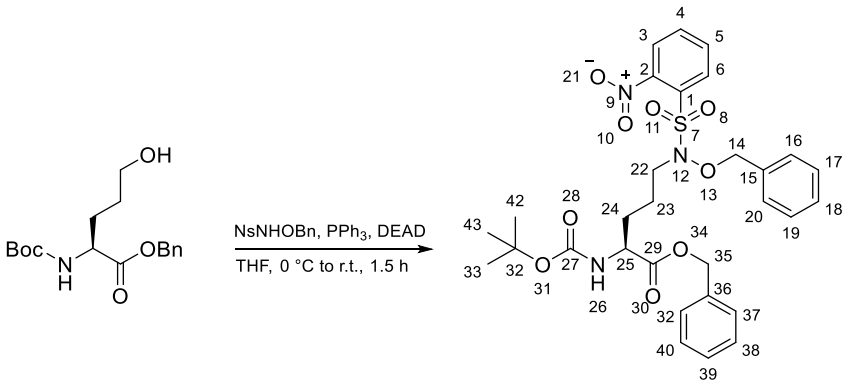

To a 50 mL round bottom flask was add benzyl (*S*)-2-((*tert*-butoxycarbonyl)amino)-5-hydroxypentanoate (0.90 g , 2.77 mmol, 1.00 eq), triphenylphosphine (0.76 g, 2.91 mmol, 1.05 eq), *N*-(benzyloxy)-2-nitrobenzenesulfonamide (0.90 g, 2.96 mmol, 1.07 eq).

The solids were then dissolved in dry THF (25 mL) and the reaction mixture cooled to 0 °C under nitrogen atmosphere.

To the reaction mixture, DEAD (0.49 mL, 3.09 mmol, 1.12 eq) was added dropwise over 30 minutes.

After this time, the reaction mixture was allowed to warm slowly to room temperature stirred for an additional 1 h.

After which the reaction mixture was quenched with sat. aq. NH_4Cl (15 mL), the resulting slurry extracted with EtOAc (3 x 30 mL). The combined organic layers were washed with sat. aq. NH_4Cl (30 mL) and brine (40 mL), dried over anhydrous sodium sulphate and the solvent was removed under reduced pressure to give a colourless oil.

The crude product was purified via silica gel column chromatography (40-60 petrol/ethyl acetate = 3:1, column diameter = 5 cm, silica = 24 cm) to give benzyl (*S*)-5-((*N*-(benzyloxy)-2-nitrophenyl)sulfonamido)-2-((*tert*-butoxycarbonyl)amino)pentanoate as a colourless oil (1.50 g, 2.44 mmol) in an 88% yield.

Colourless oil (1.50 g, 88%).

[α]$_D$ = -0.8° (*c* = 1, MeOH).

R_f = 0.38 (40-60 petrol : EtOAc, 2:1, UV light 254nm, $KMnO_4$).

^{1}H NMR (400 MHz, Chloroform-*d*) δ 7.99 (d, *J* = 8.0 Hz, 1H, H-3), 7.74 (t, *J* = 7.8 Hz, 1H, H-5), 7.64 (t, *J* = 7.8 Hz, 1H, H-4), 7.53 (d, *J* = 8.0 Hz, 1H, H-6), 7.40 – 7.30 (m, 10H, Ar), 5.15 (s, 2H, H-35), 5.03 (s, 2H, H-14), 5.00 (s, 1H, H-26), 4.32 – 4.26 (m, 1H, H-25), 3.06 (br s, 2H, H-22), 1.91 – 1.82 (m, 1H, H-24^a), 1.68 – 1.59 (m, 1H, H-24^b), 1.56 – 1.47 (m, 2H, H-23), 1.43 (s, 9H, H-43, H-42, H-33).

^{13}C NMR (101 MHz, Chloroform-d) δ 172.2 (C-29), 155.3 (C-27), 149.8 (C-2), 135.3 (C-36), 135.0 (C-5), 134.7 (C-15), 132.7 (C-3), 131.1 (C-4), 130.1 (C-20 and C-16), 129.2 (C-39), 128.7 (Ar), 128.7 (Ar), 128.6 (C-18), 128.4 (C-41 and C-37), 125.8 (C-1), 123.7 (C-6), 80.3 (C-14), 80.0 (C-32), 67.2 (C-35), 53.2 (C-25), 52.9 (C-22), 29.9 (C-24), 28.4 (C-43, C-42 and C-33), 22.8 (C-23).

IR (neat) ν_{max}/cm^{-1}: 3420 (N-H, w), 2980 (C-H, w), 1738 (C=O, m), 1709 (C=O, m).

MS (ES+): 636.2 $[M+Na]^+$ (100%).

HRMS (TOF ES+): calcd for $C_{30}H_{35}N_3O_9SNa$ $[M+Na]^+$: 636.1992, found 636.1987.

4.3.8 Benzyl (*S*)-5-((benzyloxy)amino)-2-((*tert*-butoxycarbonyl)amino)pentanoate (49)

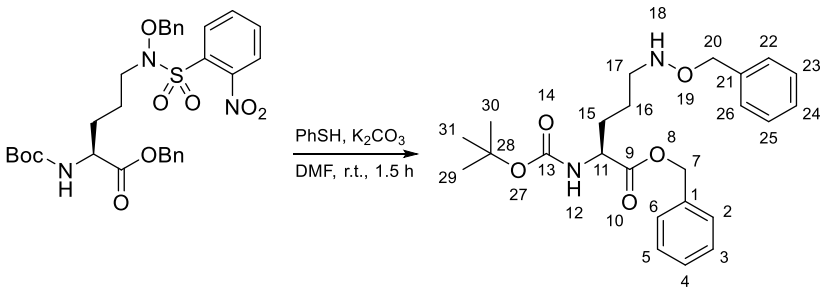

To a stirred solution of benzyl (*S*)-5-((N-(benzyloxy)-2-nitrophenyl)sulfonamido)-2-((*tert*-butoxycarbonyl)amino)pentanoate (0.54 g, 0.88 mmol, 1.00 eq) in dry DMF (4.5 mL) at room temperature under nitrogen atmosphere was added K_2CO_3 (0.13 g, 0.94 mmol, 1.07 eq). The reaction mixture was stirred for 10 min.

To the reaction mixture, thiophenol (0.11 mL, 1.06 mmol, 1.20 eq) was added via syringe.

The reaction mixture was then stirred for an additional 80 min.

After which the reaction mixture was quenched with sat. aq. NH_4Cl (20 mL), the resulting slurry extracted with EtOAc (3 x 30 mL). The combined organic layers were washed with sat. aq. NH_4Cl (30 mL) and brine (40 mL), dried over anhydrous sodium sulphate and the solvent was removed under reduced pressure to give a colourless oil.

The crude product was purified via silica gel column chromatography (40-60 petrol/ethyl acetate = 2:1, column diameter = 5 cm, silica = 20 cm) to benzyl (*S*)-5-((benzyloxy)amino)-2-((*tert*-butoxycarbonyl)amino)pentanoate as a colourless oil (0.31 g, 0.72 mmol) in a 82% yield.

Colourless oil (0.31 g, 82%).

[α]$_D$ = -13.4° (*c* = 1, MeOH).

R_f = 0.20 (40-60 petrol : EtOAc, 2:1, UV light 254nm, $KMnO_4$);

^{1}H NMR (400 MHz, Chloroform-*d*) δ 7.39 – 7.27 (m, 10H, Ar), 5.21 – 5.12 (m, 3H, H-7, H-12), (overlaps with N-H peak), 4.67 (s, 2H, H-20), 4.37 – 4.32 (m, 1H, H-11), 2.90 (t, *J* = 6.8 Hz, 2H, H-17), 1.91 – 1.82 (m, 1H, H-15^a), 1.74 – 1.65 (m, 1H, H-15^b), 1.61 – 1.49 (m, 2H, H-16), 1.44 (s, 9H, H-31, H-30, H-29).

^{13}C NMR (101 MHz, Chloroform-d) δ 172.7 (C-9), 155.5 (C-13), 138.0 (C-1), 135.6 (C-21), 128.7 (2C), 128.6 (3C), 128.5 (3C), 128.4, 128.0, 80.0 (C-28), 76.4 (C-20), 67.1 (C-7), 53.5 (C-11), 51.5 (C-17), 30.5 (C-15), 28.5 (C-31, C-30, C-29), 23.4 (C-16).

IR (neat) ν_{max}/cm^{-1}: 3354 (N-H, w), 2977 (N-H, w), 1739 (C=O, m), 1711 (C=O, s).

MS (ES+): 429.2 $[M+H]^+$ (100%).

HRMS (TOF ES+): calcd for $C_{24}H_{32}N_2O_5H$ $[M+H]^+$: 429.2390, found 429.2394.

4.3.9 Benzyl (*S*)-5-(*N*-(benzyloxy)formamido)-2-((*tert*-butoxycarbonyl)amino)pentanoate (63)

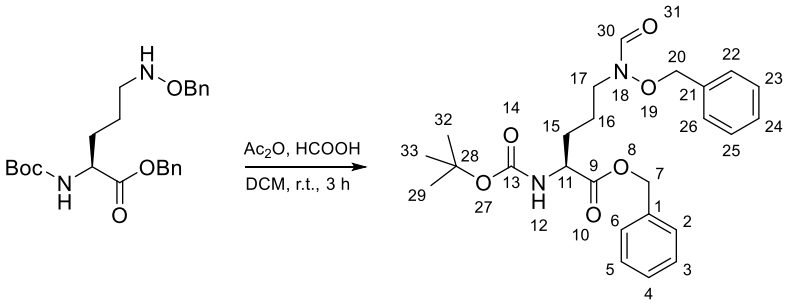

A mixed anhydride solution was prepared by mixing of acetic anhydride (92.64 µL, 0.98 mmol, 2.10 eq) and formic acid (73.95 µL, 1.96 mmol, 4.20 eq) for 1 h.

After this time, the mixture was poured into a solution benzyl (*S*)-5-((benzyloxy)amino)-2-((*tert*-butoxycarbonyl)amino)pentanoate (200 mg, 0.47 mmol, 1.00 eq) in dry DCM (2.3 mL) at room temperature under nitrogen atmosphere.

The reaction mixture was then stirred for additional for 1.5 h.

After which the reaction mixture was diluted with DCM (15 mL) and washed with sat. aq. $NaHCO_3$ (20 mL), dried over anhydrous sodium sulphate and the solvent was removed under reduced pressure to give benzyl (*S*)-5-(*N*-(benzyloxy)formamido)-2-((*tert*-butoxycarbonyl)amino)pentanoate (197 mg, 0.43 mmol)as a colourless oil in a 92% yield.

Colourless oil (197 mg, 92%).

[α]$_D$ = -8.26° (*c* = 1, MeOH).

R_f = 0.34 (40-60 petrol : EtOAc, 3:2, UV light 254nm, $KMnO_4$);

^{1}H NMR (400 MHz, Chloroform-*d*) δ 8.17 (br s, 1H, H-30), 7.42 – 7.28 (m, 10H, Ar), 5.18 (d, *J* = 12.3 Hz, 1H, H-7^a), 5.13 (d, *J* = 12.3 Hz, 1H, H-7^b), 5.08 – 5.03 (m, 1H, H-12), 4.79 (s, 2H, H-20), 4.41 – 4.25 (m, 1H, H-11), 3.56 – 3.27 (m, 2H, H-17), 1.91 – 1.76 (m, 1H, H-15^a), 1.71 – 1.58 (m, 3H, H-16, H-15^b),1.43 (s, 9H, H-33, H-32, H-29).

^{1}H NMR (300 MHz, Acetone-d_6) δ 8.22 (br s, 1H, H-30, mix with rotamer), 7.48 – 7.28 (m, 10H, Ar), 6.37 (d, *J* = 8.5 Hz, 1H, H-12, major rotamer, 5.95 minor), 5.18 (d, *J* = 12.5 Hz, 1H, H-7^a), 5.13 (d, *J* = 12.6 Hz, 1H, H-7^b), 4.94 (s, 2H, H-20), 4.28 – 4.20 (m, 1H, H-11), 3.61 (br s, 2H, H-17), 1.90 – 1.83 (m, 1H, H-15^a), 1.81 – 1.68 (m, 3H, H-15^b, H-16), 1.39 (s, 9H, H-33, H-32, H-29).

^{13}C NMR (101 MHz, Chloroform-d) δ 172.4 (C-9), 163.3 (C-30), 155.5 (C-13), 135.4 (C-1), 129.6 (3C), 129.3 (C-21), 128.9, 128.7 (3C), 128.6, 128.4 (C-6, C-2), 80.1 (C-28), 77.9 (C-20), 67.3 (C-7), 53.3 (C-11), 43.8 (C-17), 30.0 (C-15), 28.4 (C-33, C-32, C-29), 23.1 (C-16).

IR (neat) ν_{max}/cm^{-1}: 3331 (b, w), 2980 (N-H, w), 1800, 1739, 1710.

MS (ES+): 935.4 $[2M+Na]^+$ (25%), 479.2 $[M+Na]^+$ (100%).

HRMS (TOF ES+): calcd for $C_{50}H_{64}N_4O_{12}Na$ $[2M+Na]^+$: 935.4418, found 935.4427.

HRMS (TOF ES+): calcd for $C_{25}H_{32}N_2O_6Na$ $[M+Na]^+$: 479.2158, found 479.2138.

4.3.10 (*S*)-1-(Benzyloxy)-5-(*N*-(benzyloxy)formamido)-1-oxopentan-2-aminium trifluoroacetate (58)

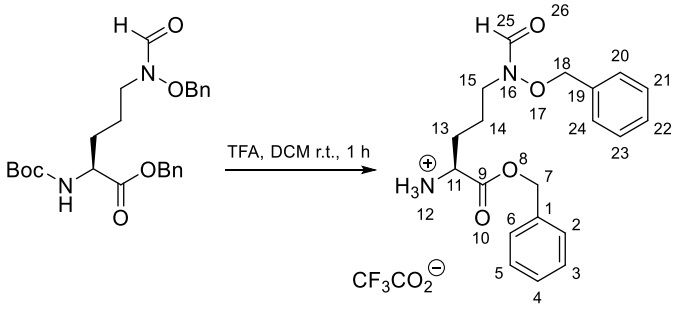

To a 5 mL Schlenk flask under an atmosphere of nitrogen at room temperature containing benzyl (*S*)-5-(N-(benzyloxy)formamido)-2-((*tert*-butoxycarbonyl)amino)pentanoate (171 mg, 0.37 mmol) was added dry DCM (1 mL) followed by TFA (1 mL). The reaction mix was stirred at room temperature for 2 hours after which time the reaction mix was concentrated under reduced pressure to yield (S)-1-(benzyloxy)-5-(N-(benzyloxy)formamido)-1-oxopentan- 2-aminium trifluoroacetate (0.35 mmol, 160 mg) as colourless oil in a 95% yield.
Which was used in the next reaction without further purification.

Colourless oil

^{1}H NMR (400 MHz, Chloroform-*d*) δ 8.56 (br s, 3H, H-12), 8.06 (s, 1H, H-25), 7.40 – 7.23 (m, 10H, Ar), 5.17 (d, *J* = 12.3 Hz, 1H, H-7^{a}), 5.11 (d, *J* = 12.1 Hz, 1H, H-7^{b}), 4.87 – 4.73 (m, 2H, H-18), 4.10 – 4.06 (m, 1H, H-11), 3.59 – 3.19 (m, 2H, H-15), 2.02 – 1.90 (m, 2H, H-13^{a}, H-14^{a}), 1.81 – 1.62 (m, 2H, H-13^{b}, H-14^{b}).

^{13}C NMR (101 MHz, Chloroform-d) δ 169.3 (C-9), 163.7 (C-25), 134.5 (C-1), 129.6 (3C), 129.3 (C-19), 128.8 (2C), 128.7 (3C), 128.5 (C-6, C-2), 77.8 (C-18), 68.4 (C-7), 52.7 (C-11), 43.2 (C-15), 27.4 (C-13), 22.3 (C-14).

4.3.11 Benzyl (*S*)-2-((*S*)-5-(((benzyloxy)carbonyl)amino)-2-(2,3-bis (benzyloxy) benzamido)pentanamido)-5-(*N*-(benzyloxy)formamido)pentanoate (45)

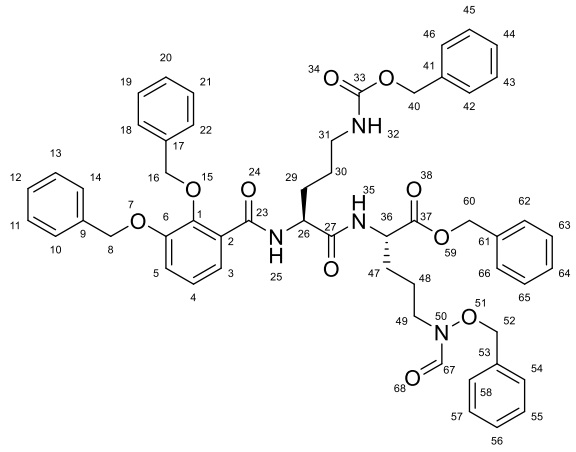

To a 5 mL Schlenk flask, (*S*)-5-(((benzyloxy)carbonyl)amino)-2-(2,3-bis(benzyloxy)benzamido) pentanoic acid (194.7 mg, 0.33 mmol, 1.03 eq) and HATU (133.8 mg, 0.35 mmol, 1.09 eq) were added at 0 °C under nitrogen atmosphere.

Then the dry DMF (0.9 mL) was added, the reaction mixture was stirred for 15 min.

To a separate 5 mL round bottom flask, (*S*)-1-(benzyloxy)-5-(*N*-(benzyloxy)formamido)-1-oxopentan-2- aminium trifluoroacetate (150.8 mg, 0.32 mmol, 1.00 eq) was dissolved with dry DMF (0.9 mL) at 0 °C under nitrogen atmosphere. After which the second mixture was transferred into the first-round bottom flask by syringe. To the reaction mixture, DIPEA (0.22 mL, 1.28 mmol, 4.00 eq) was added dropwise over 1 min. After being stirred for 30 min at the same temperature, the reaction mixture was allowed to warm slowly to room temperature stirred for addition 15.5 h. After which the reaction mixture was quenched with sat. aq. NH_4Cl (4 mL), the resulting slurry extracted with EtOAc (3 x 10 mL). The combined organic layers were washed with sat. aq. NH_4Cl (30 mL) and brine (40 mL), dried over anhydrous sodium sulphate and the solvent was removed under reduced pressure.

The crude product was purified via silica gel column chromatography ($CHCl_3$/Actone/MeOH = 70:10:1, column diameter = 2.5 cm, silica = 20 cm) to give benzyl (*S*)-2-((*S*)-5- (((benzyloxy)carbonyl)amino)-2-(2,3-bis(benzyloxy)benzamido)pentanamido)-5-(*N*- (benzyloxy)formamido)pentanoate as a colourless oil (224 mg, 3.95 mmol) in a 75% yield.

Colourless oil

R_f = 0.68 ($CHCl_3$: Acetone : MeOH, 50:10:1, UV light 254nm).

R_f = 0.32 (DCM : MeOH, 50:1, UV light 254nm).

^{1}H NMR (400 MHz, Chloroform-*d*) δ 8.43 (dd, *J* = 7.6 Hz, 4.2 Hz, 1H, H-25), 8.01 (s, 1H, H-67), 7.64 (t, *J* = 7.8 Hz, 1H, H-3), 7.41 – 7.38 (m, 2H, H-14, H-10), 7.36 – 7.17 (m, 23H, Ar), 7.11 – 7.02 (m, 2H, H-5, H-4), 5.14 (d, *J* = 10.5 Hz, 1H, H-16^a), 5.10 – 4.99 (m, 7H), 4.85 – 4.78 (m, 1H), 4.68 – 4.61 (m, 2H, H-52^b, H-26), 4.58 – 4.51 (m, 1H, H-36), 3.48 – 3.46 (m, 1H, H-49^a), 3.20 – 3.11 (m, 1H, H-31^a), 3.07 – 3.02 (m, 1H, H-32), 2.98 – 2.90 (m, 1H, H-31^b), 1.82 – 1.80 (m, 1H, H-47^a), 1.66 – 1.55 (m, 4H, H-47^b, H-29^a, H-48), 1.36 – 1.22 (m, 3H, H-30, H-29^b).

^{1}H NMR (300 MHz, Methanol-d_4) δ 8.67 (t, *J* = 6.9 Hz, 1H), 8.40 (d, *J* = 7.9 Hz), 8.02 (s, H-67, minor), 7.86 (s, H-67, major), (can see from COSY), 7.47 – 7.39 (m, 3H, Ar), 7.35 – 7.18 (m, 22H, Ar), 7.07 (t, , *J* = 8.0 Hz, 1H, H-4), 5.14 – 5.05 (m, 4H), 5.05 – 4.95 (m, 3H), 4.84 (s, 2H), 4.78 – 4.74 (m, 1H), 4.60 – 4.54 (m, 1H), 4.53 – 4.48 (m, 1H), 3.58 – 3.50 (m, 1H), 2.97 (m, 1H), 1.87 – 1.78 (m, 1H), 1.70 – 1.55 (m, 4H), 1.50 – 1.39 (m, 3H), 1.31 – 1.27 (m, 2H).

^{1}H NMR (700 MHz, Chloroform-*d*, 328 K) δ 8.39 (d, *J* = 7.5, 1H, H-25), 8.17 – 8.00 (m, 1H, H-67), 7.71 (ddd, *J* = 14.8, 7.9, 1.7 Hz, 1H, H-3), 7.45 (t, *J* = 7.5 Hz, H-14, H-10), 7.41 – 7.38 (m, 3H, Ar), 7.37 – 7.24 (m, 19H, Ar), 7.20 – 7.11 (m, 2H, Ar, H-5), 7.10 (t, *J* = 8.0, 1H, H-4), 5.20 (d, *J* = 10.7 Hz), 5.17 – 5.11 (m, 5H), 5.10 – 5.05 (m, 3H), 4.98 – 4.87 (m, 1H), 4.83 – 4.72 (m, 2H), 4.63 – 4.58 (m, 2H), 4.64 – 3.38 (m, 2H, H-49^a, H-31^a), 3.19 – 3.09 (m, 2H, H-49^b, H-31^b), 1.92 – 1.85 (m, 1H, H-47^a), 1.74 (q, *J* = 6.6 Hz, 1H), 1.71 – 1.62 (m, 3H), 1.43 – 1.37 (m, 3H), 1.31 – 1.28 (m, 2H).

^{13}C NMR (101 MHz, Chloroform-d) δ 171.8 (C-37, C-27), 165.4 (C-23), 163.2 (C-67), 156.8 (C-33), 151.9 (C-6), 147.1 (C-1), 136.7, 136.4 (2C), 135.4, 134.3, 129.6 (2C), 129.1, 129.0, 128.8 (3C), 128.7, 128.7 (4C), 128.6 (3C), 128.4, 128.1, 128.1, 127.8 (C-14, C-10), 126.6 (C-2), 124.4 (C-4), 123.3 (C-3), 117.5 (C-5), 77.5 (C-52), 76.2 (C-16), 71.4 (C-8), 67.2 (C-60), 66.7 (C-40), 52.6 (C-26), 52.1 (C-36), 43.6 (C-49), 39.9 (C-31), 29.2, 29.0, 26.1 (C-30), 23.3 (C-48).

^{13}C NMR (75 MHz, Methanol-d_4) δ 174.0 (C-37 or C-27), 172.9 (C-37 or C-27), 167.4

(C-23), 164.6 (C-67), 158.7 (C-33), 153.3 (C-6), 147.8 (C-1), 138.3, 137.9, 137.8, 137.0, 135.8, 130.8, 130.0, 129.6, 129.6, 129.5, 129.4, 129.3, 129.2, 129.0, 128.9, 128.7, 125.5 (C-4), 123.2 (C-3), 118.5 (C-5), 79.4 (CDCl3), 78.3 (C-52), 76.8 (C-16), 72.2 (C-8), 68.0 (C-60), 67.3 (C-40), 54.3 (C-26), 53.3 (C-36), 44.1 (C-49), 41.0 (C-31), 30.7 (C-47 or C-29), 29.5, (C-47 or C-29), 27.0 (C-30), 24.2 (C-48).

IR (neat) ν_{max}/cm^{-1}: 3316 (N-H, w), 2937 (C-H, w), 1716 (C=O, m).

MS (ES+): 943.4 $[M+Na]^+$ (100%), 921.4 $[M+H]^+$ (41%)

HRMS (TOF ES+): calcd for $C_{54}H_{56}N_4O_{10}Na$ $[M+Na]^+$ 943.3894, found 943.3925.

HRMS (TOF ES+): calcd for $C_{54}H_{56}N_4O_{10}H[M+H]^+$ 921.4075, found 921.4133.

4.3.12 Benzyl methyl (2-(benzyloxy)benzoyl)-*D*-serinate (77)

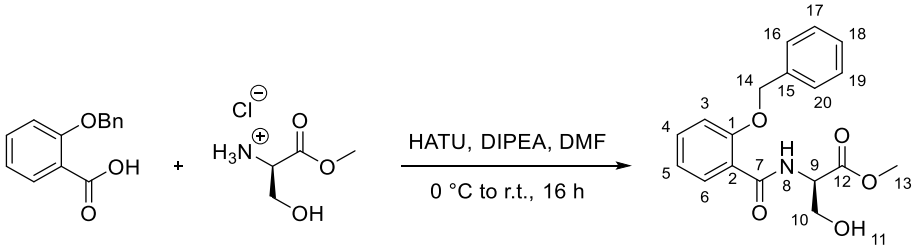

To a 150 mL round bottom flask, 2-(benzyloxy)benzoic acid (1.14 g, 5.00 mmol, 1.00 eq) and HATU (1.98 g, 5.20 mmol, 1.04 eq) were added at 0 °C under nitrogen atmosphere.

Then the dry DMF (25 mL) was added, the reaction mixture was stirred for 15 min.

To a separate 50 mL round bottom flask, methyl D-serinate hydrochloride (0.78 g, 5.00 mmol, 1.00 eq) was dissolved with dry DMF (20 mL) at 0 °C under nitrogen atmosphere.

After which the second mixture was transferred into the first-round bottom flask by syringe.

To the reaction mixture, DIPEA (3.35 mL, 19.24 mmol, 3.85 eq) was added dropwise over 5 min.

After being stirred for 30 min at the same temperature, the reaction mixture was allowed to warm slowly to room temperature stirred for addition 15 h.

After which the reaction mixture was quenched with sat. aq. NH_4Cl (4 mL), the resulting slurry extracted with EtOAc (3 x 10 mL). The combined organic layers were washed with sat. aq. NH_4Cl (30 mL) and brine (40 mL), dried over anhydrous sodium sulphate and the solvent was removed under reduced pressure.

The crude product was purified via silica gel column chromatography (DCM/EtOAc = 3:1, column diameter = 5 cm, silica = 24 cm) to give benzyl methyl (2-(benzyloxy)benzoyl)-D-serinate as a colourless solid (1.30 g, 3.95 mmol) in a 79% yield.

X-Ray grade crystals were grown from slow evaporation of a 20 mg/mL solution in methanol.

Colourless solid (1.30 g, 79%).

Mp: 128-129 °C (MeOH).

[α]$_D$ = -16.2° (*c* = 1, MeOH).

R_f = 0.30 (DCM : EtOAc, 3:1; UV light 254nm).

^{1}H NMR (400 MHz, Chloroform-*d*) δ 8.78 (d, *J* = 7.0 Hz, 1H, H-8), 8.15 (d, *J* = 7.7 Hz, 1H, H-6), 7.46 (d, *J* = 7.4 Hz, 2H, H-16, H-20), 7.43 – 7.31 (m, 4H, H-4, H-17, H-18, H-19), 7.06 – 7.01 (m, 2H, H-5, H-3), 5.22 (d, 1H, *J* =11.2 Hz, H-14^a), 5.19 (d, 1H, *J* = 11.9 Hz, H-14^b), 4.81 (dt, *J* = 7.5, 3.9 Hz, 1H, H-9), 3.89 (dd, 1H, *J* = 11.4, 4.4 Hz, H-10^a), 3.85 (dd, 1H, *J* = 11.2, 3.7 Hz, H-10^b), 3.65 (s, 3H, H-13), 2.74 (br-s, 1H, H-11).

^{13}C NMR (101 MHz, Chloroform-*d*) δ 170.9 (C-12), 165.6 (C-7), 157.0 (C-2), 135.6 (C-15), 133.2 (C-4), 132.3 (C-6), 128.8 (C-17, C-19), 128.6 (C-18), 128.1 (C-16, C-20), 121.5 (C-5), 121.2 (C-1), 112.9 (C-3), 71.3 (C-14), 63.4 (C-10), 55.3 (C-9), 52.5 (C-13).

IR (neat) ν_{max}/cm^{-1}: 3371.1 (N-H, w), 3323.6(O-H, m), 2954.9 (C-H, w), 1735.0 (C=O, s), 1624.1 (C=O, s).

MS (ES+): 330.1 $[M+H]^+$ (11%), 352.1 $[M+Na]^+$ (100%).

HRMS (TOF ES+): calcd for $C_{18}H_{19}NNaO_5$ $[M+Na]^+$ 352.1161, found 352.1149.

X-Ray code: mjh230002_fa

4.3.13 (2-(Benzyloxy)benzoyl)-*D*-serine (66)

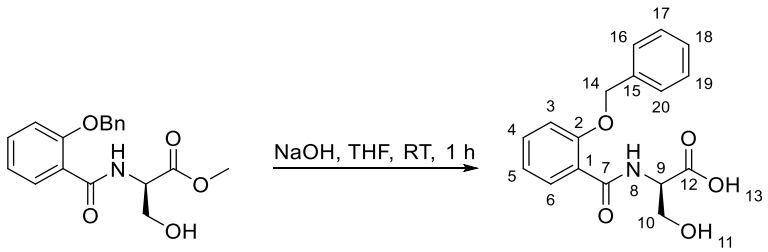

To a stirred suspension of methyl (2-(benzyloxy)benzoyl)-D-serinate (1.39 g, 4.20 mmol) in THF (8 mL) was added 2 M NaOH solution (2 mL).

Then the reaction mixture stirred for 1 hour, monitor by TLC.

After this time, the reaction mixture was diluted with EtOAc (20 mL) and extracted with sat. aq. $NaHCO_3$ (20 mL).

The aqueous layer was acidified with a dropwise addition of 2M HCl until pH 2 was reached (pH paper).

The acidified aqueous layer was then extracted with EtOAc (3 x 40 mL).

The combined organic layers were then washed with water (30 mL) and brine (30 mL), dried over anhydrous sodium sulphate and the solvent was removed under reduced pressure to give (2-(benzyloxy)benzoyl)-D-serine as a colourless solid (1.20 g, 3.80mmol) in a 91% yield.

Colourless solid (1.20 g, 91%).

Mp: 131-132 °C (MeOH).

[α]$_D$ = -24.8° (*c* = 1, MeOH).

R_f = 0.28 (40-60 petrol : EtOAc, 3:2; UV light 254nm).

^{1}H NMR (400 MHz, DMSO-d_6) δ 8.65 (d, *J* = 7.5 Hz, 1H, H-8), 7.94 (dd, *J* = 7.8, 1.4 Hz, 1H, H-6), 7.57 (d, *J* = 7.4 Hz, 2H, H-16, H-20), 7.48 (td, *J* = 7.8, 1.3 Hz, 1H, H-4), 7.40 - 7.36 (m, 2H, H-17, H-19) 7.33 (d, *J* = 7.1 Hz, 1H, H-3), 7.28 (d, *J* = 8.4 Hz, 1H, H-18), 7.07 (t, *J* = 7.5 Hz, 1H, H-5), 5.37 (d, *J* = 13.2 Hz, 1H, H-14^a), 5.33(d, *J* = 13.3 Hz, 1H, H-14^b) 4.54 (dt, *J* = 7.5, 4.0 Hz, 1H, H-9), 3.78 (dd, *J* = 10.9, 4.5 Hz, 1H, H-10^a); 3.72 (dd, *J* = 10.9, 4.0 Hz, 1H, H-10^b);

^{13}C NMR (101 MHz, DMSO-d_6) δ 171.9 (C-12), 164.2 (C-7), 156.3 (C-2), 136.2 (C-15), 132.8 (C-4), 131.2 (C-6), 128.5 (C-17, C-19), 128.0 (C-18), 127.76 (C-16, C-20), 122.0 (C-1), 121.0 (C-5), 113.9 (C-3), 70.2(C-14), 61.33(C-10), 55.05(C-9).

IR (neat) ν_{max}/cm^{-1}: 3350.4 (O-H, w), 2981.6 (C-H, w), 1744.7 (C=O, m), 1639.2 (C=O, s).

MS (ES+): 338.1 $[M+Na]^+$ (82%)

HRMS (TOF ES+): calcd for $C_{17}H_{17}NNaO_5$ $[M+Na]^+$ 338.1004, found 338.0981.

calcd for $C_{17}H_{18}NO_5$ $[M+H]^+$ 316.1185, found 316.1155.

4.3.14 Methyl 3-(2-(((benzyloxy)carbonyl)amino)acetamido)propanoate (78)

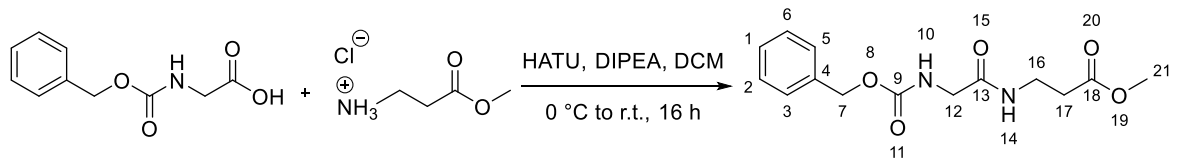

To a 250 mL round bottom flask, ((benzyloxy)carbonyl)glycine (1.00 g, 4.78 mmol, 1.00 eq), β-alanine methyl ester hydrochloride (0.73 g, 5.26 mmol, 1.10 eq) and HATU (2.00 g, 5.26 mmol, 1.10 eq) were added at 0 °C under nitrogen atmosphere.

Then the dry DCM (80 mL) was added.

To the reaction mixture, DIPEA (3.3 mL, 19.12 mmol, 4.00 eq) was added dropwise over 5 min.

After being stirred for 30 min at the same temperature, the reaction mixture was allowed to warm slowly to room temperature stirred for addition 15 h.

After which the reaction mixture was washed with sat. aq. NH_4Cl (50 mL), sat. aq. $NaHCO_3$ (50 mL) and then brine (60 mL), dried over anhydrous sodium sulphate and the solvent was removed under reduced pressure.

The crude product was purified via silica gel column chromatography (EtOAc/40-60 petrol = 3:1, column diameter = 5 cm, silica = 20 cm) to give methyl 3-(2-(((benzyloxy)carbonyl)amino)acetamido)propanoate as a colourless solid (1.13 g, 3.82 mmol) in an 85% yield.

Colourless solid (1.13 g, 80%).

Mp: 94-95 °C [lit. 93-94 °C]

R_f = 0.26 (EtOAc : 40-60 petrol, 3:1; UV light 254nm, $KMnO_4$).

^{1}H NMR (400 MHz, Chloroform-*d*) δ 7.37 – 7.29 (m, 5H, H-1, H-2, H-6, H-3, H-5), 6.61 (br-s, 1H, H-14), 5.51 (br-s, 1H, H-10), 5.12 (s, 2H, H-7), 3.83 (d, *J* = 5.0 Hz, 2H, H-12), 3.68 (s, 3H, H-21), 3.52 (q, *J* = 6.0 Hz, 2H, H-16), 2.53 (t, *J* = 6.0 Hz, 2H, H-17);

^{1}H NMR (400 MHz, Chloroform-*d*) δ 7.38 – 7.29 (m, 5H, H-1, H-2, H-6, H-3, H-5), 7.11 (**t**, *J* = 6.0 Hz, 1H, H-14), 6.15 (**t**, *J* = 5.8 Hz, 1H, H-10), 5.12 (s, 2H, H-7), 3.85 (d, *J* = 5.5 Hz, 2H, H-12), 3.66 (s, 3H, H-21), 3.51 (q, *J* = 6.2 Hz, 2H, H-16), 2.53 (t, *J* = 6.0 Hz, 2H, H-17);

^{13}C NMR (101 MHz, Chloroform-*d*) δ 172.9 (C-18), 169.0 (C-13), 156.7 (C-9), 136.3 (C-4), 128.7 (C-2, C-6), 128.4 (C-1), 128.2 (C-3, C-5), 67.3 (C-7), 52.0 (C-21), 44.7 (C-12), 35.0 (C-16), 33.8 (C-17);

IR (neat) ν_{max}/cm^{-1}: 3310.6 (N-H, m), 1730.3 (C=O, s), 1687.9 (C=O, s), 1642.6 (C=O, s), 1531.5 (N-H, s).

MS (ES+): 317.1 $[M+Na]^+$ (100%), 318.2 $[M+Na+H]^+$ (15%).

HRMS (TOF ES+): calcd for $C_{14}H_{18}N_2NaO_5$ $[M+Na]^+$ 317.1113, found 317.1128.

[lit.] R. Livingston, D. G. Doherty and H. Zeldes, *J. Am. Chem. Soc.*, 1975, **97**, 3198–3204.

4.3.15 Methyl 3-(2-aminoacetamido)propanoate hydrobromide (67)

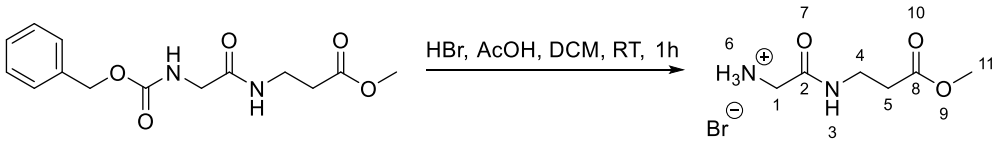

To a stirred solution of methyl 3-(2-(((benzyloxy)carbonyl)amino)acetamido)propanoate (1.07 g, 3.64 mmol) in DCM (25 mL) was added HBr (33 wt. % in acetic acid) (25 mL).

After being stirred at room temperature for 1 h, the reaction mixture was concentrated under a stream of nitrogen.

Then the residue was dissolved in $CHCl_3$ (20 mL) and concentrated under reduced pressure.

The residue was triturated by dissolving in the minimum amount of MeOH followed by the addition of an equal volume of Hexane and the stoppered solution left to stir overnight. The resulting solid was then collected via filtration to give methyl 3-(2-aminoacetamido)propanoate hydrobromide as an orange solid (0.74 g, 1.41 mmol) in an 84% yield.

Orange solid (0.74 g, 84%).

^{1}H NMR (400 MHz, DMSO-d_6) δ 8.43 (t, *J* = 4.8 Hz, 1H, H-3), 7.95 (br-s, 3H, H-6), 3.61 (s, 3H, H-11), 3.51 (s, 2H, H-1), 3.36 (q, *J* = 6.3 Hz, 2H, H-4, overlaps with residual water peak), 2.51 (t, *J* = 6.9 Hz, 2H, H-5, overlaps with residual DMSO peak).

^{1}H NMR (300 MHz, Methanol- d_4), δ 4.84 (s, 3H, H-6, overlaps with residual water peak), 3.67 (s, 5H, H-11, H-1), 3.49 (t, *J* = 6.5 Hz, 2H, H-4), 2.57 (t, *J* = 6.5 Hz, 2H, H-5).

^{13}C NMR (101 MHz, Methanol-d_4) δ 173.5 (C-8), 167.2 (C-2), 52.3 (C-11), 41.5 (C-1), 36.3 (C-4), 34.5 (C-5).

IR (neat) ν_{max}/cm^{-1}: 3314.7 (N-H, m), 3078.7 (N-H, m), 2954.1 (C-H, m), 2869.8 (C-H, m), 1724.3 (C=O, s), 1659.2 (C=O, s).

MS (ES+): $[M+Na]^+$ (100%)

HRMS (TOF ES+): calcd for $C_6H_{12}N_2NaO_3$ $[M+Na]^+$ 183.0746, found 183.0752.

4.3.16 Methyl (*R*)-3-(2-(2-(2-(benzyloxy)benzamido)-3-hydroxypropanamido)acetamido)propanoate (80)

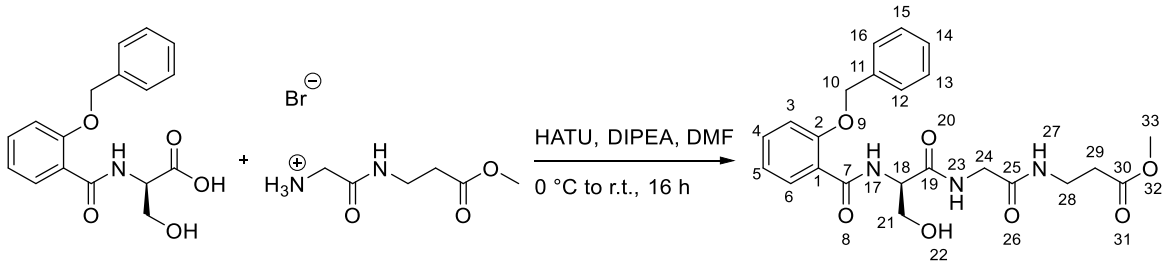

To a stirred solution of (2-(benzyloxy)benzoyl)-D-serine (1.05 g, 3.33 mmol, 1.00 eq) in dry DMF (20 mL) at 0 °C under nitrogen atmosphere was added HATU (1.51 g, 3.97 mmol, 1.19 eq). The reaction mixture was stirred for 15 min.

To a separate 50 mL round bottom flask, methyl 3-(2-aminoacetamido)propanoate hydrobromide (0.96 g, 3.98 mmol, 1.20 eq) was dissolved with dry DMF (15 mL) at 0 °C under nitrogen atmosphere.

After which the second mixture was transferred into the first-round bottom flask by syringe.

To the reaction mixture, DIPEA (2.32 mL, 13.33 mmol, 4.00 eq) was added dropwise over 5 min.

After being stirred for 30 min at the same temperature, the reaction mixture was allowed to warm slowly to room temperature stirred for an additional 15 h.

After which the reaction mixture was diluted with brine (10 mL), the resulting slurry extracted with EtOAc (3 x 50 mL). The combined organic layers were washed with 0.2 M HCl (30 mL), sat. aq. $NaHCO_3$ (30 mL) and then brine (60 mL), dried over anhydrous sodium sulphate and the solvent was removed under reduced pressure.

The crude product was purified via silica gel column chromatography (EtOAc/MeOH = 20:1, column diameter = 5 cm, silica = 20 cm) to give methyl (R)-3-(2-(2-(2-(benzyloxy)benzamido)-3-hydroxypropanamido)acetamido)propanoate as a colourless solid (0.76 g, 1.67 mmol) in a 49% yield.

Colourless solid (0.76 g, 49%).

Mp: 145-146 °C

R_f = 0.24 (EtOAc : MeOH, 20:1; UV light 254nm).

^{1}H NMR (400 MHz, Chloroform-*d*) δ 8.70 (d, *J* = 6.7 Hz, 1H, H-17), 8.08 (dd, *J* = 7.9, 1.8 Hz, 1H, H-6), 7.47 – 7.43 (m, 3H, H-23, H-16, H-12), 7.42 – 7.32 (m, 4H, H-4, H-15, H-13, H-14), 7.11 (t, *J* = 6.1 Hz, 1H, H-27), 7.08 – 7.03 (m, 2H, H-5, H-3), 5.24 (d, *J* = 11.2 Hz, 1H, H-10^a), 5.20 (d, *J* = 11.6 Hz, 1H, H-10^b), 4.60 (q, *J* = 5.2, 1H, H-18), 3.96 (dd, *J* = 11.1, 3.8 Hz, 1H, H-21^a), 3.90 – 3.77 (m, 2H, H-24), 3.62 (s, 3H, H-33), 3.58 (dd, *J* = 11.1, 5.7 Hz, 1H, H-21^b), 3.46 (q, *J* = 6.4 Hz, 2H, H-28), 3.08 (br-s, 1H, H-22), 2.51 (t, *J* = 6.4 Hz, 2H, H-29);

^{1}H NMR (400 MHz, DMSO-d_6) δ 8.61 (d, *J* = 6.7 Hz, 1H, H-17), 8.29 (t, *J* = 5.9 Hz, 1H, H-23), 7.89 (d, *J* = 7.6 Hz, 1H, H-6), 7.86 (t, *J* = 5.6 Hz, 1H, H-27), 7.55 (d, *J* = 7.4 Hz, 2H, H-16, H-12), 7.48 (t, *J* = 7.7 Hz, 1H, H-4), 7.38 (t, *J* = 7.3 Hz, 2H, H-15, H-13), 7.32 (t, *J* = 7.2 Hz, 1H, H-14), 7.27 (d, *J* = 8.4 Hz, 1H, H-3), 7.06 (t, *J* = 7.5 Hz, 1H, H-5), 5.33 (s, 2H, H-10), 5.13 (br-s, 1H, H-22), 4.47 (q, *J* = 5.8 Hz, 1H, H-18), 3.67 – 3.63 (m, 3H, H-21^a, H-24), 3.60 – 3.56 (m, 4H, H-33, H-21^b), 3.29 (q, *J* = 6.5 Hz, 2H, H-28, overlaps with residual DMSO peak), 2.46 (t, *J* = 7.0 Hz, 2H, H-29, overlaps with residual DMSO peak).

^{13}C NMR (101 MHz, Chloroform-*d*) δ 172.7 (C-30), 171.6 (C-19), 169.3 (C-25), 166.1 (C-7), 157.0 (C-2), 135.5 (C-11), 133.4 (C-4), 132.0 (C-6), 128.9 (C-15, C-13), 128.7 (C-14), 128.1 (C-16, C-12), 121.6 (C-5), 121.1 (C-1), 113.0 (C-3), 71.4 (C-10), 62.6 (C-21), 55.8 (C-18), 51.8 (C-33), 43.2 (C-24), 35.2 (C-28), 33.7 (C-29).

IR (neat) ν_{max}/cm^{-1}: 3310.0 (O-H, m), 3290.5 (N-H, m), 2928.0 (C-H, w), 1729.1 (C=O, m), 1664.2 (C=O, s), 1642.0 (C=O, s).

MS (ES+): 480.2 $[M+Na]^+$ (100%), 481.2 $[M+Na+H]^+$ (22%), 482.2 $[M+Na+2H]^+$ (5%)

HRMS (TOF ES+): calcd for $C_{23}H_{27}N_3O_7Na[M+Na]^+$ 480.1747, found 480.1740

4.3.17 (*R*)-3-(2-(2-(2-(Benzyloxy)benzamido)-3-hydroxypropanamido)acetamido)propanoic acid (64)

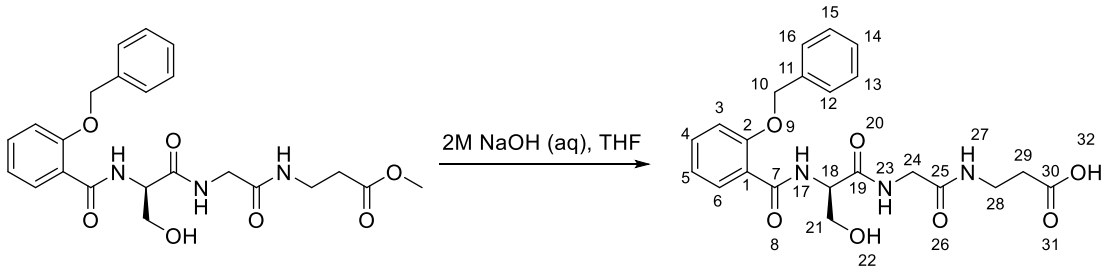

To a stirred suspension of methyl (R)-3-(2-(2-(2-(benzyloxy)benzamido)-3-hydroxypropanamido)acetamido)propanoate (0.71 g, 1.55 mmol)in THF (10 mL) was added 2 M NaOH solution (10 mL).

Then the reaction mixture stirred for 1 h, monitor by TLC.

After this time the reaction mixture was diluted with water (50 mL) and washed with EtOAc (2 x 50 mL).

The aqueous layer was acidified with a dropwise addition of 2M HCl until pH 2 was reached (pH paper).

The acidified aqueous layer was then extracted with EtOAc (3 x 50 mL).

The combined organic layers were then washed with brine (30 mL), dried over anhydrous sodium sulphate and the solvent was removed under reduced pressure to give (R)-3-(2-(2-(2-(benzyloxy)benzamido)-3-hydroxypropanamido)acetamido)propanoic acid as a colourless solid (0.62 g, 1.40 mmol) in a 90% yield.

Colourless solid (0.62 g, 90%).

Mp: 42.5-43.0 °C

[α]$_D$ = -20.6° (*c* = 1, MeOH).

R_f = 0.40 (DCM : MeOH, 9:1; UV light 254nm).

^{1}H NMR (400 MHz, Chloroform-*d*) δ 8.76 (d, *J* = 6.6 Hz, 1H, H-17), 8.00 (d, *J* = 7.8 Hz, 1H, H-6), 7.82 (t, *J* =6.6 Hz, 1H, H-23), 7.60 (t, *J* = 6.0 Hz, 1H, H-27), 7.41 – 7.39 (m, 2H, H-16, H-12), 7.37 – 7.34 (m, 1H, H-4), 7.33 – 7.28 (m, 3H, H-15, H-13, H-14), 7.00 – 6.94 (m, 2H, H-5, H-3), 5.18 (d, *J* = 11.8 Hz, 1H, H-10^a), 5.14 (d, *J* = 11.9 Hz, 1H, H-10^b), 4.60 (q, *J* = 5.9 Hz, 1H, H-18), 3.95 – 3.84 (m, 2H, H-24^a, H-21^a), 3.79 (dd, *J* = 17.0, 5.6 Hz, 1H, H-24^b), 3.56 (dd, *J* = 11.0, 6.3 Hz, 1H, H-21^b), 3.36 (qd, *J* = 13.9, 6.7 Hz, 2H, H-28), 2.47 – 2.38 (m, 2H, H-29).

^{13}C NMR (101 MHz, Chloroform-*d*) δ 174.9 (C-30), 171.8 (C-19), 170.2 (C-25), 166.3 (C-7), 157.1 (C-2), 135.5 (C-11), 133.6 (C-4), 132.1 (C-6), 129.0 (C-15, C-13), 128.7 (C-14), 128.0 (C-16, C-12), 121.6 (C-5), 120.9 (C-1), 113.1 (C-3), 71.4 (C-10), 62.6 (C-21), 55.9 (C-18), 43.1 (C-24), 35.4 (C-28), 33.7 (C-29).

IR (neat) ν_{max}/cm^{-1}: 3342.1 (O-H, b, w), 2981.4 (C-H, w), 1716.8 (C=O, w), 1634.4 (C=O, m);

MS (ES+): 444.2 $[M+H]^+$ (11%), 466.2 $[M+Na]^+$ (100%), 467.2 $[M+Na+H]^+$ (22%).

HRMS (TOF ES+): calcd for $C_{22}H_{25}N_3O_7Na$ $[M+Na]^+$ 466.1590, found 466.1590 $C_{22}H_{26}N_3O_7$ $[M+H]^+$ 444.1771, found 444.1753.

4.3.18 (*S*,*E*)-5-(Benzylideneamino)-2-(((benzyloxy)carbonyl)amino)pentanoic acid (83)

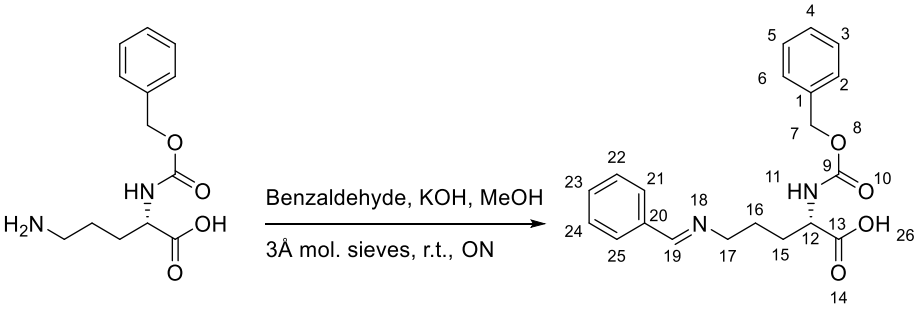

To a stirred solution of KOH (1.14 g, 20.28 mmol, 1.08 eq) in dry MeOH (50 mL) at room temperature under a nitrogen atmosphere was added (S)-5-amino-2-(((benzyloxy)carbonyl)amino)pentanoic acid (5.00 g, 18.78 mmol, 1.00 eq).

After the solids had dissolved, benzaldehyde (2.07 mL, 20.28 mmol, 1.08 eq) was added followed by 3 Å molecular sieves.

The reaction mixture was stirred at room temperature for 16 h.

After which the molecular sieves were filtered off and washed with MeOH.

The filtrate was concentrated under reduced pressure to give (*S*,*E*)-5-(benzylideneamino)-2-(((benzyloxy)carbonyl)amino)pentanoic acid as a hygroscopic pale yellow foam (6.59 g, 18.59 mmol) in a quantitative yield.

Pale yellow foam (6.59 g, quantitative).

$[\alpha]_D$ = +10° (*c* = 0.5, MeOH).

^{1}H NMR (400 MHz, DMSO-d_6) δ 8.27 (s, 1H, H-19), 7.72 – 7.70 (m, 2H, H-25, H-21), 7.43 – 7.42 (m, 3H, H-23, H-24, H-22), 7.34 – 7.27 (m, 5H, H-5, H-3, H-6, H-2, H-4), 6.68 (d, *J* = 6.8 Hz, 1H, H-11), 5.00 (s, 2H, H-7), 3.80 (q, *J* = 5.9 Hz, 1H, H-12), 3.52 (t, *J* = 6.9 Hz, 2H, H-17), 1.79 – 1.76 (m, 1H, H-15^a), 1.64 – 1.58 (m, 3H, H-16, H-15^b);

^{13}C NMR (101 MHz, DMSO-d_6) δ 174.9 (C-13), 160.3 (C-19), 155.4 (C-9), 137.4 (C-1), 136.2 (C-20), 130.4 (C-23), 128.6 (C-24, C-22), 128.3 (C-5, C-3), 127.8 (C-25, C-21), 127.6 (C-4), 127.6 (C-6, C-2), 65.0 (C-7), 60.8 (C-17), 55.6 (C-12), 30.8 (C-15), 26.9 (C-16).

IR (neat) ν_{max}/cm^{-1}: 3341.9 (O-H, b, w), 3031.8 (C-H, w), 2928.8 (C-H, w), 1688.2 (C=N, m).

MS (ES+): 355.2 $[M+H]^+$ (100%), 377.2 $[M+Na]^+$ (38%).

HRMS (TOF ES+): calcd for $C_{20}H_{23}N_2O_4$ $[M+H]^+$ 355.1658, found 355.1912. $C_{20}H_{22}N_2NaO_4$ $[M+Na]^+$ 377.1477, found 377.1764.

Observed data (1H, 13C, IR) are consistent with that previous reported by Miller *et al*.[95]

4.3.19 (*S*,*Z*)-*N*-(4-(((benzyloxy)carbonyl)amino)-4-carboxybutyl)-1-phenylmethanimine oxide (76)

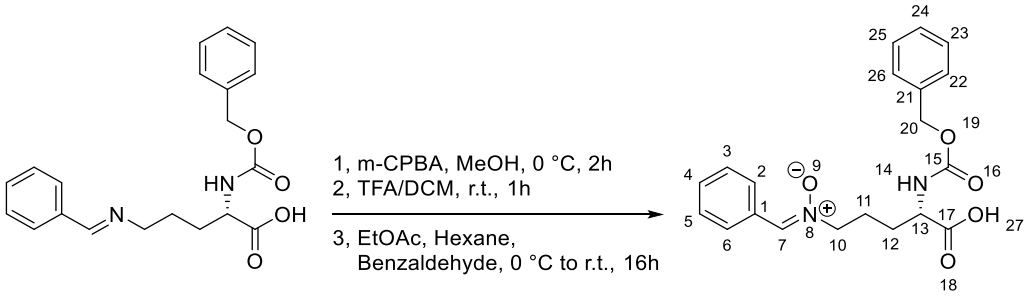

A stirred solution of (S,E)-5-(benzylideneamino)-2-(((benzyloxy)carbonyl)amino)pentanoic acid (6.90 g, 19.47 mmol) in dry MeOH (34 mL) was cooled to 0 °C in an ice bath.

Freshly prepared dry mCPBA (3.86 g, 22.39 mmol) was dissolved in dry MeOH (12 mL).

The mCPBA solution was then added dropwise to the reaction mixture over 20 min.

The resulting solution was stirred for an addition 1.5 h at 0 °C under nitrogen atmosphere.

After this time the reaction mixture was concentrated under a stream of nitrogen.

The resulting residue was partitioned between H_2O (50 mL) and EtOAc (50 mL).

The aqueous layer was acidified with a dropwise addition of 2M HCl until pH 2 was reached (pH paper).

The layers were then separated, and the aqueous layer was extracted with EtOAc (50 mL).

The combined organic layers were then washed with sat. aq. $Na_2S_2O_3$ (50 mL) and brine (50 mL), dried over anhydrous sodium sulphate and the solvent was removed under reduced pressure to give crude oxaziridine as a pale yellow solid, which was used without further purification.

To the crude oxaziridine was added TFA (15 mL) followed by CH_2Cl_2 (15 mL) and the resulting solution was stirred at room temperature for 1 h.

After this time the solution was concentrated under reduced pressure.

The resulting slurry was dissolved in EtOAc (30 mL) and cooled to 0 °C under nitrogen atmosphere. Hexane (60 mL) was then added, followed by the addition of benzaldehyde (1.5 mL, 14.60 mmol) and the reaction mixture was stirred for 16 h while coming to room temperature. (yielding a cloudy suspension)

The reaction mixture was cooled to 0 °C in an ice bath for 2 h.

The resulting solid was filtered off, washed with cold EtOAc (3 x 40 mL), and dried to give (S,Z)-N-(4-(((benzyloxy)carbonyl)amino)-4-carboxybutyl)-1-phenylmethanimine oxide (4.82 g, 13.01 mmol, 67%) as a pale pink solid.

Pale pink solid (4.82 g, 67%)

Mp: 148.4-149.7 °C [lit. 150.5 – 151 °C][95]

[α]$_D$ = -9.6° (*c* = 1, MeOH).

^{1}H NMR (400 MHz, DMSO-d_6) δ 12.70 (br-s, 1H, H-27), 8.25 – 8.23 (m, 2H, H-6, H-2), 7.87 (s, 1H, H-7), 7.68 (d, *J* = 8.1 Hz, 1H, H-14), 7.45 – 7.42 (m, 3H, H-5, H-3, H-4), 7.36 – 7.28 (m, 5H, H-25, H-23, H-26, H-22, H-24), 5.03 (s, 2H, H-20), 4.01 (td, *J* = 8.5, 4.6 Hz, 1H, H-13), 3.91 (t, *J* = 6.7 Hz, 2H, H-10), 1.90 (p, *J* = 8.3 Hz, 2H, H-11), 1.79 – 1.71 (m, 1H, H-12^a), 1.68 – 1.58 (m, 1H, H-12^b).

^{13}C NMR (101 MHz, DMSO-d_6) δ 173.6 (C-17), 156.2 (C-15), 137.0 (C-21), 133.4 (C-7), 131.0 (C-1), 129.8 (C-4), 128.4 (C-25, C-23, C-5, C-3), 127.9 (C-6, C-2), 127.8 (C-24), 127.7 (C-26, C-22), 65.5 (C-10), 65.5 (C-20), 53.5 (C-13), 27.8 (C-12), 24.1 (C-11).

^{1}H NMR (700 MHz, DMSO-d_6) δ 12.65 (br-s, 1H, H-27), 8.24 (dd, *J* = 7.8, 1.7 Hz, 2H, H-6, H-2), 7.86 (s, 1H, H-7), 7.66 (d, *J* = 8.0 Hz, 1H, H-14), 7.44 – 7.39 (m, 3H, H-5, H-3, H-4), 7.37 – 7.33 (m, 4H, H-25, H-23, H-26, H-22), 7.32 – 7.29 (m, 1H, H-24), 5.03 (s, 2H, H-20), 4.01 (ddd, *J* = 13.1, 7.9, 4.9 Hz, 1H, H-13), 3.91 (t, *J* = 6.9 Hz, 2H, H-10), 1.95 – 1.86 (m, 2H, H-11), 1.75 (dtd, *J* = 14.5, 10.6, 5.5 Hz, 1H, H-12^a), 1.63 (dtd, *J* = 14.7, 9.7, 5.7 Hz, 1H, H-12^b).

^{13}C NMR (176 MHz, DMSO-d_6) δ 173.6 (C-17), 156.1 (C-15), 137.0 (C-21), 133.3 (C-7), 131.0 (C-1), 129.8 (C-4), 128.3 (C-25, C-23, C-5, C-3), 127.9 (C-6, C-2), 127.8 (C-24), 127.7 (C-26, C-22), 65.5 (C-10), 65.4 (C-20), 53.5 (C-13), 27.8 (C-12), 24.1 (C-11).

IR (neat) ν_{max}/cm^{-1}: 3334.8 (N-H, w), 1720.0 (C=O, w), 1690.2 (C=O, s).

MS (ES+): 371.2 $[M+H]^+$ (100%), 372.2 $[M+2H]^+$ (22%), 393.1 $[M+Na]^+$ (28%).

HRMS (TOF ES+): calcd for $C_{20}H_{23}N_2O_5$ $[M+H]^+$ 371.1607, found 371.1616.

calcd for $C_{20}H_{22}N_2NaO_5$ $[M+Na]^+$ 393.1426, found 393.1435

Observed data (1H, 13C, IR) are consistent with that previous reported by Miller *et al*.[95]

4.3.20 Benzyl (*S*)-(1-(benzyloxy)-2-oxopiperidin-3-yl)carbamate (86)

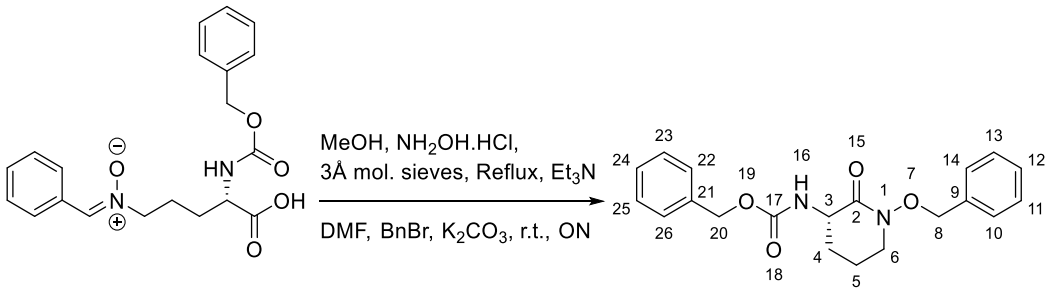

To a stirred solution of (Z)-N-(4-(((benzyloxy)carbonyl)amino)-4-carboxybutyl)-1-phenylmethanimine oxide (3.00 g, 8.10 mmol, 1.00 eq) in dry MeOH (80 mL) at room temperature under a nitrogen atmosphere was added hydroxylamine hydrochloride (0.67 g, 9.61 mmol, 1.20 eq). The reaction mixture was heated to reflux and stirred for 1 h. After this time 3 Å mol. sieves were added followed by Et_3N (2.26 mL, 16.20 mmol, 2.00 eq). The reaction mixture was refluxed for an additional 2 h and filtered through a pad of Celite. The filtrate was concentrated under reduced pressure. The resulting residue was partitioned between EtOAc (80 mL) and water (25 mL).

After separation of the layers, the organic layer was dried over anhydrous sodium sulphate and the solvent was removed under reduced pressure to give the crude hydroxamic acid as a red residue.

The residue was dissolved in Dry DMF (13 mL). To the reaction mixture, K_2CO_3 (11.19 g, 80.99 mmol, 10.00 eq) was added followed by BnBr (4.81 mL, 40.50 mmol, 5.00 eq).

The reaction mixture was stirred for an addition 16 h at room temperature under nitrogen atmosphere.

After which the residue diluted with EtOAc (50 mL). The resulting slurry was then washed with water (3 x 50 mL) and brine (50 mL), dried over anhydrous sodium sulphate and the solvent was removed under reduced pressure.

The crude product was purified via silica gel column chromatography (DCM/EtOAc = 9:1, column diameter = 8 cm, silica = 25 cm) to give benzyl (S)-(1-(benzyloxy)-2-oxopiperidin-3-yl)carbamate as a colourless solid (2.05 g, 5.78 mmol) in a 71% yield.

Colourless solid (2.05 g, 71%).

Mp: 86 – 87 °C [lit. 86 – 88 °C][95]

[α]$_D$ = +22° (*c* = 1, MeOH).

R_f = 0.30 (DCM : EtOAc, 9:1; UV light 254nm, $KMnO_4$).

^{1}H NMR (400 MHz, Chloroform-*d*) δ 7.41 (dd, *J* = 6.6, 2.8 Hz, 2H, H-14, H-10), 7.38 – 7.28 (m, 8H, Ar), 5.92 (d, *J* = 5.7 Hz, 1H, H-16), 5.13 (d, *J* = 12.1 Hz, 1H, H-20^a), 5.08 (d, *J* = 12.5 Hz, 1H, H-20^b), 4.95 (d, *J* = 10.5 Hz, 1H, H-8^a), 4.87 (d, *J* = 10.4 Hz, 1H, H-8^b), 4.19 (td, *J* = 12.0, 6.0 Hz, 1H, H-3), 3.39 (td, *J* = 10.8, 5.7 Hz, 1H, H-6^a), 3.31 – 3.26 (m, 1H, H-6^b), 2.33 – 2.28 (m, 1H, H-4^a), 1.83 – 1.74 (m, 2H, H-5), 1.58 (qd, *J* = 12.2, 4.6 Hz, 1H, H-4^b).

^{13}C NMR (101 MHz, Chloroform-*d*) δ 167.8 (C-2), 156.4 (C-17), 136.4 (C-21), 135.1 (C-9), 129.5 (C-14, C-10), 128.7 (C-12), 128.4 (C-25, C-23, C-13, C-11), 128.0 (C-26, C-22, C-24), 75.8 (C-8), 66.7 (C-20), 52.7 (C-3), 51.1 (C-6), 28.0 (C-4), 20.8 (C-5).

^{1}H NMR (700 MHz, Chloroform-*d*, 298 K) δ 7.40 (dd, *J* = 7.3, 2.4 Hz, 2H, H-14, H-10), 7.35 – 7.31 (m, 7H, H-12, H-26, H-22, H-13, H-11, H-25, H-23), 7.30 – 7.27 (m, 1H, H-24), 5.99 – 5.96 (m, 1H, H-16), 5.13 (d, *J* = 12.2 Hz, 1H, H-20^a), 5.07 (d, *J* = 12.5 Hz, 1H, H-20^b), 4.94 (d, *J* = 10.6 Hz, 1H, H-8^a), 4.86 (d, *J* = 10.4 Hz, 1H, H-8^b), 4.19 (td, *J* = 12.4, 6.4 Hz, 1H, H-3), 3.39 (td, *J* = 11.7, 5.8 Hz, 1H, H-6^a), 3.29 – 3.27 (m, 1H, H-6^b), 2.29 – 2.19 (m, 1H, H-4^a), 1.80 – 1.72 (m, 2H, H-5), 1.59 (qd, *J* = 12.5, 3.8 Hz, 1H, H-4^b).

^{13}C NMR (176 MHz, Chloroform-*d*, 298 K) δ 167.7 (C-2), 156.4 (C-17), 136.4 (C-21), 135.1 (C-9), 129.4 (C-14, C-10), 128.6 (C-12), 128.3 (C-25, C-23, C-13, C-11), 127.9 (C-26, C-22, C-24), 75.7 (C-8), 66.6 (C-20), 52.6 (C-3), 50.9 (C-6), 27.9 (C-4), 20.7 (C-5).

IR (neat) ν_{max}/cm^{-1}: 3318.3 (N-H, w), 3010.7 (C-H, w), 2950.3 (C-H, w), 1714.2 (C=O, m), 1666.6 (C=O, m).

MS (ES+): 355.2 $[M+H]^+$ (25%), 377.1 $[M+Na]^+$ (100%).

HRMS (TOF ES+): calcd for $C_{20}H_{22}N_2NaO_4$ $[M+Na]^+$ 377.1477, found 377.1477.

Observed data (1H, 13C, IR) are consistent with that previous reported by Miller *et al*.[95]

4.3.21 (*S*)-3-Amino-1-(benzyloxy)piperidin-2-one hydrobromide (68)

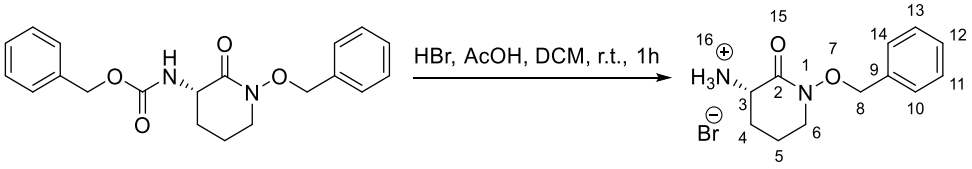

To a solution of benzyl (S)-(1-(benzyloxy)-2-oxopiperidin-3-yl)carbamate (1.26 g, 3.56 mmol, 1.00 eq) in dry DCM (34 mL) at room temperature under a nitrogen atmosphere was added HBr (33 wt. % in acetic acid) (34 mL).

After being stirred at room temperature for 1 h, the reaction mixture was concentrated under a stream of nitrogen.

Then the residue was dissolved in $CHCl_3$ (20 mL) and concentrated under reduced pressure.

The residue was triturated by dissolving in the minimum amount of $CHCl_3$ followed by the addition of an equal volume of Hexane and the stoppered solution left to stir overnight.

The resulting solid was then collected via filtration to give 3-amino-1-(benzyloxy)piperidin-2-one hydrobromide as an red powder (1.02 g, 3.39 mmol) in a 95% yield.

Red powder (1.02 g, 95%).

Mp: 191 – 192 °C [lit. 194 – 195 °C][90]

^{1}H NMR (400 MHz, Deuterium Oxide) δ 7.49 – 7.47 (m, 2H, H-14, H-10), 7.45 – 7.43 (m, 3H, H-13, H-12, H-11) 4.95 (s, 2H, H-8), 4.06 (dd, *J* = 11.8, 5.8 Hz, 1H, H-3), 3.61 – 3.57 (m,-2H, H-6), 2.28 – 2.21 (m, 1H, H-4^{a}), 2.10 – 2.04 (m, 1H, H-5^{a}), 1.98 – 1.88 (m, 1H, H-5^{b}), 1.82 (qd, *J* = 12.7, 3.0 Hz, 1H, H-4^{b}).

^{13}C NMR (75 MHz, Deuterium Oxide) δ 164.8 (C-2), 134.0 (C-9), 130.0 (C-14, C-10), 129.4 (C-12), 128.8 (C-13, C-11), 75.8 (C-8), 50.3 (C-3), 49.7 (C-6), 24.6 (C-4), 19.7 (C-5).

^{13}C NMR (75 MHz, DMSO-d_6) δ 163.7 (C-2), 135.2 (C-9), 129.3 (C-14, C-10), 128.7 (C-12), 128.4 (C-13, C-11), 74.9 (C-8), 49.9 (C-3), 49.7 (C-6), 25.1 (C-4), 19.8 (C-5).

IR (neat) ν_{max}/cm^{-1}: 3395.0 (N-H, w), 2947.6 (C-H, m), 1660.4 (C=O, s).

MS (ES+): 221.1 $[M+H]^+$ (100%), 222.1 $[M+2H]^+$ (14%).

HRMS (TOF ES+): calcd for $C_{12}H_{17}N_2O_2$ $[M+H]^+$ 221.1290, found 221.1288.

4.3.22 (*S*,*Z*)-*N*-(4-(((Benzyloxy)carbonyl)(methyl)amino)-4-carboxybutyl)-1-phenylmethanimine oxide (68)

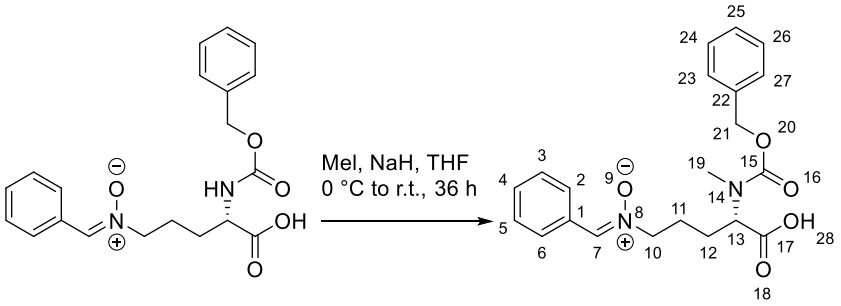

To a stirred suspension of (S,Z)-N-(4-(((benzyloxy)carbonyl)amino)-4-carboxybutyl)-1-phenylmethanimine oxide (1.00 g, 2.70 mmol, 1.00 eq) and NaH (0.33 g, 8.10 mmol, 3.00 eq, 60 % weight dispersion in mineral oil) in dry THF (40 mL) at 0 °C under a nitrogen atmosphere was added MeI (1.35 mL, 21.60 mmol, 8.00 eq).

After being stirred for 30 min at the same temperature, the reaction mixture was allowed to warm slowly to room temperature stirred for addition 35 h.

After which the reaction mixture was quenched with MeOH (20 mL).

After this time the reaction mixture was concentrated under a stream of nitrogen. (until a yellow residue resulted)

The resulting residue was partitioned between Et_2O (75 mL) and H_2O (40 mL).

The aqueous layer was acidified with a dropwise addition of 2M HCl until pH 2 was reached (pH paper).

The acidified aqueous layer was extracted with EtOAc (3 x 30 mL).

The combined organic layers were then washed with brine (50 mL), dried over anhydrous sodium sulphate and the solvent was removed under reduced pressure to give a pale-yellow oil.

The residue was triturated from Hexane and Et_2O to give the methylation product as a light-yellow foam (0.70 g) in a 67% yield.

Light yellow foam (0.70 g, 67%).

[α]$_D$ = -38.7° (*c* = 0.3, MeOH).

^{1}H NMR (700 MHz, DMSO-*d*$_6$, 343 K) δ 12.62 (br-s, 1H, H-28), 8.24 (dd, *J* = 7.9, 1.5 Hz, 2H, H-6, H-2), 7.79 – 7.78 (m, 1H, H-7), 7.43 – 7.40 (m, 3H, H-5, H-3, H-4), 7.35 – 7.33 (m, 4H, H-26, H-24, H-27, H-23), 7.31 – 7.28 (m, 1H, H-25), 5.11 (s, 2H, H-21), 4.56 (br-s, 1H, H-13), 3.94 (dt, 10.4, 6.8 Hz 2H, H-10), 2.83 (s, 3H, H-19), 1.96 – 1.92 (m, 1H, H-12^a), 1.89 – 1.78 (m, 3H, H-11, H-12^b).

^{13}C NMR (176 MHz, DMSO-*d*$_6$, 343 K) δ 171.8 (C-17), 155.8, 136.6 (C-22), 132.7 (C-7), 130.8 (C-1), 129.3 (C-4), 130.0 (C-26, C-24), 127.9 (C-5, C-3), 127.6 (C-6, C-2), 127.4 (C-25), 127.0 (C-27, C-23), 66.2 (C-21), 65.1 (C-10), 58.0 (C-13), 30.2, 24.0 (C-12), 23.8 (C-11).

^{13}C NMR (75 MHz, Chloroform-*d*, 298 K) δ 173.1 (C-17, major),173.0 (minor), 157.1, 156.3 (C-15, major), 156.2 (C-15, minor), 137.8 (major), 137.5 (minor), 136.2 (C-22, major), 136.2 (C-22, minor), 131.4 (C-1, minor), 131.3 (C-1, major), 129.5, 129.4, 128.5, 128.4, 127.9, 127.8, 127.7, 127.5, 67.5 (C-21), 65.6 (C-10, minor), 65.4 (C-10, major), 58.2 (C-13, minor), 57.7 (C-13, major), 31.0 (C-19, minor), 30.5 (C-19, major), 25.7 (C-12, minor), 25.2 (C-12, major), 24.3 (C-11, minor), 24.0 (C-11, major).

IR (neat) ν_{max}/cm^{-1}: 2946.0 (O-H, w), 1693.7 (C=O, s), 1452.3.

MS (ES+): 385.2 $[M+H]^+$ (100%), 407.2 $[M+Na]^+$ (6%).

HRMS (TOF ES+): calcd for $C_{21}H_{25}N_2O_5$ $[M+H]^+$ 385.1764, found 385.1749.

calcd for $C_{21}H_{24}N_2NaO_5$ $[M+Na]^+$ 407.1583, found 407.1576.

X-Ray code: mjh200061; mjh200065

4.3.23 (*Z*)-*N*-((*S*)-5-(((*S*)-1-(Benzyloxy)-2-oxopiperidin-3-yl)amino)-4-(((benzyloxy)carbonyl)(methyl)amino)-5-oxopentyl)-1-phenylmethanimine oxide (88)

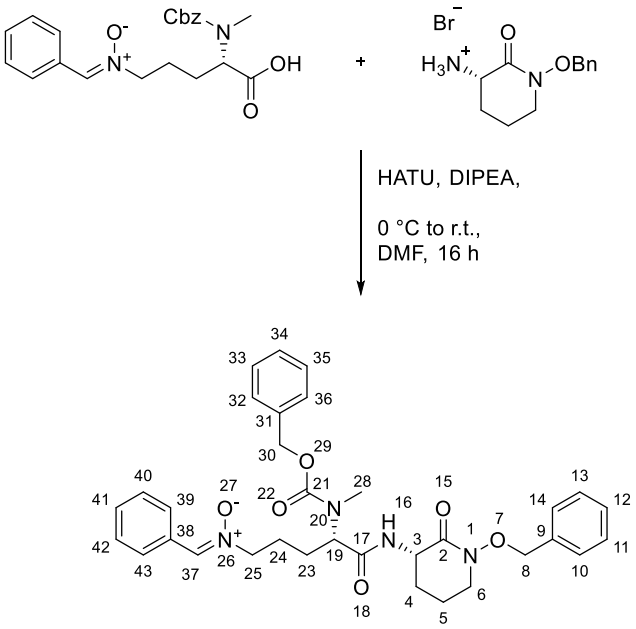

To a stirred solution of (S,Z)-N-(4-(((benzyloxy)carbonyl)(methyl)amino)-4-carboxybutyl)-1-phenylmethanimine oxide (1.59 g, 4.14 mmol, 1.08 eq) in dry DMF (20 mL) at 0 °C under nitrogen atmosphere was added HATU (1.67 g, 4.40 mmol, 1.15 eq). The reaction mixture was stirred for 15 min.

To a separate 50 mL round bottom flask, (S)-3-amino-1-(benzyloxy)piperidin-2-one hydrobromide (1.15 g, 3.83 mmol, 1.00 eq) was dissolved with dry DMF (35 mL) at 0 °C under nitrogen atmosphere.

After which the second mixture was transferred into the first-round bottom flask by syringe.

To the reaction mixture, DIPEA (2.67 mL, 15.30 mmol, 4.00 eq) was added dropwise over 10 min.

After being stirred for 30 min at the same temperature, the reaction mixture was allowed to warm slowing to room temperature stirred for an additional 15 h.

After which the reaction mixture was diluted with water (20 mL), the resulting slurry extracted with DCM (4 x 40 mL). The combined organic layers were washed with sat.

aq. $NaHCO_3$ (50 mL), 0.2 M HCl (50 mL), H_2O (3 x 40 mL) and then brine (60 mL), dried over anhydrous sodium sulphate and the solvent was removed under reduced pressure.

The crude product was purified via silica gel column chromatography (DCM/MeOH = 40 : 1 to 25 : 1, column diameter = 4 cm, silica = 25 cm) to give (Z)-N-((S)-5-(((S)-1-(benzyloxy)-2-oxopiperidin-3-yl)amino)-4-(((benzyloxy)carbonyl)(methyl)amino)-5-oxopentyl)-1-phenylmethanimine oxide as a colourless foam (1.36 g, 2.32 mmol) in a 61% yield.

Colourless foam (1.36 g, 61%).

[α]$_D$ = +17.6° (*c* = 1, MeOH).

R_f = 0.22 (DCM : MeOH, 24:1; UV light 254nm, $KMnO_4$).

^{1}H NMR (700 MHz, DMSO-d_6, 368 K) δ 8.24 (d, *J* = 1.9 Hz, 1H, H-43), 8.23 (d, *J* = 1.6 Hz, 1H, H-39), 7.87 (d, *J* = 8.0 Hz, 1H, H-16), 7.76 (s, 1H, H-37), 7.43 – 7.33 (m, 12H, Ar), 7.29 – 7.27 (m, 1H, Ar), 5.15 (d, *J* = 12.8 Hz, 1H, H-30^a), 5.12 (d, *J* = 12.7 Hz, 1H, H-30^b), 4.90 (d, *J* = 10.6 Hz, 1H, H-8^a), 4.89 (d, *J* = 10.5 Hz, 1H, H-8^a), 4.62 (dd, *J* = 9.2, 5.5 Hz, 1H, H-19), 4.31 (ddd, *J* = 11.0, 8.0, 5.5 Hz, 1H, H-3), 3.96 (t, *J* = 6.9 Hz, 2H, H-25), 3.49 (d, *J* = 3.9 Hz, 1H, H-6^a), 3.48 (d, *J* = 4.0 Hz, 1H, H-6^b), 2.86 (s, 3H, H-28), 1.99 – 1.94 (m, 1H, H-23^a), 1.92 – 1.85 (m, 4H, H-5^a, H-4^a, H-24), 1.84 – 1.78 (m, 1H, H-5^b), 1.77 – 1.72 (m, 1H, H-4^b), 1.71 – 1.67 (m, 1H, H-23^b).

^{13}C NMR (176 MHz, DMSO-d_6, 378 K) δ 169.4 (C-17), 165.6 (C-2), 155.5 (C-21), 136.5 (C-31), 135.3 (C-9), 132.3 (C-37), 130.7 (C-38), 128.9 (C-41), 128.4 (C-14, C-10), 127.7 (2C), 127.7 (C-34), 127.6 (2C), 127.6 (2C), 127.3 (C-43, C-39), 127.1 (C-12), 126.8 (C-36, C-32), 74.2 (C-8), 66.0 (C-30), 65.2 (C-25), 57.9 (C-19), 50.1, 49.5, 29.5 (C-28), 26.9 (C-4), 25.2 (C-23), 23.8 (C-24), 20.1 (C-5).

IR (neat) ν_{max}/cm^{-1}: 3313.1 (N-H, w), 3061.9 (C-H, w), 2945.9 (C-H, w), 1667.8 (C=O, s).

MS (ES+): 587.3 $[M+H]^+$ (64%), 609.3 $[M+Na]^+$ (100%).

HRMS (TOF ES+): calcd for $C_{33}H_{39}N_4O_6$ $[M+H]^+$ 587.2870, found 587.2877.

calcd for $C_{33}H_{38}N_4NaO_6$ $[M+Na]^+$ 609.2689, found 609.2716.

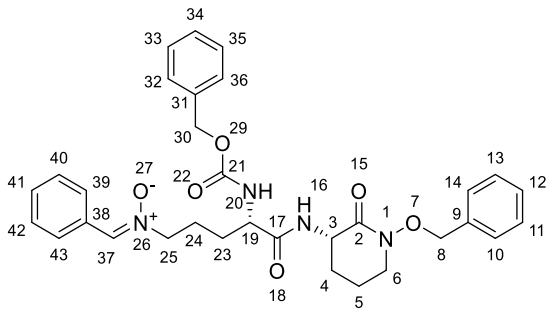

(**89**)

R_f = 0.18 (DCM : MeOH, 24:1; UV light 254nm, $KMnO_4$).

^{1}H NMR (300 MHz, DMSO-d_6) δ 8.26 – 8.21 (m, 3H, H-16, H-43, H-39), 7.87 (s, 1H,

H-37), 7.48 (d, *J* = 8.2 Hz, 1H, H-20), 7.43 – 7.28 (m, 14H, Ar), 5.05 (d, *J* = 12.8 Hz, 1H, H-30^{a}), 5.00 (d, *J* = 12.8 Hz, 1H, H-30^{b}), 4.87 (d, *J* = 10.6 Hz, 1H, H-8^{a}), 4.83 (d, *J* = 10.3 Hz, 1H, H-8^{b}), 4.39 – 4.31 (m, 1H, H-3), 4.06 (td, *J* = 8.1, 5.6 Hz, 1H, H-19), 3.92 (t, *J* = 6.8 Hz, 2H, H-25), 3.44 (m, overlaps with residual water peak, 2H, H-6), 1.94 (dd, *J* = 14.0, 7.0 Hz, 2H, H-24), 1.86 – 1.81 (m, 2H, H-4^{a}, H-5^{a}), 1.79 – 1.72 (m, 2H, H-5^{b}, H-23^{a}), 1.66 – 1.56 (m, 2H, H-4^{b}, H-23^{b}).

^{13}C NMR (75 MHz, DMSO-*d*$_6$) δ 171.5 (C-17), 166.2 (C-2), 156.0 (C-21), 137.1 (C-31), 135.6 (C-9), 133.6 (C-37), 131.1 (C-38), 130.0 (C-41), 129.3 (C-14, C-10), 128.6, 128.5 (C-43, C-39, Ar), 128.1, 127.9, 127.8, 74.7 (C-8), 65.8 (C-25), 65.6 (C-30), 54.4 (C-19), 50.1 (C-3, C-6), 29.2 (C-23), 27.6 (C-4), 24.1 (C-24), 20.7 (C-5).

^{1}H NMR (300 MHz, Chloroform-*d*) δ 8.21 (dd, *J* = 6.7, 3.2 Hz, 2H, H-43, H-39), 7.70 (d, *J* = 7.3 Hz, 1H, H-16), 7.46 (s, 1H, H-37), 7.39 – 7.23 (m, 13H, Ar), 6.11 (d, *J* = 8.0 Hz, H-20), 5.06 (s, 2H, H-30), 4.92 (d, *J* = 10.5 Hz, 1H, 8^{a}), 4.82 (d, *J* = 10.5 Hz, 1H, 8^{b}), 4.44 – 4.38 (q, *J* = 6.2 Hz, 1H, H-3), 4.36 – 4.30 (q, *J* = 5.5 Hz, 1H, H-19), 3.94 (m or td ?, *J* = 12.6, 6.3 Hz, 2H, H-25), 3.36 (dt, *J* = 11.0, 5.5 Hz, 1H, H-6^{a}), 3.28 – 3.22 (m, 1H, H-6^{b}), 2.31 – 2.20 (m, 1H, H-24^{a}), 2.16 – 2.08 (m, 1H, H-4^{a}), 2.06 – 1.91 (m, 2H, H-24^{b}, H-23^{b}), 1.84 – 1.69 (m, 3H, H-23^{b}, H-5), 1.55 (td, *J* = 11.8, 4.5 Hz, 1H, H-4^{b}).

^{13}C NMR (75 MHz, Chloroform-*d*) δ 171.8 (C-17), 167.3 (C-2), 156.1 (C-21), 136.4 (C-31), 135.4 (C-37), 135.2 (C-9), 130.5, 130.4, 129.5 (C-14, C-10), 128.8, 128.7, 128.5, 128.0, 128.0 (C-36, C-32), 75.8 (C-8), 66.8 (C-30), 66.3 (C-25), 54.1 (C-19), 51.1 (C-3), 51.0 (C-6), 30.4 (C-23), 27.6 (C-4), 23.7 (C-24), 20.9 (C-5).

MS (ES+): 573.3 $[M+H]^+$ (56%), 595.3 $[M+Na]^+$ (100%)

HRMS (TOF ES+): calcd for $C_{32}H_{37}N_4O_6$ $[M+H]^+$ 573.2713, found 573.2721. $C_{32}H_{36}N_4O_6Na$ $[M+Na]^+$ 595.2532, found 595.2528.

4.3.24 *N*-((*S*)-5-(((*S*)-1-(benzyloxy)-2-oxopiperidin-3-yl)amino)-4-(((benzyloxy)carbonyl)(methyl)amino)-5-oxopentyl)hydroxylammonium chloride (65)

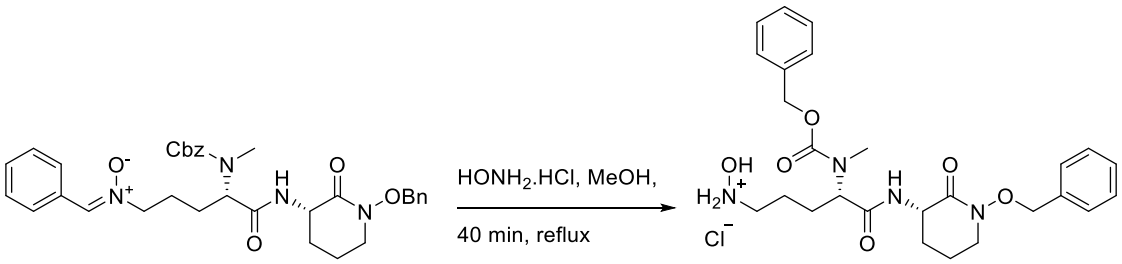

To a stirred suspension of (*Z*)-*N*-((*S*)-5-(((*S*)-1-(benzyloxy)-2-oxopiperidin-3-yl)amino)-4-(((benzyloxy)carbonyl)(methyl)amino)-5-oxopentyl)-1-phenylmethanimine oxide (535.6 mg, 0.91 mmol, 1.00 eq) in dry MeOH (10 mL) at room temperature under a nitrogen atmosphere was added hydroxylamine hydrochloride (73.0 mg, 1.05 mmol, 1.15 eq).

The reaction mixture was heated to reflux and stirred 40 min, monitor by TLC.

After which the reaction mixture was concentrated under reduced pressure.

The residue was triturated with MeOH/Et_2O (1:3) to give crude N-((S)-5-(((S)-1-(benzyloxy)-2-oxopiperidin-3-yl)amino)-4-(((benzyloxy)carbonyl)(methyl)amino)-5-oxopentyl)hydroxylammonium chloride as a colourless solid (442.5 mg) which used without further purification.

HRMS (TOF ES+): calcd for $C_{26}H_{35}N_4O_6$ $[M+H]^+$ 499.2557, found 499.2575.

calcd for $C_{26}H_{34}N_4NaO_6$ $[M+Na]^+$ 521.2376, found 521.2355.

4.3.25 Benzyl ((3*R*,16*S*)-17-(((*S*)-1-(benzyloxy)-2-oxopiperidin-3-yl)amino)-1-(2-(benzyloxy)phenyl)-12-hydroxy-3-(hydroxymethyl)-1,4,7,11,17-pentaoxo-2,5,8,12-tetraazaheptadecan-16-yl)(methyl)carbamate (90)

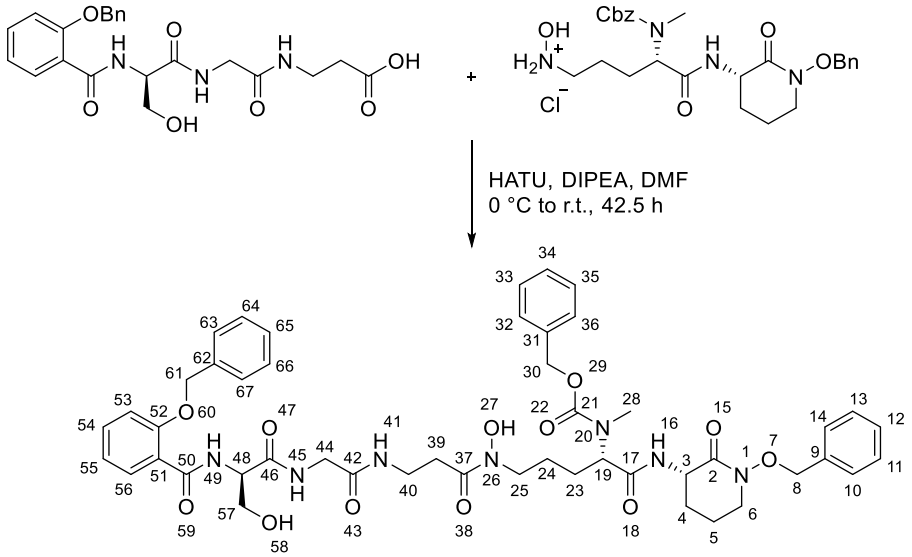

A stirred solution of N-((S)-5-(((S)-1-(benzyloxy)-2-oxopiperidin-3-yl)amino)-4-(((benzyloxy)carbonyl)(methyl)amino)-5-oxopentyl)hydroxylammonium chloride (0.90 g, 1.68 mmol, 1.40 eq) in dry DMF (15 mL) was cooled to 0 °C in an ice bath under nitrogen atmosphere. To the reaction mixture, HATU (0.51 g, 1.32 mmol, 1.11 eq) and (R)-3-(2-(2-(2-(benzyloxy)benzamido)-3-hydroxypropanamido)acetamido)propanoic acid (0.54 g, 1.20 mmol, 1.00 eq) were added. After which DIPEA (0.84 mL, 4.81 mmol, 4.00 eq) was added. After being stirred for 30 min at the same temperature, the reaction mixture was allowed to warm slowly to room temperature stirred for an additional 42 h. After which the reaction mixture was diluted with water (15 mL), the resulting slurry extracted with EtOAc (3 x 40 mL). The combined organic layers were washed with 5% aq. $NaHCO_3$ (40 mL), 0.2 M HCl (40 mL), H_2O (3 x 30 mL) and then brine (50 mL), dried over anhydrous sodium sulphate and the solvent was removed under reduced pressure. The crude product was purified via silica gel column chromatography (DCM/MeOH = 20:1 to 10:1, column diameter = 4 cm, silica = 25 cm) to give benzyl ((3R,16S)-17-(((S)-1-(benzyloxy)-2-oxopiperidin-3-yl)amino)-1-(2-(benzyloxy)phenyl)-12-hydroxy-3-(hydroxymethyl)-1,4,7,11,17-pentaoxo-2,5,8,12-tetraazaheptadecan-16-yl)(methyl)carbamate as a colourless oil (0.58 g, 0.63 mmol)

in a 53% yield.

Colourless oil (0.58 g, 53%)

[α]$_D$ = -7.2° (*c* = 1, MeOH). **R_f** = 0.18 (DCM : MeOH, 20:1; UV light 254nm).

IR (neat) ν_{max}/cm^{-1}: 3301.1 (O-H, w), 3063.4 (N-H, w), 2938.0 (C-H, w), 1643.5 (C=O, s), 1599.6, 1520.4. **MS** (ES+): 946.4 $[M+Na]^+$ (100%), 924.4 [M+H] (21%).

HRMS (TOF ES+): calcd for $C_{48}H_{58}N_7O_{12}$ $[M+H]^+$ 924.4144, found 924.4192.

$C_{48}H_{57}N_7NaO_{12}$ $[M+Na]^+$ 946.3963, found 946.3958.

^{1}H NMR (700 MHz, Chloroform-*d*, 328 K) δ 9.11 (br-s, 1H), 8.62 (t, *J* = 6.9 Hz, 1H, H-49), 8.06 – 8.02 (m, 1H, H-56), 7.68 (t, *J* = 5.9 Hz, 1H, H-45), 7.64 (t, *J* = 6.2 Hz, 1H), 7.42 – 7.42 (m, 1H), 7.41 – 7.40 (m, 1H), 7.39 – 7.37 (m, 1H, H-41), 7.36 – 7.36 (m, 1H, H-54), 7.35 – 7.28 (m, 12H, Ar), 7.23 (t, *J* = 7.5 Hz, 1H), 7.01 (d, *J* = 7.6 Hz, 1H, H-55), 6.99 (d, *J* = 8.3 Hz, 1H, H-53), (better spectrum dispersion at 298 K, clear shows t and d), 5.19 (d, *J* = 11.7 Hz, 1H, H-61^a), 5.16 (d, *J* = 11.6 Hz, 1H, H-61^b), 5.12 – 5.09 (m, 2H, H-30), 4.88 (dd, *J* = 10.5, 2.3 Hz, 1H, H-8^a), 4.82 (d, *J* = 10.6 Hz, 1H, H-8^b), 4.78 – 4.70 (m, 1H, H-19), 4.64 (q, *J* = 5.8 Hz, 1H, H-48), 4.43 – 4.38 (m, 1H, H-3), 3.90 (dd, *J* = 10.6, 5.0 Hz, 1H, H-57^a), 3.84 (dd, *J* = 16.9, 5.9 Hz, 1H, H-44^a), 3.79 – 3.77 (m, 1H, H-25^a), 3.74 (dd, *J* = 16.8, 5.8 Hz, 1H, H-44^b), 3.68 -3.68 (m, 0.3H), 3.62 (dd, *J* = 10.7, 6.0 Hz, 1H, H-57^b), 3.52 (td, *J* = 13.2, 6.6 Hz, 1H,H-40^a), 3.49 -3.43 (m, 1H), 3.41 – 3.35 (m, 2H, H-40^b, H-6^a), 3.29 – 3.27 (m, 1H, H-6^b), 2.88 (s, 3H, H-28), 2.78 – 2.72 (m, 1H, H-39^a), 2.66 – 2.59 (m, 1H, H-39^b), 2.07 – 2.05 (m, 1H, H-4^a), 1.89 (br-s, 1H, H-23^a), 1.81 – 1.77 (m, 1H, H-5^a), 1.75 – 1.71 (m, 2H, H-5^b, H-23^b), 1.66 (q, *J* = 7.0 Hz, 1H, H-24^a), 1.51 (br-s, 2H, H-4^b, H-24^a).

^{13}C NMR (176 MHz, Chloroform-*d*, 328 K) δ 172.7, 171.9 (C-46), 171.7 (C-37 or C-17), 171.6 (C-17 or C-37), 169.7 (C-42), 167.6 (C-2), 166.0 (C-50), 157.0 (C-21, C-52), 136.6 (C-31), 135.7 (C-62), 135.2 (C-9), 133.1 (C-54), 131.9 (C-56), 129.4 (C-14, C-10), 128.8, 128.8, 128.5, 128.5, 128.0, 127.9, 127.9, 127.7, 121.7 (C-51), 121.5 (C-55), 113.3 (C-53), 75.9 (C-8), 71.5 (C-61), 67.5 (C-30), 62.7 (C-57), 58.2 (C-19), 55.9 (C-48), 50.9 (C-6), 50.9 (C-3), 47.1 (C-25), 43.3 (C-44), 35.5 (C-40), 32.1 (C-39), 30.3 (C-28), 27.6 (C-4), 25.4 (C-23), 22.9 (C-24), 20.9 (C-5).

References

1. G. F. Bills and J. B. Gloer, *Microbiol*. *Spectr*., 2016, **4**, 4.6.01.
2. D. J. Newman and G. M. Cragg, *J. Nat. Prod.*, 2020, **83**, 770–803.
3. Y. Tu, *Angew. Chemie (International ed.)*, 2016, **55**, 10210–10226.
4. M. J. R. Desborough and D. M. Keeling, *Br. J. Haematol.*, 2017, **177**, 674–683.
5. K. Priyadarshini and U. Keerthi Aparajitha, *Med*. *Chem*., 2012, **2**, 139-141.
6. M. Grobbelaar, G. E. Louw, S. L. Sampson, P. D. Van Helden, P. R. Donald and R. M. Warren, *Infect. Genet. Evol.*, 2019, **74**, 103937.
7. D. Konz, A. Klens, K. Schörgendorfer and M. A. Marahiel, *Chem. Biol.*, 1997, **4**, 927–937.
8. R. C. Hider and X. Kong, *Nat*. *Prod*. *Rep*., 2010, **27**, 637-657.
9. C. J. Carrano and K. N. Raymond, *J. Am. Chem. Soc.*, 1979, **101**, 5401–5404.
10. J. B. Neilands, *J. Biol. Chem.*, 1995, **270**, 26723–26726.
11. M. G. P. Page, *Ann. N. Y. Acad. Sci.*, 2013, **1277**, 115–126.
12. P. Martin, S. Tronnet, C. Garcie and E. Oswald, *IUBMB Life*, 2017, **69**, 435–441.
13. E. Ahmed and S. J. M. Holmström, *Microb. Biotechnol.*, 2014, **7**, 196–208.
14. K. Kamińska, A. Mular, E. Olshvang, N. M. Nolte, H. Kozłowski, E. Wojaczyńska and E. Gumienna-Kontecka, *RSC Adv.*, 2022, **12**, 25284–25322.
15. J. Horáček and R. Přibil, *Talanta*, 1969, **16**, 1495–1499.
16. L. D. Loomis and K. N. Raymond, *Inorg. Chem.*, 1991, **30**, 906–911.
17. A. Evers, R. D. Hancock, A. E. Martell and R. J. Motekaitis, *Inorg. Chem.*, 1989, **28**, 2189–2195.
18. C. J. Carrano, H. Drechsel, D. Kaiser, G. Jung, B. Matzanke, G. Winkelmann, N. Rochel and A. M. Albrecht-Gary, *Inorg. Chem.*, 1996, **35**, 6429–6436.
19. M. Tsuda, M. Yamakawa, S. Oka, Y. Tanaka, Y. Hoshino, Y. Mikami, A. Sato, H. Fujiwara, Y. Ohizumi and J. Kobayashi, *J. Nat. Prod.*, 2005, **68**, 462–464.
20. J. M. Harrington, H. Park, Y. Ying, J. Hong and A. L. Crumbliss, *Metallomics*, 2011, **3**, 464–471.
21. J. M. Mitchell and J. T. Shaw, *Org. Lett.*, 2007, **9**, 1679–1681.

22. E. Mazzei, M. Iorio, S. I. Maffioli, M. Sosio and S. Donadio, *J. Antibiot. (Tokyo).*, 2012, **65**, 267–269.
23. A. R. Tyler, H. Mosaei, S. Morton, P. G. Waddell, C. Wills, W. McFarlane, J. Gray, M. Goodfellow, J. Errington, N. Allenby, N. Zenkin and M. J. Hall, *J. Nat. Prod.*, 2017, **80**, 1558–1562.
24. K. Harada, K. Tomita, K. Fujii, K. Masuda, Y. Mikami, K. Yazawa and H. Komaki, *J. Antibiot. (Tokyo)*., 2004, **57**, 125–133.
25. X. Zhang, H. He, R. Ma, Z. Ji, Q. Wei, H. Dai, L. Zhang and F. Song, *J. Ind. Microbiol. Biotechnol.*, 2017, **44**, 589–594.
26. J.-X. Yan, M. G. Chevrette, D. R. Braun, M. K. Harper, C. R. Currie and T. S. Bugni, *Org. Lett.*, 2019, **21**, 6275–6279.
27. M.-K. Bill, Y. Kleiner, J. L. Flügel, M. Kurz, M. Spohn, M. Marner, S. Mihajlovic, A. Vilcinskas, T. F. Schäberle, P. E. Hammann, M. A. Patras and S. M. M. Schuler, *J. Antibiot. (Tokyo)*., 2022, **75**, 576–582.
28. World Health Organization, Global antimicrobial resistance and use surveillance system (GLASS) report, 2022.
29. A. G. Atanasov, S. B. Zotchev, V. M. Dirsch, *et al*., *Nat. Rev. Drug Discov.*, 2021, **20**, 200–216.
30. E. Sauvage, F. Kerff, M. Terrak, J. A. Ayala and P. Charlier, *FEMS Microbiol. Rev.*, 2008, **32**, 234–258.
31. R. R. Yocum, J. R. Rasmussen and J. L. Strominger, *J. Biol. Chem.*, 1980, **255**, 3977–3986.
32. T. J. Silhavy, D. Kahne and S. Walker, *Cold Spring Harb. Perspect. Biol.*, 2010, **2**, a000414–a000414.
33. M. Pazos and K. Peters, ed. A. Kuhn, Springer International Publishing, Cham, 2019, pp. 127–168.
34. S. Brown, J. P. Santa Maria and S. Walker, *Annu. Rev. Microbiol.*, 2013, **67**, 313–336.
35. J. G. Swoboda, J. Campbell, T. C. Meredith and S. Walker, *Chembiochem*, 2010, **11**, 35–45.

36. N. F. C. and B. James, *Microbiol. Mol. Biol. Rev.*, 2003, **67**, 686–723.
37. A. Gründling and O. Schneewind, *Proc. Natl. Acad. Sci.*, 2007, **104**, 8478–8483.
38. O. Yusuke, K. Kenji, M. Miki, Y. Sakuo, L. Bok-Luel and S. Kazuhisa, *J. Bacteriol.*, 2009, **191**, 141–151.
39. K. Schirner, J. Marles-Wright, R. J. Lewis and J. Errington, *EMBO J.*, 2009, **28**, 830–842.
40. G. Garufi, A. P. Hendrickx, K. Beeri, J. W. Kern, A. Sharma, S. G. Richter, O. Schneewind and D. Missiakas, *J. Bacteriol.*, 2012, **194**, 4312–4321.
41. M. E. Wörmann, R. M. Corrigan, P. J. Simpson, S. J. Matthews and A. Gründling, *Mol. Microbiol.*, 2011, **79**, 566–583.
42. J. Jumper, R. Evans, A. Pritzel, *et al.*, *Nat.*, 2021, **596**, 583–589.
43. M. Varadi, S. Anyango, M. Deshpande, *et al.*, *Nucleic Acids Res.*, 2022, **50**, D439–D444.
44. C. R. Vickery, B. M. Wood, H. G. Morris, R. Losick and S. Walker, *J. Am. Chem. Soc.*, 2018, **140**, 876–879.
45. S. G. Richter, D. Elli, H. K. Kim, A. P. A. Hendrickx, J. A. Sorg, O. Schneewind and D. Missiakas, *Proc. Natl. Acad. Sci.*, 2013, **110**, 3531–3536.
46. X. Chee Wezen, A. Chandran, R. S. Eapen, E. Waters, L. Bricio-Moreno, T. Tosi, S. Dolan, C. Millership, A. Kadioglu, A. Gründling, L. S. Itzhaki, M. Welch and T. Rahman, *J. Chem. Inf. Model.*, 2022, **62**, 2586–2599.
47. M. G. Percy and A. Gründling, *Annu. Rev. Microbiol.*, 2014, **68**, 81–100.
48. H. J. D. Soufo and P. L. Graumann, *Curr. Biol.*, 2003, **13**, 1916–1920.
49. K. Schirner and J. Errington, *J. Bacteriol.*, 2009, **191**, 1404–1413.
50. H. Pu, T. Jiang, D. Peng, J. Xia, J. Gao, Y. Wang, X. Yan, X. Huang, Y. Duan and Y. Huang, *Org. Biomol. Chem.*, 2022, **20**, 5066–5070.
51. S. Kishimoto, S. Nishimura, A. Hattori, M. Tsujimoto, M. Hatano, M. Igarashi and H. Kakeya, *Org. Lett.*, 2014, **16**, 6108–6111.
52. T. W. Giessen, K. B. Franke, T. A. Knappe, F. I. Kraas, M. Bosello, X. Xie, U. Linne and M. A. Marahiel, *J. Nat. Prod. (Washington, D.C.)*, 2012, **75**, 905–914.
53. S. Kishimoto, S. Nishimura and H. Kakeya, *Chem. Lett.*, 2015, **44**, 1303–1305.

54. M. Bosello, M. Zeyadi, F. I. Kraas, U. Linne, X. Xie and M. A. Marahiel, *J. Nat. Prod. (Washington, D.C.)*, 2013, **76**, 2282–2290.
55. A.Tyler, PhD thesis, Newcastle University, 2018.
56. P. Marfey, *Carlsberg Res. Commun.*, 1984, **49**, 591.
57. K. Fujii, Y. Ikai, H. Oka, M. Suzuki and K. Harada, *Anal. Chem.*, 1997, **69**, 5146–5151.
58. R. Bhushan and H. Brückner, *Amino Acids*, 2004, **27**, 231–247.
59. T. Emery and J. B. Neilands, *J. Am. Chem. Soc.*, 1961, **83**, 1626–1628.
60. H. A. Akers and J. B. Neilands, *Biochemistry*, 1973, **12**, 1006–1010.
61. R. E. Moore and T. Emery, *Biochemistry*, 1976, **15**, 2719–2723.
62. T. Emery, *Biochim. Biophys. Acta - Gen. Subj.*, 1980, **629**, 382–390.
63. F. A. Fekete, R. A. Lanzi, J. B. Beaulieu, D. C. Longcope, A. W. Sulya, R. N. Hayes and G. A. Mabbott, *Appl. Environ. Microbiol.*, 1989, **55**, 298–305.
64. S. Kishimoto, S. Nishimura, M. Hatano, M. Igarashi and H. Kakeya, *J. Org. Chem.*, 2015, **80**, 6076–6082.
65. D. M. Shendage, R. Fröhlich and G. Haufe, *Org. Lett.*, 2004, **6**, 3675–3678.
66. Sigma-Aldrich Safety Data Sheet, https://www.sigmaaldrich.com/GB/en/sds/ALDRICH/T24503, (accessed March 2023).
67. D. Marcovici-Mizrahi, H. E. Gottlieb, V. Marks and A. Nudelman, *J. Org. Chem.*, 1996, **61**, 8402–8406.
68. A. K. Ghosh and M. Brindisi, *J. Med. Chem.*, 2015, **58**, 2895–2940.
69. T. Kan and T. Fukuyama, *Chem. Commun.*, 2004, 353–359.
70. C.C. Marvin, in *Comprehensive Organic Synthesis*, ed. G. A. Molander and P. Knochel, Elsevier Science, Amsterdam, 2nd edn, 2014, vol. 6, pp. 34–99.
71. P. A. Reddy, O. F. Schall, J. R. Wheatley, L. O. Rosik, J. P. McClurg, G. R. Marshall and U. Slomczynska, *Synth.*, 2001, **2001**, 1086–1092.
72. C. J. M. Brown, M. P. Gotsbacher, J. P. Holland and R. Codd, *Inorg. Chem.*, 2019, **58**, 13591–13603.
73. T. Fukuyama, C.-K. Jow and M. Cheung, *Tetrahedron Lett.*, 1995, **36**, 6373–6374.

74. S. Sikandar, A. F. Zahoor, S. Naheed, B. Parveen, K. G. Ali and R. Akhtar, *Mol. Divers.*, 2022, **26**, 589–628.
75. S. Yokoshima, H. Tokuyama and T. Fukuyama, *Chem. Rec.*, 2010, **10**, 101–118.
76. R. P. Volante, *Tetrahedron Lett.*, 1981, **22**, 3119–3122.
77. C. W. HUFFMAN, *J. Org. Chem.*, 1958, **23**, 727–729.
78. S. Kokubo, K. Suenaga, C. Shinohara, T. Tsuji and D. Uemura, *Tetrahedron*, 2000, **56**, 6435–6440.
79. R. A. Johnson, O. M. Manley, A. M. Spuches and N. E. Grossoehme, *Biochim. Biophys. Acta*, 2016, **1860**, 892–901.
80. J. J. Christensen, R. M. Izatt and D. Eatough, *Inorg. Chem.*, 1965, **4**, 1278–1280.
81. T. Wiseman, S. Williston, J. F. Brandts and L.-N. Lin, *Anal. Biochem.*, 1989, **179**, 131–137.
82. Malvern Panalytical Instrumentation company, https://www.malvernpanalytical.com/en/products/technology/microcalorimetry/isothermal-titration-calorimetry, (accessed March 2023).
83. Reaction Biology Corporation Biotech company, https://www.reactionbiology.com/services/biophysical-assays/isothermal-titration-calorimetry-itc, (accessed March 2023).
84. L. C. O'Brien, H. B. Root, C.-C. Wei, D. Jensen, N. Shabestary, C. De Meo and D. J. Eder, *J. Chem. Educ.*, 2015, **92**, 1547–1551.
85. B. Kepplinger, X. Wen, A. R. Tyler, B.-Y. Kim, J. Brown, P. Banks, Y. Dashti, E. S. Mackenzie, C. Wills, Y. Kawai, K. J. Waldron, N. E. E. Allenby, L. J. Wu, M. J. Hall and J. Errington, *Front. Microbiol.*, 2022, **13**, 1004737.
86. L. A. Maldonado, J. E. M. Stach, W. Pathom-aree, A. C. Ward, A. T. Bull and M. Goodfellow, *Antonie Van Leeuwenhoek*, 2005, **87**, 11–18.
87. H. Huang, W. Yang, Z. Chen, Z. Lai and J. Sun, *Chem. Sci.*, 2019, **10**, 9586–9590.
88. W. Dan, H. Geng, J. Qiao, R. Guo, S. Wei, L. Li, W. Wu and J. Zhang, *Molecules*, 2016, 21.
89. K. Kamińska, A. Mular, E. Olshvang, N. M. Nolte, H. Kozłowski, E. Wojaczyńska

and E. Gumienna-Kontecka, *RSC Adv.*, 2022, **12**, 25284–25322.

90. L. Dong and M. J. Miller, *J. Org. Chem.*, 2002, **67**, 4759–4770.
91. P. J. Maurer and M. J. Miller, *J. Am. Chem. Soc.*, 1983, **105**, 240–245.
92. R. Livingston, D. G. Doherty and H. Zeldes, *J. Am. Chem. Soc.*, 1975, **97**, 3198–3204.
93. M. Drag and J. Oleksyszyn, *Tetrahedron Lett.*, 2005, **46**, 3359–3362.
94. T. Maki, T. Tsuritani and T. Yasukata, *Org. Lett.*, 2014, **16**, 1868–1871.
95. Y.-M. Lin and M. J. Miller, *J. Org. Chem.*, 1999, **64**, 7451–7458.
96. A. Horn and U. Kazmaier, *European J. Org. Chem.*, 2018, **2018**, 2531–2536.
97. T. Kolasa and M. J. Miller, *J. Org. Chem.*, 1990, **55**, 1711–1721.
98. P. R. Sridhar, B. C. Venkatesh, S. Kalesha and C. Sudharani, *Org. Biomol. Chem.*, 2018, **16**, 3732–3740.
99. A. J. Phillips, Y. Uto, P. Wipf, M. J. Reno and D. R. Williams, *Org. Lett.*, 2000, **2**, 1165–1168.

Appendix 1

Chiral HPLC method for analysis of protected *ent*-(*S*,*S*)-and (*R*,*R*)-mirubactin C (**45**)

Samples of protected (*R*,*R*)-mirubactin C (**45**) and *ent*-(*S*,*S*)-mirubactin C (**45**) at a concentration of 10 mg/1 mL in MeOH. The separation was performed in iPrOH/MeOH or MeOH/EtOH system with CHIRALCEL® OD-H column, CHIRALPAK ® AD-H column and CHIRALPAK ® IC column.

Entry	Column	IPA/MeOH	Time	Amount	Outcome
1	OD-H	90%-100%	40 min	5 µL	very close
2	OD-H	90%-100%	60 min	5 µL	very close
3	OD-H	70%-100%	120 min	5 µL	Broad 8 min
4	OD-H	70%-100%	120 min	1 µL	Broad 8 min
5	AD-H	70%-100%	70 min	30 µL	Broad 23 min
		MeOH/EtOH			
6	OD-H	70%-100%	30 min	10 µL	Broad
		IPA/MeOH			
7	IC	50%-50%	30 min	5 µL	overlapping
8	IC	50%-50%	60 min	10 µL	separated
9	IC	50%-50%	60 min	10 µL	separated
10	IC	50%-50%	60 min	10 µL	separated

Appendix 2

Rotamers of benzyl protected cyclised ornithine (*S*-**86**) as observed by variable temperature ^{1}H NMR from 248 K (top) to 298 K (top) in $CDCl_3$ (700 MHz).

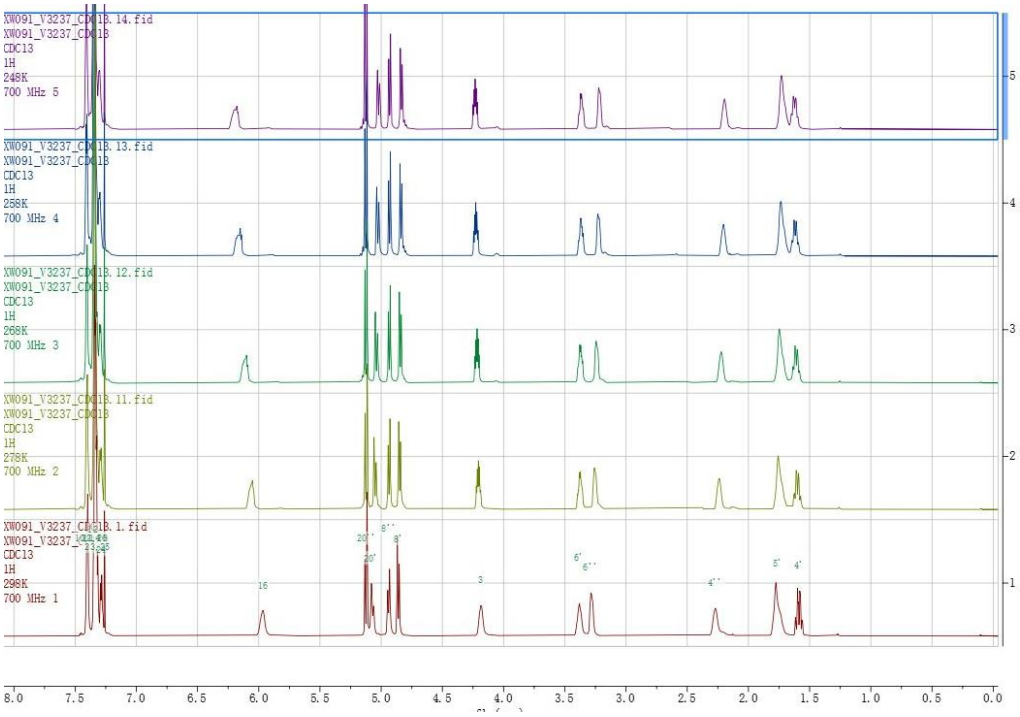

Appendix 3

Full assignment table of protected pentapeptide (**90**)

Atom no.	δC	^{1}H (CDCl3 - 298K - 400 MHz)						1H (CDCl3 - 298K - 700 MHz)				1H (CDCl3-328K - 700 MHz)			
		δH	Number of protons	Multiplicity	J (Hz)	^{1}H-^{1}H (COSY)	^{13}C-^{1}H (HMBC)	δH	Number of protons	Multiplicity	J (Hz)	δH	Number of protons	Multiplicity	J (Hz)
25(N-H)	-	8.50	1	dd	7.5, 4.3	4.37,4.68, 4.63	52.6 (C-**26**), 165.4 (C-**23**)	8.51	1	d	7.1	8.38	1	dd	7.4, 4.7
67 minor	-	8.12	-	s	-	8.08 (67 major)	-	8.12	-	s	-	-	-	-	-
67 major	163.40	8.08	-	s	-	8.12 (67 minor)	-	8.08	-	s	-	8.12 - 8.10	-	m	-
3 minor	123.33	7.73	-	d	1.6	7.15 (**5 major**), 7.12 (**4 major**)	7.15 (**5**), 7.10 (**4**)	7.72	-	dd	7.9, 1.4	7.72	-	dd	7.9, 1.5
3 major	123.29	7.70	-	dd	7.3, 1.7	7.15 (**5 major**), 7.12 (**4 major**)	7.15 (**5**), 7.10 (**4**)	7.701	-	dd	7.8, 1.2	7.701	-	dd	7.9, 1.5
10 minor	127.8 (overlaps with 14)	7.48 (overlaps with 10 major, 14 major, 14 minor)	-	m	-	-	-	7.48	-	d	2.04	7.46	-	d	1.7
10 major	127.8 (overlaps with 14)	7.47 - 7.43 (overlaps with 10 minor, 14 major, 14 minor)	1	m	-	7.40, 7.38	7.33, 5.13	7.49	1	d	7.26	7.45	1	d	7.47
14 minor	127.8 (overlaps with 10)	7.48 (overlaps with 14 major, 10 major, 10 minor)	-	m	-	-		7.48	-	d	2.04	7.46	-	d	1.7
14 major	127.8 (overlaps with 10)	7.47 - 7.43 (overlaps with 14 minor, 10 major, 10 minor)	1	m	-	7.40, 7.38	7.33, 5.13	7.49	1	d	7.26	7.45	1	d	7.47
5	117.50	7.15 (overlaps with 4 and 5X)	1	d	6.9	7.06 (**4**), 7.64 (**3**), 7.18 (5X)	7.64 (**3**)	7.15	1	d	8	7.15	1	dd	8.10, 1.4
5X	117.58	7.18 (overlaps with 5)	-	m	-	7.15 (5), 7.11 (4)	-	7.17	-	d	7.17	7.19	-	d	8.26
5X-b	-	-	-	-	-	-	-	7.13 (overlaps with 5)	-	s	-	7.13	-	s	-
5X-c	-	-	-	-	-	-	-	-	-	-	-	7.16	-	dd	8.26, 1.67
4	124.40	7.11	1	t	7.7	7.15 (**5**), 7.72 (**3**)	-	7.11 (overlaps with 4x)	1	t	8.1	7.101	1	t	8
4X	124.44	-	-	-	-	-	-	7.12 (overlaps with 4)	-	-	-	7.11 (overlaps with 4)	-	d	7.9
16^{a}	76.21	5.21	1	d	10.6	5.09 (**16^{b}**), 5.06 (?)	7.34 (maybe is 18,20)	5.21	1	d	10.4	5.2	1	d	10.6
16^{b}	76.21	5.10	1	m	-	5.21 (**16^{b}**)	7.34 (maybe is 18,20)								
52^{a}	77.5 (overlaps with CDCl3)	4.71	1	m	-	4.75 (52b)	-								
52^{b}	77.5 (overlaps with CDCl3)	-	1	m	-	4.72 (52a)	-								
26	52.63	4.666 (HSQC spot overlaps with 36)	1	m	-	8.508 (N-H,25)	8.475 (N-H,25)								
36	52.12 (peak brod)	4.62 - 4.60 (HSQC spot overlaps with 26)	1	m	-	1.88 (**47^{a}**), 1.69 (**47^{b}**), 1.66 (**48^{a}**)	-	4.62 - 4.61	1	br-s	-	4.62 - 4.58	1	m	-
49	43.60	3.54	-	br-s	-	1.652 (48a), 1.60 (48b)	-	3.58 - 3.50	-	m	-	3.48	-	br-s	-
31a	39.85	3.27 - 3.18	1	m	-	3.007 (31b major),1.408 (30a)	-	3.23 - 3.19	1	m	-	3.19	1	br-s	-
31b minor	39.85	3.14 - 3.09	-	m	-	3.007 (31b major)	-	3.11	-	m	-	3.11 - 3.10	-	m	-
31b major	39.85	3.05 - 2.97	1	m	-	3.23 (31a), 3.11 (31b minor),1.397 (30a/b)	-	3.02 - 3.001	1	m	-	3.03	1	dt	13.1, 6.5
47^{a}	29.2 or 29.0	1.89 - 1.87	1	m	-	1.69 (47b), 4.62 (36)	-	1.93 - 1.87	1	m	-	1.82 - 1.85	1	m	-
47a-X	-	-	-	-	-	-	-	1.84 - 1.82	-	m	-	-	-	-	-
47^{b}	29.2 or 29.0	1.68(overlaps with 29a, 48a, 48b)	1	m	-	1.87 (47a), 3.55 (49), 4.62 (36)	-					1.74 - 1.72	1	q	6.6
29^{a}	28.80	1.68(overlaps with **47^{b}** and **48a and 48b)**	1	m	-	1.432(29b), 1.35 (30), 4.62 (36)	-					1.70 - 1.69 (overlaps with 48a, 48b)	1	m	-
48	23.30	1.66 (overlaps with 29a and 47b)	2	m	-	1.87 (47a), 3.55 (49)	-					1.69 - 1.67 (overlaps with 29a)	2	m	-
48-X								1.64 - 1.59				1.65 - 1.62			
30	26.10	1.38 (overlaps with **29^{b}**)	2	m	-	1.71 (**29^{a}**),3.23 (**31^{a}**), 3.01(**31^{b}**)	-					1.43 - 1.39 (overlaps with 29b)	2	m	-
29b	28.80	1.33 (overlaps with **30**)	1	m	-	not sure						1.39 - 1.36	1	m	-

37	174.00	-	-	-	-	-	5.14 , 5.10									
27	174.00	-	-	-	-	-	5.14 , 5.10									
23	165.40	-	-	-	-	-	8.49 (**25**, N-H), 7.69 (**3**)									
33	156.80	-	-	-	-	-	5.09, 5.02									
6	153.30	-	-	-	-	-	7.70 (**3**), 7.15 (**5**),7.11 (4), 5.14									
1	147.10	-	-	-	-	-	7.70 (**3**), 7.15 (**5**),7.11 (4), 5.20 (16), 5.07									
2	126.60	-	-	-	-	-	7.11 (4)									
8	71.40	5.14 (overlaps with **60**)	2	m	-	-	7.47 (**14**,**10**)									
60	67.20	5.13 (overlaps with **40**)	2	m	-	-	7.30, 7.25									
40	66.70	5.07 (overlaps with **60**)	2	m	-	-	7.33									
major	136.79	-	-	-	-	-	7.33, *7.15,7.13(spot overlaps)*									
minnor	136.74	-	-	-	-	-	7.33									
major	136.35	-	-	-	-	-	7.26, 5.13									
minor of 136.35 peak	136.25	-	-	-	-	-	7.26, 5.13									
	135.36	-	-	-	-	-	7.30, 7.25, 5.16,5.13,5.10									
	134.30	-	-	-	-	-										
2C overlaps	129.57	7.42 - 7.25 (HSQC spot overlaps)		m												
	129.07	7.42 - 7.25 (HSQC spot overlaps)		m			5.10, spot overlaps									
C-18, C-22	129.00	7.42 - 7.25 (HSQC spot overlaps)		m			5.10,5.21 (**16a**) spot overlaps									
	128.78	7.42 - 7.25 (HSQC spot overlaps)		m			spot 5.10,overlaps									
	128.76	7.42 - 7.25 (HSQC spot overlaps)		m			5.10, spot overlaps									
	128.71	7.42 - 7.25 (HSQC spot overlaps)		m			5.10, spot overlaps									
	128.66	7.28 (HSQC spot overlaps)		m			5.10, 7.26									
	128.62	7.42 - 7.25 (HSQC spot overlaps)		m			5.10									
	128.55	7.42 - 7.25 (HSQC spot overlaps)		m			5.10, 7.30									
	128.37	7.42 - 7.25 (HSQC spot overlaps)		m			5.10,5.17, 5.13 spot overlaps									
	128.11	7.42 - 7.25 (HSQC spot overlaps)		m			5.10,5.17,5.13, 7.32									
	128.09	7.42 - 7.25 (HSQC spot overlaps)		m			5.10, 5.13									
	128. 9	7.43 - 7.42	1	m	-	7.28										
		7.41				7.38, 7.28										
		7.40				7.40, 7.37										
		7.39														
		7.38														
		7.37														
		7.34				7.33										
		7.33				7.31, 7.34										
		7.31				7.33										
		7.28				7.26										
		7.28														
		7.26				7.28										
		5.17														
		5.15														
		5.14				5.11, 5.09										
		5.12														
		5.11				5.14										
		5.09				5.14, 5.11, 5.03										
		5.08														
		5.07														
		5.06														
		5.06				5.03										
		5.03				5.06, 5.10										

X-Ray Crystallographa Data

The following crystal structure data were collected on a Xcalibur (Atlas, Gemini Ultra) diffractometer equipped with a proper sealed X-ray tube ($\lambda_{CuK\alpha}$ = 1.54184 Å) and an Oxford Cryosystems CryostreamPlus open-flow N_2 cooling device. The X-ray diffraction data analysis for all the following compounds was carried out by Dr Paul Waddell.

Benzyl 2,3-bis(benzyloxy)benzoate (54)

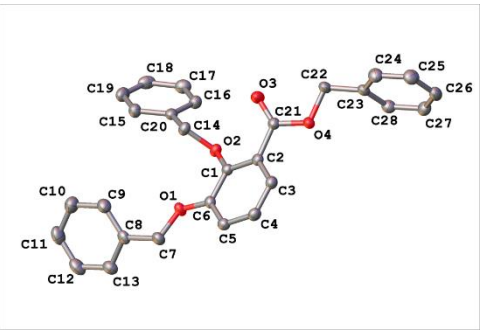

Identification code	mjh200063
Empirical formula	$C_{28}H_{24}O_4$
Formula weight	424.47
Temperature/K	150.0(2)
Crystal system	monoclinic
Space group	$P2_1/c$
a/Å	11.2319(2)
b/Å	8.59750(10)
c/Å	22.4293(3)
α/°	90
β/°	92.7230(10)
γ/°	90
Volume/Å^3	2163.47(5)

Z	4
ρ_{calc}g/cm^3	1.303
μ/mm^{-1}	0.693
F(000)	896.0
Crystal size/mm^3	0.35 × 0.15 × 0.12
Radiation	Cu Kα (λ = 1.54184)
2Θ range for data collection/°	7.88 to 133.802
Index ranges	-13 ≤ h ≤ 13, -10 ≤ k ≤ 10, -26 ≤ l ≤ 26
Reflections collected	30201
Independent reflections	3850 [R_{int} = 0.0563, R_{sigma} = 0.0284]
Data/restraints/parameters	3850/0/290
Goodness-of-fit on F^2	1.048
Final R indexes [I>=2σ (I)]	R_1 = 0.0389, wR_2 = 0.0979
Final R indexes [all data]	R_1 = 0.0465, wR_2 = 0.1051
Largest diff. peak/hole / e Å^{-3}	0.18/-0.19

_N_-(benzyloxy)-2-nitrobenzenesulfonamide (61)

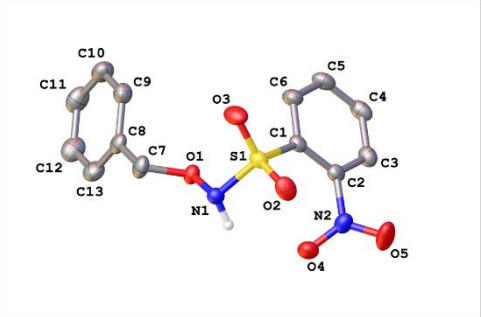

Identification code	mjh200049
Empirical formula	$C_{13}H_{12}N_2O_5S$
Formula weight	308.31
Temperature/K	150.0(2)
Crystal system	monoclinic
Space group	$P2_1/n$
a/Å	13.3591(2)
b/Å	7.85340(10)
c/Å	13.9530(3)
α/°	90
β/°	104.590(2)
γ/°	90
Volume/Å^3	1416.66(4)
Z	4
ρ_{calc}g/cm^3	1.446
μ/mm^{-1}	2.262
F(000)	640.0
Crystal size/mm^3	0.17 × 0.14 × 0.13
Radiation	CuKα (λ = 1.54184)
2Θ range for data collection/°	8.19 to 133.858
Index ranges	-13 ≤ h ≤ 15, -9 ≤ k ≤ 9, -16 ≤ l ≤ 16

Reflections collected	19438
Independent reflections	2521 [R_{int} = 0.0384, R_{sigma} = 0.0195]
Data/restraints/parameters	2521/0/194
Goodness-of-fit on F^2	1.053
Final R indexes [I>=2σ (I)]	R_1 = 0.0288, wR_2 = 0.0678
Final R indexes [all data]	R_1 = 0.0353, wR_2 = 0.0730
Largest diff. peak/hole / e $Å^{-3}$	0.24/-0.24

Methyl (2-(benzyloxy)benzoyl)-*D*-serinate (77)

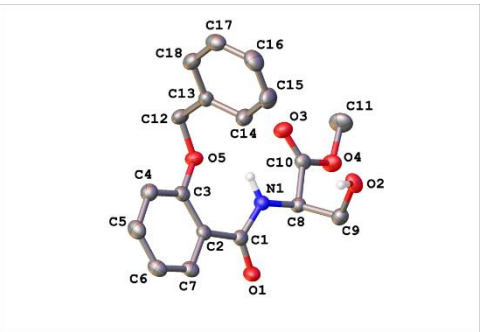

Identification code	mjh230002_fa
Empirical formula	$C_{18}H_{19}NO_5$
Formula weight	329.34
Temperature/K	150.0(2)
Crystal system	orthorhombic
Space group	$P2_12_12_1$
a/Å	8.3118(2)
b/Å	12.5695(3)
c/Å	15.6625(4)
α/°	90
β/°	90
γ/°	90
Volume/Å^3	1636.34(7)
Z	4
ρ_{calc}g/cm^3	1.337
μ/mm^{-1}	0.812
F(000)	696.0
Crystal size/mm^3	0.17 × 0.13 × 0.05
Radiation	Cu Kα (λ = 1.54184)
2Θ range for data collection/°	9.02 to 155.908
Index ranges	-9 ≤ h ≤ 4, -15 ≤ k ≤ 15, -19 ≤ l ≤ 19
Reflections collected	7891
Independent reflections	3226 [R_{int} = 0.0335, R_{sigma} = 0.0366]

Data/restraints/parameters	3226/0/225
Goodness-of-fit on F^2	1.049
Final R indexes [I>=2σ (I)]	R_1 = 0.0321, wR_2 = 0.0777
Final R indexes [all data]	R_1 = 0.0350, wR_2 = 0.0799
Largest diff. peak/hole / e $Å^{-3}$	0.14/-0.13
Flack parameter	-0.07(13)

(*S*,*Z*)-*N*-(4-(((benzyloxy)carbonyl)amino)-4-carboxybutyl)-1-phenylmethanimine oxide (76)

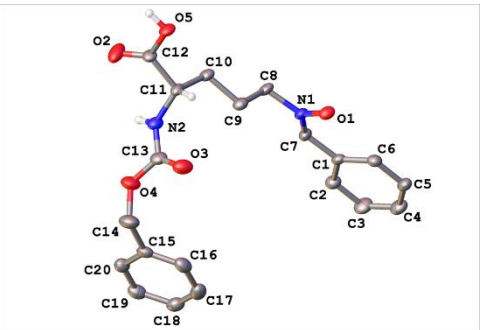

Identification code	mjh200061
Empirical formula	$C_{20}H_{22}N_2O_5$
Formula weight	370.39
Temperature/K	100.0(2)
Crystal system	monoclinic
Space group	$P2_1$
a/Å	14.3933(3)
b/Å	5.1806(2)
c/Å	15.0922(2)
α/°	90
β/°	116.8480(10)
γ/°	90
Volume/Å^3	1004.06(5)
Z	2
ρ_{calc}g/cm^3	1.225
μ/mm^{-1}	0.083
F(000)	392.0
Crystal size/mm^3	0.156 × 0.026 × 0.013
Radiation	Synchrotron (λ = 0.6889)
2Θ range for data collection/°	2.932 to 63.558
Index ranges	-20 ≤ h ≤ 9, -4 ≤ k ≤ 7, -21 ≤ l ≤ 22
Reflections collected	4349

Independent reflections	3610 [R_{int} = 0.0193, R_{sigma} = 0.0408]
Data/restraints/parameters	3610/2/250
Goodness-of-fit on F^2	1.087
Final R indexes [I>=2σ (I)]	R_1 = 0.0495, wR_2 = 0.1432
Final R indexes [all data]	R_1 = 0.0567, wR_2 = 0.1463
Largest diff. peak/hole / e $Å^{-3}$	0.26/-0.26
Flack parameter	-0.4(10)

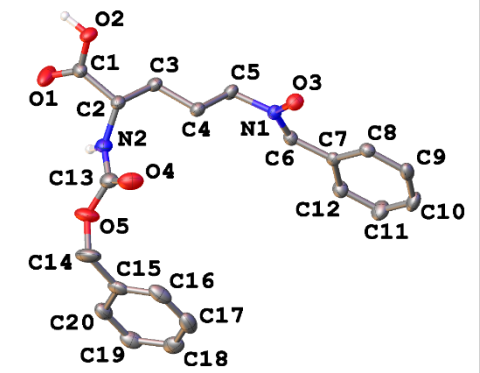

Identification code	mjh200065
Empirical formula	$C_{20}H_{22}N_2O_5$
Formula weight	370.39
Temperature/K	100.0(2)
Crystal system	monoclinic
Space group	$P2_1$
a/Å	14.3030(8)
b/Å	5.2106(3)
c/Å	15.0565(7)
α/°	90
β/°	116.669(4)
γ/°	90
Volume/Å^3	1002.74(10)
Z	2
ρ_{calc}g/cm^3	1.227
μ/mm^{-1}	0.083
F(000)	392.0
Crystal size/mm^3	0.21 × 0.016 × 0.012
Radiation	Synchrotron (λ = 0.6889)
2Θ range for data collection/°	2.934 to 53.144
Index ranges	-20 ≤ h ≤ 21, -7 ≤ k ≤ 7, -21 ≤ l ≤ 22
Reflections collected	16669
Independent reflections	4515 [R_{int} = 0.0494, R_{sigma} = 0.0810]
Data/restraints/parameters	4515/191/250

Goodness-of-fit on F^2	0.990
Final R indexes [I>=2σ (I)]	R_1 = 0.0374, wR_2 = 0.0971
Final R indexes [all data]	R_1 = 0.0442, wR_2 = 0.0991
Largest diff. peak/hole / e $Å^{-3}$	0.18/-0.15
Flack parameter	-0.2(5)

frontiers | Frontiers in Microbiology

TYPE Original Research
PUBLISHED 13 October 2022
DOI 10.3389/fmicb.2022.1004737

OPEN ACCESS

EDITED BY
Christian Sohlenkamp,
National Autonomous University of Mexico, Mexico

REVIEWED BY
Béatrice Roche,
University of Basel, Switzerland
Chris Sham,
National University of Singapore, Singapore
Robson Francisco De Souza,
University of São Paulo, Brazil

*CORRESPONDENCE
Jeff Errington
jeff.errington@ncl.ac.uk

SPECIALTY SECTION
This article was submitted to Microbial Physiology and Metabolism, a section of the journal Frontiers in Microbiology

RECEIVED 27 July 2022
ACCEPTED 22 September 2022
PUBLISHED 13 October 2022

CITATION
Kepplinger B, Wen X, Tyler AR, Kim B-Y, Brown J, Banks P, Dashti Y, Mackenzie ES, Wills C, Kawai Y, Waldron KJ, Allenby NEE, Wu LJ, Hall MJ and Errington J (2022) Mirubactin C rescues the lethal effect of cell wall biosynthesis mutations in *Bacillus subtilis*. *Front. Microbiol.* 13:1004737. doi: 10.3389/fmicb.2022.1004737

Mirubactin C rescues the lethal effect of cell wall biosynthesis mutations in *Bacillus subtilis*

Bernhard Kepplinger[1], Xin Wen[2], Andrew Robert Tyler[2], Byung-Yong Kim[3], James Brown[1], Peter Banks[4], Yousef Dashti[1], Eilidh Sohini Mackenzie[4], Corinne Wills[2], Yoshikazu Kawai[1], Kevin John Waldron[4], Nicholas Edward Ellis Allenby[3], Ling Juan Wu[1], Michael John Hall[2] and Jeff Errington[1,3]*

[1]Centre for Bacterial Cell Biology, Newcastle University, Newcastle upon Tyne, United Kingdom, [2]Chemistry, School of Natural and Environmental Sciences, Newcastle University, Newcastle upon Tyne, United Kingdom, [3]Odyssey Therapeutics Inc., Newcastle upon Tyne, United Kingdom, [4]Faculty of Medical Sciences, Bioscience Institute, Newcastle University, Newcastle upon Tyne, United Kingdom

Growth of most rod-shaped bacteria is accompanied by the insertion of new peptidoglycan into the cylindrical cell wall. This insertion, which helps maintain and determine the shape of the cell, is guided by a protein machine called the rod complex or elongasome. Although most of the proteins in this complex are essential under normal growth conditions, cell viability can be rescued, for reasons that are not understood, by the presence of a high (mM) Mg^{2+} concentration. We screened for natural product compounds that could rescue the growth of mutants affected in rod-complex function. By screening > 2,000 extracts from a diverse collection of actinobacteria, we identified a compound, mirubactin C, related to the known iron siderophore mirubactin A, which rescued growth in the low micromolar range, and this activity was confirmed using synthetic mirubactin C. The compound also displayed toxicity at higher concentrations, and this effect appears related to iron homeostasis. However, several lines of evidence suggest that the mirubactin C rescuing activity is not due simply to iron sequestration. The results support an emerging view that the functions of bacterial siderophores extend well beyond simply iron binding and uptake.

KEYWORDS

mirubactin, *B. subtilis*, cell wall mutants, siderophore, chemical biological activity

Introduction

Gram-positive bacteria surround their cell membrane with a thick layer of peptidoglycan (PG), which gives the bacteria their shape and protects them from fluctuations in internal osmotic pressure (Koch, 2006). PG synthesis is highly conserved across bacterial taxa and several components of the PG synthetic machinery are hugely important antibiotic targets. The cell envelopes of Gram-positive bacteria usually contain other highly abundant anionic polymers called teichoic acids (TAs), which can be either anchored into the cell membrane (lipoteichoic acids, LTA) or to the peptidoglycan (wall teichoic acids, WTA) (Archibald et al., 1961). The specific functions of these polymers are not well understood but this certainly includes a role in metal homeostasis (Archibald et al., 1961; Heptinstall et al., 1970) and they can be important virulence determinants in pathogens (Morath et al., 2001; Weidenmaier et al., 2004; Fittipaldi et al., 2008).

Cell wall synthesis is supported by various synthetic systems. In most rod-shaped bacteria cell elongation is governed by various general elements: a "Rod complex," which includes a glycosyl transferase, RodA, and associated transpeptidases called class B penicillin-binding proteins (bPBPs); autolytic hydrolases such as CwlO and LytE in *Bacillus subtilis* (Masayuki et al., 2012), which break bonds to allow cell wall expansion; and a topological regulator, the actin-like protein MreB, and its associated factors MreC and MreD. Some TA-synthetic enzymes and PG precursor synthetic proteins are also probably associated with the Rod complex (Bhavsar et al., 2001).

In *B. subtilis*, there are three MreB paralogues, which have overlapping functions (Kawai et al., 2009). MreB and Mbl ("MreB-like") (Levin et al., 1992; Varley and Stewart, 1992; Lee and Price, 1993; Abhayawardhane and Stewart, 1995) are both essential in typical microbiological growth media but, curiously, this growth deficiency can be rescued by addition of high concentrations of magnesium (Mg^{2+}) to the culture medium (Formstone and Errington, 2005). Intriguingly, growth of mutants that lack one of several other factors in the Rod complex can also be rescued or greatly enhanced by Mg^{2+} supplementation, including *mreC*, *mreD* and *rodA* (Jones et al., 2001; Formstone and Errington, 2005; Leaver and Errington, 2005; Dominguez-Cuevas et al., 2012). *B. subtilis*, like most other bacteria, has a second PG synthetic machinery based around bifunctional (glycosyl transferase, transpeptidase) class A penicillin-binding proteins (aPBPs) (Meeske et al., 2016; Emami et al., 2017; Dion et al., 2019). Growth of mutants affected in the major aPBP gene, *ponA*, are also rescued by Mg^{2+} (Murray et al., 1998). The molecular basis for this Mg^{2+} effect remains unclear. Formstone and Errington suggested two potential mechanisms: stiffening of the cell wall or inhibition of autolytic enzymes (Formstone and Errington, 2005; Dajkovic et al., 2017; Tesson et al., 2022). Dajkovic et al. (2017) subsequently presented evidence to exclude mechanical changes in the cell wall, and provided strong evidence for the reduction of autolytic activity. Wilson and Garner (2021) identified LytE as a likely target for this inhibition.

The TAs are underexplored potential antibiotic targets for Gram-positive pathogens. Compounds active on WTA (Campbell et al., 2012) or LTA (Richter et al., 2013; Vickery et al., 2018) have been described but, so far, have not yet entered clinical development. The key enzyme in LTA synthesis, LTA synthase (LtaS), is a particularly interesting antibiotic target because it is essential under normal conditions in *Staphylococcus aureus* (Oku et al., 2009; Corrigan et al., 2011), but specific inhibitors would not affect Gram-negative nor many other Gram-positive bacteria. Furthermore, the enzyme's active site is located outside the cytoplasmic membrane, excluding cell permeability and efflux mechanisms as sources of resistance. Lastly there is no equivalent in mammalian cells.

We previously described the discovery of mutations in *ltaS* as potent suppressors of the Mg^{2+}-dependence of *mbl* mutants in *B. subtilis* (Schirner et al., 2009). This suggested that inhibitors of LtaS might also rescue the growth of an *mbl* mutant cultured in the absence of Mg^{2+}, providing the basis for a powerful chemical biology screen for LtaS inhibitors. Even if compounds rescuing the growth of an *mbl* mutant did not directly target LtaS they might still be of interest by providing insights into the molecular basis for the Mg^{2+}-rescue effect and the functions of TAs.

Actinomycetes have been a rich source of bioactive natural products including many diverse drugs, particularly antibiotics (Genilloud, 2017). By screening a collection of actinomycete extracts we were able to identify, isolate and characterize a small natural product molecule, mirubactin C (Pu et al., 2022), which efficiently rescues the growth of an *mbl* mutant in the absence of added Mg^{2+}. We used bioactivity-guided fractionation to purify the molecule and determined its structure by a combination of NMR and high resolution mass spectrometry. The molecule turns out to be identical to a fragment of a known siderophore antibiotic called mirubactin (Giessen et al., 2012; Kishimoto et al., 2015b). To validate the source of the observed bioactivity, mirubactin C was synthesized, and the synthetic molecule was also able to rescue growth of *mbl* and *mreB* mutants of *B. subtilis* but was toxic at higher concentrations, probably due to iron sequestration. The results provide new insights into the intricate connections between metal homeostasis and cell envelope synthesis systems, as well as highlighting how poorly we understand the complex chemical exchanges between microorganisms inhabiting the soil.

Results

A screen for natural product compounds that rescue growth of an *mbl* mutant

Previous results showed that disruption of the *mbl* gene is normally lethal on standard culture media but that the mutant can be rescued by the addition of a high concentration (e.g., 20 mM) of Mg^{2+}. Cells of the *mbl* mutant cultured in the presence of Mg^{2+} and then diluted into medium with no added Mg^{2+} failed to grow, except after prolonged incubation, at which time it appeared that suppressor mutations emerged that relieve the Mg^{2+} dependence, as described by Schirner et al. (2009). We established a protocol for culturing *mbl*-mutant cells in 96 well plates. **Supplementary Figure 1** shows that, under these conditions, addition of 20 mM Mg^{2+} resulted in growth albeit slower than that of isogenic wild type cells (*B. subtilis* 168CA). Lower concentrations of Mg^{2+} (down to 5 mM) allowed equivalent growth rates but with an increasingly long delay. We do not understand the basis of this but a similar effect has been described by Pi et al. (2022). Agar plate crush extracts (see Materials and methods) of strains from a large collection of actinomycetes that is both diverse and low in replicate organisms were obtained from Demuris Ltd. A total of 2,070 extracts were screened, from organisms belonging to many Genera, including: *Actinomadura, Amycolatopsis, Dactylosporangium, Gordonia, Micromonospora, Norcardia, Rhodococcus, Streptacidiphilus, Streptomyces* and *Streptosporangium*. The collection is known to contain a high proportion of antibiotic producers, with about 25% of organisms capable of producing secondary metabolites that kill *B. subtilis* in simple plug assays. Five of the strain extracts were found reproducibly to enhance the growth of the *mbl* mutant in the absence of added Mg^{2+}, giving growth rates similar to 5–10 mM of Mg^{2+} (representative plots shown in **Supplementary Figure 1**).

Genome sequencing of the producer strains

To facilitate purification of the active compounds we tested the supernatants of the five positive strains for the *mbl*-rescuing activity. Of the five strains, only TW 167, MEX267 and MDA8-470 produced *mbl*-rescuing activity under these conditions, so we focused on these three strains. As a method to determine what kind of bioactive natural products these organisms might make and whether they were likely to make similar or different compounds, we carried out whole genome sequencing (WGS) by a combination of Minion and Illumina sequencing methods (NCBI accession numbers: JANADG000000000 TW 167, CP098740 MDA8-470, JANADF000000000 Mex267). Analyses of the predicted natural product biosynthetic gene clusters in each of the three strains are shown in **Supplementary Table 1** through antiSMASH output of the prioritized strains. This analysis revealed that TW 167 and MDA8-470 are closely related strains, whereas MEX267 is evolutionarily distant. The nearest described type strains were *Streptomyces drozdowiczii* for TW 167 and MDA8-470 and *Nocardia zapadnayensis* for MEX267. We chose MDA8-470 as the focus of further work since in repeated growth experiments it tended to provide bioactivity more consistently than the other strains.

Purification and structure determination of the active compound from MDA8-470

We purified the active component from supernatants of strain MDA8-470 by activity-guided isolation using the *mbl*-rescue bioassay. MDA8-470 was cultured for 76.5 h at 26 L volume in a stirred tank reactor. The culture broth was treated with XAD-16 resin and absorbed compounds were eluted with methanol. Hydrophobic compounds were removed by partitioning between ethyl acetate (EtOAc) and water (pH 4). The active compound stayed in the aqueous phase which was further purified by C18 flash chromatography followed by LH20 size exclusion in water and then freeze dried to give a light brown powder with a molecular ion by high resolution mass spectrometry (HRMS) of *m/z* 427.1815 $[M + H]^+$.

Mirubactin C is a fragment of the siderophore antibiotic mirubactin A

The molecular structure of the active compound was determined by a combination of HRMS and NMR spectroscopy (**Supplementary Table 3** and **Supplementary Figure 2**). HRMS suggested a molecular formula of $C_{18}H_{25}O_8N_4$, implying eight double bond equivalents in the structure. ^1H NMR in D_2O allowed the identification of 18 hydrogens, suggesting the presence of 7 exchangeable protons, whilst ^{13}C NMR showed the presence of a benzene ring and four carbonyl-containing functional groups. Further analysis by ^{15}N NMR confirmed the presence of four nitrogen atoms, one amine and three amide-like groups. This, combined with additional 2D experiments, allowed us to propose a linear polypeptide-like structure, including both a 2,3-dihydroxybenzoyl and a hydroxamic acid group typical of bacterial siderophores (**Figure 1**).

The structure of the compound turned out to be identical to a recently described compound, Mirubactin C (Pu et al., 2022), which belongs to a family of related compounds including

10.3389/fmicb.2022.1004737

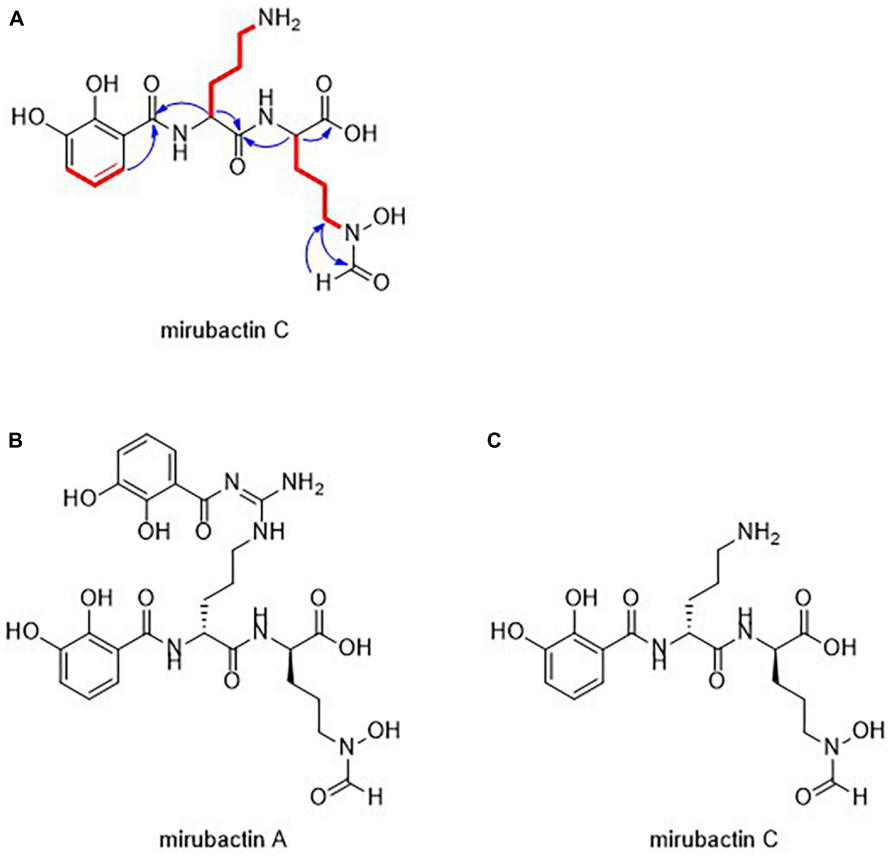

FIGURE 1
(A) Structural assignment of mirubactin C (COSY = red, selected HMBC = blue) **(B)** Structures of mirubactin A **(C)** mirubactin C.

mirubactin A, chlorocatechelin A and chlorocatechelin B. Mirubactin C is identical to mirubactin A, except that it is missing one of its 2,3-dihydroxybenzoid acid moieties and has lost the guanidine group. The relationship between mirubactin A and mirubactin C is similar to that of chlorocatechelin A to B (Kishimoto et al., 2014). Indeed, mirubactin C differs from chlorocatechelin B only in the lack of a chlorine substituent on the aromatic ring. Kishimoto et al. (2014, 2015a) proposed that chlorocatechelin A spontaneously decomposes to give chlorocatechelin B under acidic conditions, (Kishimoto et al., 2014, 2015a) raising the possibility that mirubactin C has a similar relationship as a degradation product of mirubactin A (**Supplementary Figure 4**). This was recently shown by Pu et al. (2022). To check whether mirubactin A was produced by MAD8-470, the strain was cultured in 50 ml of GYM media for 3 days and, after removing the bacterial cells, the chemical profile of culture media was directly analysed by LC-MS. Mirubactin A was detected in both apo (*m/z* 605.2) and holo (*m/z* 658.1) forms (Giessen et al., 2012).

Marfy's analysis was used to determine the stereochemistry of the two constituent ornithine amino acid moieties, which were both found to be in the D-form, matching those of mirubactin A and the chlorocatechelins (**Supplementary Figure 3**).

We identified a mirubactin-like gene cluster in the genome sequence of MDA8-470 by a combination of antiSMASH analysis and alignments with the mirubactin A gene cluster from *Actinosynnema mirum* DSM 43827 (**Figure 2** and **Supplementary Figure 2**). The gene cluster borders on the gene cluster of coelichelin (an unrelated siderophore) and is consequently not immediately identified as mirubactin by antiSMASH. However, the subcluster analysis found the mirubactin gene cluster with an identity of 72%. The gene cluster appears to be truncated on both sides, while the core biosynthetic pathway is conserved. The biosynthetic genes [*mrbA, mrbC* and *mrbD*; gene designations as assigned by Giessen et al. (2012)] for the 2,3-dihydroxybenzoic acid groups (DHAB) appear to be missing from the main cluster. However, genes sharing homology with *mrbC* (57%), *mrbA* (56%) and *mrbD* (55%) were found in an operon approximately 130 kb upstream of the gene cluster. Genes *mrbL-mrbO* appear to be missing in MDA8-470 but they were annotated as unknown function and regulatory in the original mirubactin cluster, and therefore may not be required for the synthesis of mirubactin A.

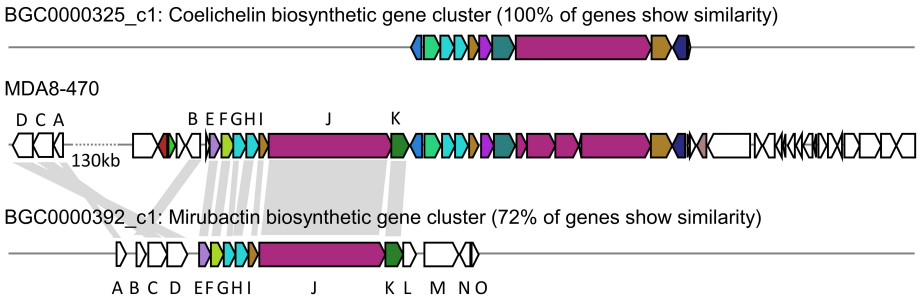

FIGURE 2
Comparative genomic analysis between *Streptomyces drozdowiczii* MDA8-470, *Streptomyces coelicolor A3*(2) and *Actinosynnema mirum* DSM 43827 in regards to the genetic locus of coelichelin and mirubactin. **(Top)** coelichelin biosynthetic gene cluster from *Streptomyces coelicolor A3*(2). **(Middle)** Genetic locus of the mirubactin and coelichelin gene cluster in *Streptomyces drozdowiczii* MDA8-470. **(Bottom)** mirubactin gene cluster from *Actinosynnema mirum* DSM 43827. Homology indicated by gray blocks based on BlastP analysis.

Synthetic mirubactin C rescues growth of the *mbl* mutant

To confirm that mirubactin C was responsible for the rescue of *mbl* mutant growth we undertook a total synthesis of the compound and compared the activity of this synthetic material to the natural product. Synthetic mirubactin C rescued growth at the same concentration as the purified natural compound (**Figures 3A,B**). We therefore conclude that the structure shown in **Figure 1** (mirubactin C) is indeed the compound responsible for the *mbl*-growth-rescue effect in extracts from strain MDA8-470. Detailed dose response curves for rescue by the compound (also observed with the original culture extracts) revealed an optimal rescue concentration at 4 μg/ml: above this concentration, growth rescue was progressively less effective (**Figure 3A**). To ascertain how specific this effect is we also purified mirubactin A and tested it in the *mbl*-recovery assay (**Figure 3C**). Mirubactin A only showed slight rescue of the *mbl* mutant and required 8 times the concentration (32 μg/ml vs 4 μg/ml). A concentration of 32 μg/ml of mirubactin C already had an adverse effect on the growth of the *mbl* mutant. The failure to rescue growth of the *mbl* mutant at higher concentrations of mirubactin C appeared to be an inhibitory activity, as growth of wild type *B. subtilis* was also impaired at the higher concentrations (**Figure 3D**). Addition of the optimal concentration of mirubactin C not only rescued growth of the *mbl* mutant, it also largely restored a normal cell morphology, although the cells seemed more prone to chaining than normal (**Figure 4**).

Mirubactin C also rescues the growth of MreB but not aPBP mutants

Previous work has revealed that various mutations affecting PG synthesis are lethal under "normal" culture conditions but can be rescued by addition of high concentrations of Mg^{2+}, including *mreB*, *mreC*, *mreD*, *rodA* and *ponA*, and that this is likely due to the inhibition of PG hydrolases (see above). We therefore tested whether mirubactin C could rescue other mutants with a Mg^{2+}-dependent phenotype. As shown in **Figure 4**, mirubactin C rescued the growth of the Δ*mreB* mutant, but not that of the Δ*4* mutant (which lacks *ponA* and the 3 other class A PBPs) (Emami et al., 2017). Although growth of the Δ*mreB* mutant was restored, the cells were highly abnormal morphologically, being bloated and lytic (**Figure 4**).

The inhibitory effect of mirubactin C is associated with iron homeostasis

The mechanism whereby mirubactin C rescues growth of the *mbl* and *mreB* mutants was not clear but we reasoned that a clue might come from further investigation of the inhibitory effect. As one way to investigate this we took a library of *B. subtilis* deletion mutants (Koo et al., 2017) and tested the set for growth at a subinhibitory concentration of mirubactin C. Three genes *odhA odhB* and *gpsA* (enzymes involved in the TCA cycle and biosynthesis of phospholipids) grew better in the presence of mirubactin C (**Supplementary Figure 5**). The nine most severely affected mutants are listed in **Table 1** and the full data set is provided in **Supplementary Figure 5**. Interestingly five of the nine genes are involved in iron (Fe) homeostasis. These findings suggested that mirubactin C binds iron and that at concentrations above 4 μg/ml, under the conditions used, it causes iron limitation resulting in growth inhibition. To test this idea, we determined the Fe and Mg^{2+} content of wild type and mutant *B. subtilis* cells by inductively coupled plasma mass spectrometry (ICP-MS) (**Figure 5**) after culture in the presence of Mg^{2+} or mirubactin C. We observed that cells treated with mirubactin C contained significantly lower Mg^{2+} and Fe content. Interestingly, growth-restoring concentrations of mirubactin C did not rectify the Mg^{2+} deficiency of *mreB* or *mbl* cells, confirming that the

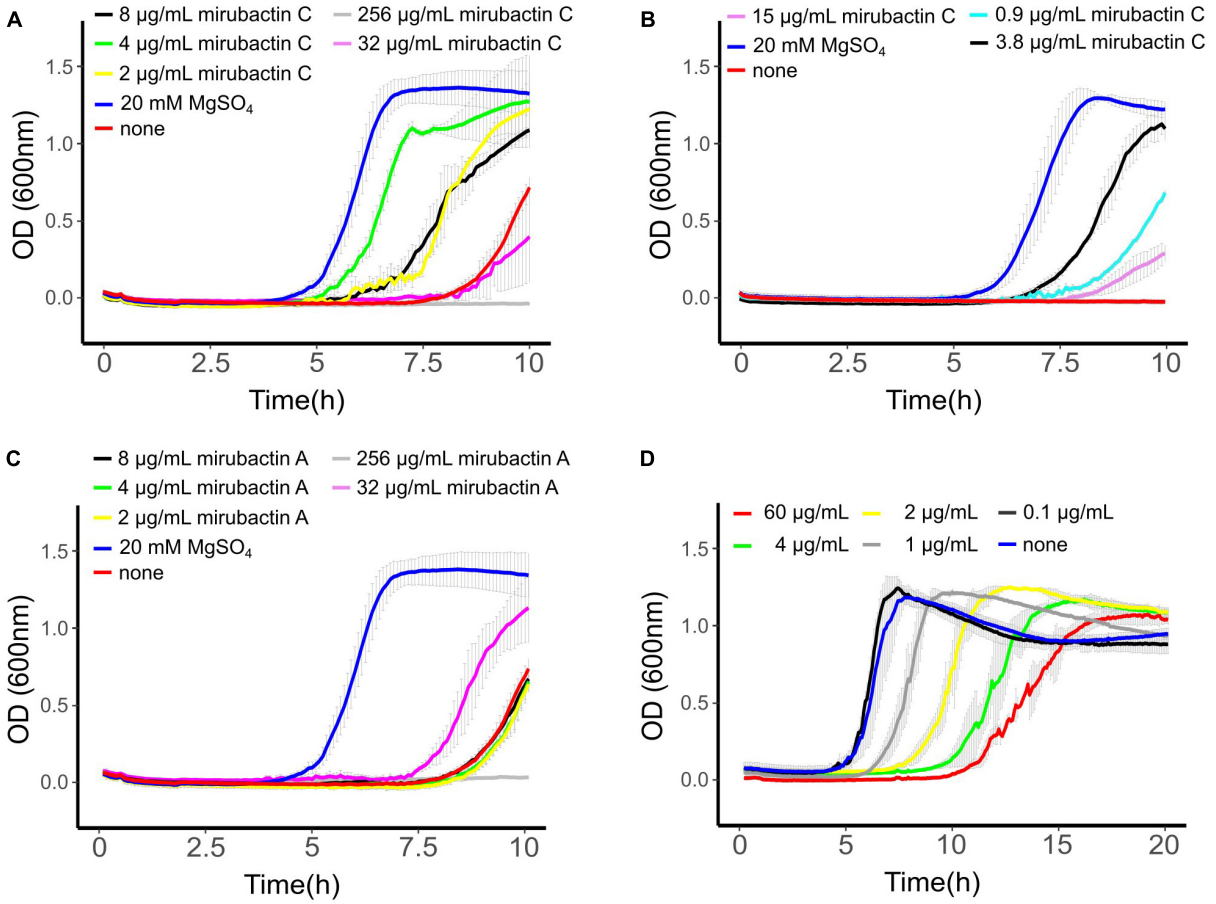

FIGURE 3
(A) *mbl*-recovery assay with mirubactin C (256 µg/ml gray, 32 µg/ml magenta, 8 µg/ml black, 4 µg/ml green, 2 µg/ml yellow) 20 mM $MgSO_4$ (blue), no addition (red). **(B)** *mbl*-recovery assay with chemically synthesized mirubactin C (15 µg/ml purple, 3.8 µg/ml black, 0.9 µg/ml turquoise), no addition (red), 20 mM $MgSO_4$ (blue) **(C)** *mbl*-recovery assay with mirubactin A (256 µg/ml gray, 32 µg/ml magenta, 8 µg/ml black, 4 µg/ml green, 2 µg/ml yellow), 20 mM $MgSO_4$ (blue), no addition (red). **(D)** Activity of purified mirubactin C against *Bacillus subtilis* 168CA, no addition (blue) and various concentrations of mirubactin C in gray. Error bars as a result of three technical replicates are shown in gray.

metabolite restores their growth through a mechanism distinct from that of Mg^{2+} (Figure 5). To confirm the role of Fe, we incubated wild type *B. subtilis* with an inhibitory concentration of mirubactin C (60 µg/ml) and supplemented the culture with $FeCl_3$. As shown in Figure 6, growth was partially restored at 3 µM Fe^{3+} and fully restored at 50 µM. This indicates that toxicity of mirubactin C at concentrations above 4 µg/ml is likely due to Fe starvation, consistent with the idea that this compound, like its larger relative mirubactin A, binds iron.

Discussion

The main motivation for developing our chemical biology screen was to find potential inhibitors of the LtaS protein, a potential antibiotic target, given that Schirner et al. (2009) had shown that deletion of the *ltaS* gene rescues growth of *mbl* mutants. However, since Schirner et al. (2009) found suppressor mutations in several other genes, the screen might also identify compounds acting on other targets. Further studies of the hit compounds might also provide insights into the enigmatic ability of Mg^{2+} to rescue the growth of mutants affected in various other cell wall functions. In this work we only screened about 2,000 natural product extracts but this unearthed mirubactin C, plus at least one other structurally and functionally distinct compound that awaits further investigation. It is likely that a screen of larger numbers of extracts would yield yet more interesting compounds, including potential antibiotics. Thus, further screening of synthetic or natural compounds via the *mbl*-rescue assay is warranted.

One of the historical difficulties with screens of natural product compounds was that of dereplicating the hits, i.e., identifying strains likely to be making the same compound and therefore reducing the number of active strains to study via

10.3389/fmicb.2022.1004737

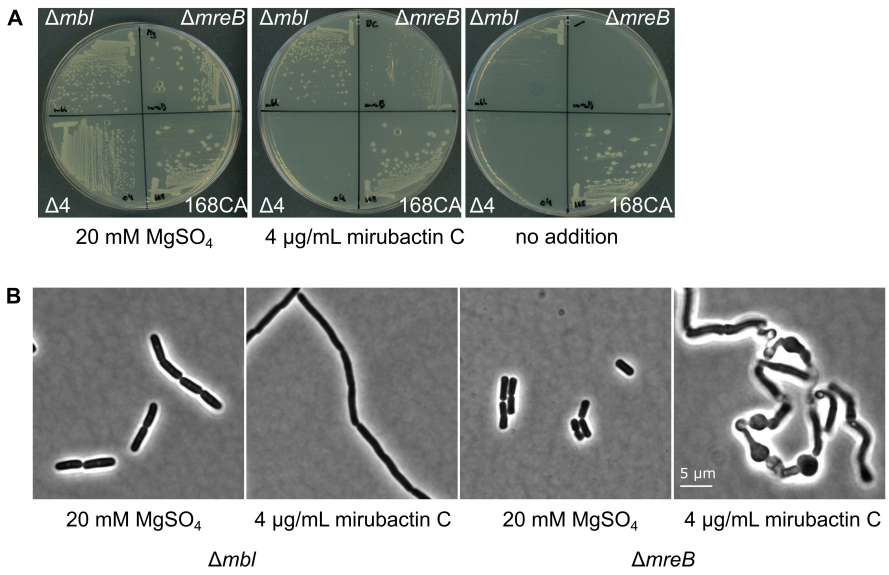

FIGURE 4
Effects of divalent cations and mirubactin C on several $MgSO_4$-dependent cell wall mutants. **(A)** Growth behavior of *Bacillus subtilis* 168CA (wt) and Δ*mbl*, Δ*mreB*, Δ*4* mutant (which lacks *ponA* and genes for the 3 other class A PBPs) on PAB plates in the presence of 20 mM $MgSO_4$, 4 µg/ml mirubactin C and in the absence of any additive. **(B)** Phenotype of *Bacillus subtilis* mutants Δ*mbl* and Δ*mreB* in the presence of $MgSO_4$ and 4 µg/ml mirubactin C.

TABLE 1 Deletion strains that exhibit hypersensitivity to mirubactin C.

Gene	Proposed function according to Subtiwiki (Pedreira et al., 2022)
feuA	ABC transporter for the siderophores Fe-enterobactin and Fe-bacillibactin (binding protein), with YusV as ATPase
yusV	ABC transporter for the siderophores Fe-enterobactin and Fe-bacillibactin, as well as for the siderophores schizokinen and arthrobactin (ATPase)
cpgA	Ribosome assembly GTPase, activity stimulated by ribosomes, may be involved in the maturation of the 30S subunit of the ribosome, detoxification of 4-phosphoerythronate
yqhY	Modulator of lipid biosynthesis
feuB	ABC transporter for the siderophores Fe-enterobactin and Fe-bacillibactin (integral membrane protein)
feuC	ABC transporter for the siderophores Fe-enterobactin and Fe-bacillibactin (integral membrane protein)
flhA	Part of the flagellar type III export apparatus (flagellar Type III secretion system), part of the CORE complex required for flagellum and nanotube assembly
fur	Transcription regulator of iron homoeostasis, sensor of Fe sufficiency
sdhA	Succinate dehydrogenase (flavoprotein subunit)

culture scale-up and compound purification. Rapid WGS of the three main hits revealed that two strains were almost identical and therefore likely to be making the same active compound. It was therefore only necessary to follow up one of these strains, illustrating the power of the genomic dereplication approach. The sequencing and analysis also revealed that the third strain is very different to the others and therefore is likely to make an unrelated compound. We intend to follow this up in the future.

The purified active compound turned out to be a smaller version of a known siderophore antibiotic, mirubactin. Total synthesis of the structure deduced for mirubactin C confirmed that this is the active compound in extracts of the producer strain. The genome sequence suggests that strain MDA8-470 contains all necessary genes for biosynthesis of mirubactin and metabolic profile of culture media of strain MDA8-470 confirmed production of mirubactin. Thus, it seems likely that mirubactin C is either a shunt metabolite in the biosynthesis of mirubactin a or a breakdown product of mirubactin A (**Supplementary Figure 4**), which would mirror the findings of Kishimoto et al. (2014) with the related chlorocatechelin A and B compounds. Mirubactin A has a high affinity for Fe^{3+} due to its hexadentate coordination potential based on its DHBA (x2) and hydroxamate moieties. Mirubactin C has a lower affinity for Fe^{3+} because of the absence of one of the DHBA groups (Pu et al., 2022). However, mirubactin C is clearly capable of binding Fe because: first, the inhibitory effect we saw in cultures treated with $\geq$ 16 µg/ml mirubactin C was exacerbated by various mutations affected in iron uptake

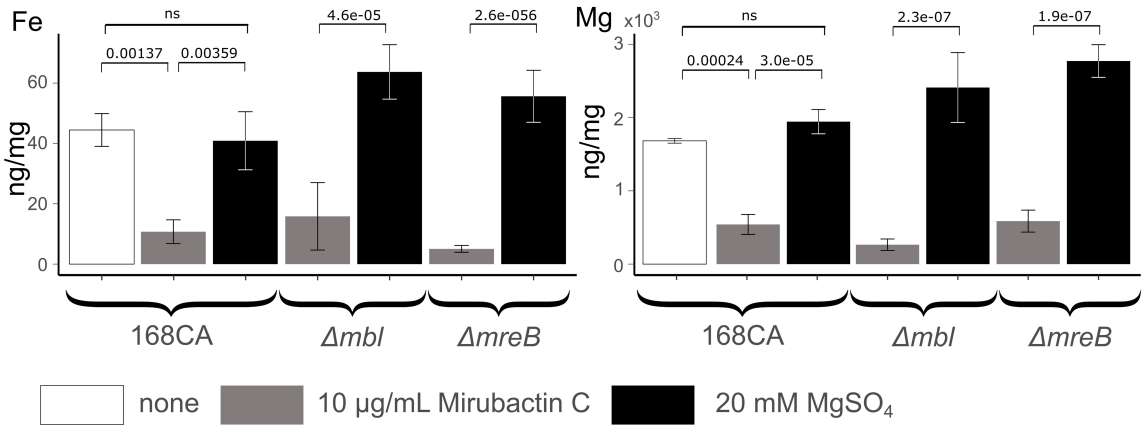

FIGURE 5
Cellular Fe and Mg content of *Bacillus subtilis* 168CA and Δ*mbl*, Δ*mreB*, mutant cells, as determined by ICP-MS, after culture in PAB medium with/without supplementation with 20 mM $MgSO_4$ or 10 μg/ml mirubactin C. *P*-values are given for selected conditions which were calculated using the pairwise *t*-test function of the ggpubr package in R.

or homeostasis; second, the inhibitory effect was alleviated by Fe supplementation in the growth medium. Nevertheless, the rescuing effect of mirubactin C at low Fe concentrations is not simply due to it acting to import iron because mirubactin A hardly rescued the *mbl* mutant. Furthermore, although most actinomycete bacteria produce iron siderophores, only a tiny proportion of the > 2,000 culture extracts we tested rescued growth of the mutant. One mechanistic hypothesis worthy of future testing is that mirubactin C moderates siderophore transport in *Bacillus*. This could occur by affecting import through the FeuABC siderophore transporter, in which the FeuA component is known to exhibit promiscuous siderophore binding (Peuckert et al., 2011), by interfering with *feuABC* regulation by interacting with its regulator Btr, which contains a FeuA-like sensory domain (Gaballa and Helmann, 2007), or by modifying the activity of the siderophore esterase, BesA (Miethke et al., 2006). Further work will be needed to establish the mechanism whereby mirubactin C rescues growth of the Rod complex mutants. The finding of a natural product compound that has a growth restorative effect on mutants of the Rod pathway highlights that there is much still to be learned about the complex chemical genetic interactions between soil microbes.

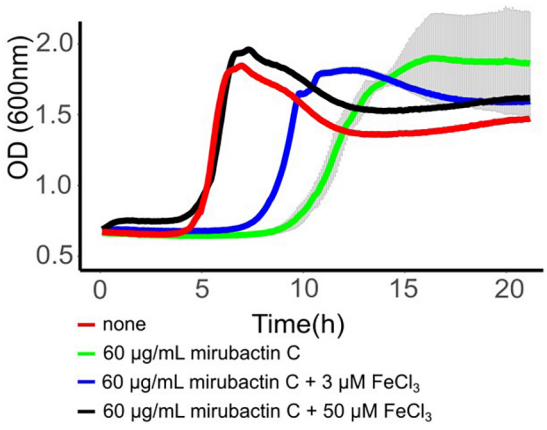

FIGURE 6
Rescue of mirubactin C toxicity in the presence of iron. Growth behavior of *Bacillus subtilis* 168CA; no addition (red), 60 μg/ml mirubactin C (green), 60 μg/ml mirubactin C and 3 μM $FeCl_3$ (blue) and 60 μg/ml mirubactin C and 50 μM $FeCl_3$ (black).

Materials and methods

Development of a robust high throughput assay for rescue of *mbl*-mutant growth

The *mbl* mutant was cultured in nutrient broth (NB) containing 20 mM Mg^{2+} under defined conditions and then diluted 10^{-4}-fold into fresh medium containing no added Mg^{2+} and chloramphenicol or spectinomycin (to inhibit growth of the actinomycetes; see below). The mutant culture was dispensed into the wells of a 96 well microtiter plate containing various controls and test samples. To calibrate the assay, several defined concentrations of Mg^{2+} were included. The plates were cultured at 37°C for 15 h, and growth was monitored by following the optical density (OD_{600}). A wild type culture was also included, with no added Mg^{2+}. No growth of the *mbl* mutant was seen in the absence of Mg^{2+} but addition of different concentrations of Mg^{2+} resulted in growth after a delay, which was roughly proportional to the amount of Mg^{2+} added. A typical result is shown below (**Supplementary Figure 1**), with time (min) along

the x-axis and optical density (OD_{600}) on the y-axis. Remaining wells in the plate were occupied by test extracts from the Demuris actinomycete collection. After testing various methods, a freeze-thaw-centrifuge procedure was adopted for preparation of extracts. Individual actinomycete strains were cultured on an appropriate agar growth medium. The agar was harvested and fragmented into 50 ml conical tubes, which were frozen at –20°C overnight, then thawed and centrifuged. The supernatant was collected, filtered and stored at –20°C until used. Positives in the primary assay were identified by growth stimulation similar to Mg^{2+} addition. Candidate extracts were retested using new extracts prepared via regrowth of the actinomycete strains. Five positive producers were identified, strains TW 167, A51P1, Mex267, MDA8-470 and MDA8-566.

Genome sequencing and analyses

The strains TW 167 and MEX267 were grown in 10 ml of liquid GYM and incubated for 3 days at 30°C and 120 rpm. Genomic DNA was extracted using the Quick-DNA HMW MagBead Kit (Zymo Research, cat. no. D6060). Aliquots (300 µl) of the cultured cells were spun at 13,000 × *g* for 2 min to pellet. The cells were resuspended in 200 µl DNA/RNA Shield (Zymo Research, cat. no. R1100-50). Microbial lysis and DNA extraction (including RNAse treatment) were performed according to the manufacturer's instructions. DNA quality was assessed by agarose gel electrophoresis to ensure no trace amounts of RNA. DNA concentration was assessed using the dsDNA assay on a Qubit fluorometer.

The strains TW 167 and MEX267 were part of a multiplexed nanopore MinION sequencing (12 strains in total) using the Native Barcoding Expansion 1–12 (EXP-NDB104), in conjunction with the Ligation Sequencing Kit (SQK-LSK109). A DNA fragmentation step was not performed. Priming and loading the SpotON flow cell was performed according to the manufacturer's instructions using R9.4.1 flow cells (FLO-MIN106D, ONT). The flow cell was mounted on a MinION Mk1B device (ONT) for sequencing and was controlled using Oxford Nanopore Technologies MinKNOW software. Base calling and data conversion was performed in parallel using Albacore v1.2.4 (Oxford Nanopore Technologies). The sequences were exported in FASTQ format and used for an assembly with CANU v1.5 (Koren et al., 2017).

For the Illumina Sequencing the genomic DNA libraries were prepared using the Nextera XT Library Prep Kit (Illumina, San Diego, USA) following the manufacturer's protocol with the following modifications: input DNA was increased 2-fold, and PCR elongation time was increased to 45 s. DNA quantification and library preparation were carried out on a Hamilton Microlab STAR automated liquid handling system (Hamilton Bonaduz AG, Switzerland). Pooled libraries were quantified using the Kapa Biosystems Library Quantification Kit for Illumina. Libraries were sequenced using Illumina sequencers (HiSeq/NovaSeq) using a 250 bp paired-end protocol.

The resulting reads were mapped onto the contigs produced by Canu using Minimap and the resulting consensus sequences exported. The contigs were annotated using Prokka 1.11 (Seemann, 2014). The corrected genome sequences were analysed with the online version of antiSMASH 6.0.1 (Blin et al., 2021).

MDA8-470 was sequenced using the Pacific Biosciences single-molecule, real-time DNA sequencing technology performed by the University of Maryland School of Medicine Genomics Resource Centre who also assembled the genome. The resulting four contigs were further polished using paired-end Illumina MiSeq data and annotated using RAST (Aziz et al., 2008).

Purification of mirubactin C

The *Streptomyces* isolate MDA8-470 was grown in GYM medium (4 g/L glucose, 4 g/L yeast extract, 10 g/L malt extract) for 76.5h (30 degrees) in two stirred tank bioreactors at a combined volume of 26 L. The combined culture supernatant was subjected to a batch absorption of 1.5 kg Amberlite XAD-16N resin. The resin was eluted with 2.5 L of methanol and evaporated to yield in 900 ml of aqueous extract. The extract was twice extracted at pH 4 with an equal volume of ethyl acetate. Bioactivity-guided fractionation showed that the compound stayed in the aqueous phase. We therefore subjected the active aqueous extract in five batches of about 180 ml to 60 g reverse phase flash chromatography from water (0.1% formic acid) to methanol (0.1% formic acid) (Gradient 1 column volume (CV) water, 10 CV 0–20% methanol, 2 CV 20–100% methanol, 1.5 CV 100% methanol). Mirubactin C eluted at about 10% methanol. The active fractions were combined and freeze-dried to a viscous oil of 5 ml. To remove the formic acid and other minor components we finally subjected the semi pure mirubactin C to a LH20 size exclusion column (85 cm x 3 cm) at a flow rate of 1 ml/min. The active fractions were freeze-dried to give a light brown powder.

Purification of mirubactin A

A mirubactin producing strain *Streptomyces sanglieri* 2161 (from the Demuris library) was cultured in 1 L GYM media for 3 days. The culture was centrifuged and the supernatant was filtered to remove the cells. The filtrate was passed through a Hypersep C18 (10 g) column using a vacuum pump. The column was then eluted stepwise with 100/0, 90/10, 50/50 and 0/100 of water/methanol. LC-MS analysis showed that mirubactin A eluted in the fraction with 10% methanol. The compound was then further purified on an Agilent 1260 Infinity II preparative HPLC connected to a single-Q mass

spectrometer using the following HPLC method: initial isocratic conditions of 5% acetonitrile for 5 min followed by linear gradient from 5 to 50% acetonitrile over 45 min; then to 100% acetonitrile in 1 min; continued by isocratic flow for an additional 9 min at a fellow rate of 12 ml/min. To avoid degradation of mirubactin during chromatography, solvents without acid additives were used. A molecular formula of $C_{26}H_{32}N_6O_{11}$, consistent with mirubactin A, was generated for the purified compound based on HRESIMS *m/z* 605.2198 $[M + H]^+$ (calculated for $C_{26}H_{33}N_6O_{11}{}^+$, 605.2201).

Bacillus subtilis deletion strain library

The strains from a comprehensive *B. subtilis* deletion library (Koo et al., 2017) were transferred onto agar plates containing LB-Miller agar either with or without 200 μg/ml mirubactin C using a SINGER ROTOR colony pinning robot with 384 long pin pads. The agar plates were incubated overnight at 37°C before being imaged on an S&P robotics SP Imager. The IRIS programme (Kritikos et al., 2017) was used to analyse the agar plate photos and determine individual colony size and the mean of four independent pinning experiments was plotted in **Supplementary Figure 5**.

Effect of mirubactin C on the growth of *Bacillus subtilis* 168CA, Δ*mbl*, Δ*mreB* and Δ*ponA*

Bacillus subtilis wild type 168CA, and isogenic strains bearing mutations Δ*mbl*, Δ*mreB* and Δ*ponA* were grown on nutrient agar plates overnight in the presence of 20 mM Mg^{2+}. Single colonies of each strain were inoculated into 10 ml PAB medium and grown to an OD_{600nm} of ∼0.1, before diluting 10^{-4} into PAB (Difco Antibiotic Medium 3) containing no Mg^{2+}. Mirubactin C was dissolved to 10 mg/ml in water prior to making dilutions in PAB medium to reach the final concentrations shown. $FeCl_3$ was dissolved in water to a concentration of 100 mM prior to making dilutions in PAB to reach the final concentrations. Growth was monitored in 96 well microtiter plate. For microscopy analysis the strain was grown to mid logarithmic phase in a 96 well plate prior to microscopic analysis. Microscopy was carried out with Nikon Eclipse Ti (Nikon Plan Apo 1.40 Oil Ph3 objective) and the images were acquired with a Prime 4.2 sCMOS camera (Photometrics) and Metamorph 7 (Molecular Devices).

Elemental analysis of *Bacillus subtilis* cells

Overnight cultures of *B. subtilis* strains grown in 10 ml of PAB medium (Difco Antibiotic Medium 3) supplemented with 20 mM Mg^{2+}. The cultures were washed twice with magnesium free medium (equal volume), diluted 1:1000 and subsequently cultured in PAB medium (37 degrees), supplemented with 20 mM Mg^{2+} or with 10 μg/ml mirubactin C, to OD_{600nm} ∼0.6 (in biological triplicates). Cells were harvested by centrifugation and washed in 1 ml of 20 mM HEPES buffer, pH 7.4, followed by a wash in 20 mM EDTA to remove surface-associated metals, then finally washed twice in PBS to remove trace EDTA. The wet cell weight of the samples was determined and then the pellets were digested in 440 μl concentrated nitric acid before 10-fold dilution for elemental analysis. ICP-MS analysis was performed by Durham University Bio-ICP-MS Facility using a set of matrix-matched standard solutions containing defined concentrations of Mg^{2+} and Fe, using Sc and Bi as internal standards in all samples and standards. The p-values were calculated using the pairwise *t*-test function in the ggpubr package in R.

Data availability statement

The datasets presented in this study can be found in online repositories. The names of the repository/repositories and accession number(s) can be found in the article/**Supplementary material**.

Author contributions

BK: investigation, visualization, and writing – original draft. YD, XW, AT, PB, JB, EM, and B-YK: investigation. CW and NA: supervision. YK: conceptualization and writing – review and editing. LW and KW: supervision and writing – review and editing. NA and MH: writing-original draft and supervision. JE: conceptualization, writing – original draft, review and editing, supervision, project administration, and funding acquisition. All authors contributed to the article and approved the submitted version.

Funding

Work in the JE lab was supported by a BBSRC Follow-on Fund grant (BB/FOF/319) and a Wellcome Investigator Award (209500).

Acknowledgments

We thank Newcastle University for Ph.D. studentships, Dr. Alex Charlton (SAgE Mass Spectrometry Facility, Newcastle

University) for mass spectrometry support, Prof. William McFarlane (Newcastle University) for NMR support, and Dr. Richard Daniel for the use of the Bacillus subtilis knock out library.

Conflict of interest

NA and B-YK were an employee of and JE scientific founder of and shareholder in Demuris Ltd. (now Odyssey Therapeutics Inc.).

The remaining authors declare that the research was conducted in the absence of any commercial or financial relationships that could be construed as a potential conflict of interest.

Publisher's note

Supplementary material

The Supplementary Material for this article can be found online at: https://www.frontiersin.org/articles/10.3389/fmicb.2022.1004737/full#supplementary-material

References

Abhayawardhane, Y., and Stewart, G. C. (1995). *Bacillus subtilis* possesses a second determinant with extensive sequence similarity to the *Escherichia coli* mreB morphogene. *J. Bacteriol.* 177, 765–773. doi: 10.1128/jb.177.3.765-773.1995

Archibald, A. R., Armstrong, J. J., Baddiley, J., and Hay, J. B. (1961). Teichoic acids and the structure of *Bacterial* walls. *Nature* 191, 570–572. doi: 10.1038/191570a0

Aziz, R. K., Bartels, D., Best, A. A., DeJongh, M., Disz, T., Edwards, R. A., et al. (2008). The RAST server: rapid annotations using subsystems technology. *BMC Genom.* 9:75. doi: 10.1186/1471-2164-9-75

Bhavsar, A. P., Beveridge, J. T., and Brown, D. E. (2001). Precise deletion of tagD and controlled depletion of its product, glycerol 3-phosphate cytidylyltransferase, leads to irregular morphology and lysis of *Bacillus subtilis* grown at physiological temperature. *J. Bacteriol.* 183, 6688–6693. doi: 10.1128/JB.183.22.6688-6693.2001

Blin, K., Shaw, S., Kloosterman, A. M., Charlop-Powers, Z., van Wezel, G. P., Medema, M. H., et al. (2021). antiSMASH 6.0: improving cluster detection and comparison capabilities. *Nucleic Acids Res.* 49:W29–W35. doi: 10.1093/nar/gkab335

Campbell, J., Singh, A. K., Swoboda, G. J., Gilmore, M. S., Wilkinson, J. B., and Walker, S. (2012). An antibiotic that inhibits a late step in wall teichoic acid biosynthesis induces the cell wall stress stimulon in *Staphylococcus aureus*. *Antimicrob. Agents Chemother.* 56, 1810–1820. doi: 10.1128/AAC.05938-11

Corrigan, R. M., Abbott, J. C., Burhenne, H., Kaever, V., and Gründling, A. (2011). c-di-AMP is a new second messenger in *Staphylococcus aureus* with a role in controlling cell size and envelope stress. *PLoS Pathog.* 7:e1002217. doi: 10.1371/journal.ppat.1002217

Dajkovic, A., Tesson, B., Chauhan, S., Courtin, P., Keary, R., Flores, P., et al. (2017). Hydrolysis of peptidoglycan is modulated by amidation of meso-diaminopimelic acid and Mg2+ in *Bacillus subtilis*. *Mol. Microbiol.* 104, 972–988. doi: 10.1111/mmi.13673

Dion, M. F., Kapoor, M., Sun, Y., Wilson, S., Ryan, J., Vigouroux, A., et al. (2019). *Bacillus subtilis* cell diameter is determined by the opposing actions of two distinct cell wall synthetic systems. *Nat. Microbiol.* 4, 1294–1305. doi: 10.1038/s41564-019-0439-0

Dominguez-Cuevas, P., Mercier, R., Leaver, M., Kawai, Y., and Errington, J. (2012). The rod to L-form transition of *Bacillus subtilis* is limited by a requirement for the protoplast to escape from the cell wall sacculus. *Mol. Microbiol.* 83, 52–66. doi: 10.1111/j.1365-2958.2011.07920.x

Emami, K., Guyet, A., Kawai, Y., Devi, J., Wu, L. J., Allenby, N., et al. (2017). RodA as the missing glycosyltransferase in *Bacillus subtilis* and antibiotic discovery for the peptidoglycan polymerase pathway. *Nat. Microbiol.* 2:16253. doi: 10.1038/nmicrobiol.2016.253

Fittipaldi, N., Sekizaki, T., Takamatsu, D., Harel, J., Dominguez-Punaro, M., de la, C., et al. (2008). D-alanylation of lipoteichoic acid contributes to the virulence of *Streptococcus suis*. *Infect. Immun.* 76, 3587–3594. doi: 10.1128/IAI.01568-07

Formstone, A., and Errington, J. (2005). A magnesium-dependent mreB null mutant: implications for the role of mreB in *Bacillus subtilis*. *Mol. Microbiol.* 55, 1646–1657. doi: 10.1111/j.1365-2958.2005.04506.x

Gaballa, A., and Helmann, J. D. (2007). Substrate induction of siderophore transport in *Bacillus subtilis* mediated by a novel one-component regulator. *Mol. Microbiol.* 66, 164–173. doi: 10.1111/j.1365-2958.2007.05905.x

Genilloud, O. (2017). Actinomycetes: still a source of novel antibiotics. *Nat. Prod. Rep.* 34, 1203–1232. doi: 10.1039/C7NP00026J

Giessen, T. W., Franke, K. B., Knappe, T. A., Kraas, F. I., Bosello, M., Xie, X., et al. (2012). Isolation, structure elucidation, and biosynthesis of an unusual hydroxamic acid ester-containing siderophore from actinosynnema mirum. *J. Nat. Prod.* 75, 905–914. doi: 10.1021/np300046k

Heptinstall, S., Archibald, A. R., and Baddiley, J. (1970). Teichoic Acids and Membrane Function in *Bacteria*. *Nature* 225, 519–521. doi: 10.1038/225519a0

Jones, L. J. F., Carballido-López, R., and Errington, J. (2001). Control of cell shape in *Bacteria*: helical, actin-like filaments in *Bacillus subtilis*. *Cell* 104, 913–922. doi: 10.1016/S0092-8674(01)00287-2

Kawai, Y., Daniel, R. A., and Errington, J. (2009). Regulation of cell wall morphogenesis in *Bacillus subtilis* by recruitment of PBP1 to the MreB helix. *Mol. Microbiol.* 71, 1131–1144. doi: 10.1111/j.1365-2958.2009.06601.x

Kishimoto, S., Nishimura, S., and Kakeya, H. (2015b). Total synthesis and structure revision of mirubactin, and its iron binding activity. *Chem. Lett.* 44, 1303–1305. doi: 10.1246/cl.150520

Kishimoto, S., Nishimura, S., Hatano, M., Igarashi, M., and Kakeya, H. (2015a). Total synthesis and antimicrobial activity of chlorocatechelin A. *J. Org. Chem.* 80, 6076–6082. doi: 10.1021/acs.joc.5b00532

Kishimoto, S., Nishimura, S., Hattori, A., Tsujimoto, M., Hatano, M., Igarashi, M., et al. (2014). Chlorocatechelins A and B from Streptomyces sp.: New siderophores containing chlorinated catecholate groups and an acylguanidine structure. *Org. Lett.* 16, 6108–6111. doi: 10.1021/ol502964s

Koch, A. L. (2006). The exocytoskeleton. *Microb. Physiol.* 11, 115–125. doi: 10.1159/000094048

Koo, B. M., Kritikos, G., Farelli, J. D., Todor, H., Tong, K., Kimsey, H., et al. (2017). Construction and analysis of two genome-scale deletion libraries for *Bacillus subtilis*. *Cell Syst.* 4, 291–305.e7. doi: 10.1016/j.cels.2016.12.013

Koren, S., Walenz, B. P., Berlin, K., Miller, J. R., Bergman, N. H., and Phillippy, A. M. (2017). Canu: scalable and accurate long-read assembly via adaptive k-mer

weighting and repeat separation. *Genome Res.* 27, 722–736. doi: 10.1101/gr.215087.116

Kritikos, G., Banzhaf, M., Herrera-Dominguez, L., Koumoutsi, A., Wartel, M., Zietek, M., et al. (2017). A tool named Iris for versatile high-throughput phenotyping in microorganisms. *Nat. Microbiol.* 2:17014. doi: 10.1038/nmicrobiol.2017.14

Leaver, M., and Errington, J. (2005). Roles for MreC and MreD proteins in helical growth of the cylindrical cell wall in *Bacillus subtilis*. *Mol. Microbiol.* 57, 1196–1209. doi: 10.1111/j.1365-2958.2005.04736.x

Lee, S., and Price, C. W. (1993). The minCD locus of *Bacillus subtilis* lacks the minE determinant that provides topological specificity to cell division. *Mol. Microbiol.* 7, 601–610. doi: 10.1111/j.1365-2958.1993.tb01151.x

Levin, P. A., Margolis, P. S., Setlow, P., Losick, R., and Sun, D. (1992). Identification of *Bacillus subtilis* genes for septum placement and shape determination. *J. Bacteriol.* 174, 6717–6728. doi: 10.1128/jb.174.21.6717-6728.1992

Masayuki, H., Seika, O., and Junichi, S. (2012). Synthetic lethality of the lytE cwlO genotype in *Bacillus subtilis* Is caused by lack of d,l-endopeptidase activity at the lateral cell wall. *J. Bacteriol.* 194, 796–803. doi: 10.1128/JB.05569-11

Meeske, A. J., Riley, E. P., Robins, W. P., Uehara, T., Mekalanos, J. J., Kahne, D., et al. (2016). SEDS proteins are a widespread family of *Bacterial* cell wall polymerases. *Nature* 537, 634–638. doi: 10.1038/nature19331

Miethke, M., Klotz, O., Linne, U., May, J. J., Beckering, C. L., and Marahiel, M. A. (2006). Ferri-bacillibactin uptake and hydrolysis in *Bacillus subtilis*. *Mol. Microbiol.* 61, 1413–1427. doi: 10.1111/j.1365-2958.2006.05321.x

Morath, S., Geyer, A., and Hartung, T. (2001). Structure–function relationship of cytokine induction by lipoteichoic acid from *Staphylococcus aureus*. *J. Exp. Med.* 193, 393–398. doi: 10.1084/jem.193.3.393

Murray, T., Popham, D. L., and Setlow, P. (1998). *Bacillus subtilis* cells lacking penicillin-binding protein 1 require increased levels of divalent cations for growth. *J. Bacteriol.* 180, 4555–4563. doi: 10.1128/JB.180.17.4555-4563.1998

Oku, Y., Kurokawa, K., Matsuo, M., Yamada, S., Lee, B. L., and Sekimizu, K. (2009). Pleiotropic roles of polyglycerolphosphate synthase of lipoteichoic acid in growth of *Staphylococcus aureus* cells. *J. Bacteriol.* 191, 141–151. doi: 10.1128/JB.01221-08

Pedreira, T., Elfmann, C., and Stülke, J. (2022). The current state of SubtiWiki, the database for the model organism *Bacillus subtilis*. *Nucleic Acids Res.* 50:D875–D882. doi: 10.1093/nar/gkab943

Peuckert, F., Ramos-Vega, A. L., Miethke, M., Schwörer, C. J., Albrecht, A. G., Oberthür, M., et al. (2011). The Siderophore binding protein FeuA shows limited promiscuity toward exogenous triscatecholates. *Chem. Biol.* 18, 907–919. doi: 10.1016/j.chembiol.2011.05.006

Pi, H., Wendel, B., and Helmann, J. (2022). Dysregulation of magnesium transport protects *Bacillus subtilis* against manganese and cobalt intoxication. *J. Bacteriol.* 202:e711–e719. doi: 10.1128/JB.00711-19

Pu, H., Jiang, T., Peng, D., Xia, J., Gao, J., Wang, Y., et al. (2022). Degradation of mirubactin to multiple siderophores with varying Fe(iii) chelation properties. *Org. Biomol. Chem.* 20, 5066–5070. doi: 10.1039/D2OB00942K

Richter, S. G., Elli, D., Kim, H. K., Hendrickx, A. P., Sorg, J. A., Schneewind, O., et al. (2013). Small molecule inhibitor of lipoteichoic acid synthesis is an antibiotic for Gram-positive *Bacteria*. *Proc. Natl. Acad. Sci. U.S.A.* 110, 3531–3536. doi: 10.1073/pnas.1217337110

Schirner, K., Marles-Wright, J., Lewis, R. J., and Errington, J. (2009). Distinct and essential morphogenic functions for wall- and lipo-teichoic acids in *Bacillus subtilis*. *EMBO J.* 28, 830–842. doi: 10.1038/emboj.2009.25

Seemann, T. (2014). Prokka: rapid prokaryotic genome annotation. *Bioinformatics* 30, 2068–2069. doi: 10.1093/bioinformatics/btu153

Tesson, B., Dajkovic, A., Keary, R., Marlière, C., Dupont-Gillain, C. C., and Carballido-López, R. (2022). Magnesium rescues the morphology of *Bacillus subtilis* mreB mutants through its inhibitory effect on peptidoglycan hydrolases. *Sci. Rep.* 12:1137. doi: 10.1038/s41598-021-04294-5

Varley, A. W., and Stewart, G. C. (1992). The divIVB region of the *Bacillus subtilis* chromosome encodes homologs of *Escherichia coli* septum placement (minCD) and cell shape (mreBCD) determinants. *J. Bacteriol.* 174, 6729–6742. doi: 10.1128/jb.174.21.6729-6742.1992

Vickery, C. R., Wood, B. M., Morris, H. G., Losick, R., and Walker, S. (2018). Reconstitution of *Staphylococcus aureus* lipoteichoic acid synthase activity identifies congo red as a selective inhibitor. *J. Am. Chem. Soc.* 140, 876–879. doi: 10.1021/jacs.7b11704

Weidenmaier, C., Kokai-Kun, J. F., Kristian, S. A., Chanturiya, T., Kalbacher, H., Gross, M., et al. (2004). Role of teichoic acids in *Staphylococcus aureus* nasal colonization, a major risk factor in nosocomial infections. *Nat. Med.* 10, 243–245. doi: 10.1038/nm991

Wilson, S., and Garner, E. (2021). An exhaustive multiple knockout approach to understanding cell wall hydrolase function in *Bacillus subtilis*. *bioRxiv* 2021.02.18.431929 [Preprint]. doi: 10.1101/2021.02.18.431929